

# **ASSESSMENT OF SEISMIC HAZARD AND PATTERN RECOGNITION FOR REGION AROUND KANGRA**

**Ph.D. THESIS**

**By**

**MRIDULA**



**DEPARTMENT OF EARTHQUAKE ENGINEERING  
INDIAN INSTITUTE OF TECHNOLOGY ROORKEE  
ROORKEE - 247 667 (INDIA)  
MAY -2016**



# **ASSESSMENT OF SEISMIC HAZARD AND PATTERN RECOGNITION FOR REGION AROUND KANGRA**

**A THESIS**

*Submitted in partial fulfillment of the  
requirements for the award of the degree  
of*

**DOCTOR OF PHILOSOPHY**

*in*

**EARTHQUAKE ENGINEERING**

**By**

**MRIDULA**



**DEPARTMENT OF EARTHQUAKE ENGINEERING  
INDIAN INSTITUTE OF TECHNOLOGY ROORKEE  
ROORKEE - 247 667 (INDIA)  
MAY -2016**







**©INDIAN INSTITUTE OF TECHNOLOGY ROORKEE, ROORKEE-2016**

**ALL RIGHTS RESERVED**



# INDIAN INSTITUTE OF TECHNOLOGY ROORKEE ROORKEE

## CANDIDATE'S DECLARATION

I hereby certify that the work which is being presented in the thesis entitled “**ASSESSMENT OF SEISMIC HAZARD AND PATTERN RECOGNITION FOR REGION AROUND KANGRA**” in partial fulfillment of the requirements for the award of the Degree of Doctor of Philosophy and submitted in the Department of Earthquake Engineering of the Indian Institute of Technology Roorkee, Roorkee is an authentic record of my own work carried out during a period from December, 2010 to May, 2016 under the supervision of Dr. (Mrs.) Amita Sinvhal, Professor and Dr. H. R. Wason, Emeritus Fellow, Department of Earthquake Engineering, Indian Institute of Technology Roorkee, Roorkee.

The matter presented in the thesis has not been submitted by me for the award of any other degree of this or any other Institute.

**(MRIDULA)**

This is to certify that the above statement made by the candidate is correct to the best of our knowledge.

(Dr. (Mrs.) A. Sinvhal)

(Dr. H. R. Wason)

Date:.....

Supervisor

Supervisor



## ABSTRACT

This research work was carried out with the following objectives: to identify seismically susceptible areas using Pattern Recognition (PR); segmentation of longer tectonic units using PR and assessment of seismic hazard by two methods: Deterministic Seismic Hazard Assessment (DSHA) and Probabilistic Seismic Hazard Assessment (PSHA) in a  $7^\circ$  by  $7^\circ$  area, defined by longitudes  $73^\circ\text{E}$  to  $80^\circ\text{E}$  and latitudes  $29^\circ\text{N}$  to  $36^\circ\text{N}$ , centered on the epicenter of the great Kangra earthquake of 1905. An earthquake catalogue compiled for the study area consisted of 1172 main events with moment magnitude ( $M_w$ ) ranging from 3.5 – 8.0 for the period 1552-2012. This catalogue is referred to as the Merged, Homogenized and Declustered, MHD, catalogue for western Himalaya. Another catalogue, MHD catalogue-2, compiled for validation of results, contained 80 earthquakes with  $M_w$  4.5 – 5.7 for the period January 2013 to September 2015. Tectonic data for the study area was compiled from Seismotectonic Atlas of India and its Environs (SEISAT, 2000). Initially 26 tectonic units were considered, in subsequent studies these were increased to 118.

The PR technique consisted of six steps: identification and extraction of features, classification of data, discriminant analysis, i.e. training exercise, decision making based on results of training exercise and validation of results. This PR technique was used twice, once for identification of seismically susceptible areas and again for segmentation of MBT and MCT. A circle of 25 km radius was drawn around each epicenter of the MHD catalogue, which was a central earthquake. Twelve features were extracted from this circle. All epicenters in the MHD catalogue were classified into two training classes according to magnitude. 15 iterations of discriminant analyses were carried out by varying number of features and classification criteria. The best result in terms of percentage of classification of epicenters was retained for further analysis. A linear combination of extracted features and discriminant functions  $\lambda_2, \lambda_3, \dots, \lambda_{12}$  was used to compute seismic score for each earthquake,  $R_i$ . This transformed the original set of features of an earthquake into a single seismic score. This was used to maximize the difference between the two training classes

Multivariate mean of the two classes was subsequently used for decision making. 196 grid points at half degree intervals were considered in the study area and the same 11 features were extracted from a circle of radius 25 km drawn around each site. Using  $\lambda_2, \lambda_3, \dots, \lambda_{12}$  values obtained

in the training exercise a seismic score was computed for each grid point. These were compared to the multivariate means obtained in the training exercise and this was used to assign new classes to each site, henceforth named as classes, 'A', 'B' and 'C'. Envelopes were drawn around clusters of same class and after validation three areas were identified as: Area A: most susceptible, Area B: moderately susceptible and Area C: least susceptible.

The next step was segmentation of MBT and MCT using the PR technique. All epicenters in the MHD catalogue were again divided into two classes with respect to distance from MBT. Discriminant analysis was repeated with four features. Graphical representation of seismic scores indicated four prominent clusters of crossover epicenters which were located at same position in all iterations. These clusters of seismicity within a well defined tectonic environment together with presence of transverse tectonic units, change in seismicity pattern along the thrust and change in strike were used for segmentation of the MBT. The six segments identified are: Poonch segment, Udhampur segment, Kangra segment, Solan segment, Dehradun segment and Nainital segment. A similar exercise carried out for MCT yielded 5 segments: Mashko segment, Chenab segment, Kinnaur segment, Uttarkashi segment and Bageshwar segment. Tectonic units in the study area increased from 118 to 127 after segmentation and these were used for hazard assessment.

Hazard maps were prepared for DSHA study with two different approaches: DSHA-1 and DSHA-2, for the entire study area. The map prepared for DSHA-1 showed that PGA varied between 0.012 - 0.470g. This study was repeated by refining several aspects such as 127 tectonic units, assigning maximum magnitude to each tectonic unit and calculating PGA using Boore and Atkinson, 2008 relationship. A hazard map was prepared which revealed that PGA in the study area was substantially higher than in the previous study and varied between 0.039 - 0.581g.

For PSHA study the study area was divided into nine seismogenic source zones (SSZ). These are named as SSZ1 to SSZ9 and are: the Kangra SSZ, Uttarakhand SSZ, Kashmir Syntaxis SSZ, Kaurik SSZ, Kargil Laddakh SSZ, Western Nepal SSZ, Karakoram SSZ, Jhelum SSZ, and Indo Gangetic SSZ. Hazard parameters were computed for each source zone. GMPE's given by Abrahamson and Litehiser (1989) and Boore and Atkinson (2008) were used to estimate PGA in each SSZ. PGA in the entire study area was estimated to vary between 0.039 - 0.289g for 10% probability of exceedance in 50 years for a return period of 475 years. PGA varied between 0.038 - 0.723 g for 2% probability of exceedance in 50 years, for a return period of 2,475 years. By

retaining the SSZ and hazard parameters of the earlier exercise the PSHA was repeated to study the effect of varying GMPE's on PGA. PGA in the study area varied between 0.013-0.315g for 10% probability of exceedance in 50 years for a return period of 475 years and varied between 0.024 - 0.780g for 2% probability of exceedance in 50 years for a return period of 2,475 years. Four hazard maps were developed for PSHA studies. Validation of results of return periods for  $M_w \leq 5.7$  was carried out for each of the nine seismogenic source zones. This could not be validated for higher magnitudes as no earthquake of magnitude  $M_w > 5.7$  occurred after 2012, as per the MHD catalogue-2 for validation. These earthquakes were not part of the data set used for computation of hazard parameters.

Seismic hazard parameters computed for each SSZ showed that the most hazardous zone in the entire  $7^\circ$  by  $7^\circ$  study area is the Kangra seismogenic source zone, SSZ1. This zone is currently going through a rapid phase of techno-economic development and hydro electric potential is tremendous in this Himalayan zone due to the presence of many rivers and their tributaries. Return period computed for an earthquake of magnitude  $M_w = 8.0$  revealed that it will occur somewhere between the years 2003 to 2109, earthquakes of magnitude  $M_w 7.0$  and  $6.0$  are overdue since 1964 and 1966, respectively, and earthquakes of magnitude  $M_w 5.0 - 5.7$  are occurring more frequently than computed. This indicates that an impending earthquake disaster is overdue in the Kangra source zone and underlines the urgency of estimating future implications for the Kangra source zone.

Susceptible areas superimposed on SSZ map showed that almost 73% area of Kangra SSZ comprised of susceptible area  $A'$ , i.e. approximately  $17,500 \text{ km}^2$ . Therefore the Kangra SSZ was narrowed down to this truncated area. Recent epicenters from MHD catalogue-2 overlaid on the Kangra SSZ revealed that 23 out of the 24 epicenters were within this truncated area. Therefore, the truncated area can be considered where most current events are located. PGA contours in the truncated area varied between 0.37g and 0.58g as per DSHA. Risk to loss of human life calculated for five districts located within the truncated area indicated that Kangra district would suffer maximum human casualties and injuries followed by Mandi, Hamirpur, Bilaspur and Chamba districts. It is pertinent to note that PGA computed was much higher than that assigned to zone V in the seismic zoning map of India as per, BIS 1893- 2002; therefore, actual casualty figures and injured may be much higher than computed. Iseismals of four destructive earthquakes plotted on

truncated area showed that maximum damage due to these four events is concentrated within the truncated area. Therefore, this area is under an enhanced threat perception.

After all these studies the following can be deduced for the truncated area. It is an area where the following are concentrated: (1) Return period for an earthquake of magnitude  $M_w = 8.0$  is between the years 2003 to 2109, an earthquake of  $M_w 7.0$  and  $6.0$  is overdue since 1964 and 1966, respectively, and earthquakes of magnitude  $M_w 5.0-5.7$  are occurring more frequently than computed, (2) Computed PGA values are very high and are in the range  $0.37g$  to  $0.58g$ , (3) current seismic events are located, (4) meizo-seismal areas of four destructive earthquakes are located, and (5) risk to population is very high. This has tremendous implications in the Kangra SSZ for future.

Starting with a  $7^\circ$  by  $7^\circ$  study area the results were narrowed down to hypothesize a predictive model for a smaller area,  $17,500 \text{ km}^2$ , where frequent destructive earthquakes are expected in the near future. Therefore, urgent preparedness, emergency responses and disaster mitigation measures are required in this area. The results presented here for the Kangra SSZ can be obtained similarly for all the other eight SSZs and risk implications can be estimated.



## ACKNOWLEDGMENT



Foremost of all, I bow my head to the **Almighty God**, for granting me the wisdom, strength and health, to accomplish this chapter of my life.

First of all I express my immense gratitude and indebtedness to my supervisor, **Dr. (Mrs.) Amita Sinvhal**, Professor, Department of Earthquake Engineering (DEQ), for her constant inspiration, guidance, encouragement and insightful suggestions that inspired me to dedicate myself to this research work. Under her guidance I successfully overcame many difficulties and learned a lot. I can't forget her hard times. Despite of her ill health, she used to review my thesis progress, make corrections and give valuable suggestions. Her unflinching courage and conviction will always inspire me.

I am also extremely indebted to my supervisor **Dr. H.R. Wason**, Emeritus Fellow, Department of Earthquakes Engineering (DEQ), for his valuable guidance, support, consistent encouragement and helpful suggestions throughout my Ph.D. He always made himself available to clarify my doubts despite his busy schedules and I consider it as a great opportunity to do my doctoral program under his guidance and to learn from his research expertise.

Special thanks to my research committee, **Prof. J. P Narayan**, Department of Earthquake Engineering and **Prof. Anand Joshi**, Department of Earth Sciences (DES), for their support and helpful suggestions. I highly appreciate their contribution of time and ideas which inspired me to carry out my Ph.D. work. Some faculty members of the institute have been very kind enough to extend their help at various phases of this research, whenever I approached them. I am thankful to **Prof. A. D. Pandey** (DEQ), **Prof. Ashwini Kumar** (Professor, DEQ), **Prof I.D. Gupta** (visiting Professor, DEQ), **Ajay Gairola** (Professor, Civil Engineering department), **Dr. Arun Kumar** (Professor, AHEC) and **Mr. Sushil Dubey** (Project Associate, AHEC) Indian Institute of Technology Roorkee, for providing departmental facilities for carrying out my research work.

I would like to thank the department and the Head **Prof. Yogendra Singh, IIT Roorkee**, and **Prof. M. L. Sharma** (former head), for providing academic support to carry out this research work. I also thank to the **Indian Meteorological Department**, New Delhi, for the epicentral data provided and **Geological Survey of India** and **Survey of India** for providing maps. I am grateful

to the **Ministry of Human Resource Development (MHRD)** for financial support provided for the study.

I am also thankful to **Mr. Subodh Saini**, for helping me in various stages of preparation of my thesis. I owe my thanks to **Mr. P. L Gupta, Mr. Sudan, Ms. Rekha, Mr. R. Giri, and Mr. Narendra Sharma** for providing me with help with departmental issues.

I am also thankful to family members of Dr. (Mrs.) Amita Sinvhal, **Dr. Harshvardhan Sinvhal** (former deputy director, IIT Roorkee), **Major Yashvardhan Sinvhal, Ms. Nidhi Sinvhal** and her granddaughter **Ms. Sadhika Sinvhal** for their support throughout this study.

I am indebted to my friends and colleagues, **Dr. Ranjeet Das, Dr. Madan Mohan Rout, Ms. Shermi, Prabhat Kumar, his wife Swati** for providing a fun filled environment and lively company on various occasions during the tenure of research work. My special thanks go to **Dr. Darakhshan Sahar** for her friendship and encouragement. I would also like to extend thanks to **Ms. Swati Singh Rajput** for helping me in preparing maps and lovely company.

Words fail me in expressing my heartfelt thanks to my family members for their blessings, unquestioning love and longed to see this achievement come true. I am grateful to my parents (**Mrs. Arunima and Dr. Harilal, DGM, ONGC**, who has been my role-model for hard work) and in-laws (**Mrs. Bala Devi and Mr. Yashpal Singh**) for their patience, understanding and belief in my effort, and for their constant support and prayers. Special thanks to my sisters (**Dr. Manisha and Ms. Abhilasha**), sister in-laws (**Ms. Neelam and Ms. Abhilasha**).

Finally, and most importantly, I would like to thank my husband **Dr. Brij Mohan Singh** for his continued and unwavering love. His support and encouragement was in the end what made this thesis possible.

I dedicate this Ph.D. thesis to my two lovely children **Harshit** and **Anwita**, for their continuous patience for their mother spending so much time away from them working on her thesis. Both of you are the pride and joy of my life.

**MRIDULA**

## CONTENTS

<b>ABSTRACT</b>	i
<b>ACKNOWLEDGEMENT</b>	v
<b>CONTENTS</b>	vii
<b>LIST OF FIGURES</b>	x
<b>LIST OF TABLES</b>	xvii
<b>LIST OF ABBREVIATIONS</b>	xxii
<b>LIST OF SYMBOLS</b>	xxv
<b>CHAPTER 1: INTRODUCTION</b>	<b>1-25</b>
1.1 Introduction	1
1.2 Literature Review	2
1.2.1 Review of pattern recognition	2
1.2.2 Review of Segmentation	13
1.2.3 Review of deterministic seismic hazard assessment	14
1.2.4 Review of probabilistic seismic hazard assessment	17
1.2.5 Seismic zoning map of India	20
1.3 Identification of Gaps	23
1.4 Objectives	24
1.5 Organization of the Thesis	24
<b>CHAPTER 2: DATA USED IN THE STUDY AREA</b>	<b>26-74</b>
2.1 Introduction	26
2.2 Study Area	29
2.3 Seismicity of the Study Area	33
2.3.1 Data treatment	35
2.3.1.1 Merging of catalogues	35
2.3.1.2 Homogenization of catalogues	36
2.3.1.3 Declustering of catalogue	37
2.3.2 MHD catalogue	40
2.3.2.1 Completeness of MHD earthquake catalogue	42
2.3.2.2 Use of MHD catalogues in this research work	45
2.4 Tectonics of the Study Area	48
2.4.1 Identification of tectonic data	48
2.4.2 Data collection	49
2.4.3 Digitization of tectonic data	57
2.4.4 Tectonic units	63
2.4.5 Use of tectonic data in this research work	64
2.4.6 Seismotectonics of the study area	64
2.4.7 Fault plane solutions	70
2.4.8 MHD catalogue-2, for validation of results	70
2.5 Conclusions	74

<b>CHAPTER 3: PATTERN RECOGNITION</b>	<b>75-105</b>
3.1 Introduction	75
3.2 Major Steps of Pattern Recognition	75
3.3 Identification of Features	76
3.4 Extraction of Features	78
3.5 Classification Criteria	85
3.6 Discriminant Analysis	86
3.7 Interpretation of Results	90
3.8 Validation of Results	101
3.9 Segmentation of Long Tectonic Units	101
3.10 Conclusions	105
<b>CHAPTER 4: IDENTIFICATION OF SEISMICALLY SUSCEPTIBLE AREAS IN WESTERN HIMALAYA</b>	<b>106-125</b>
4.1 Introduction	106
4.2 Features Used for Discriminant Analysis in Model PR4	108
4.3 Classification Criteria	109
4.4 Discriminant Analysis	110
4.5 Interpretation and Decision Making	116
4.6 Validation of Results	119
4.7 Comparisons	122
4.8 Conclusions	124
<b>CHAPTER 5: SEGMENTATION OF MAIN BOUNDARY THRUST AND MAIN CENTRAL THRUST IN WESTERN HIMALAYA</b>	<b>126-145</b>
5.1 Introduction	126
5.2 Equal Segmentation of Long Tectonic Units	126
5.3 Segmentation of Main Boundary Thrust (MBT)	130
5.3.1 Features used	130
5.3.2 Classification criteria	131
5.3.3 Discriminant analysis	131
5.3.4 Results and decision making	134
5.4 Segmentation of Main Central Thrust (MCT)	138
5.5 Validation of Results of Segmentation	144
5.6 Conclusions	145
<b>CHAPTER 6 :DETERMINISTIC SEISMIC HAZARD ASSESSMENT (DSHA)</b>	<b>146-186</b>
6.1 Introduction	146
6.2 Deterministic Seismic Hazard Assessment (DSHA-1)	149
6.3 Deterministic Seismic Hazard Assessment (DSHA-2)	158
6.4 Discussion	177
6.5 Conclusions	185

<b>CHAPTER 7: PROBABILISTIC SEISMIC HAZARD ASSESSMENT (PSHA)</b>	<b>187-211</b>
7.1 Introduction	187
7.2 Methodology	190
7.2.1 Identification of Seismogenic source zones	190
7.2.2 Validation of SSZ as per MHD catalogue-2	192
7.2.3 Seismic hazard parameters	195
7.2.4 Significance of ‘a’ and ‘b’ values in different SSZs	198
7.2.5 Return periods	200
7.2.6 Validation of return periods in terms of MHD catalogue-2	201
7.2.7 Hazard maps	203
7.2.8 Interpretation of PSHA hazard map	206
7.3 Discussion	207
7.4 Conclusions	210
<b>CHAPTER 8: DISCUSSION AND CONCLUSIONS</b>	<b>212-221</b>
8.1 Summary	212
8.2 Integrated Results for Kangra SSZ	213
8.3 Predictive Model for Kangra SSZ	216
8.4 Conclusions	220
8.5 Future Scope	221
<b>BIBLIOGRAPHY</b>	<b>222-252</b>
<b>LIST OF PUBLICATIONS</b>	<b>253</b>



## LIST OF FIGURES

Figure no.	Caption	Page
Figure 1.1	Seismic zoning map of India shown for the study area (redrawn after BIS 1893: 2002). Places are as per SEISAT (Narula <i>et al.</i> 2000).	22
Figure 2.1	Isoseismals of the great Kangra earthquake of 1905, on RF scale, (after Middlemiss, 1910), epicenter of the great Kangra earthquake is shown by yellow circle. Rivers, place names and MBT (shown in red) are as per (Narula <i>et al.</i> 2000).	29
Figure 2.2	(a) Study area encompassed between latitude: 29°N to 36°N and longitude 73°E to 80°E, shown by box. MBT, MCT and the epicenter of great Kangra earthquake of 1905 shown by yellow circle. All boundaries are as per Survey of India, (2011) maps. (b) Study area shown by box with epicenter of great Kangra earthquake of 1905 at its center on Google earth map.	30
Figure 2.3	Study area divided into 196 quadrangles in the Lambert conformal conical projection. Midpoint of each was considered as a site for hazard assesment.	31
Figure 2.4	Seismicity of the study area as per MHD catalogue for the space defined by longitude: 73°E to 80°E and latitude: 29°N to 36°N, time period 1552-2012 and magnitude range $3.5 \leq M_w \leq 8.0$	40
Figure 2.5	Variation of $\sigma_\lambda$ with time interval and magnitude and lines with slope $(1/\sqrt{T})$ for testing completeness of earthquake data of the study area.	47
Figure 2.6	Frequency Magnitude Distribution (FMD) for estimation of minimum magnitude of completeness of the homogenized catalogue.	47
Figure 2.7	Nine SEISAT sheets considered for the present study, (redrawn after Narula <i>et al.</i> 2000).	50
Figure 2.8	Simplified version of the four subdivisions of the Himalayan tectonic zone which are separated by mega faults, e.g. ITSZ = Indian Suture Zone, MCT = Main Central Thrust, MBF = Main Boundary Fault and FFT = Frontal Foothill Thrust, (After Sinvhil, 2010).	51
Figure 2.9	26 tectonic units used for initial study of DSHA. Tectonic units are numbered as per table 2.12. 1. Alaknanda fault (AF); 2. Drang thrust (DT); 3. Indus Suture Zone (ISZ); 4. Jhelum fault; 5. Jwalamukhi thrust (JMT); 6. Karakoram fault (KF); 7. Kishtwar fault (KiF); 8. Mahendragarh-Dehradun fault (MHD-DDN F); 9. Mastgarh anticline (MA); 10. Main Boundary thrust (MBT); 11. MBT-A ; 12. Main	60

Central Thrust (MCT); 13. Main Frontal thrust (MFT); 14. Main Mantle thrust (MMT); 15. North Almora thrust (NAT); 16. Ramgarh thrust (RT); 17. Reasi thrust (ReT); 18. Ropor fault (RF); 19. Shyok Suture (SS); 20. South Almora thrust (SAT); 21. Sundarnagar fault (SNF); 22. Closed thrust, T1; 23. Closed thrust, T2; 24. Closed thrust, T3; 25. Closed thrust, T4; 26. Closed thrust, T5.

Figure 2.10	118 tectonic units in the study area, where abbreviations of tectonic units are as per table 2.13. AF: Alaknanda fault; Bg Co: Beng Co fault; DT: Drang thrust; ISZ: Indus Suture Zone; JF: Jhelum fault; JMT: Jwalamukhi thrust; KF: Karakoram fault; KFS: Kaurik fault System; KiF: Kishtwar fault; MA: Mastgarh anticline; MBT: Main Boundary thrust; MCT: Main Central Trust; MF: Mangla fault; MHDDDN: Mahendragarh Dehradun fault; MMT: Main Mantle thrust; NAT: North Almora thrust; ReT: Reasi thrust; SAT: Saouth Almora thrust; SNF: Sundarnagar fault; SRT: Salt Range thrust; SS: Shyok Suture; T1, T2, ..., T7: Closed thrust between MBT and MCT; Tso M F: Tso Morari fault; VT: Vaikrita thrust.	62
Figure 2.11	Seismotectonics of the study area in western Himalaya emerged by overlaying the figure 2.4 and figure 2.10.	69
Figure 2.12	Fault plane solutions of 27 earthquakes listed in table 2.16.	72
Figure 2.13	Seismicity as per MHD catalogue-2 for validation of results.	73
Figure 3.1	Major steps of Pattern Recognition (PR) technique.	76
Figure 3.2	DEM data available for portions shown in brown, from ISRO website. Features F10, F11 and F12 were extractable in these areas only.	78
Figure 3.3	(a) An example of extracted features for the great Kangra earthquake of 4 <sup>th</sup> April, 1905, $M_w = 8.0$ (MHD catalogue); (b): Elevation contours as per ISRO website within the circle around the Great Kangra earthquake of 1905, at 500 m interval. Minimum elevation is shown by green and maximum elevation is shown by red triangle. Accompanying table shows the numerical values of the extracted features, F1, F2, F3, ..., F12. These are described in section 3.4.	80
Figure 3.4 (a-h)	Feature extraction shown for different earthquakes, where <b>F2</b> : number of earthquake epicenters other than central earthquake; <b>F3</b> : number of tectonic units; <b>F4</b> : number of intersections between two tectonic units; <b>F5</b> : number of intersections between tectonic unit and river; <b>F6</b> : distance of central earthquake from nearest tectonic feature (km); <b>F7</b> : distance of central earthquake from nearest tectonic intersection (km); <b>F8</b> : length of river (km); <b>F9</b> : combination of number of earthquakes and number of tectonic features (F2+F3); <b>F10</b> : maximum elevation, $E_{max}$ (meters); <b>F11</b> : minimum elevation, $E_{min}$ (meters) and <b>F12</b> : difference in elevation ( $E_{max} - E_{min}$ ) (meters).	84



Figure 3.5 (a-o)	$R_A$ , $R_B$ and $R_0$ values and histograms for different analysis carried out for identification of susceptible areas. Classification criteria and number of features selected for each PR model is as per table 3.2.	100
Figure 3.6 (a-l)	Histograms for different analysis carried out for segmentation of longer tectonic units, classification criteria and number of earthquake epicenters in each class and number of tectonic units is as per table 3.3.	105
Figure 4.1 (a)	Steps used for training exercise for identification of seismically susceptible areas	107
Figure 4.1 (b)	Decision making exercise	108
Figure 4.2	Epicentral map of the study area, showing classification of epicenters as per classification criteria-II, i.e., Class A: $M_w \geq 5.5$ , shown in red and Class B: $4.5 \leq M_w \leq 5.4$ , shown in blue.	110
Figure 4.3	Plot of seismic scores, $R_A$ , $R_B$ and $R_0$ for the training exercise. Red represents Class A and blue represents Class B.	113
Figure 4.4	Epicentral map of the study area, after discriminant analysis. Epicenters in purple with question mark show 42 misclassified events, all from Class B. List of these 42 epicenters is given in table 4.2.	114
Figure 4.5	The study area is divided into a grid of $0.5^\circ$ by $0.5^\circ$ , which resulted in 196 quadrangles. Midpoint of every quadrangle was considered as a site. Circle represents an area of 25 km radius drawn around each site for extraction of features.	115
Figure 4.6	Eleven features F2-F12, extracted from within a circle of radius 25 km drawn around site # 105, Lat: $32.32^\circ\text{N}$ , Long: $76.25^\circ\text{E}$ . This is the nearest site to the great Kangra earthquake of 1905. Yellow represents the epicenter of 1905 Kangra earthquake.	115
Figure 4.7	Plot of seismic scores, $R_A$ , $R_B$ and $R_0$ for sites for decision making exercise. Red represents Class A, blue represents Class B' and green represents Class C that were considered neither in Class A' nor Class B'.	116
Figure 4.8	196 sites divided into one of the three classes Class A, Class B' and Class C, identified after the training exercise and decision making exercise.	117
Figure 4.9	Three types of susceptible areas. Red represents 'area A' most susceptible area; Yellow represents area B': Moderately susceptible area; and green represents area C: Least susceptible area. This is obtained after making envelopes and smoothing the results of figure 4.8. Map also shows districts as per Survey of India, (2011).	118

Figure 4.10	Seismicity as per MHD catalogue-2 superimposed on susceptible areas for validation of results	122
Figure 4.11	Susceptible area map (as per figure 4.8) superimposed on the map of potential knots of $M_w \geq 6.5$ nodes of Bhatia <i>et al.</i> ( 1992)	123
Figure 4.12	Susceptible area map (as per figure 4.8) superimposed on the map of potential knots of $M_w \geq 7.0$ nodes of Bhatia <i>et al.</i> ( 1992).	124
Figure 5.1 (a)	Segmentation of Karakoram fault (KF), Drang thrust (DT), Main Mantle Thrust (MMT), Shyok Suture (SS), Main Boundary Thrust (MBT) and Main Central Thrust (MCT) into equal segments.	129
Figure 5.1 (b)	Seismicity of the study area as per MHD catalogue superimposed on the equal segments of MBT and MCT.	130
Figure 5.2	Classification of epicenters of MHD catalogue as per classification criteria-III. Purple belt indicates area 25 km on either side of MBT, epicenters within this belt are classified as Class $S_{B1}$ and Class $S_{B2}$ defines epicenters outside this belt. Legend for seismicity and tectonics is as per figure 2.11.	132
Figure 5.3	Seismic scores for the 1172 epicenters in the study area, model PR26. Blue represents Class $S_{B1}$ and red represents Class $S_{B2}$ epicenters. $R_{SB1}$ , $R_{SB2}$ and $R_0$ , are also plotted to show the separation between the two classes of epicenters. $R_{SB1} = -0.225$ , $R_{SB2} = -35.768$ and $R_0 = -17.997$ .	133
Figure 5.4	X shows cross over epicenters after discriminant analysis, and are significant while segmentation.	134
Figure 5.5	Figure shows MBT in red and tectonic units transverse to it which were used for segmentation. These are Kishtwar fault (KiF), Ropor fault (RF), Sundarnagar fault (SNF) and lineaments L22, L24 and L26.	136
Figure 5.6	Six segments of MBT in western Himalaya.	138
Figure 5.7	Classification of epicenters of MHD catalogue as per classification criteria-IV. Green belt indicates area 25 km on either side of MCT, epicenters within this belt are classified as Class $S_{C1}$ and Class $S_{C2}$ defines epicenters outside this belt. Legend for seismicity and tectonics is as per figure 2.11.	140
Figure 5.8	Seismic scores for the 1172 epicenters in the study area. Blue represents Class $S_{C1}$ and red represents Class $S_{C2}$ epicenters. $R_{SC1}$ , $R_{SC2}$ and $R_0$ , are also plotted to show the separation between the two classes of epicenters. $R_{SC1} = -0.027$ , $R_{SC2} = -8.748$ and $R_0 = -4.387$ .	141
Figure 5.9	X shows cross over epicenters after discriminant analysis, and are significant while segmentation.	141

Figure 5.10	Figure shows MCT in black and tectonic units transverse to it which were used for segmentation. These are Kishtwar fault (KiF), Sundarnagar fault (SNF), Kaurik fault system (KFS) and lineaments L26.	143
Figure 5.11	Five segments of MCT in western Himalaya.	144
Figure 5.12	Recent epicenters from MHD catalogue-2, plotted on segments of MBT and MCT. These were used for validation of seismicity of these segments.	145
Figure 6.1	Major steps in Deterministic Seismic Hazard Assessment (DSHA) approach (after Reiter, 1990)	147
Figure 6.2	Various measures of distance used in strong-ground predictive relationships (After Shakal and Bernreuter, 1981).	147
Figure 6.3 (a)	Contour map for PGA as per DSHA-1, at contour interval 0.01 g.	157
Figure 6.3 (b)	Hazard map for PGA as per DSHA-1. Map also shows state boundaries as per Survey of India, 2011, MBT and MCT.	158
Figure 6.4	(a) Site characteristics of strong ground motion accelerograph stations, redrawn after Mittal <i>et al.</i> , 2012. Site class A, B and C are defined in section 6.3 (b) Site class considered for grid points in the present study.	164
Figure 6.5	Fault model prepared for calculation of Joyner and Boore $R_{JB}$ distance, as shown in figure 6.6. Box showing various distances used for computations. NSD: non seismicogenic depth.	165
Figure 6.6 (a-d)	Illustration showing $R_{JB}$ considered for different fault types.	165
Figure 6.7 (a)	Contour map for PGA as per DSHA-2 at contour interval 0.01 g. Box shows contour intervals around the highest PGA in the study area.	176
Figure 6.7 (b)	Hazard map as per DSHA-2. State boundaries are as per Survey of India (2011). This map is referred to as DSHA hazard map.	177
Figure 6.8	Comparison of PGA computed in the present study, shown in figure 6.7(a), with the PGA recorded at near field stations for several recent earthquakes. Recording station is shown by colored triangle, color of station is as per site classification given in figure 6.4(a), magnitude of epicenter is as per seismicity map (figure 2.4), and site at which maximum PGA obtained in this study is shown by hollow triangle. (a) Dharamshala earthquake of 26th April, 1986, $M_w = 5.8$ , (b) Uttarkashi earthquake of 20 <sup>th</sup> October, 1991, $M_w = 6.8$ , (c) Chamoli earthquake of 28 <sup>th</sup> March 1999, $M_w = 6.7$	182
Figure 6.9	Hazard map as shown in figure 6.7(b) superimposed on seismic zoning map of India (BIS, 2002) as shown in figure 1.1.	184

Figure 7.1	Major steps of probabilistic seismic hazard assessment approach (Reiter, 1990)	188
Figure 7.2	a. Seismogenic source zones delineated in the study area, where SSZ1: Kangra source zone; SSZ2: Uttarakhand source zone; SSZ3: Kashmir syntaxis source zone; SSZ4: Kaurik source zone; SSZ5: Kargil Laddakh source zone; SSZ6: Western Tibet source zone; SSZ7: Karakoram source zone; SSZ8: Jhelum source zone; SSZ9: Indo Gangetic source zone. b. Seismicity as per figure 2.4, superposed on seismogenic source zones. c. Tectonics as per figure 2.10, superposed on seismogenic source zones. d. Districts of Himachal Pradesh and Uttarakhand as per Survey of India, (2011) superimposed on SSZ map.	194
Figure 7.3	Epicenters of MHD catalogue-2 for validation of results plotted on SSZ map.	195
Figure 7.4	Frequency magnitude distribution plotted for estimation of seismic hazard parameters $M_c$ , 'a' and 'b' value for all nine SSZ.	198
Figure 7.5	Hazard maps as per PSHA-1 for (a) 10% probability of exceedance in 50 years for a return period of 475 years, (b) 2% probability of exceedance in 50 years for a return period of 2,475 years	205
Figure 7.6	Hazard maps as per PSHA-2 for; (a) 10% probability of exceedance in 50 years for a return period of 475 years, (b) 2% probability of exceedance in 50 years for a return period of 2,475 years.	206
Figure 7.7	Comparison of PGA computed in the present study, with the PGA recorded at near field stations for several recent earthquakes. Recording station is shown by colored triangle, color of station is as per site classification given in figure 6.4, magnitude of epicenter is as per legend of seismicity map (figure 2.4), and site at which maximum PGA obtained in this study is shown by hollow triangle. (a) Dharamshala earthquake of 26 <sup>th</sup> April, 1986, $M_w = 5.8$ , (b) Uttarkashi earthquake of 20 <sup>th</sup> October, 1991, $M_w = 6.8$ , (c) Chamoli earthquake of 28 <sup>th</sup> March 1999, $M_w = 6.7$	209
Figure 8.1	Districts of Himachal Pradesh, drawn after Survey of India (2011), and rivers (redrawn after SEISAT) superimposed on Kangra SSZ.	214
Figure 8.2	Seismically susceptible areas, as per figure 4.9, superimposed on seismogenic source zones, as per figure 7.2. (a) for the entire study area. Common area of Kangra SSZ and largest area of susceptible areas A is shown by box. This area is called truncated area, henceforth.	215

Figure 8.3	Seismicity as per MHD catalogue-2 plotted on the truncated area.	215
Figure 8.4	PGA contours, as per figure 6.7(a), superimposed on the truncated area.	215
Figure 8.5	Isoseismals of four destructive earthquakes plotted on the truncated area	217
	(a) The great Kangra earthquake of 4 <sup>th</sup> April, 1905. Isoseismals are on RF scale (Redrawn after Middlemiss, 1910).	
	(b) Dharamshala earthquake of 26 <sup>th</sup> April, 1986. Isoseismals are on MMI scale (Redrawn after SEISAT, 2010).	
	(c) Chamba earthquake of 22 <sup>nd</sup> June, 1945. Isoseismals are on MM scale (Redrawn after SEISAT, 2010).	
	(d) Chamba earthquake of 24 <sup>th</sup> March, 1995. Isoseismals are on MSK scale (Redrawn after SEISAT, 2010).	



## LIST OF TABLES

<b>Table no.</b>	<b>Caption</b>	<b>Page</b>
Table 1.1	Applications of pattern recognition (PR) in different fields.	3
Table 1.2	Pattern Recognition (PR) studies for identification of earthquake prone areas.	6
Table 1.3	Maximum magnitude, Peak acceleration, Intensity (MM) and perceived damage implications assigned to different seismic zones as per BIS (BIS: 1893:2002).	23
Table 2.1	Salient features of the great Kangra earthquake of 4 <sup>th</sup> April, 1905.	28
Table 2.2	Salient features of various catalogues studied for the study area between latitude: 23° N-37°N; longitude: 72° E- 87°E.	35
Table 2.3	Salient features of merged earthquake catalogues for the study area between latitude: 29°N -36°N and longitude 73°E - 80°E.	36
Table 2.4	Time and space windows for identification of aftershocks for an earthquake of a given magnitude M, where L is estimated distance interval and T is estimated time interval, (after Gardener and Knopoff, 1974).	39
Table 2.5	Reasenberg parameters (after Reasenberg, 1985) for declustering of an earthquake catalogue. $\tau_{\min}$ (days) is minimum value of look-ahead time for building clusters when the event is not clustered; $\tau_{\max}$ (days) is maximum value of look ahead time for building clusters; P1 is the probability of detecting the next clustered event used to compute the look ahead time; $x_k$ is increase in the lower cut-off magnitude during clusters; $x_{\text{meff}} = x_{\text{meff}} + x_k M$ , (where M is the magnitude of the largest earthquake) is effective lower magnitude cut off for catalogue; and $r_{\text{fact}}$ is number of crack radii surrounding each earthquake within new events considered to be part of the cluster.	39
Table 2.6	A page from MHD catalogue, arranged chronologically. <b>Y</b> : Year; <b>M</b> : Month; <b>D</b> : Day; <b>H</b> : Hour; <b>Mn</b> : Min; <b>S</b> : seconds; <b>Long</b> : longitude (°E) ; <b>lat</b> : latitude (°N); <b>Dep</b> : Depth (km); <b>Source</b> : catalogue source; <b>Remarks</b> : A: description in text, B: description available in papers, C: fault plain solutions available.	41
Table 2.7	Number of events in different magnitude ranges for MHD earthquake catalogue.	42
Table 2.8	List of earthquakes with $M_w \geq 6.0$ , in the environs of Main Boundary Thrust (MBT) and Main Central Thrust (MCT), chronologically arranged. Cluster 1: Srinagar Baramula region (6 earthquakes), Cluster 2: West of Kishtwar fault (2 earthquakes), Cluster 3: Chamba region (2 earthquakes), Cluster 4: Bageshwar Region	43

(2 earthquakes). \* indicates earthquake considered for hazard assessment in DSHA Chapter 6.

Table 2.9	Rate of earthquake occurrence of different magnitude ranges (N/T) and time intervals for computing time completeness of MHD catalogue, where N is the cumulative number of earthquakes in time interval T.	44
Table 2.10	Standard deviation, $\sigma$ , of the estimates of mean recurrence rate per year, used in equation, $\sigma_\lambda = (\lambda/T)^{1/2}$ , where $\lambda$ is the mean rate per unit time interval, N is the cumulative number of earthquakes in time interval T.	46
Table 2.11	Salient features of 9 SEISAT sheets used in the present study. These include SEISAT sheet number, coordinates covered in each sheet, geographical area covered, important localities, important physiographic features and important tectonic units.	52
Table 2.12	List of 26 tectonic units in the study area, (in alphabetical order). Only those major named units were considered which were prominent or close to either the MBT or the MCT. This list includes 5 closed unnamed thrusts, which are between the MBT and MCT. * indicates ISZ, which consists of three closely spaced parallel features, ** indicates MBT and its closely spaced parallel feature. This data was used for a preliminary estimation of DSHA.	59
Table 2.13	List of 118 tectonic units in the study area as per SEISAT sheets.	61
Table 2.14	Convergence between different notations used for fault type, as per SEISAT, Wells and Coppersmith, (1994) formulation (W&C) and this study. Relations (equations 2.4-2.6) for computing maximum magnitude are different for each type of fault and depend on rupture length.	64
Table 2.15	List of 118 tectonic units, its length, (computed from ARCGIS), type of faulting, (strike slip: SS, thrust: T, Gravity fault: N, fault: F, Unspecified: U), computed maximum magnitude $M_w$ and down dip rupture width RW, using Wells and Coppersmith (1994) formulation. * longest sliver of the three parallel portions of ISZ was retained.	65
Table 2.16	Fault plane solutions of 27 earthquakes from MHD catalogue	71
Table 2.17	Salient features of earthquake catalogues used for compilation of MHD catalogue-2 for the study area.	72
Table 2.18	Magnitude wise breakup of earthquakes from MHD catalogue-2 for validation of results.	73
Table 3.1	Salient features of model PR1, classification criteria I was considered i.e. Class I: epicenters having magnitude $M_w \geq 6.0$ , which contained 45 epicenters and Class II: epicenters having $4.5 \leq M_w \leq 5.9$ , which contained 492 epicenters. Features F2-F12	89



were extracted for 537 epicenters of  $4.5 \leq M_w \leq 8$ . Vector mean of Class I, Vector mean of Class II, Vector of mean differences of both classes, coefficients of discriminant function i.e.  $\lambda$  values and percentage contribution computed for each feature are shown in the table.

Table 3.2	Percentage of classification of either Class by varying classification criteria and number of features, step wise exclusion of one feature out of 11 features are shown from row number 5 to 15. The combination of classification criteria and number of features at S.No. 4, model PR4, gives the best results, and model PR15 gives second best result.	90
Table 3.3	Salient features of different PR models. $\lambda$ values and percentage contribution of each feature by varying seismicity and number of tectonic units. Classification was done in terms of distance from either MBT of MCT. <b>F1</b> : magnitude of central earthquake; <b>F2</b> : Number of earthquake epicenters other than central earthquake; <b>F3</b> : Number of tectonic units; <b>F4</b> : Number of intersections between two tectonic units.	102
Table 4.1	Salient features of model PR4, vector mean of Class A, vector mean of Class B, Vector of mean differences of both classes, discriminant function, i.e. $\lambda$ values and percentage contribution of each feature, for model PR4.	111
Table 4.2	List of 42 epicenters of Class B which are misclassified as Class A after discriminant analysis.	112
Table 4.3	Magnitude wise break up of 80 recent earthquakes from MHD catalogue-2 for validation of results of susceptible areas "A", "B" and "C".	120
Table 4.4	States and districts identified in Areas "A", "B" and "C".	121
Table 5.1	List of tectonic units, longer than 294 km that were segmented into equal portions, shown in figure 5.1.	128
Table 5.2	Salient features of model PR26: classification criteria-III was considered, i.e., Class $S_{B1}$ contained 164 epicenters which are within a 25 km belt on either side of MBT, and Class $S_{B2}$ contained 1008 epicenters outside this belt. Features used were F1-F4. Vector means of Classes $S_{B1}$ , $S_{B2}$ , difference of both Classes, discriminant function, i.e., $\lambda$ values and percentage contribution computed for each feature is shown in the table.	133
Table 5.3	Initial four segments of MBT	135
Table 5.4	Six segments of MBT, from west to east, its given name, length (L), tectonic units demarcating the segment and places that define its extent and coordinates.	137
Table 5.5	Salient features of model PR27: classification criteria-IV was	142

considered i.e. Class  $S_{C1}$  contained 199 epicenters which are within a belt defined by a distance of 25 km on either side of MCT, and Class  $S_{C2}$  contained epicenters 973 outside this belt. Features used were F1-F4. Vector means of class  $S_{C1}$ ,  $S_{C2}$ , difference of both classes, discriminant function i.e.  $\lambda$  values and percentage contribution computed for each feature is shown in the table.

Table 5.6	Five segments of MCT, from west to east, its given name, length (L), tectonic units demarcating the segment and places that define its extent and coordinates.	142
Table 6.1	Salient features of 40 tectonic units considered in DSHA-1, (in alphabetical order) including segments of the larger units are shown in this table. Column 2: Tectonic unit, column 3: its length, column 4: maximum earthquake, $M_w$ , assigned to each tectonic unit, column 5 and 6: epicenter (Longitude °E, latitude °N), column 7: depth (km) and column 8: descriptive identifier of earthquake.	150
Table 6.2	Table shows computed PGA for 196 sites as per DSHA-1 study. Column 1: site number, column 2: tectonic unit nearest to site, column 3: epicentral distance, column 4: PGA (g) as per Abrahamson and Litehiser (1989) formulation. Length and maximum magnitude are given in table 6.1.	151
Table 6.3	Salient features of 127 tectonic units, its type (F: Fault; SS: Strike Slip; GF: Gravity Fault, as per SEISAT), surface length, (computed from ARCGIS), computed $M_w$ (Wells and Coppersmith, 1994). * longest sliver of the three was retained. This tectonic data was used for DSHA-2 study.	161
Table 6.4	Calculation of PGA for DSHA-2, site wise. Column 1: site number; 2: Nearest tectonic unit to site; 3: Fault type (from SIESAT); 4: length of tectonic unit in km, length from ArcGIS-9.3; 5: Estimated $M_w$ W&C94; 6: Calculated Rupture Width (RW), from W&C94; 7: Dip ( $\delta$ ) (Assumed, $15^\circ$ for thrust/reverse sources, $50^\circ$ for normal and $90^\circ$ for strike slip sources (Ni and Barazangi, 1984)); 8: surface projection of fault rupture km ( $RW \cdot \cos\delta$ ); 9: Epicentral Distance; 10: Joyner and Boore Distance ( $R_{jb}$ ); 11: Site classification (Mittal et al., 2012); 12: $V_{s,30}$ ; 13: Focal Plane Mechanism (as per BA08: -1: Unknown, 0: Strike Slip, 1: Normal, 2: Thrust); 14: PGA (g) as per BA08	168
Table 6.5	PGA values computed in this study compared with observed PGA, from DSHA hazard map for Dharamshala earthquake, Uttarkashi earthquake and Chamoli earthquake. Computed Maximum magnitude, causative fault, fault length and epicentral distance for the nearest site are given in table 6.4. ( <sup>1</sup> Chandrasekaran, 1988; <sup>2</sup> Chandrasekaran and Das, 1991, 1992; <sup>3</sup> DEQ report, 2000).	180

Table 6.6	PGA values computed by different authors compared with this study	185
Table 7.1	Seismicity and tectonic distribution within each seismogenic source zone are shown in this table. This includes area (km <sup>2</sup> ), magnitude wise distribution of earthquakes, total number of earthquakes and prominent tectonic units in each SSZ.	193
Table 7.2	Magnitude wise break up of recent epicenters from MHD catalogue-2 for validation of seismic zones and return periods in each SSZ.	195
Table 7.3	Salient features of maximum observed earthquake, ( $M_{\max,obs}$ ), in each SSZ as per MHD catalogue. YYYY: Year, MM: month, DD: Day, Long: Longitude, Lat: Latitude, D: Depth, $M_{\max,obs}$ : Maximum observed magnitude, district / place where it was observed, and its nearest prominent tectonic unit.	197
Table 7.4	Seismic hazard parameters computed for each seismogenic source zone. $M_c$ : magnitude of completeness, $a$ value, $b$ value and error in $b$ value, $\delta b$ , mean annual rate of exceedance, $\lambda_m$ , and maximum magnitude computed with standard deviation, $M_{\max,cal} \pm s.d.$ , range of return period for earthquakes of magnitude 5.5, 6, 7 and 8.	199
Table 7.5	Temporal range in years computed for $M_{\max,obs}$ and other large earthquakes observed in the same SSZ for each SSZ, and predictive implications of the same. T1: Temporal range for $M_{\max,obs}$ , T2: Temporal range for other large earthquakes observed in the same SSZ, Implications: $T_{overdue}$ : overdue for the relevant $M_w$ .	201
Table 7.6	Range of PGA values for 10% and 2% probability of exceedance in 50 years, calculated using different attenuation relationships. AL89: Abrahamson and Litehiser (1989), BA08: Boore and Atkinson (2008), CY08: Chiou and Youngs (2008). BA08+AL89 and BA08+CY08: PGA value computed by subjecting attenuation relations to logic tree.	205
Table 7.7	Comparison of highest PGA values obtained in PSHA-1 and PSHA-2, for 10% and 2% probabilities of exceedance in 50 years.	205
Table 7.8	PGA values computed in this study compared with observed PGA, for Dharamshala earthquake of 1986, Uttarkashi earthquake of 1991 and Chamoli earthquake of 1999. <sup>1</sup> Chandrasekaran, 1988 <sup>2</sup> Chandrasekaran and Das, 1991; 1992, <sup>3</sup> DEQ report, 2000.	209
Table 7.9	PGA values for 10% probability of exceedance computed by different authors compared with this study.	210

Table 8.1 District wise and tehsil wise breakup of truncated area according to PGA are shown in this table. 218

**A:** Intensities of the great Kangra earthquake of 4<sup>th</sup> April, 1905 on RF scale.

**B:** Intensities of Dharamshala earthquake of 26<sup>th</sup> April, 1986 on MMI scale.

**C:** Intensities of Chamba earthquake of 22<sup>nd</sup> June, 1945 on MM scale.

**D:** Intensities of Chamba earthquake of 24<sup>th</sup> March, 1995 on MSK scale.

## LIST OF ABBREVIATIONS

A	Acceleration
AF	Alaknanda fault
AL89	Abrahamson and Litehiser (1989) attenuation relationship
ANN	Artificial neural network
Area A''	Identified area A''
Area B''	Identified Susceptible area B''
Area C''	Identified Susceptible area C''
BA08	Boore and Atkinson (2008) GMPE
BIS	Bureau of Indian Standards
Class A	Class of epicenters used in identification of susceptible areas, $M_w \geq 5.5$
Class A'	Class of sites after classification in identification of susceptible areas, $M_w \geq 5.5$
Class B	Class of epicenters used in identification of susceptible areas , $4.6 \leq M_w \leq 5.4$
Class B'	Class of sites after classification in identification of susceptible areas, $4.6 \leq M_w \leq 5.4$
Class C''	Class of sites after classification in identification of susceptible areas, neither in Class A' nor in class B'
CMT	Centroid Moment Tensor
CY08	Chiou and Youngs (2008) GMPE
DEM	Digital Elevation Model
DSHA	Deterministic Seismic Hazard Assessment
DT	Drang Thrust
EMR	Entire magnitude range
ESRI	Environmental Systems Research Institute
F1	Magnitude of central earthquake
F10	Mzximum elevation
F11	Minimum elevation
F12	Difference in elevation (Max. elevation- min elevation)
F2	Number of other earthquake epicentres
F3	Number of tectonic units
F4	Number of tectonic intersections

F5	Distance of central earthquake from nearest tectonic feature
F6	Distance of central earthquake from nearest tectonic intersection
F7	Length of river
F8	Number of tectonic river intersections
F9	Combination of number of earthquakes and number of tectonic features
GIS	Geographic Information System
GMPE	Ground Motion Prediction Equation
GOR	General Orthogonal Relation
GSHAP	Global Seismic Hazard Program
GSI	Geological Survey of India
HP	Himachal Pradesh
IMD	Indian Meteorological Department
ISC	International Seismological Centre
ISRO	Indian Space Research Organization
ISZ	Indus Suture Zone
J&K	Jammu and Kashmir
JF	Jhelum fault
JMT	Jwalamukhi thrust
KFS	Kaurik Fault System
KiF	Kishtwar fault
MA	Mastgarh Anticline
Matlab/MATLAB	Matrix Laboratory
MBT	Main Boundary thrust
MCT	Main Central thrust
ME	Maximum Earthquake
MF	Mangla fault
MFT	Main Frontal thrust
MHD catalogue	Merged Homogenized De-clustered catalogue
MHD-DDN F	Mahendragarh Dehradun fault
MKT	Main Karakoram thrust
MMI	Modified Mercalli intensity scale
MMT	Main Mantle thrust
MSK	Medvedev- Sponheuer- Karnik intensity scale

NAT	North Almora thrust
NDMA	National Disaster Management Authority
NEIC	National Earthquake Information Center
PGA	Peak Ground Acceleration
PGV	Peak Ground Velocity
PR	Pattern Recognition
PSHA	Probabilistic Seismic Hazard Assessment
ReT	Reasi Thrust
RF	Rossi Forel intensity scale
RT	Ramgarh thrust
RW	Down dip rupture width
SAT	South Almora thrust
S <sub>B1</sub>	Classification of epicenters with respect to MBT, closer to MBT
S <sub>B2</sub>	Classification of epicenters with respect to MBT, far from MBT
S <sub>C1</sub>	Classification of epicenters with respect to MCT, closer to MCT
S <sub>C2</sub>	Classification of epicenters with respect to MCT, far from MCT
sec	seconds
Site class A	Site classification as per $V_{s30}$ , Hard rock
Site Class B	Site classification as per $V_{s30}$ , Firm Rock
Site Class C	Site classification as per $V_{s30}$ , Soft Rock
SRL	Surface rupture length
TIN	Triangular Irregular Network
UK	Uttarakhand
USGS	United States Geological Survey
VT	Vaikrita thrust





## LIST OF SYMBOLS

$E_{\max}$	Maximum elevation
$E_{\min}$	Minimum elevation
$M_L$	Richter magnitude, Local magnitude
$M_{\max,cal}$	Calculated maximum magnitude
$M_{\max,obs}$	Observed maximum magnitude
$M_s$	Surface wave Magnitude
$M_w$	Moment magnitude
$R_0$	Discriminant index (midpoint between $R_A$ and $R_B$ )
$R_A$	Multivariate mean of class A
$R_B$	Multivariate mean of class B
$R_{jb}$	Joyner Boore Distance
$R_{rup}$	Distance to rupture of fault, site
$Y$	Peak Ground Acceleration
$\delta$	Dip angle
$\Delta E$	Difference in elevation
$\lambda_1, \lambda_2, \dots, \lambda_{12}$	Coefficients of discriminant function
$\lambda$	Mean rate per unit time interval and is given as : $\lambda = \left(\frac{1}{2}\right) \sum_{i=1}^n k_i, k_i,$ $k_2..k_n$ are the number of earthquake per unit time interval.
$\lambda_m$	Mean annual rate of exceedance

# CHAPTER 1

## INTRODUCTION

---

### 1.1 Introduction

Earthquakes cause tremendous loss of life and devastation of the built environment. Due to ongoing continent-continent collision between the Indian plate and the Eurasian plate, major seismic activity in India is concentrated along seismo-tectonically active and geologically young Himalayan arc. The Himalayan arc is a part of Alpine-Himalayan seismic belt, which has experienced four great earthquakes within a short temporal range between the years 1897 and 1950 i.e. within 53 years. One of these great earthquakes is the great Kangra earthquake of 4<sup>th</sup> April, 1905. The epicenter of this great earthquake was in the Himachal Pradesh (HP) and in the vicinity of the Main Boundary Thrust (MBT), in western Himalaya. Besides great earthquakes, the region has also experienced several moderate to large-sized earthquakes. However, it is pertinent to note that after 1950, no great earthquake has occurred within the Himalayan arc. Phenomenal damage to the built environment and ground was observed in the meizo-seismal and adjoining areas of this great earthquake. Since, the seismicity in the region is highly variable and the region is also going through a phase of techno-economic development, therefore, it is pertinent to identify seismically susceptible areas and to assess seismic hazard in view of the available seismicity and tectonic database.

Western Himalayas comprises of the states of, Himachal Pradesh (HP), Jammu & Kashmir (J&K), Uttarakhand (UK), Punjab, Haryana, union territory of Chandigarh and Uttar Pradesh. In western Himalaya different areas exhibit different patterns of seismicity, i.e., some parts of the Himalayan arc show dense seismicity, and other parts exhibit sparse seismicity. Also, this region is infested with complex tectonics. Therefore, the following section deals with the literature review of the studies carried out for identification of earthquake prone areas using pattern recognition.

## 1.2 Literature Review

Following section deals applications of pattern recognition (PR) techniques in non-seismological and seismological field. It then specifically reviews PR technique used for identification of earthquake prone areas. Literature review of segmentation of long tectonic units, Deterministic seismic hazard assessment and probabilistic seismic hazard assessment is also presented here.

### 1.2.1 Review of pattern recognition

Pattern recognition (PR) is the study which aims to recognize objects or patterns into different classes based either on *a priori* knowledge extracted from the training samples (Robbert, 1992; Aguilar, 2004). Pattern recognition has numerous applications in both non-seismological and seismological fields. Following shows the applications in non-seismological fields. It has applications in medical image processing such as abnormality detection (Chu *et al.* 1976; Chawla *et al.* 2008). In image processing it has been used for segmentation, texture analysis and computer vision (Gonzalez, 2008); automatic cancer detection (Petricoin and Liotta, 2004); automatic analysis of MRI, X-ray CT scan and ultrasound images (Bezdek *et al.* 1993; Zhang and Chen, 2004; Hofmann *et al.* 2008; Zhu *et al.* 2008; Srivastava, 2009; Shrimali *et al.* 2009) and blood cells analysis (Shitong *et al.* 2006; Shin and Markey, 2006). Pattern recognition is used in video surveillance systems such as military security (Miller *et al.* 1998); law enforcement (Green, 1999); human activity detection (Ali and Aggarwal, 2001); smart video data mining (Matsuo *et al.* 2003; Zhu *et al.* 2005); detecting unusual activity in video (Zhong *et al.* 2004); event detection (Smith *et al.* 2005) and public and commercial security (Srinivasan *et al.* 2009). In the field of document analysis and recognition the applications are for optical character recognition (Singh *et al.* 2011a, 2011b) and vehicle number plate recognition (Chang *et al.* 2013). In bioinformatics area it is useful in microarray data analysis (Valafar, 2002) and sequence analysis (Liew *et al.* 2005). In biometric recognition, it is used for person identification (Delac and Grgic, 2004; Jain *et al.* 2004; Jain, 2007). In data mining, it has applications in searching meaningful patterns, data warehousing, business analysis (Wu *et al.* 2008). In remote sensing, pattern recognition is used in boundary detection, region segmentation, forecasting crop yield (Chen and Ho, 2008). In multi-media database retrieval, the uses of pattern recognition are in internet search, event detection, and video /

audio clip retrieval from database (Antani *et al.* 2002). It is also used in industrial automation: printed circuit board inspection (Fukuda and Shibata, 1992), in speech recognition and analysis: telephone directory enquiry without assistance of operator (Itakura and Saito, 1970; Gonzalez, 2008). In food sciences, the applications are, wine analysis, edible oils analysis, honey analysis, dairy foods analysis, meat analysis, alcoholic beverages, orange juice, milk, tonic, food additives, beers (Berrueta *et al.* 2007). In communications, the uses are in data compression, speech recognition, telephone (Rabiner *et al.* 1979, 2004; Andras, 2005; Ustundag, 2008). In robotics, automation, measuring and processing 2-D and 3-D data, diffusion of bombs, coal mining, wars, dangerous situations (Fukui, 1981; Courtney, 1984; Nitzan, 1988; Nagy, 2005; Alfehaid, 2012) are some applications. In automatic target recognition (ATR), it is used for image processing and image understanding (Rosenfield, 1976). These applications are listed in table 1.1.

**Table 1.1:** Applications of Pattern Recognition (PR) in different fields.

S. No.	Field	Applications	Input	Algorithm Used
1.	Seismology	Discrimination Between Earthquakes and Nuclear Detonations; Earthquake and Tsunami Prediction; Hazard Analysis; Oil Explorations; Seismic Risk	Seismicity; Tectonics; Seismograms ; Seismic Signals	CORA-3; Discriminant Analysis Artificial Neural Networks (ANN)
2.	Disaster Management	Natural Disaster Management: Tropical Cyclones; Flood; Drought; Land Sliding; Tsunami	Quantity; Measures; Numeric Readings	Support Vector Machines; Neural Network
3.	Video Surveillance	Human Activity Detection; Law Enforcement; Military Security; Detecting Unusual Activity in Video; Event Detection; Public and Commercial Security; Smart Video Data Mining	Video Clip	Support Vector Machines; Hidden Morkov Models; k-Nearest Neighbor; Neural Network; Baysian Model
4.	Medical Image Processing	Cancer Detection; Abnormality Detection; Diseases Detection and Diagnosis; Blood Cells Analysis; Automatic Analysis of MRI; X-Ray; CT Scan; and Ultrasound Images	Image Features	Support Vector Machines; Hidden Morkov Models; k-Nearest Neighbor; Neural Network; Baysian Model
5.	Document Analysis and Recognition	Vehicle Number Plate Recognition; Optical Character Recognition; Video Surveillance	Text Image	Support Vector Machines; Hidden Morkov Models; k-Nearest Neighbor;

<b>S. No.</b>	<b>Field</b>	<b>Applications</b>	<b>Input</b>	<b>Algorithm Used</b>
				Neural Network; Bayesian; Naïve; Decision Trees; Logistic Regression; Linear Regression; Locally Weighted Regression
6.	Bioinformatics	Sequence Analysis; Microarray Data Analysis	DNA/ Protein Sequence	Support Vector Machines; k-Nearest Neighbor; Neural Network
7.	Biometric Recognition	Personal Identification	Face; Iris; Finger Print	Support Vector Machines; Hidden Markov Models; K-Nearest Neighbor; Neural Network; Bayesian; Naïve; Decision Trees
8.	Data Mining	Searching for Meaningful Patterns; Data Warehousing; Business Analysis	Points in Multi-Dimensional Space	k-Means Algorithm; Support Vector Machines;
9.	Remote Sensing	Boundary Detection; Region Segmentation; Forecasting Crop Yield	Multi-Spectral Image	Support Vector Machines; Hidden Markov Models; k-Nearest Neighbor; Neural Network
10.	Multi-Media Database Retrieval	Internet Search; Event Detection; Video/ Audio Clip Retrieval From Database	Video/ Audio Clip	Support Vector Machines; Hidden Markov Models; k-Nearest Neighbor; Neural Network
11.	Automation in Industries	PCB Inspection	Intensity or Range Image	Support Vector Machines; Neural Network
12.	Speech Recognition and Analysis	Telephone Directory Enquiry Without Assistance of Operator	Speech Waveform	Support Vector Machines; Hidden Markov Models; k-Nearest Neighbor; Neural Network; Bayesian; Naïve; Decision Trees
13.	Food Sciences	Wine Analysis; Edible Oils Analysis; Honey Analysis; Dairy Foods Analysis; Meat Analysis; Alcoholic Beverages; Orange Juice; Milk; Tonic; Food Additives; Beers	Food Item Features	Support Vector Machines; Neural Network
14.	Communications	Data Compression; Speech Recognition; Telephone	Signal Features	Support Vector Machines; Neural Network
15.	Robotics	Automation; Measuring and Processing 2-D and 3-D Data; Diffusion of Bombs; Coal Mining; Wars; Dangerous Situations	2D and 3D Feature Information	Support Vector Machines; k-Nearest Neighbor; Neural Network

S. No.	Field	Applications	Input	Algorithm Used
16.	Automatic Target Recognition (ATR)	Image Processing and Image Understanding	Sequence of Images	Support Vector Machines; k-Nearest Neighbor; Neural Network
17.	Document Classification	Internet Search	Text Document	Support Vector Machines; Neural Network

PR has applications in different fields of seismology, for example, discrimination between earthquakes and explosions (Davies, 1971; Gir *et al.* 1977, 1978; Gir and Gir, 1979, 1981; Gir and Chaudhary, 1979; Kebeasy *et al.* 1998; Scarpetta *et al.* 2005; Walter *et al.* 2007; Sayed and Hasib, 2009, and Esteban *et al.* 2010). It has applications in the fields of seismic interpretation for oil exploration (Huang and Fu, 1987; Chen and Fu, 1987; Aminzadeh *et al.* 1984, 1987, 2005; Kaman *et al.* 1987; Sinvhal *et al.* 1979; Sinvhal and Khattri, 1983; Sinvhal *et al.* 1984; Sinvhal and Sinvhal, 1992; Sinvhal, 2012a). Some other applications are tsunami prediction (Shah *et al.* 2011; Jain *et al.* 2011), seismic risk assessment (Gupta and Sinvhal, 2010) and hazard analysis (Dong *et al.* 1984, 1990). In disaster management, the applications are natural disaster management: tropical cyclones, flood, drought, land sliding, Tsunami (Faulkner, 2001; Göbel *et al.* 2005). It has its applications in determining earthquake prone areas in different regions of the world which are discussed in following section.

The earliest known research paper in identification of earthquake prone areas harks back to 1972. Gelfand *et al.* (1972, 1973a) showed that in Central Asia epicentres of strong earthquakes in the time window 1885-1971, with magnitude  $\geq 6.5$  were situated within disjunctive knots, i.e., in zones of intersection of major neo tectonic faults. Strong events nucleate at specific structures that are formed at intersections of lineaments, i.e., at morphosturctural knots (nodes). All dangerous nodes were recognized in the zones of sharp contrast, near mountain countries, like the Tien Shan-Pamir region (nodes #23, #26, #31), Tien - N. Tarim region (41), Kuen Lun-Tarim region (knot #34), and Pamir – Hindu Kush region (knot #37). Since 1972 PR has been applied for recognition of earthquake prone areas for different threshold magnitudes in many seismic regions of the world, for example, (in alphabetical order the of study area), Alborz (Gorshkov *et al.* 2009); Alps and Dinarides (Gorshkov *et al.* 2004); Anatolia (Turkey) and adjacent regions (Gelfand *et al.* 1973a); andean South America (Gvishiani and Soloviev, 1984); California and Nevada (Gelfand *et al.*

1976); Carpatho-Balkan mountain belt (Gorshkov *et al.* 2000); Caucasus region (Soloviev *et al.* 2013); Ecuador (Chunga *et al.* 2010); greater Caucasus (Gvishiani *et al.* 1988); Himalaya (Bhatia *et al.* 1992); Iberian Peninsula region (Gorshkov *et al.* 2010); Italy (Caputo *et al.* 1980; Gorshkov *et al.* 2002; Peresan, 2015); Kamchatka (Gvishiani *et al.* 1984); Kopet Dagh (Novikova and Gorshkov, 2013); Kumaon Himalaya (Varunoday and Wason, 1979); lesser Caucasus (Gorshkov *et al.* 1991); North Vietnam (Tuyen *et al.* 2012); north-eastern Italy (Peresan *et al.* 2002; Peresan *et al.* 2011); Po-plain of Northern Italy (Peresan *et al.* 2015); Pyrenees (Gvishiani *et al.* 1987); Tien Shan and Pamir region (Gelfand *et al.* 1973b); united region of Balkans, Asia Minor, Transcaucasia (Gelfand *et al.* 1974a, 1974b) and western Alps (Cisternas *et al.* 1985). All these studies are listed in table 1.2 which shows author(s), year, study area, features considered and their results.

**Table 1.2:** Pattern Recognition (PR) studies for identification of earthquake prone areas.

Author(s)	Year	Area	Features considered	Result
Gelfand <i>et al.</i>	1972	Eastern Central Asia	Transverse faults; type of junction; number of faults; faults separation; distance from the fault separating mountain countries; combination of geomorphological features; height difference; total length of major fault; relative area of soft sediments and strong earthquake epicenters in the years 1885 to 1971	Tien Shan-Pamir (knots #23, #26 and #31), Kuen Lun-Tarim (knot #34) and Tien & n-N. Tarim (knot #41) were recognized as dangerous knots.
Gelfand <i>et al.</i>	1973a	Pamir and Tien Shan region	-	These papers are in Russian and are cross referenced here.
Gelfand <i>et al.</i>	1973b	central Asia to Anatolia (Turkey)	-	
Gelfand <i>et al.</i>	1974a	Asia Minor and S-E Europe	-	
Gelfand <i>et al.</i>	1974b	-	-	

Author(s)	Year	Area	Features considered	Result
Gelfand <i>et al.</i>	1976	California	Transverse faults; type of junction; number of faults; faults separation; distance from the fault separating mountain countries; combination of geomorphological features; height difference; total length of major fault.	Nearest intersections or nearest ends of major faults from a node and relatively low elevation areas were identified as dangerous.
Varunoday <i>et al.</i>	1979	Kumaon Himalayan	Gradient; soft sediment area; rock type, number of contacts; number of thrust; number of faults; number of closed thrusts, number of intersections, total number of ends and intersections, distance from nearest intersection of sharp bends	Out of the 51 objects considered, 33 appear as dangerous and 18 as non-dangerous
Caputo <i>et al.</i>	1980	Italy	Elevation; maximum elevation; minimum elevation; number of lineaments departing from intersection; soft sediments area; nearest distance to lineament; to lineament of first rank; nearest distance to second lineament of first and second rank; nearest distance to second longitudinal lineament; maximum difference of elevation; number of intersections	Two clusters of dangerous points were observed in north Apennines and central Apennines
Bhatia <i>et al.</i>	1992	Himalayan Arc	Minimum altitude in the vicinity of knot; Difference between maximum and minimum altitudes; Gradient of altitudes; Combinations of relief types: (mountain/plain, mountain/piedmont/plain, mountain/piedmont, mountain/upland, mountain/mountain); Distance from the intersection to the nearest lineament of II rank;	Two studies were carried out for $M \geq 6.5$ and $M \geq 7.0$ . Out of 97 knots 48 knots are seismically potential for $M \geq 6.5$ and 36 knots are seismically potential for $M \geq 7.0$ .



Author(s)	Year	Area	Features considered	Result
			Distance from intersection to the nearest intersection.	
Gorshkov <i>et al.</i>	2000	Carpatho-Balkan mountain belt situated in the most seismically active Circum-Pannonian region in Hungary, Poland and Romania region	Longitudinal and transverse lineaments; nearest distance to intersection.	Sixty-four dangerous nodes were identified. Seven of these nodes were validated for earthquakes of $M_s \geq 6.0$ .
Gorshkov <i>et al.</i>	2002	Adria Margin in peninsular Italy	Topographic parameters (Maximum altitude; minimum altitude, distance between maximum altitude and minimum altitude and relief energy); Geologic parameters (the portion of soft (Quaternary) parameters); Gravity parameters (maximum and minimum values of Bouguer anomaly, difference between maximum and minimum values of Bouguer anomaly); parameters from the morphostructural map (number of lineaments within node, lineament of highest rank within node, distance to the nearest first and second rank lineament, nearest distance to the node); Morphological parameters (mountain/plain, piedmont/plain, mountain/piedmont, mountain/upland, mountain/mountain, piedmont only, plain only)	Total of 81 nodes were identified to be prone to earthquake of magnitude $M_w \geq 6.0$ . All earthquake of magnitude $M_w \geq 6.0$ in their catalogue are within the node, however 13 out of 15 of magnitude $M_w \geq 6.5$ were inside nodes.

Author(s)	Year	Area	Features considered	Result
Gorshkov <i>et al.</i>	2004	Italian mountain ranges Alps and Dinarides	Same as Gorshkov <i>et al.</i> (2002)	In the Alps, recognised D nodes cover approximately 38% of the entire area of the region, while in Dinarides the area occupied by D nodes is about 27-28%.
Gorshkov <i>et al.</i>	2009	Alborz Region	Same as Gorshkov <i>et al.</i> (2002)	Of 134 nodes, 79 (58%) are classified as dangerous and 65 (49%) as Non-dangerous
Gorshkov <i>et al.</i>	2010	Iberian Peninsula	Same as Gorshkov <i>et al.</i> (2002)	Most of the dangerous nodes were scattered at the Peninsula periphery.
Peresan <i>et al.</i>	2011	North-Eastern Italy	Elevation in mountain belts; variations in elevation in mountain belts; elevation in watershed areas; variations in elevation in watershed areas; orientation of linear topographic features; linear topographic features density; type and density of drainage pattern.	Dangerous nodes were identified as the circles of radius 25 km.
Tuyen <i>et al.</i>	2012	North Vietnam	Same as Gorshkov <i>et al.</i> (2002)	Of the 134 nodes, 92 ( 68% ) were classified as D and 42 (32%) as N. All earthquakes with $M_w \geq 5.0$ recorded in North Vietnam are close to the D nodes.
Peresan <i>et al.</i>	2015	Po- Plain Italy	Same as Gorshkov <i>et al.</i> (2002)	Of 102 nodes in the region, 60 are located in lowland environments of Po plain and 42 divides the Po plain from the surrounding mountain chains.
Sinvhal <i>et al.</i>	1991, 1992	Tehri region, Uttarakhand	Magnitude of earthquake; Number of major thrusts; Distance to end of major thrust; Number of lineaments, (identified through satellite imageries); Number of intersection of lineaments; Length of river course/ tributary; Number of	Three distinct types of zones were identified: <ul style="list-style-type: none"> <li>○ S1 was identified as a highly critical zone, 100 sq. km in area, with three major thrusts within the area: Krol, Garhwal and Tons thrusts.</li> </ul>

Author(s)	Year	Area	Features considered	Result
			epicenters	<ul style="list-style-type: none"> <li>○ S2 was identified as a moderately critical zone and existed in three separate places, and was marked by two major thrusts: Bhatwari and Munsiri thrust.</li> <li>○ S3 was identified as a critical zone, and existed along all the major thrusts.</li> </ul>

The methodology used by authors listed in above section, was based on the assumption that strong events originate at intersections of lineaments, i.e., at morphostructural knots. Here, strong events mean earthquakes of magnitude  $M$ , which are not lower than some pre decided threshold magnitude,  $M_0$ . Different authors consider different thresholds of magnitude,  $M_0$ . The PR algorithm used consists of three steps: Learning, voting and control experiments. The knots used in the learning stage are divided into two classes: A knot is considered to be of dangerous class,  $D_0$ , if an earthquake with  $M \geq M_0$  had occurred during the past history within that knot. In case of absence of earthquakes of  $M \geq M_0$  within the knots, they are considered as non dangerous class,  $N_0$ . Different combinations of features were used by different authors for identifying areas where epicenters of strong earthquakes may occur in future. Some of these features are listed in table 1.2. These features are: topographic features, geological features, features from morphostructural map, morphological features, gravity features and several other features from tectonics and drainage (transverse faults; type of junction; number of faults; number of major thrusts; number of lineaments; number of intersection of lineaments; faults separation; distance from the fault separating mountain countries; total length of major fault; relative area of soft sediments; elevation in mountain belts; elevation in watershed areas; variations in elevation in watershed areas; orientation and density of linear topographic features; type and density of drainage pattern; magnitude of earthquake; distance to end of major thrust; length of river course/ tributary; number of epicenters; total number of ends and intersections; distance from nearest intersection of sharp bends).

Of all the above discussed studies, two studies were for identification of earthquake prone areas within Himalayan arc. Varunoday *et al.* (1979) applied the PR technique to predict the location of future earthquakes of magnitude equal to or greater than 5.5 in the Kumaon Himalaya. Six earthquakes of magnitudes greater than or equal to 5.5, occurred between 1900-1976, were used in learning exercise to develop decision rules. Features used were: type of rocks, number of contacts, number of thrusts, number of faults, number of closed thrusts, number of intersections, total number of ends and intersections and distance from nearest intersection or sharp bends, area of soft segments and gradient. Out of the 51 potential knots identified, 33 appeared as dangerous i.e. knots supporting earthquake of magnitude greater than 5.5 and 18 as non-dangerous.

Identification of seismogenic potential knots for two magnitudes ranges  $M_w \geq 6.5$  and  $M_w \geq 7.0$  for the entire Himalayan arc was again attempted by Bhatia *et al.* (1992). Features considered were: topographic, geological and tectonic maps, in addition, satellite imageries were also included. A total of 97 intersections (knots) were identified throughout the Himalayan arc. 48 knots were found to be seismically potential for magnitude,  $M_w \geq 6.5$ . Also, 36 knots were found to be seismically potential for  $M_w \geq 7.0$ . Gorshkov *et al.* (2012) reconsidered and validated maps obtained by Bhatia *et al.* (1992) and found that three out of four post-publication earthquakes occurred within the dangerous knot, **D**. Uttarkashi earthquake of 1991 occurred within knot #24, Chamoli earthquake of 1999 occurred within knot #35 and the Kashmir earthquake of 2005 occurred within **D** knot #5. The Sikkim earthquake of 2011 originated between two knots #66 and #71.

For all the above studies, the methodology rely on an analysis of available geological and morphostructural data, founded on a set of parameters based on relief, topography, drainage, geology, sediments and faults. These methods used hierarchical logical decision making, which is essentially a qualitative pattern recognition technique, for morphosturctural zoning and then to recognize seismogenic knots. Therefore, these methodologies are independent of past seismicity and are particularly useful in areas where information on historical seismicity is sparse (Peresan *et al.* 2015). However, seismogenic knots that are not related with known active faults or past earthquakes still need investigation. In addition, epicentral data, though used in analysis, was not a discriminant parameter. This feature was taken care of and enhanced by the PR technique developed by Sinvhal *et al.* (1990, 1991), as a quantitative approach was applied and epicentral

data was part of extracted features in the PR analysis. Three distinct types of zones for Tehri region were identified by PR method which was based on linear discriminant analysis. The features identified were based on tectonic density, drainage density and seismic density. These were: 1) magnitude of earthquake; 2) number of major thrusts; 3) distance to end of major thrust; 4) number of lineaments (identified through satellite imageries); 5) number of intersections of lineaments; 6) length of river course/ tributary; 7) number of epicenters. Three distinct types of zones were identified: S1 was identified as a highly critical zone, approximately 100 sq. km in area, with three major thrusts within the area: Krol, Garhwal and Tons thrusts. Narendra Nagar, Devprayag, Kirtinagar, Chamba, Jhaknidhar and Rishikesh are within this critical zone. S2 was identified as a moderately critical zone and existed in three separate islands, and was marked by two major thrusts: Bhatwari and Munsiri thrust. The three islands were centered around, a) Badhani, Bhudna; b) between North Almora thrust and Tons Nayar thrust, centred at Tehri; and c) Garhwal thrust and Krol thrust, centred at Rishikesh. S3 was identified as a critical zone, and existed along all the major thrusts.

A hypothetical disaster scenario together with vulnerability and risk analysis was conceived for Narendranagar in the highly critical zone, S1, by Gupta *et al.* (2006). Fifty-nine percent population of Narendranagar was prone to damage associated with accelerations as high as 0.41g. This risk will increase substantially if the larger magnitude earthquake originates. The risk could be even higher at intersection and vicinity of faults, and river. Forty-seven villages and one urban center with 32.4% of the total population of Narendranagar were at higher risk.

Hypocenter of the modeled Uttarkashi earthquake was in the moderately critical zone, S2, and that of the Chamoli earthquake of 1999 was below an extension of the same zone; implying that S2 seems to have tremendous seismogenic potential, (Gupta and Sinvhal, 2010; Sinvhal and Gupta, 2010).

With this background, therefore, one of the objective of the present study is to divide the western Himalayas into several seismically susceptible areas using PR technique and then to validate these areas according to their seismogenic potential.

### 1.2.2 Review of segmentation

All the above pattern recognition problems consider tectonics of the region as one of the important features. While addressing the PR problem for identification of earthquake prone areas the longer long tectonic units can be considered as one long unit as it does not deal with the maximum earthquake that it can produce. But, while estimating hazard of the region the maximum earthquake that a fault can support plays an important role. Therefore, before assessing hazard of the region it is necessary to study the tectonics of the region and proper segmentation of any longer tectonic unit should be considered.

It was observed that in western Himalaya several long tectonic units exist. Seismicity in the western Himalayas is highly variable. Seismicity along the Himalayan arc varies significantly with well defined patterns following segments of seismic sources. Many seismic sources in the western Himalaya, in the form of faults, thrusts and lineaments, are capable of producing an earthquake of significant magnitude. These sources, from small tectonic units to mega thrusts like the Main Boundary Thrust (MBT) and Main Central Thrust (MCT), can have highly variable seismicity and lengths. During an earthquake the longer lineaments do not rupture over their entire length. This leads to the fact that the longer lineaments are active in segments (King and Yielding, 1984; King and Nábělek, 1985; King, 1986; Coppersmith, 1991; Ikeda *et al.* 2009; Mukhopadhyay, 2011; Mukhopadhyay *et al.*, 2011). However, the question is, to what desirable length the rupture exist, or is there any physical boundary in the fault that controls and defines the extent and location of rupture? The solution to this problem may be formulated by the fact that the segments of longer lineaments are governed by several factors such as presence of transverse tectonic features, change in seismicity along the fault, difference in slip rates, occurrence of significant lithologic changes, strike of fault etc (Schwartz and Coppersmith, 1986).

The concept of segmentation of long tectonic units and their impact on hazard assessment has been considered by several authors. Allen (1968) considered the segments of San andreas Fault Zone in California, based on historical and paleoseismicity data, data on displacement per event, and historically defined segments to suggest maximum size of earthquakes that might be generated in any area on the basis of its distinctive geologic features. It was found that the two segments of the San andreas fault that were characterized by great earthquakes within the historic record, in

1857 and 1906, had likewise generated infrequent great shocks throughout the recent geologic past, and that the present absence of small earthquakes and creep is typical of the past and probable future behavior between large shocks. Schwartz *et al.* (1984) considered it for the Wasatch fault zone, Utah; Yielding *et al.* (1981) and King and Yielding (1984) considered the Oued Fodda Fault Zone, in Algeria; and Scott *et al.* (1985) considered the Lost river fault zone, Idaho. DePolo *et al.* (1991), considered basin and range province of western North - America. Ikeda *et al.* (2009) considered segmentation of the most active Median Tectonic Line active fault system of Shikoku, Japan which is a strike-slip fault. a model for fault segmentation was developed using geological and geophysical data information about faults. Mukhopadhyay (2011) studied clusters of moderate size earthquakes along MCT and suggested that MCT is not dormant but active in segments.

Segmentation provides a physical basis for selecting rupture lengths which is later used in calculation of maximum earthquakes. The fault segmentation and behavior of independent segments has important implications in seismic hazard assessment. The seismic hazard posed by segmented fault may be different, than what is posed by a non segmented entire length. In keeping with this trend, equal segments of long tectonic units and segments of the MBT and the MCT using PR technique are discussed in the present study and the segments were used subsequently for assessing seismic hazard.

### **1.2.3 Review of deterministic seismic hazard assessment**

The potentially damaging phenomena associated with earthquakes, such as surface fault rupture, landslides, ground shaking, fissures and soil liquefaction are defined as seismic hazard. Seismic hazard assessment is an attempt to quantify seismic hazard in terms of Peak Ground Acceleration (PGA). This could result in significant implications to society which includes built environment destruction and life loss. Two different approaches of seismic hazard assessment are: 1) deterministic seismic hazard assessment (DSHA) and 2) probabilistic seismic hazard assessment (PSHA). When a particular earthquake scenario is assumed hazard can be assessed deterministically, whereas, when uncertainties in earthquake location, time of occurrence and size, are explicitly considered hazard can estimated probabilistically (Kramer, 2009).

Both methods have their own advantages and disadvantages that often make the use of one advantageous over the other. The deterministic approach focuses on a single event, which ensures

that the event is realistic and probability of occurrence of that earthquake is finite. The probabilistic approach on other hand can be viewed as inclusive of all deterministic events with a finite probability of occurrence (McGuire, 2004). The choice of the method depends on several factors such as seismotectonic environment, site position, and the type of decisions to be made. In this research work both deterministic and probabilistic seismic hazard methods have been studied in detail.

Deterministic Seismic Hazard Assessment (DSHA) is the frequently used method to assess hazard in many seismically active regions of the world, for example in Northwest Oregon, USA (Hull *et al.* 2003); California (Mualchin, 2005); Bangladesh (Khan and Hossain, 2005; Joshi and Khan, 2009; Khan, 2012, 2014); Iran (Hamzehloo *et al.* 2005, 2007, 2010; Ma'hood *et al.* 2009); USA (Kripakaran *et al.* 2007, 2008; Gupta *et al.* 2005); Greece (Moratto *et al.* 2007); Quetta, Pakistan (Shah *et al.* 2012); Thailand and adjacent areas (Pailoplee *et al.* 2010 ); and Taiwan (Wang *et al.* 2012). Several other authors also attempted DSHA (Joshi *et al.* 1999, 2009, 2013a; Gupta, 2002; Tewatia *et al.* 2006, 2007, 2013).

DSHA has been used for assessing hazard for several states or cities of India. These are in alphabetical order of state/city are, Andaman and Nicobar islands (Katariya *et al.* 2013); Bangalore (Sitharam *et al.* 2006); Central India (Kumar *et al.* 1997, 1999, 2005, 2008, 2011, 2012; Sinha *et al.* 1998, 2001a, 2001b, 2006; Maity *et al.* 2010); Chennai (Boominathan *et al.* 2008); Dehradun (Kumar *et al.* 2013); Goa (Naik and Chaudhary, 2015); Gujarat (Nath *et al.* 2010a; Shukla and Chaudhary, 2012); India subcontinent and adjacent areas (Parvez *et al.* 2003); Indian Subcontinent (Nath *et al.* 2010b); Mumbai (Desai and Choudhury, 2014); north-east Himalayas and northeast India (Nath *et al.* 2008); Uttarakhand Himalayas (Mohan *et al.* 2008; Joshi *et al.* 2009, 2010a, 2010b); Tamil Nadu (Ganapathy, 2010); Tripura and Mizoram (Sitharam and Sil, 2014); and Uttarakhand (Kumar *et al.* 2011; Joshi *et al.* 2013b; Kumar *et al.* 2014). DSHA carried out for either northwest Himalayas or states in Northwest Himalaya are discussed here.

Mohan *et al.* (2008) assessed seismic hazard for Uttarakhand Himalayas and north-east Himalayas using deterministic approach. The zonation map was prepared for magnitude  $M_w \geq 6.0$  in Uttarakhand Himalayas. It showed that Almora, Dharchula, Karanparyag, Lohaghat, Munsiri, Nainital, Pithoragarh and Uttarkashi had peak ground acceleration greater than equal to 400



cm/sec<sup>2</sup> and were in Zone V (BIS: 1983-2002). Sobla and Gopeshwar lie in Zone IV with peak ground acceleration greater than equal to 250 cm/sec<sup>2</sup>.

Kumar *et al.* (2011) identified 32 seismo-tectonic sources in Uttarakhand. Maximum PGA was computed at 180 sites and a seismic zoning map was prepared. The PGA in the area varied in the range 0.06g to 0.50g. Highest seismic hazard was estimated in the vicinity of MCT and the MBT, North Almora Thrust, Ramgarh thrust and complex tectonic units in the form of closed loops named as TZ1, TZ2 and TZ7, between MBT and MCT.

Kumar *et al.* (2013) carried out seismic hazard assessment for the Dehradun city of Uttarakhand and its adjoining region. 24 seismotectonic sources were identified in the area. Two attenuation relations viz. Abrahamson and Litehiser (1989) attenuation relation and Sharma (2000) attenuation relation, were used for estimation of PGA. Maximum PGA of 0.475g by Abrahamson and Litehiser (1989) attenuation relationship along MBT was estimated. Maximum PGA estimated using Sharma (2000) attenuation relationship was 0.334g along MBT.

Joshi *et al.* (2013b), used semi empirical method for seismic hazard zonation of Uttarakhand Himalayas. Strong ground motion at a site was simulated to develop an attenuation relation. The developed attenuation relation was used to estimate peak ground acceleration. Hazard map was prepared and it showed that Almora, Bageshwar, Chamoli, Devprayag, Pauri, Srinagar and Tehri fall in a zone of peak ground acceleration of 200 gals.

Seismic hazard assessment (mean and mean plus one standard deviation Peak Horizontal Accelerations) has been carried out for Uttarakhand by Kumar *et al.* (2014), using Boore and Atkinson (2008) ground motion prediction model. The seismicity data and tectonic data were same as for Kumar *et al.* (2011). The estimated PGA (mean) was in the range of 0.07 g to 0.605 g and PGAs (mean plus one standard deviation) varied from 0.127 g to 1.06 g in the state.

In spite of being in use by several researchers DSHA suffers from various disadvantages. (Krinitzsky, 2003). Ground motion at a site varies with variation in maximum magnitude, distance from source, site condition and empirical relations used. Moreover, different empirical relations give different ground motion at the same site. The deterministic approach provides no information about the time of occurrence of the maximum earthquake and the level of shaking that might be

expected during a finite period of time. To overcome some of these disadvantages the application of PSHA came into vogue.

#### **1.2.4 Review of probabilistic seismic hazard assessment**

The goal of Probabilistic seismic hazard assessment (PSHA) is to quantify the probability of exceeding ground-motion level at a site given by all possible earthquakes. It explicitly takes care of some of the uncertainties inherent in DSHA, such as maximum magnitude considered and the ground motion attenuation. The probability distribution is defined in terms of the annual rate of exceeding the ground motion level at the site, due to all possible pairs of magnitude and epicentral distance of the controlling earthquake, (M, R) (Rieter, 1990). PSHA has been carried out using the approach formulated by Cornell (1968) that was further developed by McGuire (1976). The combined approach is known as the Cornell–McGuire approach (Rieter, 1990).

PSHA has been used to assess hazard in many seismically active regions of the world and in India, for example, in Bangalore (Anbazhagan *et al.* 2009); Canterbury region, UK (Stirling *et al.* 2002); central and south India (Jaiswal and Sinha, 2008); Dehradun (Sharma and Lindholm, 2012); Delhi (Sharma *et al.* 2003; Sharma and Wason, 2004); Eskisehir, Turkey (Orhan *et al.* 2007); Greece (Tselentis and Danciu, 2010; Tselentis *et al.* 2010 ); Global Seismic Hazard Assessment Program, GSHAP (Giardini *et al.* 1999); Himachal Pradesh and adjacent areas (Patil *et al.* 2014); Indian subcontinent (Basu and Nigam, 1977, 1978; Khattri *et al.* 1984, Bhatia *et al.* 1999,2010; Parvez and Ram, 1999; Smith *et al.* 2009; NDMA, 2011; Grzelak *et al.* 2011; Nath and Thingbaijam, 2012); Kozani-Grevena Region, Greece (Theodulidis *et al.* 1997); Maharashtra (Gupta *et al.* 2001); New Madrid seismic zone (Cramer, 2001); Northeast India (Das *et al.* 2006; Sharma and Malik, 2006; Gupta and Pattanur, 2012); Northeast India and Hindukush Regions (Parvez and Ram; 1997); Northern and Central Italy (Lombardi *et al.* 2005); Italian sites (Sabetta *et al.* 2005); north-west Himalaya (Mahajan *et al.* 2010; Yadav *et al.* 2012; Rout *et al.* 2015); Norway (Lindholm and Bungum, 2000); Romania (Mantyniemi *et al.* 2003; Ardeleanu *et al.* 2005; Sokolov *et al.* 2007, 2009); South Spain (Muñoz and Udías, 1992; Benito *et al.* 2010); Horn of Africa, i.e. peninsula in Northeast Africa (Kebede and Van Eck, 1996); southeast Spain (Mayordomo *et al.* 2007); Tamil Nadu (Menon *et al.* 2010); Tripura and Mizoram (Sil *et al.* 2013). Several other authors also attempted PSHA (Veneziano *et al.* 1984; Kijko and Graham, 1998,

1999; Orozova and Suhadolc 1999; Kijko and Oncel, 2000; Ameer *et al.* 2005 Bommer *et al.* 2005; Scherbaum *et al.* 2005).

Khattari *et al.* (1984) delineated 24 seismogenic sources for India and carried out PSHA to prepare the zoning map for 10% probability of exceedance for a return period of 475 years at bedrock level. Sharma and Wason, (2004) estimated hazard for Delhi region considering 300 km area around Delhi divided into six seismogenic sources. Peak ground accelerations (PGA) for 20% exceedance in 50 years were estimated. The isoacceleration map for Delhi region was prepared. Two seismogenic zones viz. Mathura fault zone and Sohna Fault Zone were found to govern the pattern of isoacceleration map for Delhi region. National Disaster Management Authority (NDMA) (2011) carried out PSHA and prepared a hazard map for the entire country. 32 seismogenic source zones were delineating. For a grid interval  $0.2^\circ \times 0.2^\circ$ , PGA and pseudo spectral accelerations for spectral periods 0.5 and 1.25 sec has been estimated. Contour maps for hard rock type were prepared for return periods of 475 and 2,475 years. PGA values at forty eight important cities in India were reported. Nath and Thingbaijam (2012) carried out PSHA and computed hazard components viz. seismogenic source zonation, seismicity modelling, assessment of site conditions and a suitability test for the Ground Motion Prediction Equations (GMPEs) in the regional context. Appropriate GMPEs were used for different seismotectonic regimes. Ground motion was computed for the return periods of 475 years and 2,475 years. The tectonically active regions of the Garhwal Himalayas, parts of western Kashmir, northeast India, western Gujarat and Koyna-Warna regions indicated higher hazard area.

Bhatia *et al.* (1999) estimated hazard for India and adjoining regions by delineating 86 potential seismogenic sources and calculated PGA for a return period of 475 years. PGA for the entire India varied between 0.1g to 0.4g. It was found that region of north Indian plate boundary and the Tibetan plateau have PGA greater than or equal to 0.25g and north-east India and Hindukush region has prominently high hazard level of order 0.35 - 0.40g. PGA map in the form of seismic zoning map having four zones, with zone factors 0.1g, 0.2g, 0.3g and 0.4g was prepared. Mahajan *et al.* (2010) estimated hazard for north-west Himalaya, by delineating 19 seismogenic source zones. For PGA estimation weighted average of Abrahamson and Litehiser (1989) attenuation relationship, Hasegawa *et al.* (1981) relationship and Peng *et al.* (1985) relationship had been used. PGA was estimated for a 10% probability of exceedance in 50 years and 10 years.

Longitudinal variation in hazard level for the northwest Himalayan arc was observed. High hazard zones are observed around Kangra region (0.50g / 0.20g), Garhwal region (0.50g / 0.20g), Kaurik-Spiti region (0.45g / 0.20g), Kashmir region (0.70g / 0.35g) and Dharchula region (0.50g / 0.20g) for 50 years and 10 years, respectively.

Sharma and Lindholm (2012) estimated seismic hazard for Dehradun city, Uttarakhand. Earthquake distribution for Main Boundary Thrust (MBT) was modelled to be Poissonian, whereas for Himalayan Frontal Fault (HFF) it was modelled with to be characteristic earthquake recurrence model and a Poissonian model. PGA in the Dehradun ranges upto  $2.2 \text{ m/s}^2$  for 225 years and  $4.6 \text{ m/s}^2$  for 2,500 years. Yadav *et al.* (2012) delineated 28 seismogenic source zones in NW Himalaya and adjoining regions. Hindukush-Pamir Himalayan region, Uttarkashi- Chamoli region and Quetta region of Pakistan were estimated to have high seismic hazard. Maximum magnitude greater than 8.0, are expected in Himachal Pradesh, Kashmir, and Quetta zones. Patil *et al.* (2014) prepared hazard maps for Himachal Pradesh and adjacent areas for a return period of 475 and 2475 years at the bedrock level. Two different cases were considered (i) varying  $b$ -value for each seismogenic zone, (ii) constant  $b$ -value for the entire study area. For 475 years, the PGA values varied between 0.09g to 0.15g when  $b$ -value was varied. PGA varied in the range 0.09g to 0.26g, when  $b$ -value was considered to be constant. For 2,475 years, PGA varied in the range 0.07g to 0.24g when  $b$ -value was varied and 0.14g to 0.37g, when  $b$ -value was considered to be constant. Central water commission (Government of India organization) provided guidelines for preparation of site specific seismic study report and illustrated an example for developing target response spectra using both DSHA and PSHA methods in highly seismic Kumaun-Garhwal Himalayan region (Uttarakhand). The region was divided into five seismogenic zones. Rout *et al.* (2015), delineating 22 seismic zones and estimated hazard, for western and central Himalayas. 5 different attenuation relations were used and each was assigned to have equal weightage. PGA was estimated at bed rock level, for 10% and 2% probability of exceedance in 50 years. For the 10% and 2% probability of exceedance in 50 years, the PGA values varied in the range 0.06g - 0.36g and 0.11g - 0.65g, respectively. High PGA values around Kaurik Fault and in eastern part of the study area were observed.

PSHA also suffers from several disadvantages, such as lack of transparency of the method. The effects of individual parameters can neither be understood nor easily recognized. Moreover, sometimes an unrealistic scenario is presented, i.e., the location where actual fault exists could not be corresponded (Krinitzsky, 2003). DSHA and PSHA use the same data set, but as the results are very different it is very difficult to decide which to use. In such an undecided scenario it may be possible that Pattern Recognition (PR) may offer some alternative in decision making.

### **1.2.5 Seismic zoning map of India**

Seismic zoning is a process of dividing an area into seismic zones based on expected peak ground acceleration (PGA) and is best represented by a map.

The first seismic zoning map of India was compiled by the Geological Survey of India (GSI) in 1935 after the great Bihar – Nepal earthquake of 15<sup>th</sup> January 1934. This map was made on the basis of damage observed in past earthquakes, of intensity VII or higher on Rossi-Forel scale. In 1962, the Bureau of Indian Standards (BIS) (earlier, Indian Standards Institution) published the first seismic zonation map of India (IS: 1893-1962). It was prepared on the basis of zoning maps made by GSI in 1935, 1950, quantitative aspects of Dr. Jai Krishna's map of 1959, and earthquake epicenters provided by India Meteorological Department (IMD) and five great earthquakes: Kutch earthquake of 1819, Assam earthquake of 1897, Kangra earthquake of 1905, Bihar-Nepal earthquake of 1934 and Assam earthquake of 1950. India was divided into seven seismic zones based on the damage i.e. VI represents extensive damage and 0 represents no damage. Most of the Peninsular India was in zone 0. On the other hand zone VI was the severest zone which included meizo-seismal areas of the two great Assam earthquakes of 1897 and 1950. Zone V corresponds to the gap between the two great earthquakes of Assam and, in addition, meizo-seismal areas of Kutch earthquake of 1819, Kangra earthquake of 1905 and Bihar-Nepal earthquake of 1934.

The zoning was reviewed on the basis of geology and the tectonic units in 1966 (IS: 1893-1966). Three tectonic zones were emphasized: the Himalayan tectonic zone, the Kutch region and the seismically stable peninsular region. The map continued to have seven zones.

The zonation map was again revised after the strong earthquake of magnitude, 6.5, i.e., Koyana earthquake of 11<sup>th</sup> December, 1967, which occurred in Peninsular India. This part of the country was previously assigned as zone 0. In 1984, the zonation map was again revised (IS: 1893-1984) on the basis of past seismicity and tectonic units. Zone 0 and zone 1 and zone V and zone VI of the previous map were merged together, which resulted into five zones I, II, III, IV and V. Zone V was the severest zone and zone I was the least active of all zones.

Several damaging earthquakes occurred after the 1984 version of the zoning map. One of such earthquake was Latur earthquake of 1993, which was a strong earthquake of magnitude 6.3. Previously Latur was placed in zone I and no earthquake of comparable magnitude was expected in that zone. Casualty figures were high in stone houses in this earthquake. Also in the Kutch earthquake of January 26, 2001 the urban landscape with the new multistory buildings was adversely altered. The seismic zoning map of 1984 was again revised in 2002 on the basis of these two earthquakes. Zones I and II were merged which resulted into four zones II, III, IV and V, where zone V is the severest zone. The Latur earthquake of 1993 was placed in zone III. This map is referred to as seismic zoning map of India (BIS: 1893-2002), henceforth. The following section gives salient features of these four zones.

Zone V is the most seismically active zone. The areas under this zone are Srinagar Baramula region in Jammu and Kashmir; Chamba, Dharamshala, Hamirpur, Jogindernagar, Kangra, Kullu and Mandi in Himachal Pradesh; eastern part of Uttarakhand which includes parts of Bageshwar, Chamoli, Champawat, Pithoragarh, Pauri Garhwal, Rudraprayag and Tehri; In Bihar it includes Darbhanga, Supaul and Madhubani; the entire northeast which includes all the seven states Assam, Arunachal Pradesh, Manipur, Meghalaya, Mizoram, Nagaland and Tripura; andaman and Nicobar Islands and the Rann of Kutchh in Gujarat. Zone V can expect destruction of the built environment from earthquakes with magnitude greater than 7.0, and MM intensity greater than or equal to IX, with acceleration ranging between 0.24 - 0.36 g.

Zone IV is the next severest zone of the seismic zoning map and is comprised of Almora, Ambala, Amritsar, Chandigarh, Darjeeling, Dehradun, Gangtok, Gorakhpur, Monghyr, Moradabad, Nainital, Patna, Roorkee and Simla. This zone can expect heavy damage from

earthquakes in the magnitude range 6.5-7.0, MM intensity ranges between VIII and IX, and accelerations in the range 0.16 - 0.24 g.

Zone III is the zone of intermediate severity and due to neo tectonic activity the Narmada graben, Mahanadi Graben and Godavari Graben are assigned to zone III. This zone can expect moderate damage from earthquakes in the magnitude range between 6.0-6.5, MM intensity between VII and VIII, with accelerations of 0.16 g.

Zone II is the least active zone and some of the important places of zone II are Ajmer, Allahabad, Bangalore, Bhilai, Bhopal, Hyderabad, Jaipur, Jhansi, Madurai, Nagpur, Pondicherry, Raipur, Ranchi, Tiruchirapalli and Vishakhapattanam. Slight damage can be expected in zone II, from earthquakes in the magnitude range 5.0-6.0, MM intensity between VI and VII, with accelerations less than 0.10 g. Seismic zoning map of India is shown in figure 1.1. Table 1.3 shows maximum magnitude, maximum intensity and PGA range assigned to each seismic zone.

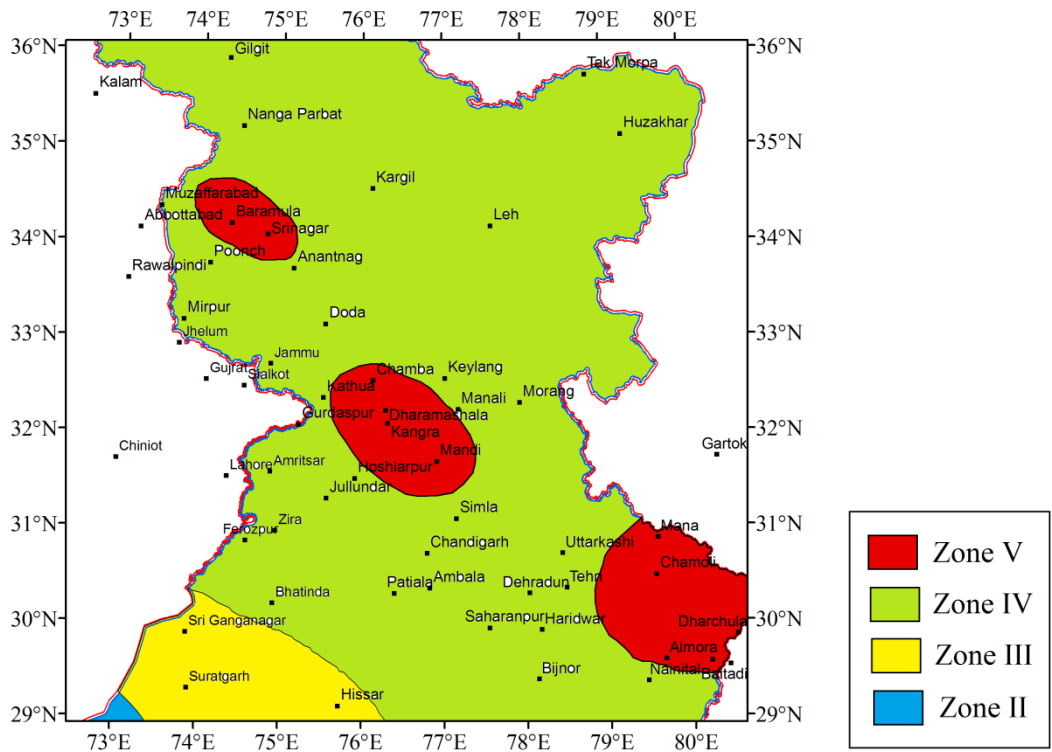


**Figure 1.1:** Seismic zoning map of India shown for the study area (redrawn after BIS 1893: 2002). Places are as per SEISAT (Narula *et al.* 2000).

**Table 1.3:** Maximum magnitude, Peak acceleration, Intensity (MM) and perceived damage implications assigned to different seismic zones as per BIS (BIS: 1893:2002).

<b>Zone</b>	<b>Intensity (MM)</b>	<b>Magnitude</b>	<b>PGA range</b>	<b>Damage implication</b>
V	IX +	> 7.0	0.24-0.36 g	Destruction
IV	between VIII and IX	6.5-7.0	0.16-0.24	Heavy damage
III	between VII and VIII	6.0-6.5	0.10-0.16	Moderate damage
II	between VI and VII	5.0-6.0	< 0.10	Slight damage

### 1.3 Identification of Gaps

Several gaps were identified in seismic hazard assessment and in pattern recognition applied to earthquake prone areas after literature review. These are enumerated below.

1. The most controversial and difficult question in SHA has often been whether one should use PSHA or DSHA. While there is a definite worldwide trend toward PSHA, the situation is by no means clear. For example, in the field of nuclear safety alone, regulators trying to define the criteria for nuclear reactors and waste repositories have switched back and forth between DSHA and PSHA. In many cases the question has been rephrased so that the issue is not “whether” but rather “to what extent” a particular approach should be used, ([www.reluis.it/doc/pdf/Accelerogrammi/PSHA\\_DSHA.pdf](http://www.reluis.it/doc/pdf/Accelerogrammi/PSHA_DSHA.pdf)).
2. Methodology adopted by authors for identification of earthquake prone areas used morphostructural zoning and then recognized seismogenic knots, using a hierarchical logical decision making process which is essentially a qualitative pattern recognition technique. In addition, epicentral data, though used in analysis, was not a discriminant parameter.
3. In seismic hazard assessment length of tectonic units plays a major role in estimating magnitude of an earthquake it can support. MBT and MCT are tectonically complex mega plate boundary thrusts, each more than 2500 km long in the Himalayan region. The entire MBT or MCT cannot be expected to rupture over its entire length in a single large earthquake. Therefore, there is an urgent need for segmentation of these mega tectonic units. Therefore, appropriate segmentation of the longest and highly contorted lineaments MBT and MCT is required by considering several factors such as presence of transverse tectonic units, change in



seismicity along the fault, change in strike, sharp bends, difference in slip rates and occurrence of significant lithologic changes.

## 1.4 Objectives

After identifying the gaps, the objectives of this research work were identified as follows:

1. Identification of seismically susceptible areas using Pattern Recognition (PR) technique.
2. Segmentation of longer tectonic units (MBT, MCT) using Pattern recognition technique.
3. Assessment of seismic hazard by two methods:
  - i. Deterministic Seismic Hazard Assessment (DSHA)
  - ii. Probabilistic Seismic Hazard Assessment (PSHA)
4. Comparison of seismic hazard maps obtained by DSHA and PSHA technique.
5. Comparison of seismic hazard maps using strong ground motion data of 3 earthquakes in the region.
6. Validation of above results using recent earthquakes.
7. Implications for probable earthquake damage in western Himalaya and particularly for Kangra region.

## 1.5 Organization of the Thesis

The thesis is divided into eight chapters. First chapter is the introduction to the thesis and the research background of the thesis is discussed. Literature review of Pattern Recognition technique used for identification of susceptible areas and segmentation of longer tectonics, Deterministic Seismic Hazard Assessment (DSHA) and Probabilistic Seismic Hazard Assessment (PSHA) is also discussed. The major objectives of the study are enumerated. The other chapters are organized according to the themes outlined within the scope of the present work.

**Chapter 2** describes the details of the study area, different types of data used to carry out various studies. It deals with seismicity data, treatment of earthquake catalog, tectonic data, digitization, treatment and characterization of tectonic data. Available fault plane solutions of several earthquakes are also discussed.

**Chapter 3** describes the pattern recognition technique, its steps and the application areas. The application of PR specific to hazard assessment is discussed in terms of identification of susceptible areas and segmentation of longer tectonic units.

**Chapter 4** describes the analysis carried out for the identification of susceptible areas in western Himalaya. It also contains the susceptibility map, its interpretation, validation and conclusions drawn from the study.

**Chapter 5** contains method of segmentation and its details of the longer tectonic units, Main Boundary Thrust (MBT) and Main Central Thrust (MCT) in the western Himalaya using pattern recognition technique.

**Chapter 6** deals with major steps of DSHA approach which includes identification and characterization of seismogenic source zones; source to site distance computation; identification of maximum earthquake; and to define seismic hazard in terms of ground motion. Computation of seismic hazard using two different approaches is discussed. Interpretation of hazard map and its comparison with different studies is also shown.

**Chapter 7** contains PSHA for the western Himalaya. It deals with major steps of PSHA which includes: identification and characterization of seismogenic source zones; seismicity characterization; strong ground motion prediction; and probability estimation. Computation of seismic hazard by varying attenuation relationships is discussed. Hazard map obtained is discussed. Interpretation of hazard map and its comparison with different studies is also shown. Validation of return periods for the different magnitude earthquakes is also discussed.

**Chapter 8** contains the implication for probable earthquake damage in western Himalaya is discussed. It is then specifically discussed for the Kangra region. This chapter then summarizes all the studies, its implication and major conclusions drawn from the study. This chapter also suggests future work which can be carried out further.



## CHAPTER 2

### DATA USED IN THE STUDY AREA

---

#### 2.1 Introduction

Seismicity in Indian subcontinent is due to the subduction of the Indian plate under the Eurasian plate (Molnar and Lyon, 1989; Ni and Barazangi, 1984). It marks the largest active continent-continent collision zone, in the Himalayan region. The Himalayan seismotectonic region has experienced four great earthquakes in a time span of 53 years and is subject to seismic hazard. The Indo Gangetic plains south of Himalayas are densely populated so the relatively lesser hazard can translate into greater risk. Therefore, it is pertinent to assess hazard and investigate the effects of such hazard on the populous regions of the area. For this reason it is necessary to consider the seismicity and tectonics of the region. Due to high level of seismicity, i.e., from small earthquakes to great earthquakes and very complex tectonics, a serious seismic hazard scenario exists for the region. One of the most devastating of all earthquakes in this region was the great Kangra earthquake of 1905.

The great Kangra earthquake of 4<sup>th</sup> April, 1905 had its epicenter in the Kangra district of Himachal Pradesh (HP), in the seismically active Himalayan arc, in the vicinity of the Main Boundary Thrust (MBT). This earthquake was one of the most devastating earthquakes of the last century and caused extensive ground damage and enormous destruction of buildings over a large area encompassing the states of Himachal Pradesh, Jammu and Kashmir and Uttarakhand. Damage was concentrated in Kangra, Dharamshala, Palampur, Mandi and adjoining regions of Himachal Pradesh, in the region around Dehradun and Mussoorie in Uttarakhand including foothills of western Himalaya and Lahore in Pakistan (Middlemiss, 1910). The earthquake was felt in large parts of northern India; in Quetta and Sind in the west, in Tapti valley in the south and in the Ganga delta in the east.

Middlemiss (1910) documented effects of this great earthquake in a Geological Survey of India memoir. Extensive ground damage was spread in a very wide area. Ground fissures and topographic changes occurred across the Main Boundary Thrust. Extensive landslides, landslips and rock falls were spread in the valleys of Rivers Beas, Jhelum, Sutlej, Ravi, Chenab and their

tributaries like Parbati and Sainj. Surface and sub surface ground water and the drainage system was altered and springs, streams and canals were disturbed. Sand vents and dust clouds were prominent at many places. Several hundred aftershocks continued for months after the main event. Between Rajpur and Mussoorie the hillsides are composed of much crushed slates and limestone. They rise steeply and culminate in the E-W Mussoorie-Landour ridge at an elevation of about 7,000-8,000 ft, (Middlemiss, 1910, page 95).

Maximum intensity assigned to this earthquake was X on the Rossi Forel (RF) scale and encompassed an area of about 200 sq miles ( $\approx$  517 sq km) in Kangra district. It includes large parts of the Kangra valley and portions of the lower slopes of the Dhauladhar range. RF intensity X refers to the highest intensity on the RF scale and indicates “an extremely high intensity tremor, a great disaster, ruins, disturbance of strata, fissures in ground and rock falls from mountains”. Isoseismal IX refers to a devastating tremor and partial or total destruction of buildings and encloses an elliptical area of about 1600 sq miles (4144 sq km) including parts of Kangra, Hamirpur, Kullu and Mandi districts of Himachal Pradesh. Isoseismals X and IX are totally within Himachal Pradesh.

RF intensity VIII refers to a damaging tremor, fall of chimneys and formation of fissures in walls of buildings. This elliptical isoseismal was in the Kangra–Kullu area and included parts of Kangra, Hamirpur, Kullu, Chamba, Mandi and Sirmour districts of Himachal Pradesh and covered an area of about 2150 sq miles ( $\approx$  5568 sq km). A separate and smaller closed curve, about 1457 sq miles ( $\approx$  3774 sq km) was in the Dehradun–Mussoorie area and included parts of districts of Dehradun, Tehri Garhwal and Uttarkashi in the adjoining state of Uttarakhand. Closest distance between two curves is approximately 85 km.

The built environment was ruined, destroyed or severely damaged, within isoseismal VIII. This included medical facilities, schools, places of worship like temples, churches, mosques; forts at Kangra and Rehlu; and roads and bridges, including masonry bridges, large iron girder bridges and suspension bridges. Likewise, government buildings were similarly ruined, e.g. post office, court house, military barracks, officers’ mess, jail and tombstones where the gate pillars twisted on their base. Fall of chimneys, canopies and cornices was common. Several tea factories and shops were ruined and the Mcleodganj bazaar was leveled to the ground with no buildings standing. Damage was irregular in private stone masonry houses; where the roof was made of heavy slate on

undressed or semi dressed stone, collapse was common, whereas in *dhajji diwari* style of construction the seismic performance was almost exemplary. Table 2.1 shows salient features of the great Kangra earthquake of 1905.

**Table 2.1:** Salient features of the great Kangra earthquake of 4<sup>th</sup> April, 1905.

Date (D/M/Y), Time	: 04.04.1905, 06:20 am (Middlemiss, 1910)
Epicenter	: Kangra, District Dharamshala, Himachal Pradesh 32.30 °N, 76.25 °N (IMD); 33.00 °N, 76.00 °N (ISC); 33.00 °N, 76.00 °N (USGS); 32.30 °N, 76.25 °N (MHD);
Magnitude	: $M_s = 7.8 \pm 0.05$ (Ambraseys and Bilham, 2000), $M_L = 8.0$ (IMD); $M_s = 8.0$ (ISC); $M_s = 8.6$ (USGS); $M_w = 8.0$ (MHD), This study
Depth of Focus	: 35 km (ISC); 25 km (USGS);
Maximum Intensity	: X Rossi Forel Scale (Middlemiss, 1910)
Casualties	: More than 19000 (Middlemiss, 1910)

RF intensity VII is the lowest intensity shown in the map; it refers to a very strong tremor, overthrow of movable objects, fall of plaster, ringing of church bells, general panic and moderate to heavy damage of buildings. This structural damage was spread in a wide region of Himachal Pradesh and adjoining states of Uttarakhand, portions of Punjab, Haryana and Jammu and Kashmir. It encloses a large area which includes districts Bilaspur, Chamba, Hamirpur, Kangra, Kinnaur, Kullu, Lahaul & Spiti, Mandi, Shimla, Sirmaur, Solan and Una in HP. In Uttarakhand (Uttarkashi, Dehradun, Tehri Garhwal, Rudraprayag, Pauri Garhwal, Chamoli, Almora and Haridwar); in Punjab (Gurdaspur, Hoshiyarpur, Amritsar, Roopnagar, Kapurthala, Mohali, Nawashahar and Jalandhar); in Haryana (Panchkula, Ambala, Yamunagar and Kurukshetra); in Uttar Pradesh (Saharanpur, Muzzafarnagar, Bijnor and Meerut.) Isoseismals of the great Kangra earthquake of 1905 is shown in figure 2.1.

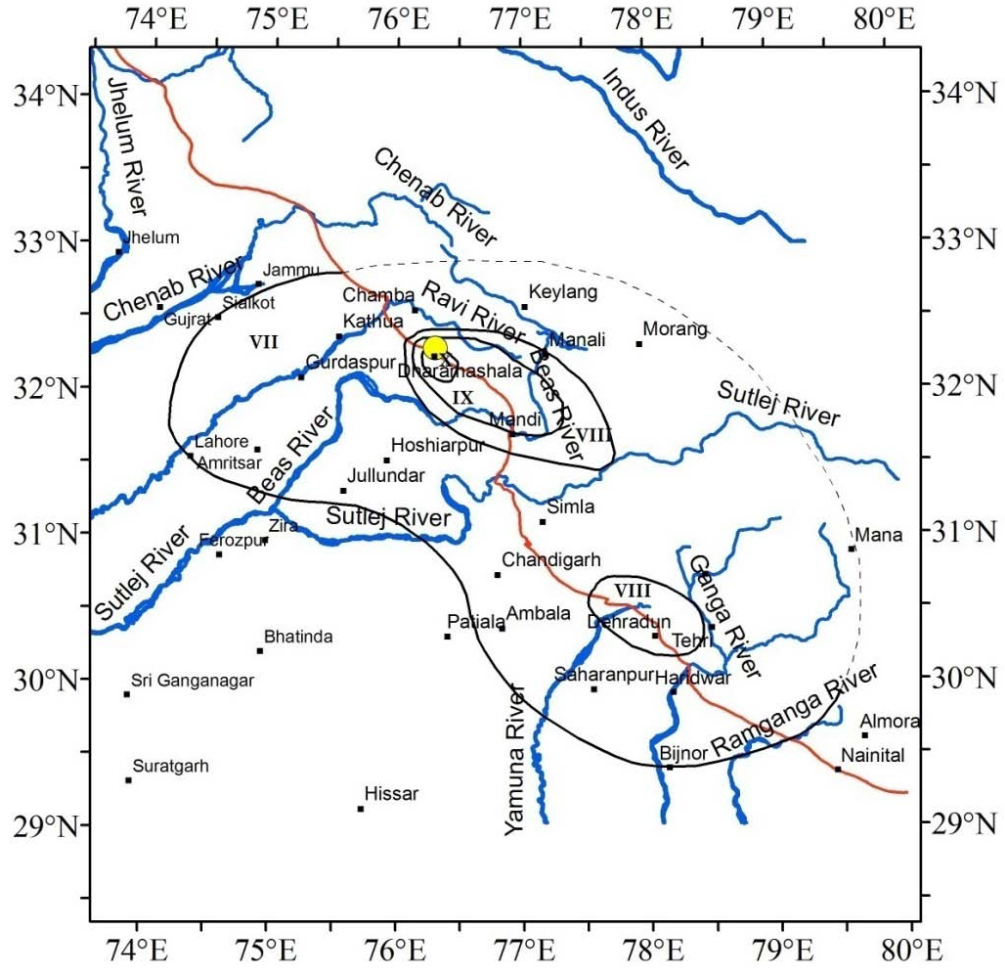


**Figure 2.1:** Isoseismals of the great Kangra earthquake of 1905, on RF scale, (after Middlemiss, 1910), epicenter of the great Kangra earthquake is shown by yellow circle. Rivers, place names and MBT (shown in red) are as per Narula *et al.* (2000).

## 2.2 Study Area

Seismic hazards described for this earthquake by Middlemiss (1910) such as landslides and fissures resulted in adverse consequences to society such as damage to buildings and loss of life. As extensive damage to built environment took place in the meizo-seismal and adjoining areas of this great earthquake, it is necessary to assess seismic hazard. Estimation of seismic hazard for this area is an urgent necessity in view of rapid techno economic development of the region and enormous increase in population. In view of this, the area around the great Kangra earthquake of 1905 was considered for this research work. The  $7^{\circ}$  by  $7^{\circ}$  area bound by coordinates longitude:

73°E to 80°E and latitude: 29°N to 36°N centered on the epicenter of the great Kangra earthquake of 1905 was considered, as shown in figures 2.2 (a) and (b).

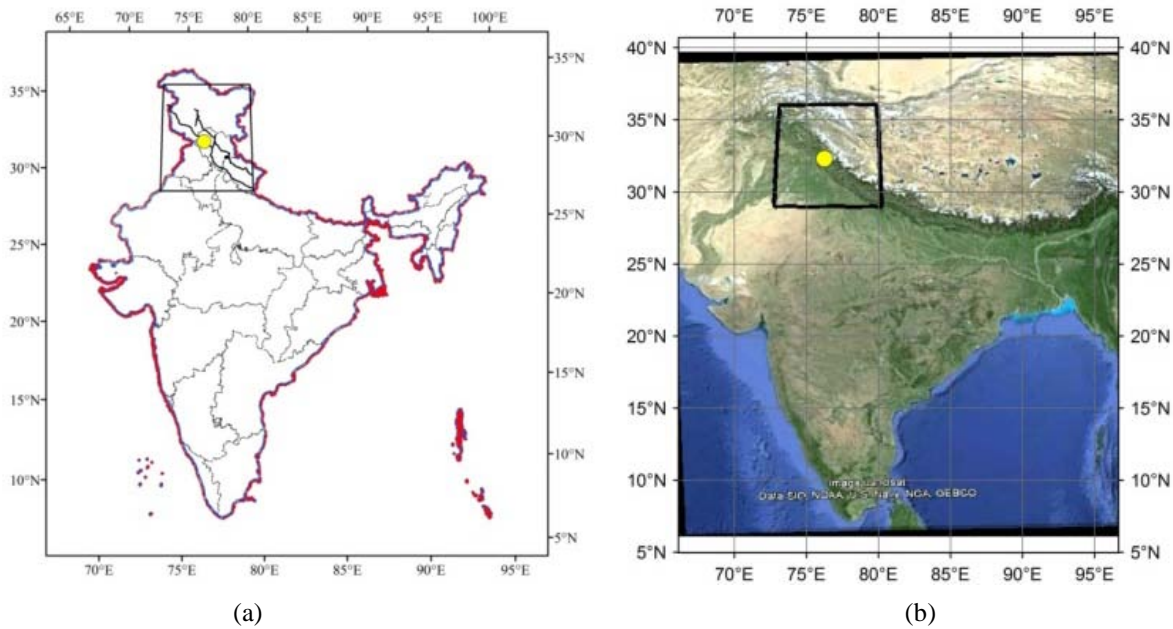


**Figure 2.2:** (a) Study area encompassed between latitude: 29°N to 36°N and longitude 73°E to 80°E, shown by box. MBT, MCT and the epicenter of great Kangra earthquake of 1905 shown by yellow circle. All boundaries are as per Survey of India, (2011) maps. (b) Study area shown by box with epicenter of great Kangra earthquake of 1905 at its center on Google earth map.

Study area comprises of Himachal Pradesh (HP) and Punjab totally and major parts of Jammu & Kashmir (J&K), Uttarakhand (UK), Uttar Pradesh (UP), Haryana and Rajasthan. It also includes parts of neighbouring countries like Pakistan, Afghanistan, China and Tibet.

The study area was divided into a grid of 0.5° by 0.5°, which resulted in 196 quadrangles in the Lambert conformal conical projection in the entire study area. Midpoint of every quadrangle was considered as a site for hazard assessment. A total of 196 sites were, therefore, considered within the study area as shown in figure 2.3. Out of 196 sites 152 are within India.

These sites were used for identification of seismically susceptible areas, in Chapter 4 and also for estimation of seismic hazard using deterministic and probabilistic approach, as given in Chapters 6 and Chapter 7. The site is also referred to as grid points at several places.



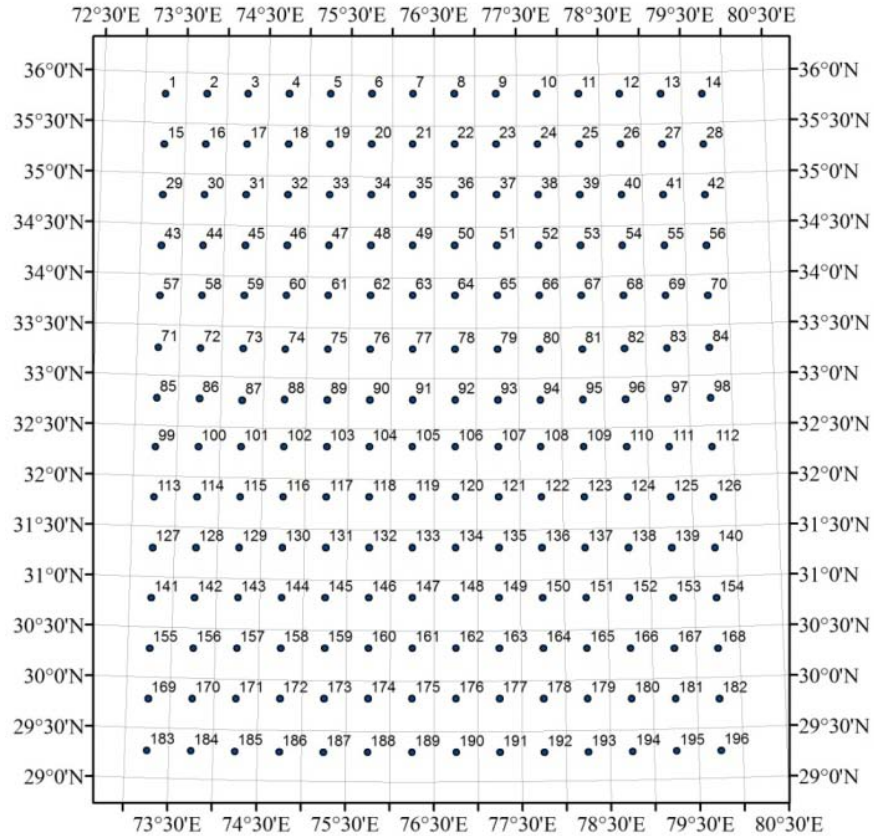


**Figure 2.3:** Study area divided into 196 quadrangles in the Lambert conformal conical projection. Midpoint of each was considered as a site for hazard assesment.

Besides the Great Kangra earthquake of 1905, the study area has witnessed several other damaging earthquakes. The Dharamshala earthquake of 26<sup>th</sup> April, 1986 occurred within the meizo-seismal area of the great Kangra earthquake of 1905. The Chamba earthquake of 22<sup>nd</sup> June, 1945 and the Kinnaur earthquake of 19<sup>th</sup> January, 1975 occurred in the Chamba and Kinnaur districts, respectively, of Himachal Pradesh. The Uttarkashi earthquake of 20<sup>th</sup> October, 1991 and the Chamoli earthquake of 29<sup>th</sup> March, 1999 occurred in the Uttarkashi and Chamoli districts, respectively, of Uttarakhand. Kashmir earthquake of 8<sup>th</sup> October, 2005 was a major destructive earthquake. Further details of these earthquakes are given in the following paragraphs. Besides these earthquakes, several other destructive and historical earthquakes were also reported in the region. Historical events with a large magnitude,  $M \geq 7.0$ , are of exceptional engineering significance. Some of the prominent historical earthquakes within the study area are the three earthquakes in the Srinagar-Baramula region: the 1552 earthquake (epicentre: 74.50°E and 34.00°N,  $M_L = 7.5$  IMD;  $M_W=7.5$ , this study), 26<sup>th</sup> June, 1828 earthquake (epicentre: 74.00°E and

34.00°N,  $M_L = 6.0$  IMD;  $M_W=6.0$ , this study) and the 30<sup>th</sup> May, 1885 earthquake (epicentre: 74.80°E and 34.10°N,  $M_L = 7.0$  IMD;  $M_W=7.0$ , this study). Details of these earthquakes are documented in Mukhopadhyay *et al.* (2015).

### ***Kashmir earthquake of 2005***

A hundred years after the great Kangra earthquake of 1905 a major destructive earthquake originated  $\approx 350$  km northwest of the Kangra earthquake, in the vicinity of the Main Boundary Thrust, in the Western Syntaxis. The Kashmir earthquake of 8<sup>th</sup> October, 2005 (epicentre: 73.64°E, 34.52°N; depth 7.9 km;  $m_b = 6.7$ ,  $M_s = 7.6$ , ISC;  $M_w = 7.5$ , USGS;  $M_L = 7.6$ , IMD;  $M_W=7.2$ , this study, fault plane solution: strike 338°, dip about 50° in the N-NE direction, EERI, 2005; northeast-dipping fault plane striking N133°E and a dip angle of 40°, Harvard), devastated Uri, Tangdhar, Baramula, Kupwara and adjoining areas in India and large parts of contiguous Pakistan. Maximum intensity assigned to this earthquake, on the basis of massive landslides, rock falls, mud slides and damage to the built environment was X+ on the MMI scale (EERI, 2005; Sinvhal *et al.* 2005; Sinvhal, 2012b).

### ***Uttarkashi earthquake of 1991***

The Uttarkashi earthquake of 20<sup>th</sup> October, 1991 (epicentre: 78.79°E, 30.77°N, depth 13.2 km, ISC,  $m_b = 6.4$ ,  $M_s = 6.9$ , ISC;  $M_w= 6.8$ , USGS;  $M_L = 6.6$ , IMD,  $M_W=6.8$ , this study, fault plane solution: strike 317°, dip 14°, HRV; strike 349°, dip 26°, Narula *et al.* 2000) occurred  $\approx 300$  km south east of the Kangra earthquake in the vicinity of Main Central Thrust (MCT). In this earthquake, 723 persons perished, thousands of people were injured and about 36,000 houses were partially or completely damaged. Maximum intensity observed was IX on MSK scale (GSI, 1992).

### ***Chamoli earthquake of 1999***

The Chamoli earthquake of 29<sup>th</sup> March, 1999 (epicentre: 79.42°E and 30.51°N, depth 22.9 km,  $M_L = 5.1$ , IMD;  $m_b = 5.4$ , USGS;  $m_b = 6.3$ ,  $M_s = 6.6$ , ISC;  $M_w = 6.7$ , this study; fault plane solution: strike 282°, dip 9°, USGS) occurred  $\approx 360$  km south east of the Kangra earthquake in the vicinity of Main Central Thrust. Maximum intensity observed was VIII on MSK scale (GSI, 2001). More than a 100 people died in this earthquake and more than 400 were injured.

### ***Kinnaur earthquake of 1975***

The Kinnaur earthquake on 19<sup>th</sup> January, 1975 (epicentre: 78.52°E and 32.50°N, depth 48 km,  $M_L = 6.8$ , IMD;  $m_b = 6.2$ ,  $M_w = 6.6$ , this study; fault plane solution: strike 360°, dip 50°, Molnar and Chen, 1983; plane I: strike N0°E, dip 31°E; plane II: strike N2°E, dip 59°W, Khattri et al., 1978) occurred  $\approx$  200 km north east of the Kangra earthquake in the vicinity of Kaurik fault system which is transverse to the MBT. Maximum intensity observed was IX on MMI scale (Singh *et al.* 1977). During this earthquake 60 persons lost their lives, a few hundred were severely injured and more than 2500 became homeless. Nearly 2000 houses suffered heavy damage. Landslides, rock falls snow avalanches, falling boulders and stones damaged or blocked the highways (Singh *et al.* 1977).

### ***Chamba earthquake of 1945***

The Chamba earthquake of 22<sup>nd</sup> June, 1945 (epicentre: 76.00°E and 32.50°N, depth 60 km,  $M_L = 6.5$ , IMD,  $M_w = 6.5$ , this study; fault plane solution: strike 349°, dip 26°, Narula *et al.* 2000) occurred  $\approx$  46 km north west of the Kangra earthquake in the vicinity of Main Boundary Thrust. Maximum intensity observed in this earthquake was VIII on MM scale (Narula *et al.* 2000).

### ***Dharamshala earthquake of 1986***

The Dharamshala earthquake of 26<sup>th</sup> April, 1986 (epicentre: 76.4°E, 32.1°N; depth 33 km;  $m_b = 5.5$ , USGS;  $M_L = 5.5$ , IMD;  $M_s = 5.2$ , ISC,  $M_w = 5.8$ , this study; fault plane solution: strike 153°, dip about 74°, Harvard; strike 143°, dip about 84°, Molnar and Lyon, 1989) occurred within the meizo-seismal area of the great Kangra earthquake of 1905, in the vicinity of Main Boundary Thrust (MBT). This earthquake took a toll of six human lives, caused considerable damage to buildings and resulted in several earth fissures and landslides (Arya *et al.* 1986). Maximum intensity observed was VII on MM scale (Narula *et al.* 2000).

## **2.3 Seismicity of the Study Area**

To assess seismic hazard of an area, a comprehensive seismicity catalog is essential for the study area, which contain source parameters such as: epicentral coordinates, time of occurrence and magnitude, for a time period as long as possible, i.e. from the earliest time to the present time. This data is not available in a single catalogue. Therefore various earthquake catalogues, from

different sources, were searched, accessed, selected, collected and subsequently studied for chronological continuity, magnitude scales and presence of foreshocks and aftershocks. These included several catalogues, viz. Oldham 1883, Indian Meteorological Department, (IMD), Indian Society of Earthquake Technology (ISET), United States Geological Survey, (USGS), International Seismological Centre (ISC), Tandon and Srivastava (1974), Chandra (1977), Rao and Rao (1984) and Srivastava and Ramachandran (1983), etc. Therefore, relevant data were sourced from several earthquake catalogues. These included India Meteorological Department (IMD), United States Geological Survey (USGS) and International Seismological Center (ISC). Data in these catalogues was studied for the space window defined by longitude:  $72^{\circ}\text{E}$ - $87^{\circ}\text{E}$ , latitude:  $23^{\circ}\text{N}$ - $37^{\circ}\text{N}$ .

Data in the India Meteorological Department (IMD) catalogue, for India and contiguous regions, contains 2743 earthquakes for the period between 1552 and 2009 AD, for earthquakes with magnitude ( $M_L$ , local magnitude) ranging from  $4.0 \leq M_L \leq 8.0$ . Origin time for each earthquake was given in Universal Time Coordinate (UTC). International Seismological Centre (ISC) provides instrumental data for the entire globe, from 1964 onwards. At the time of compilation of the catalogue for the study area in 2012, the ISC data was available upto the year 2010. Therefore, the catalogue downloaded from the ISC website was for the period 1964 – 2010. Of the 6339 earthquakes in this time and space window all earthquakes were assigned magnitude  $m_b$  and some were assigned  $M_s$ . Magnitude ranged from  $3.0 \leq m_b \leq 6.7$  and  $3.6 \leq M_s \leq 7$ . Since the data is instrumental, therefore, this catalogue furnishes the most reliable epicentral data. This data was downloaded from the website <http://www.isc.ac.uk/iscbulletin/search/bulletin>. Earthquake data for the period 2011-2012 was considered and downloaded from the National Earthquake Information Center (NEIC), USGS database. 41 earthquakes emerged which were downloaded from the website <http://earthquake.usgs.gov/earthquakes/eqarchives>. The magnitude ranged from  $4.0 \leq m_b \leq 5.1$ . This website provides a search of earthquake epicenters from within a region specified by the user for the most recent data. Salient features of these catalogues, including duration, number of events, magnitude scale, magnitude range and coordinates of area covered in each catalogue, are listed in table 2.2. Total number of events considered from these three catalogues was 9123.

**Table 2.2:** Salient features of various catalogues studied for the study area between latitude: 23° N-37°N; longitude: 72° E- 87°E.

S. No.	Catalogue	Time Period	Magnitude		No. of Events
			Scale	Range	
1	IMD	1552-2009	$M_L$	$4.0 \leq M_L \leq 8.0$	2743
2	ISC	1964-2010	$M_s, m_b$	$3.0 \leq m_b \leq 6.7$ $3.6 \leq M_s \leq 7$	6339
3	USGS (NEIC)	2011-2012	$m_b$	$4.0 \leq m_b \leq 5.1$	41
<b>Total no. of events</b>					<b>9123</b>

### 2.3.1 Data treatment

On the basis of the relevant data base, i.e., catalogues listed in table 2.2, a new catalogue was compiled for the study area, to meet the requirements of the hazard analysis. This data was prepared in several steps, starting with merging of the various catalogues, then homogenization of the various magnitudes to a single scale and then removal of aftershock and foreshock data, i.e. declustering. Seismicity data was compiled for a large area of 15° by 14° (longitude: 72°E-87°E, latitude: 23°N-37°N) and it was processed for merging, homogenization and declustering. The merged, homogenized and declustered data was then truncated for the 7° by 7° study area and all descriptions, tables and figures shown here are for this area.

#### 2.3.1.1 Merging of catalogues

As data in different catalogues were for different time durations and a catalogue that was continuous in time was required, therefore time wise merging of catalogues was required. Merging of various catalogues is an important step to obtain a working catalogue, which was subsequently used for making seismicity and seismo tectonic maps for hazard assessment. An additional purpose of merging was to remove duplicate events from the merged catalogue. The IMD catalogue was considered for historical seismicity in the area for the period 1552 to 1963. In this study 89 earthquakes emerged from the IMD catalogue. The ISC catalogue was considered for instrumental seismicity, for the period between 1964 and 2010, which yielded the largest number of events, 2619. The USGS (NEIC) catalogue was considered for the period 2010-2012, in which 41 recent events emerged. Table 2.3 shows salient features of the merged catalogue which includes the time span, number of events, magnitude scale and coordinates of area covered in each catalogue. The merged catalogue consisted of 2749 events within the study area defined by coordinates longitude

73°E - 80°E and latitude 29°N - 36°N and for duration 1552-2012. Magnitudes ranged from 3 and above and were on different scales, such as  $m_b$  (body wave magnitude),  $M_s$  (surface wave magnitude) and  $M_L$  (local magnitude). However, for hazard assessment it is preferable that all magnitudes are homogenized to a single scale.

**Table 2.3:** Salient features of merged earthquake catalogues for the study area between latitude: 29°N -36°N and longitude 73°E - 80°E.

S. No.	Catalogue	Time Period	Magnitude		No. of Events Considered
			Scale	Range	
1	IMD	1552-1963	$M_L$	$4.0 \leq M_L \leq 8.0$	89
2	ISC	1964-2010	$M_s, m_b$	$3.0 \leq m_b \leq 6.7$ $3.6 \leq M_s \leq 7$	2619
3	USGS (NEIC)	2011-2012	$m_b$	$4.0 \leq m_b \leq 5.1$	41
<b>Total no. of events</b>					<b>2749</b>

### 2.3.1.2 Homogenization of catalogues

Converting from different magnitude scales to one particular magnitude scale is known as homogenization of the earthquake catalogue (Reiter, 1990). For hazard assessment and for recognition of any useful patterns, it is necessary that all magnitudes are homogenized to a single scale. Therefore, the merged catalogue was homogenized and all magnitudes were converted to a desirable magnitude scale such as moment magnitude ( $M_w$ ). This has the advantage that moment magnitude does not depend on ground shaking levels for describing the size of very large earthquakes; rather it depends on seismic moment, which is a direct measure of factors that produce rupture along a fault. However, for other magnitude scales, the measured ground shaking characteristics become less sensitive to the size of earthquake because as the total amount of energy released during the earthquake increases, ground shaking characteristics do not necessarily increase at the same rate (Hanks and Kanamori, 1979). For assessment of seismic hazard use of moment magnitude is more appropriate.

Ristau and Cassidy (2005) considered  $M_L$  equivalent to  $M_w$ , for continental crust for magnitude  $M_L \geq 3.8$ , therefore  $M_L$  in IMD catalogue (magnitude range  $4.0 \leq M_L \leq 8.0$ ) was considered equivalent to  $M_w$ . In ISC and USGS (NEIC) catalogues  $m_b$  was specified for all events.

General orthogonal regression (GOR) relation (Wason *et al.* 2012) was used to convert  $m_b$  to  $M_w$ . Relation for converting  $m_b$  to  $M_w$  is as given by equation (2.1):

$$M_w = 1.17m_{b,obs} - 0.74 \quad (2.1)$$

where,  $m_{b,obs}$  is observed body wave magnitude. These conversions were used to modify magnitude in the merged catalogue so that all earthquakes have the same magnitude scale,  $M_w$ . These conversions result in a homogenized catalogue and were in a state where  $M_w$  could be considered for further computations. The merged and homogenized catalogue consists of main shocks, foreshocks and aftershocks and has 2749 events. The next step was to decluster the catalogue.

### **2.3.1.3 Declustering of catalogue**

Seismicity in a region can be considered to consist of two parts: main shocks, i.e. earthquakes that are independent and are mostly caused by tectonic loading; and dependent events i.e. earthquakes that depend on the main shock, like after-shocks and foreshocks. Dependent events occur as seismicity clusters. Seismicity declustering is the process by which earthquakes in a catalogue are separated into two classes, i.e., independent and dependent events, or, main shocks are separated from foreshocks and aftershocks. After merging and homogenization, the earthquake catalogue was subjected to the process of declustering. Two independent methods of declustering were tested and were applied on the merged and homogenized catalogue. These are 1) Gardner and Knopoff (1974) method also known as window method and 2) Reasenber (1985) method also known as cluster method. Declustering of the homogenized catalogue was achieved using the MATLAB tool Z-map, which is a set of tools designed to analyze catalogue data and to detect seismicity rate changes prior to major earthquakes. It is driven by a graphical user interface (GUI) and is available online, in free user domain, on the website <http://mercalli.ethz.ch/~eberhard/zmap.zip>.

#### ***Declustering by Gardner and Knopoff (1974) method***

Gardner and Knopoff's (1974) procedure for identifying aftershocks within seismicity catalogs, known as the window method, can be described briefly as follows: if an earthquake occurred within a specific time interval  $T(M_w)$  and at specific distance interval  $L(M_w)$ , it is identified as an aftershock. Same is applicable for foreshocks i.e. if any large earthquake occurs

later, the foreshock the previous shock as a foreshock. The time-space windows are reset accordingly.

An approximation of space and time window sizes is shown in equations (2.2) and (2.3) respectively and in table 2.4. As an example any earthquake within 510 days after a magnitude  $M_w = 6.0$  earthquake and within epicentral distance of 54 km was identified as an aftershock.

$$\text{Distance, } L(M_w) = 10^{0.1238-M+0.983} \text{ (km);} \quad (2.2)$$

$$\text{Time, } T(M_w) = \left. \begin{array}{l} 10^{0.032*M+2.7389}, \\ 10^{0.5409*M-0.547}, \end{array} \right\} \begin{array}{l} \text{if } M > 6.5 \\ \text{else} \end{array} \text{ (days)} \quad (2.3)$$

After declustering, of the 2749 events in the merged and homogenized catalogue, 1172 events emerged as the main shock.

### ***Declustering by Reasenber (1985) method***

A method for identifying aftershocks was introduced by Reasenber (1985). This method is also known as the cluster method. Reasenber's (1985) algorithm allowed linking up aftershock triggering within an earthquake cluster. This algorithm was based on a combined effect of time, space, magnitude and probability of dependent events, such as aftershocks and foreshocks. These values can be chosen according to the characteristics of the merged catalogue. These values are given in table 2.5. According to this algorithm if B is the aftershock of A and C the aftershock of B, then all A, B and C are considered to belong to one common cluster. Within a cluster the largest magnitude is kept as cluster's main shock. The space-time window for identification of an aftershock is based on Omori's law for its temporal dependence. This means that the time for the next aftershock is proportional to the time of main shock. After declustering, of the 2749 events in the homogenized catalogue, 1089 events emerged as the main shock. The resulting catalogue has data pertaining to main shocks only.

After applying the above two methods for declustering, the Gardner and Knopoff (1974) method was preferred over the Reasenber (1985) method due to the following reasons: Reasenber method (1985) allowed removal of dependent events of magnitude  $M \geq 4$ , whereas



**Table 2.4:** Time and space windows for identification of aftershocks for an earthquake of a given magnitude  $M$ , where  $L$  is estimated distance interval and  $T$  is estimated time interval, (after Gardner and Knopoff, 1974).

S. No.	M	L (km)	T (days)
1	2.5	19.5	6
2	3.0	22.5	11.5
3	3.5	26	22
4	4.0	30	42
5	4.5	35	83
6	5.0	40	155
7	5.5	47	290
8	6.0	54	510
9	6.5	61	790
10	7.0	70	915
11	7.5	81	960
12	8.0	94.0	985

**Table 2.5:** Reasenber parameters (after Reasenber, 1985) for declustering of an earthquake catalogue.  $\tau_{\min}$ (days) is minimum value of look-ahead time for building clusters when the event is not clustered;  $\tau_{\max}$  (days) is maximum value of look ahead time for building clusters;  $P1$  is the probability of detecting the next clustered event used to compute the look ahead time;  $x_k$  is increase in the lower cut-off magnitude during clusters;  $x_{\text{meff}} = x_{\text{meff}} + x_k M$ , (where  $M$  is the magnitude of the largest earthquake) is effective lower magnitude cut off for catalogue; and  $r_{\text{fact}}$  is number of crack radii surrounding each earthquake within new events considered to be part of the cluster.

S. No.	Parameter	Standard	Min.	Max.
1	$\tau_{\min}$ (days)	1	0.5	2.5
2	$\tau_{\max}$ (days)	10	3	15
3	$P1$	0.95	0.9	0.99
4	$x_k$	0.5	0	1
5	$x_{\text{meff}}$	1.5	1.5	1.8
6	$r_{\text{fact}}$	10	5	20

Gardner and Knopoff (1974) method allowed declustering of lower magnitude ranges too. The merged and homogenized catalogue in this study has  $M_w \geq 3.5$ . Moreover, the Gardner and Knopoff (1974) method is a widely used and quoted method (Kagan and Knopoff, 1978; Borok *et al.* 1980; Rydelek and Sacks, 1989; Borok and Kossobokov, 1990; Knopoff *et al.* 1996; Papaioannou and Papazachos, 2000; Musson *et al.* 2005; Pailoplee *et al.* 2009; Menon *et al.* 2010; NDMA, 2011; Rout *et al.* 2015; Markušić *et al.* 2016).

### 2.3.2 MHD catalogue

After merging three different earthquake catalogues, homogenization of magnitudes and declustering and truncating the data set to a  $7^\circ$  by  $7^\circ$  area, for space defined by longitude:  $73^\circ\text{E}$  to  $80^\circ\text{E}$  and latitude:  $29^\circ\text{N}$  to  $36^\circ\text{N}$ , the data set which emerged was named as the MHD earthquake catalogue. The MHD catalogue consists of 1172 main events, of magnitude range  $3.5 \leq M_w \leq 8.0$ , for the time period 1552-2012 and . The MHD catalogue was compiled in the year 2012, therefore, the data base terminates in October 2012. An example of a page from the MHD catalogue is shown in table 2.6. Salient features of MHD catalogue are given in table 2.7. Seismicity in the study area as per MHD catalogue is shown in figure 2.4.

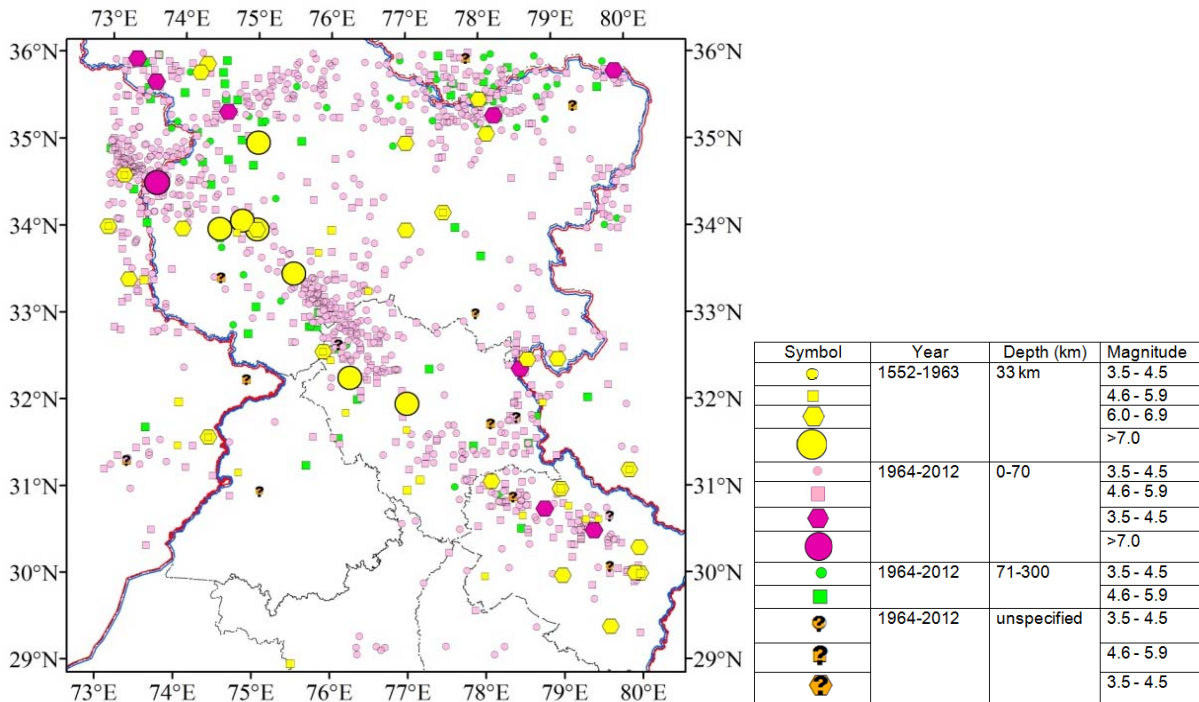


**Figure 2.4:** Seismicity of the study area as per MHD catalogue for the space defined by longitude:  $73^\circ\text{E}$  to  $80^\circ\text{E}$  and latitude:  $29^\circ\text{N}$  to  $36^\circ\text{N}$ , time period 1552-2012 and magnitude range  $3.5 \leq M_w \leq 8.0$ .

**Table 2.6:** A page from MHD catalogue, arranged chronologically. **Y:** Year; **M:** Month; **D:** Day; **H:** Hour; **Mn:** Min; **S:** seconds; **Long:** longitude ( $^{\circ}$ E) ; **lat:** latitude ( $^{\circ}$ N); **Dep:** Depth (km); **Source:** catalogue source; **Remarks:** A: description in text, B: description available in papers, C: fault plain solutions available.

S. No.	Y	M	D	H	Mn	S	Long	Lat	M <sub>w</sub>	Dep	Source	Remarks		
												A	B	C
1	1552	-	-	-	-	-	74.50	34.00	7.5	-	IMD	✓	✓	
2	1554	2	1	-	-	-	75.00	35.00	7.7	-	IMD			
3	1662	-	-	-	-	-	75.00	34.00	7.5	-	IMD	✓	✓	
4	1669	6	4	-	-	-	73.30	33.40	6.5	-	IMD			
5	1669	6	22	-	-	-	77.00	35.00	6.5	-	IMD			
6	1735	-	-	-	-	-	75.00	34.00	7.5	-	IMD	✓	✓	
7	1778	-	-	-	-	-	75.00	34.00	7.7	-	IMD	✓	✓	
8	1784	-	-	-	-	-	75.00	34.00	7.3	-	IMD	✓	✓	
9	1803	-	-	-	-	-	75.00	34.00	7.0	-	IMD	✓	✓	
10	1803	-	-	-	-	-	80.00	30.00	6.5	-	IMD			
11	1809	-	-	-	-	-	79.00	30.00	6.0	-	IMD			
12	1809	-	-	-	-	-	78.50	30.70	5.5	-	IMD			
13	1816	5	26	-	-	-	80.00	30.00	6.5	-	IMD			
14	1827	9	24	-	-	-	74.40	31.60	6.5	-	IMD			
15	1827	9	1	-	-	-	76.00	32.50	5.5	-	IMD			
16	1828	6	6	-	-	-	74.00	34.00	6.0	-	IMD			
17	1842	3	5	-	-	-	78.00	30.00	5.5	-	IMD			
18	1843	4	11	-	-	-	80.00	30.00	5.0	-	IMD			
19	1851	1	21	-	-	-	74.00	32.00	5.0	-	IMD			
20	1852	1	24	-	-	-	73.00	34.00	6.0	-	IMD			
21	1856	4	7	-	-	-	77.00	31.00	5.0	-	IMD			
22	1858	8	11	-	-	-	77.17	31.12	5.0	-	IMD			
23	1863	-	-	-	-	-	75.50	33.50	7.0	-	IMD			
24	1871	5	22	-	-	-	74.30	35.90	6.0	-	IMD			
25	1871	4	1	-	-	-	76.00	34.00	5.0	-	IMD			
26	1875	12	12	-	-	-	74.40	31.60	5.5	-	IMD			
27	1883	5	30	-	-	-	79.60	29.40	6.0	-	IMD			
28	1884	5	30	-	-	-	75.50	33.50	7.3	-	IMD			
29	1885	5	30	-	-	-	74.80	34.10	7.0	-	IMD			
30	1885	6	6	-	-	-	75.00	34.00	6.5	-	IMD			
31	1902	6	16	-	-	-	79.00	31.00	6.0	-	IMD			
32	1905	4	4	00	50	-	76.25	32.30	8.0	-	IMD	✓	✓	
33	1906	2	28	-	-	-	77.00	32.00	7.0	-	IMD			
34	1906	6	13	-	-	-	79.00	31.00	6.0	-	IMD			
35	1908	12	11	-	-	-	79.00	31.00	5.0	-	IMD			

**Table 2.7:** Number of events in different magnitude ranges for MHD earthquake catalogue.

S.No.	Magnitude range	Number of events
1.	> 7.0	14
2.	6.0 - 6.9	31
3.	4.5- 5.9	492
4.	3.5 - 4.4	635
		<b>Total=1172</b>

Of the 1172 earthquakes in the MHD catalogue, 31 events were in the magnitude range  $6.0 \leq M_w \leq 6.9$  and 14 events had a larger magnitude,  $M_w \geq 7.0$ , i.e., **45** events in the MHD catalogue are of exceptional engineering significance. It is interesting to note that more than half of these, 24, lie within a narrow belt defined by the area between the MBT and the MCT and of these 12 have  $M_w \geq 7.0$ . The details (origin time, epicentre, magnitude and depth) of all the above 24 earthquakes are given in table 2.8.

Those mentioned at serial numbers 2, 3, 4, 5, 6 and 15 have the same epicentral coordinates and are spread over a time frame of 1662 to 1885 and were assigned different magnitudes by IMD. This cluster of events, named as cluster **1**, is in the Srinagar-Baramula region. The earthquake of 1778, with the highest magnitude in this cluster,  $M_w=7.7$ , was considered for hazard assessment in chapter 6. Similarly, several other clusters were identified in table 2.8. Cluster **2**, comprises of epicenters at serial numbers 11 and 13, with the higher magnitude,  $M_w=7.3$ , for the 1884 event. This cluster is approximately 70 km south east of cluster 1 and is in the vicinity of Kishtwar Fault. Cluster **3** comprises of epicenters at serial numbers 18 and 19, with the higher magnitude,  $M_w=6.5$ , for the 1945 event and is clustered around Chamba region. Cluster **4** comprises of epicentres at serial numbers 7 and 9 and both were assigned  $M_w=6.5$  by IMD. This cluster is in Bageshwar region of Uttarakhand.

### **2.3.2.1 Completeness of MHD earthquake catalogue**

Analysis of available seismicity data set to assess the nature and degree of its completeness is an important step in any seismicity analysis. Therefore, in seismicity study where statistical assumptions have a major role, it becomes essential to assess the completeness of the dataset. Even though historical seismicity is sparse and most of the time is quite inaccurate in terms of magnitude and epicentral location, yet it is necessarily used in seismic hazard assessment.

**Table 2.8:** List of earthquakes with  $M_w \geq 6.0$ , in the environs of Main Boundary Thrust (MBT) and Main Central Thrust (MCT), chronologically arranged. Cluster 1: Srinagar Baramula region (6 earthquakes), Cluster 2: West of Kishtwar fault (2 earthquakes), Cluster 3: Chamba region (2 earthquakes), Cluster 4: Bageshwar Region (2 earthquakes). \* indicates earthquake considered for hazard assessment in DSHA Chapter 6.

S. No.	YR	MM	DD	HR	MN	Long	Lat	Mag	Depth	Source	Cluster
1 *	1552	-	-	0.00	0.00	74.50	34.00	7.50	0.00	IMD	
2	1662	-	-	0.00	0.00	75.00	34.00	7.50	0.00	IMD	Cluster-1
3	1735	-	-	0.00	0.00	75.00	34.00	7.50	0.00	IMD	Cluster-1
4 *	1778	-	-	0.00	0.00	75.00	34.00	7.70	0.00	IMD	Cluster-1
5	1784	-	-	0.00	0.00	75.00	34.00	7.30	0.00	IMD	Cluster-1
6	1803	-	-	0.00	0.00	75.00	34.00	7.00	0.00	IMD	Cluster-1
7	1803	-	-	0.00	0.00	80.00	30.00	6.50	0.00	IMD	Cluster-4
8 *	1809	-	-	0.00	0.00	79.00	30.00	6.00	0.00	IMD	
9 *	1816	5	26	0.00	0.00	80.00	30.00	6.50	0.00	IMD	Cluster-4
10*	1828	6	6	0.00	0.00	74.00	34.00	6.00	0.00	IMD	
11	1863	1	1	0.00	0.00	75.50	33.50	7.00	0.00	IMD	Cluster-2
12*	1883	5	30	0.00	0.00	79.60	29.40	6.00	0.00	IMD	
13*	1884	5	30	0.00	0.00	75.50	33.50	7.30	0.00	IMD	Cluster-2
14*	1885	5	30	0.00	0.00	74.80	34.10	7.00	0.00	IMD	
15	1885	6	6	0.00	0.00	75.00	34.00	6.50	0.00	IMD	Cluster-1
16*	1905	4	4	0.00	50.00	76.25	32.30	8.00	0.00	IMD	
17*	1906	2	28	0.00	0.00	77.00	32.00	7.00	0.00	IMD	
18*	1945	6	22	18.00	0.00	75.90	32.60	6.50	0.00	IMD	Cluster-3
19	1947	7	10	10.00	19.00	75.90	32.60	6.20	0.00	IMD	Cluster-3
20*	1955	3	12	16.00	42.00	73.20	34.60	6.00	0.00	IMD	
21*	1958	12	28	5.00	34.00	79.94	30.01	6.30	0.00	IMD	
22*	1991	10	19	9.00	23.00	78.79	30.77	6.80	13.20	ISC	
23*	1999	3	28	7.00	5.00	79.42	30.51	6.70	22.90	ISC	
24*	2005	10	8	3.00	50.00	73.64	34.52	7.20	7.90	ISC	

Instrumental records of earthquakes are often too short in time and reliable ones exist only after 1964. Most catalogs are heterogeneous in terms of magnitude and inconsistent with respect to time.

Stepp's (1972) method has been used in this study to analyze the time completeness of the MHD catalogue. In order to analyze the nature of the completeness of earthquake data set, the dataset is first grouped into different magnitude classes and then each magnitude class is modeled as a point process in time. In this method the sample mean is inversely proportional to the number

of observations in the sample. Rate of occurrence as a function of time interval for different magnitude classes was calculated. To obtain an estimate of the sample mean it was assumed that the earthquake sequences can be modeled as a Poisson distribution. Table 2.9 shows the rate of occurrence of earthquakes of different magnitudes as a function of time. Rate is given as  $N/T$ , where  $N$  is the cumulative number of earthquakes in time interval  $T$ . This data is then used to compute standard deviation of the estimates of mean, as given in table 2.10, using equation:  $\sigma_\lambda = (\lambda/T)^{1/2}$ , where  $T$  is the time interval,  $\lambda$  is the mean rate per unit time interval and is given as :  $\lambda = \left(\frac{1}{2}\right) \sum_{i=1}^n k_i$ , where,  $k_1, k_2, \dots, k_n$  are the number of earthquakes per unit time interval. The standard deviation of the mean rate as a function of sample period is plotted, along with nearly tangent lines with respect to curve of cumulative number of earthquakes, with slopes  $1/\sqrt{T}$  and is shown in figure 2.5. This indicated the period up to which a particular magnitude range may be taken to be complete. The completeness period for different magnitude ranges were estimated as follows:  $\leq 3.5$  for 32 years, 3.6-4.0 for 52 years, 4.1-4.5 for 52 years, 4.6 to 5.0 for 60 years, 5.1 to 5.5 for 92 years, 5.6 - 6.0 for 112 years and  $\geq 6.1$  for 232 years.

**Table 2.9:** Rate of earthquake occurrence of different magnitude ranges ( $N/T$ ) and time intervals for computing time completeness of MHD catalogue, where  $N$  is the cumulative number of earthquakes in time interval  $T$ .

Time period	Time interval (years)	Magnitude ( $M_w$ )													
		< 3.5		3.6-4.0		4.1-4.5		4.6-5.0		5.1-5.5		5.6-6.0		> 6.1	
		N	N/T	N	N/T	N	N/T	N	N/T	N	N/T	N	N/T	N	N/T
2001-2012	12	5	0.42	85	7.08	290	24.17	74	6.17	15	1.25	6	0.50	1	0.08
1991-2012	22	9	0.41	124	5.64	441	20.05	165	7.50	23	1.05	8	0.36	4	0.18
1981-2012	32	12	0.38	125	3.91	472	14.75	275	8.59	34	1.06	12	0.38	5	0.16
1971-2012	42	14	0.33	127	3.02	486	11.57	346	8.24	63	1.50	16	0.38	8	0.19
1961-2012	52	15	0.29	128	2.46	489	9.40	371	7.13	82	1.58	18	0.35	8	0.15
1951-2012	62	15	0.24	128	2.06	489	7.89	371	5.98	84	1.35	20	0.32	10	0.16
1941-2012	72	15	0.21	128	1.78	489	6.79	371	5.15	86	1.19	23	0.32	13	0.18
1931-2012	82	15	0.18	128	1.56	489	5.96	372	4.54	88	1.07	24	0.29	14	0.17
1921-2012	92	15	0.16	128	1.39	489	5.32	372	4.04	92	1.00	24	0.26	15	0.16
1911-2012	102	15	0.15	128	1.25	489	4.79	372	3.65	92	0.90	25	0.25	15	0.15
1901-	112	15	0.13	128	1.14	489	4.37	373	3.33	92	0.82	27	0.24	18	0.16

Time period	Time interval (years)	Magnitude ( $M_w$ )													
		< 3.5		3.6-4.0		4.1-4.5		4.6-5.0		5.1-5.5		5.6-6.0		> 6.1	
		N	N/T	N	N/T	N	N/T	N	N/T	N	N/T	N	N/T	N	N/T
2012															
1891-2012	122	15	0.12	128	1.05	489	4.01	373	3.06	92	0.75	27	0.22	18	0.15
1881-2012	132	15	0.11	128	0.97	489	3.70	373	2.83	92	0.70	28	0.21	21	0.16
1871-2012	142	15	0.11	128	0.90	489	3.44	374	2.63	93	0.65	29	0.20	21	0.15
1811-2012	202	15	0.07	128	0.63	489	2.42	378	1.87	95	0.47	31	0.15	24	0.12
1711-2012	302	15	0.05	128	0.42	489	1.62	378	1.25	96	0.32	32	0.11	29	0.10
1611-2012	402	15	0.04	128	0.32	489	1.22	378	0.94	96	0.24	32	0.08	32	0.08
1552-2012	461	15	0.03	128	0.28	489	1.06	378	0.82	96	0.21	32	0.07	34	0.07

Magnitude of completeness,  $M_c$ , is defined as the lowest magnitude at which all events in a space–time domain are detected. Magnitude of completeness ( $M_c$ ) for the MHD catalogue was computed using maximum curvature method (Wyss *et al.* 1999; Wiemer and Wyss, 2000). For calculating magnitude of completeness of the MHD catalogue cumulative number of earthquakes versus magnitude was plotted. Figure 2.6 shows the Frequency Magnitude Distribution (FMD) of earthquake of MHD catalogue for the study area. The magnitude of completeness for the entire MHD catalogue was estimated as  $M_w = 4.3$ . However, magnitude in the MHD catalogue ranges between 3.5 and 8.0 and magnitudes lower than the magnitude of completeness,  $M_w = 4.3$ , were retained in this study as these were considered as a discriminant feature in subsequent analysis.

### 2.3.2.2 Use of MHD catalogues in this research work

MHD earthquake catalogue was prepared for carrying out various analyses such as identification of susceptible areas, segmentation of longer lineaments and hazard assessment. This catalogue contained 1172 earthquakes of magnitude  $M_w = 3.5$  and above for the time span 1552-2012.

**Table 2.10:** Standard deviation,  $\sigma$ , of the estimates of mean recurrence rate per year, used in equation,  $\sigma_\lambda = (\lambda/T)^{1/2}$ , where  $\lambda$  is the mean rate per unit time interval, N is the cumulative number of earthquakes in time interval T.

Time interval (years)	Magnitude ( $M_w$ )													
	< 3.5		3.6-4.0		4.1-4.5		4.6-5.0		5.1-5.5		5.6-6.0		> 6.1	
	N/T	$\sigma$	N/T	$\sigma$	N/T	$\sigma$	N/T	$\sigma$	N/T	$\sigma$	N/T	$\sigma$	N/T	$\Sigma$
12	0.42	0.19	7.08	0.77	24.17	1.42	6.17	0.72	1.25	0.32	0.50	0.20	0.08	0.08
22	0.41	0.14	5.64	0.51	20.05	0.95	7.50	0.58	1.05	0.22	0.36	0.13	0.18	0.09
32	0.38	0.11	3.91	0.35	14.75	0.68	8.59	0.52	1.06	0.18	0.38	0.11	0.16	0.07
42	0.33	0.09	3.02	0.27	11.57	0.52	8.24	0.44	1.50	0.19	0.38	0.10	0.19	0.07
52	0.29	0.07	2.46	0.22	9.40	0.43	7.13	0.37	1.58	0.17	0.35	0.08	0.15	0.05
62	0.24	0.06	2.06	0.18	7.89	0.36	5.98	0.31	1.35	0.15	0.32	0.07	0.16	0.05
72	0.21	0.05	1.78	0.16	6.79	0.31	5.15	0.27	1.19	0.13	0.32	0.07	0.18	0.05
82	0.18	0.05	1.56	0.14	5.96	0.27	4.54	0.24	1.07	0.11	0.29	0.06	0.17	0.05
92	0.16	0.04	1.39	0.12	5.32	0.24	4.04	0.21	1.00	0.10	0.26	0.05	0.16	0.04
102	0.15	0.04	1.25	0.11	4.79	0.22	3.65	0.19	0.90	0.09	0.25	0.05	0.15	0.04
112	0.13	0.03	1.14	0.10	4.37	0.20	3.33	0.17	0.82	0.09	0.24	0.05	0.16	0.04
122	0.12	0.03	1.05	0.09	4.01	0.18	3.06	0.16	0.75	0.08	0.22	0.04	0.15	0.03
132	0.11	0.03	0.97	0.09	3.70	0.17	2.83	0.15	0.70	0.07	0.21	0.04	0.16	0.03
142	0.11	0.03	0.90	0.08	3.44	0.16	2.63	0.14	0.65	0.07	0.20	0.04	0.15	0.03
202	0.07	0.02	0.63	0.06	2.42	0.11	1.87	0.10	0.47	0.05	0.15	0.03	0.12	0.02
302	0.05	0.01	0.42	0.04	1.62	0.07	1.25	0.06	0.32	0.03	0.11	0.02	0.10	0.02
402	0.04	0.01	0.32	0.03	1.22	0.06	0.94	0.05	0.24	0.02	0.08	0.01	0.08	0.01
461	0.03	0.01	0.28	0.02	1.06	0.05	0.82	0.04	0.21	0.02	0.07	0.01	0.07	0.01



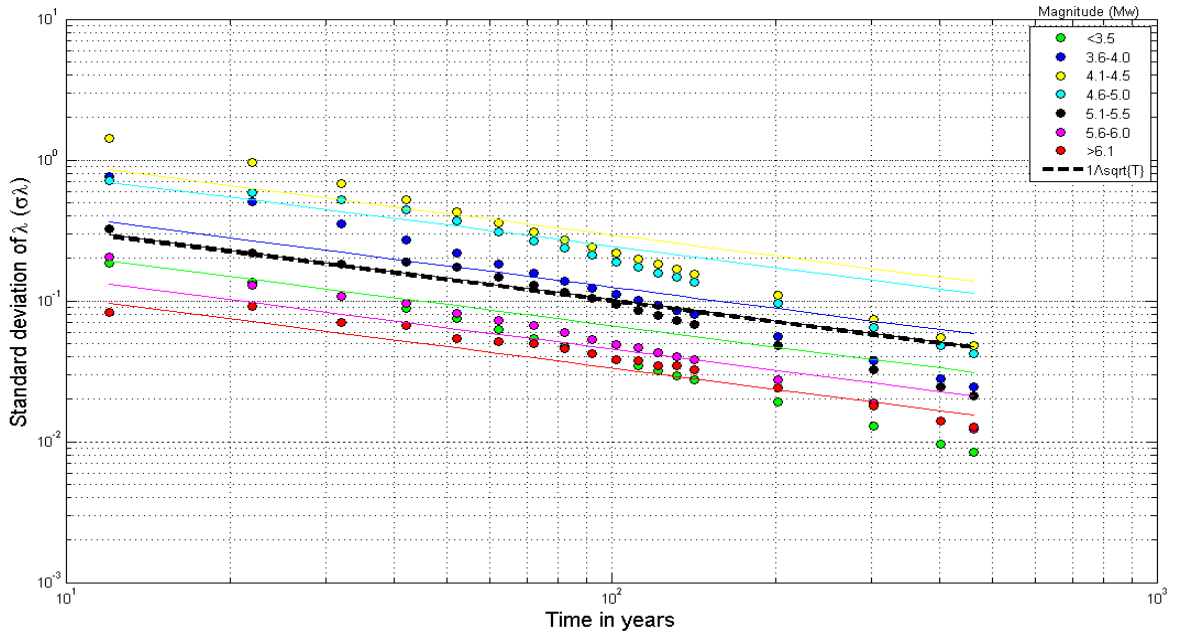


**Figure 2.5:** Variation of  $\sigma_\lambda$  with time interval and magnitude and lines with slope  $1/\sqrt{T}$  for testing completeness of earthquake data of the study area.

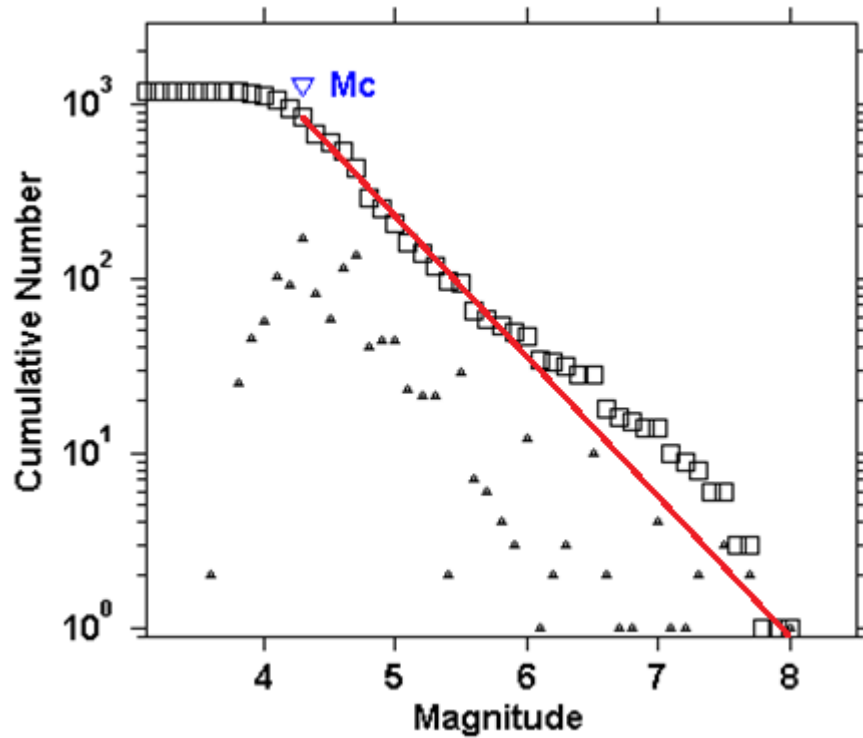


**Figure 2.6:** Frequency Magnitude Distribution (FMD) for estimation of minimum magnitude of completeness of the homogenized catalogue.

## **2.4 Tectonics of the Study Area**

After compilation of the two earthquake catalogues a comprehensive tectonic data set was compiled for the study area. Due to continent - continent collision between the Indian plate and the Eurasian plate, the study area is marked with complex tectonics and is thus prone to varying and high levels of seismic hazard. Like in the case of preparation of the MHD earthquake catalogue, tectonic data was first compiled and processed for a large area,  $12^{\circ}$  by  $12^{\circ}$  (longitude  $72^{\circ}\text{E}$  to  $84^{\circ}\text{E}$  and latitude  $25^{\circ}\text{N}$  to  $37^{\circ}\text{N}$ ) and then it was truncated to a smaller area,  $7^{\circ}$  by  $7^{\circ}$ , to meet the requirements of further analysis and for hazard assessment.

Tectonic data was prepared in several steps: identification of requirements of tectonic data, identification of various data sources, collection of relevant data, compilation of a list of tectonic units, identification of prominent and important tectonic units and digitization of tectonic data. The first exercise in hazard assessment, (given in section 6.2) was carried out with 26 prominent tectonic units, in which 6 longer tectonic units were segmented into equal portions. Details are given in Chapter 6. After this exercise it was felt that the two longest and most prominent tectonic units, the MBT and MCT be segmented as per seismicity and tectonics of the region. Segmentation of MBT and MCT was further modified in the next step. Using Pattern Recognition technique (PR), this exercise was carried out 8 times, to find the best combination of seismicity and tectonics that defined segmentation, as given in Chapters 3 and 5.

In the next stage, all tectonic units, 118, in the  $7^{\circ}$  by  $7^{\circ}$  study area, as per SEISAT were identified. Using the Pattern Recognition (PR) technique, the exercise for segmentation was carried out again, 3 times, with 118 tectonic units, as given in Chapters 3 and 5. 127 tectonic units emerged after segmentation of MBT and MCT. These 127 tectonic units were prepared for hazard assessment by assigning certain characteristics to each such as: type of fault, its length, rupture length and the maximum magnitude earthquake it can support. The 127 tectonic units, after characterization, were further used for identification of susceptible areas and for hazard assessment.

### **2.4.1 Identification of tectonic data**

Various maps available in public domain were accessed for identification of tectonic data and from these appropriate maps were identified from which tectonic data could be considered.

The different data sets which were considered included the following: Tectonic map of India, Oil and Natural Gas Commission, ONGC (Eremenko and Negi, 1968). This was available on 1:2,000,000 scale and because of inadequate data in the Himalayan region was not considered suitable for hazard analyses. Several maps available on Geological Survey of India online portal ([http://www.portal.gsi.gov.in/portal/page?\\_pageid=108,527690&\\_dad=portal&\\_schema=PORTAL](http://www.portal.gsi.gov.in/portal/page?_pageid=108,527690&_dad=portal&_schema=PORTAL)) were also studied. These included the following: geotechnical map of India, 1995, (1:2,000,000 scale); geological map of India 1998, (1:2,000,000 scale); and tectonic map of India 2001, (1:2,000,000 scale). Besides these hard copies of geological quadrangle maps, available for 1° by 1° area on 1:250,000 scale were also studied. Since these quadrangle maps were not available for the entire study area, these were not used for considering tectonics, but were referred as reference maps in case of extremely complex tectonics; geological map of the Himalaya, western Sector, scale 1:1,000,000 (2005); and Seismo-tectonic Atlas of India and its Environs (SEISAT) were also studied.

#### **2.4.2 Data collection**

Tectonic data as given in the Seismo-tectonic Atlas of India and its Environs, referred to as SEISAT, brought out by the Geological Survey of India (GSI) (Narula *et al.* 2000). SEISAT was considered appropriate for this study because of several reasons. This atlas has the most comprehensive tectonic data for the entire country and for contiguous regions, all the data is available at one place, in hard copy, in the form of an atlas. Moreover, all maps are on the same scale, 1: 1,000,000. SEISAT is a compilation of 42 sheets, each sheet is of 3° x 4° size (longitude x latitude) and each sheet is accompanied by a short write up on tectonics and seismicity of that area. For preparation of tectonic data for the study area, 9 SEISAT sheets, as shown in figure 2.7, were considered. Salient features of these 9 sheets, in terms of coordinates covered by each sheet, geographical area covered, important localities, physiographic features and rivers and important tectonic units are listed in table 2.11.

Tectonic features such as faults, thrusts, suture zones and lineaments were present across the study area. The two mega-thrusts namely, the Main Central Thrust (MCT) and the Main Boundary Thrust (MBT), separate three geologically distinct settings in this area. The Greater Himalayas lie north of the MCT, between the MCT and the Indus Suture Zone (ISZ); the Lesser Himalayas lie between the MCT and MBT; and the outer Himalaya lie south of the MBT.

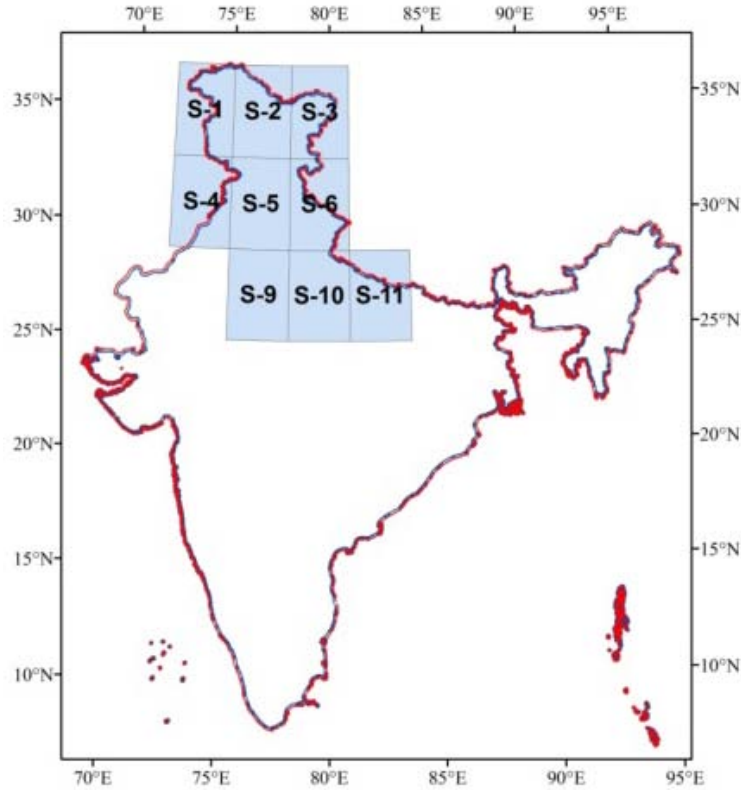


**Figure 2.7:** Nine SEISAT sheets considered for the present study, (redrawn after Narula *et al.* 2000).

The Main Frontal Thrust (MFT) is south of the MBT, is a neo-tectonic thrust and forms the foothills bordering the Indo Gangetic plains. Figure 2.8 shows four subdivisions of the Himalayan tectonic zone, which are separated by mega faults. The MBT, MCT and ISZ have a NW-SE trend and these are almost parallel to each other and to the trend of the Himalayan arc. The ISZ, MCT, MBT and MFT manifest throughout the Himalayan arc, between the Eastern and Western syntaxes and have prominent surface manifestations at several places in Western Himalaya. The MCT terminates against the Kishtwar fault in Jammu and Kashmir in the Northwest and is displaced northwest of Manali. From Manali towards east throughout the entire Himalaya almost upto the eastern syntaxis, this is considered as one of the most important tectonic surfaces.

Besides these mega Himalayan thrusts, several other faults and thrusts exist in the study area. The Karakoram Fault, (KF), a conspicuous mega structural element in the study area, north of the ISZ, exhibits a huge offset and extends for more than a 1,000 km from central Pamir to north of Kumaon Himalayas. This strike slip fault forms the eastern boundary of the Pamir syntaxis and the western boundary of the Tibetan plateau. The region between the MBT and the MFT is

traversed by several subsidiary thrusts some of which have considerable spatial extent. Prominent among these are the Jwalamukhi and Drang thrusts which can be traced over long distances. Reasi Thrust (ReT), is northward dipping and is an eastern extension of the Jwalamukhi Thrust. Neotectonic activity occurs at several places along the MBT and in western parts of Jwalamukhi Thrust. The extensive Vaikrita thrust exists in the north western part of the study area and is very close, parallel and north of the MBT. Similarly, a shorter feature, very close, parallel and south of MBT, unnamed in SEISAT, exists in the south eastern part of the study area. It was named as MBT-A for the purpose of this study. Several prominent faults and lineaments, which are transverse to the Himalayan trend, exhibit neo-tectonic activity. These are Kishtwar Fault (KiF, also known as Suru Fault), Sundarnagar Fault (SNF) and the Mahendragarh-Dehradun (MHD-DDN F) fault. The Sundernagar Fault (also known as Manali Fault) extends from the Higher Himalaya to the MBT. This fault is considered to have caused the abrupt swing of the MBT from NW-SE to N-S. The Ropor fault, occurring northwest of Chandigarh is postulated to be the southward continuation of the Sundernagar Fault. In the south eastern part of the study area, the Mahendragarh-Dehradun Fault is a sub –surface structure. Southern extension of the N-S trending Jhelum fault (JF), another major neotectonic fault, is cut across by Mangla fault and several other lineaments.

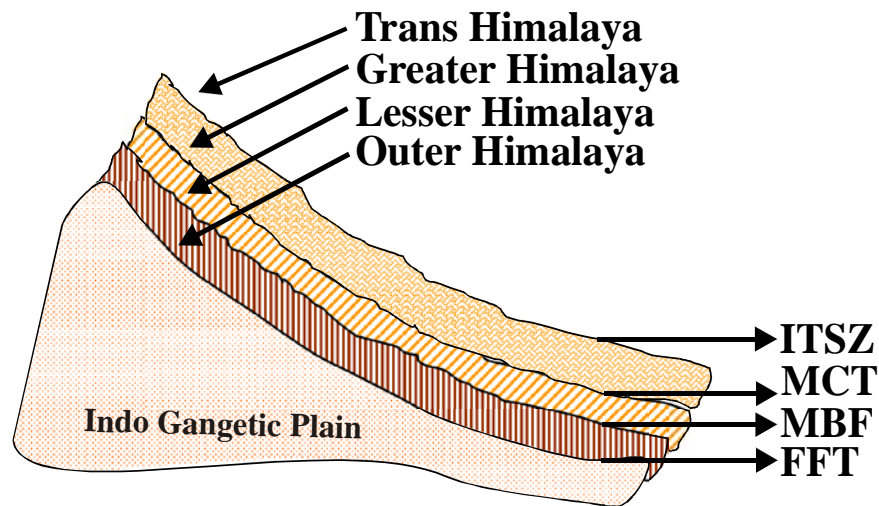


**Figure 2.8:** Simplified version of the four subdivisions of the Himalayan tectonic zone which are separated by mega faults, e.g. ITSZ = Indian Suture Zone, MCT = Main Central Thrust, MBF = Main Boundary Fault and FFT = Frontal Foothill Thrust, (After Sinval, 2012b).

**Table 2.11:** Salient features of 9 SEISAT sheets used in the present study. These include SEISAT sheet number, coordinates covered in each sheet, geographical area covered, important localities, important physiographic features and important tectonic units.

SEISAT No.	Coordinates		Sheet Name	Area	Important Localities	Important Physiographic Features	Important Tectonic Units
	Latitude	Longitude					
1	72°E - 75°E	33°N - 37°N	Western Himalayan Syntaxis between Kohistan Arc and Potwar Plateau	Parts of India, Pakistan and Afghanistan	Abbottabad Attock Baramula Gilgit Kalam Mardan Mastuj Mirpur Muzaffarabad Nanga Parbat Pindi Gheb Poonch Rawalpindi Srinagar	Great Karakoram Range, Hindukush Mountains, Pamir Plateau Kashmir basin, Peshawar basin, Potwar Plateau  <b>Rivers:</b> Abi Panja, Chenab, Indus Jhelum, Mastuj	Attock fault Jhelum fault Main Boundary Thrust Main Karakoram Thrust Main Mantle Thrust Peshawar fault Shinkhari fault Tarbela fault Western Himalayan syntaxis
2	75°E - 78°E	33°N - 37°N	Tibetan Plateau and Kashmir Ladakh Himalaya	Parts of India and China	Anantnag Doda Kargil Leh	Great Karakoram Range, Ladakh range, Pir Panjal ranges, Zaskar range  <b>Rivers:</b> Karkandor, Shyok, Indus and Chenab	Altyn Tagh fault Indus Suture zone Karakoram fault Kishtwar fault Main Boundary Thrust Shyok Suture

SEISAT No.	Coordinates		Sheet Name	Area	Important Localities	Important Physiographic Features	Important Tectonic Units
	Latitude	Longitude					
3	78°E - 81°E	33°N - 37°N	Trans Himalaya between Karakoram And Altyn Tagh faults		Huzakhar Tak Morpa	Kunlun Range, Pangong Lake, Tarim Basin, Tibetan Plateau  <b>Rivers:</b> Chira, Karakashand, Indus, Shyok	Altyn Tagh fault Beng co fault Karakoram fault
4	72°E - 75°E	29°N - 33°N	North Rajasthan and Punjab	Parts of India and Pakistan	Amritsar Bhatinda Chiniot Ferozpur Gujrat Jammu Jhelum Lahore Sialkot Sri Ganganagar Suratgarh	Indo-Gangetic alluvial plains  <b>Rivers:</b> Chenab, Jhelum, Ravi and Sutlej	Jhelum fault Kallar Kabar fault Reasi thrust Salt Range thrust Sargodha- Lahore-Delhi ridge
5	75°E - 78°E	29°N - 33°N	Himachal Himalaya and adjoining Indo-Gangetic Plains	Parts of J&K, HP, Punjab, Haryana, UP, UK, small portion of Pakistan	Ambala Chamba Chandigarh Dharamashala Gurdaspur Hissar Hoshiarpur Jullundar Kathua Keylang	Himalayan belt, Indo-Gangetic Plains  <b>Rivers:</b> Beas, Chandra, Ravi, Sutlej, Yamuna	Drang thrust Jwalamukhi thrust Mahendragarh Dehradun F Main Boundary Thrust Main Central Thrust Main Frontal Thrust Mastgarh anticline Ropor fault Sundernagar fault Vaikrita thrust

SEISAT No.	Coordinates		Sheet Name	Area	Important Localities	Important Physiographic Features	Important Tectonic Units
	Latitude	Longitude					
					Manali Mandi Morang Patiala Saharanpur Simla		
6	78°E - 81°E	29°N - 33°N	Himachal, Kumaon - Garhwal Himalayas & their Environ	Parts Kumao-Garhwal region in Uttarkahand, parts of west Nepal, HP and Laddakh	Almora Baitadi Bijnor Dehradun Dharchula Gartok Haridwar Mana Nainital Pithoragarh Tehri Uttarkashi	Indo –Gangetic plains, Tibetan Plateau  <b>Rivers:</b> Kali, Ganga, Sutlej, Ramganga, Yamuna	Indus Suture Zone Main Boundary Thrust Main Central Thrust Main Himalayan belt Trans-Himalayan tectogen Karakoram fault
9	75°E - 78°E	25°N - 29°N	North Delhi Fold belt and part of Vindhyan Basin	Parts of Rajasthan, Haryana, Uttar Pradesh and Madhya Pradehsh and Delhi	Bharatpur Bhivani Bulandshahar Bundi Delhi Jaipur Kota Mathura Rewari Rohtak Sawai Madhopur	<b>Rivers:</b> Yamuna, Banas and Chambal	Chittaurgarh-Machilpur Lineament Delhi fold belt Great Boundary fault



SEISAT No.	Coordinates		Sheet Name	Area	Important Localities	Important Physiographic Features	Important Tectonic Units
	Latitude	Longitude					
					Shivpuri Shivpuri		
10	78°E - 81°E	25°N - 29°N	Indo Gangetic plains of Uttar Pradesh and uplands of Madhya Pradesh	Parts of UP, MP and Nepal	Aligarh Banda Bareilly Bhind Etawah Farrukhabad Fatehpur Firozabad Gwalior Hamirpur Hardoi Jhansi Kanpur Lucknow Mainpuri Moradabad Orai Rampur Shahjahanpur Sitapur	Alluvial tracts, Foothills of Nepal Himalaya  <b>Rivers:</b> Ganga, Yamuna, Chambal and Sharda	Great Boundary fault Lucknow fault Moradabad fault
11	81°E - 85°E	25°N - 29°N	Nepal Himalayas and Adjoining Indo-Gangetic Plains	Parts of Nepal and Uttar Pradesh	Allahabad Annapurna Azamgarh Bahraich Basti Dhaulagiri Faizabad	Alluvial tracts of Uttar Pradesh Nepal Himalaya and its Tarai region  <b>Rivers:</b> Ganga, Ghaghara and	Main Boundary Thrust Main Central Thrust North Almora Thrust South Almora Thrust

SEISAT No.	Coordinates		Sheet Name	Area	Important Localities	Important Physiographic Features	Important Tectonic Units
	Latitude	Longitude					
					Ghazipur Gonda Gorakhpur Jaunpur Mari Mirzapur Nepal Ganj Padrauna Raibareilly Satbaria Varanasi	Yamuna	

One of the most significant extensional structures in Himachal Pradesh is the Kaurik- Fault System, (KFS). It is a normal fault with dip towards the west and its surface manifestation is provided by change in course of the Spiti river from N-S between Khab and Sumodh to west beyond these places, (Khattri *et. al.*, 1978).

The 21 prominent and named tectonic units in 9 SEISAT sheets, considered *ab initio* in this study, which were considered because these were associated with either the MBT or the MCT or were large in terms of length in the study area and given here in alphabetical order are: Alaknanda Fault (AF), Drang thrust (DT), Indus Suture Zone (ISZ), Jhelum fault (JF), Jwalamukhi thrust (JMT), Karakoram fault (KF), Kishtwar fault (KiF), Mahendragarh-Dehradun Fault (MHD-DDN F), Mastgarh Anticline (MA), Main Boundary Thrust (MBT), Main Central Thrust (MCT), Main Frontal Thrust (MFT), Main Mantle Thrust (MMT), North Almora Thrust (NAT), Ramgarh Thrust (RT), Reasi Thrust (ReT), Ropor Fault (RF), Shyok Suture (SS), South Almora Thrust (SAT) and Sundarnagar fault (SNF). The abbreviation assigned in bracket for each tectonic unit is further used in text, figures and tables. In addition, 5 closed unnamed thrusts in the form of loops which were between the MBT and MCT were also considered. This comprised the 26 tectonic units, listed in table 2.12 and shown in figure 2.9.

The next step in data collection was to compile all tectonic units in the same SEISAT sheets in the study area, including all unnamed ones, which resulted in 118 tectonic units. These were assigned names as per table 2.13 and are shown in figure 2.10.

### **2.4.3 Digitization of tectonic data**

The relevant SEISAT sheets were scanned, (which is raster data for input) and then digitized. Digitization is the representation of an image (in this case scanned SEISAT sheets), by a discrete set of its points or samples. The result is called digital representation or vector representation of the scanned image. All SEISAT sheets were digitized in 7 GIS layers: faults, thrusts, rivers, place names, gravity anomalies, seismicity and geology of the area. Maps were then projected onto Lambert Conformal Conic projection for further processing using ArcMap-9.3.

All features (color and symbol) as they appear in the SEISAT were retained during digitization. AutoCAD Map 2000i, ArcInfo 7.2.1D, ArcView 3.2A and ArcGIS-9.3 softwares were used for digitization and data processing at different stages. AutoCAD Map 2000i was used for digitizing maps

i.e. converting raster dataset (i.e. scanned SEISAT sheets) to vector dataset (i.e. digital form of scanned sheets). It was also used for Geo-referencing maps i.e. providing geographical coordinates to digitized data. ArcInfo 7.2.1 D was used for editing and correcting geometric coordinate errors in the digitized map, assembling arcs into polygons and creating feature attribute information for each polygon. ArcGIS-9.3 and ArcView-3.2 are GIS softwares provided by Environmental Systems Research Institute (ESRI). ArcGIS-9.3 was used for map composition. ArcView 3.2 was used as a supplement. Map composition consists of defining the map extent; adding map coordinate and /or geographic (latitude/longitude) coordinate grids; constructing map scales; and defining colour, symbol and label of digitized map features. Both the softwares were used for composing map at various stages.

While digitizing the SEISAT sheets several corrections were necessary. MBT is continuous between SEISAT-01 and SEISAT-02, but shows a marked discontinuity between SEISAT-02 and 05. The continuity of MBT was confirmed across these sheets by referring to geological map of the Himalaya, western Sector, scale 1:1,000,000 (2005) and the discontinuity was attributed to drafting error in SEISAT. Other features parallel to MBT in NW-SE direction were continuous. Corrections were made to make MBT continuous by shifting it for less than a degree towards west. This made MBT continuous and did not give an unnatural break in the map. Similarly in SEISAT-06 and SEISAT-05, bend of Ganga River was not complete between (78°E, 29°N) and (78°E, 30°N), therefore, continuity was corrected in the digitized version. This was also confirmed and corrected by considering the relevant Survey of India map. After corrections these 9 sheets were joined to obtain a composite map for a large area defined by the coordinates: longitude 72°E to 84°E and latitude 25°N to 37°N, the study area was totally within this large area. The composite map was then truncated for the study area (7° by 7°) for further studies.

**Table 2.12:** List of 26 tectonic units in the study area, (in alphabetical order). Only those major named units were considered which were prominent or close to either the MBT or the MCT. This list includes 5 closed unnamed thrusts, which are between the MBT and MCT. \* indicates ISZ, which consists of three closely spaced parallel features, \*\* indicates MBT and its closely spaced parallel feature. This data was used for a preliminary estimation of DSHA.

<b>S. No.</b>	<b>Tectonic Feature</b>
1.	Alaknanda fault (AF)
2.	Drang thrust (DT)
3.	Indus Suture Zone (ISZ)*
a.	ISZ 1 (northern most)
b.	ISZ 2
c.	ISZ 3 (southern most)
4.	Jhelum fault
5.	Jwalamukhi thrust (JMT)
6.	Karakoram fault (KF)
7.	Kishtwar fault (KiF)
8.	Mahendragarh-Dehradun fault (MHD-DDN F)
9.	Mastgarh anticline (MA)
10.	Main Boundary thrust (MBT)**
11.	MBT-A
12.	Main Central thrust (MCT)
13.	Main Frontal thrust (MFT)
14.	Main Mantle thrust (MMT)
15.	North Almora thrust (NAT)
16.	Ramgarh thrust (RT)
17.	Reasi thrust (ReT)
18.	Ropor fault (RF)
19.	Shyok Suture (SS)
20.	South Almora thrust (SAT)
21.	Sundarnagar fault (SNF)
22.	Closed thrust T1
23.	Closed thrust T2
24.	Closed thrust T3
25.	Closed thrust T4
26.	Closed thrust T5

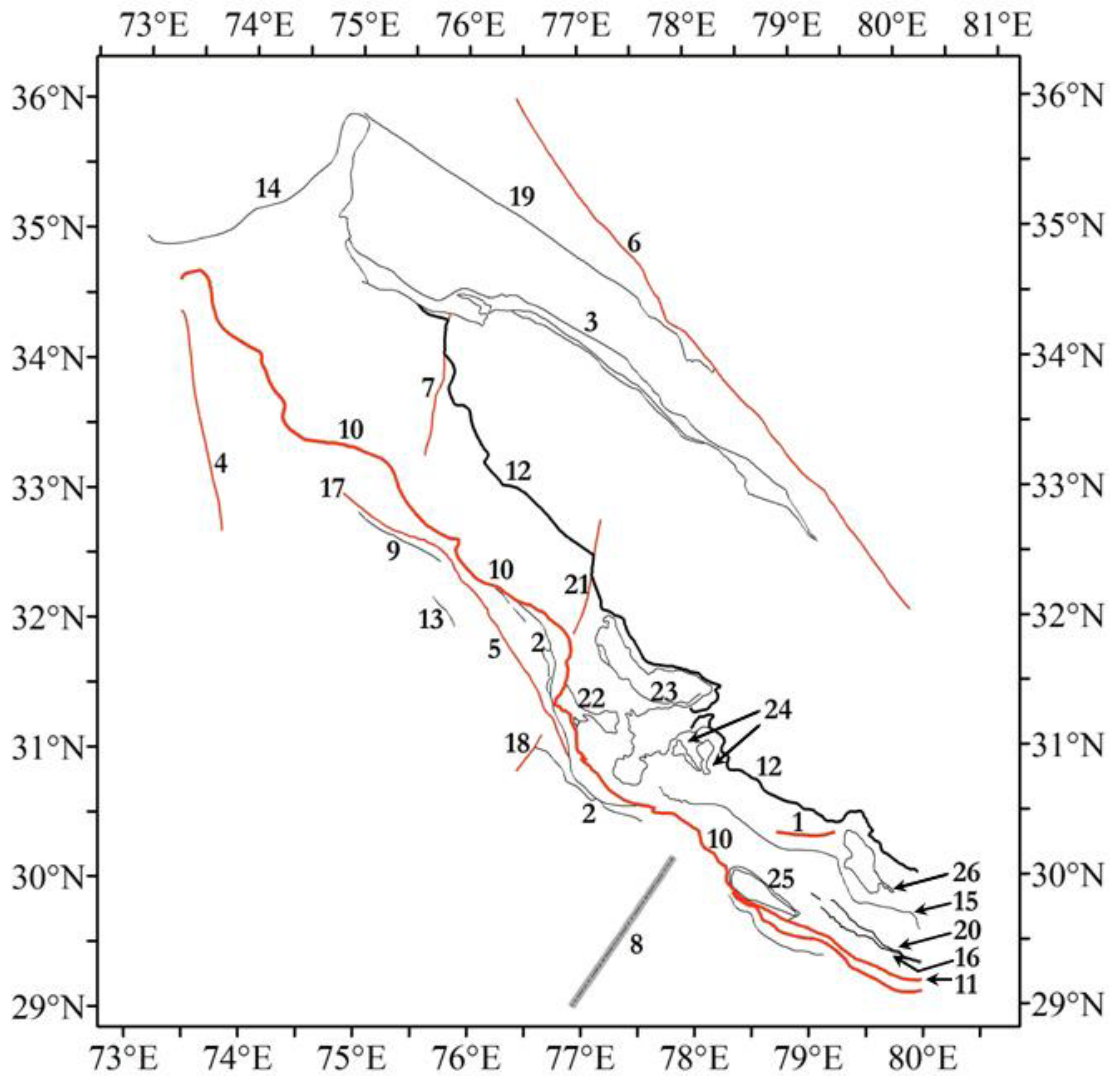


**Figure 2.9:** 26 tectonic units used for initial study of DSHA. Tectonic units are numbered as per table 2.12. 1. Alaknanda fault (AF); 2. Drang thrust (DT); 3. Indus Suture Zone (ISZ); 4. Jhelum fault; 5. Jwalamukhi thrust (JMT); 6. Karakoram fault (KF); 7. Kishtwar fault (KiF); 8. Mahendragarh-Dehradun fault (MHD-DDN F); 9. Mastgarh anticline (MA); 10. Main Boundary thrust (MBT); 11. MBT-A ; 12. Main Central Thrust (MCT); 13. Main Frontal thrust (MFT); 14. Main Mantle thrust (MMT); 15. North Almora thrust (NAT); 16. Ramgarh thrust (RT); 17. Reasi thrust (ReT); 18. Ropor fault (RF); 19. Shyok Suture (SS); 20. South Almora thrust (SAT); 21. Sundarnagar fault (SNF); 22. Closed thrust, T1; 23. Closed thrust, T2; 24. Closed thrust, T3; 25. Closed thrust, T4; 26. Closed thrust, T5.

**Table 2.13:** List of 118 tectonic units in the study area as per SEISAT sheets.

S. No.	Type of Tectonic Feature	No.	Name of Tectonic Units (alphabetical order)
1.	Thrusts	13	Drang thrust (DT), Jwalamukhi thrust (JMT), Main Boundary thrust (MBT), MBT-A, Main Central thrust (MCT), Main Frontal thrust (MFT), Main Karakoram thrust (MKT), Main Mantle thrust (MMT), North Almora thrust (NAT), Ramgarh thrust (RT), Reasi thrust (ReT), Salt Range thrust (SRT), South Almora thrust (SAT)
2.	Faults	13	Alaknanda F (AF), Altyn Tagh F (ATF), Beng Co F (Bg Co), Jhelum fault (JF), Kallar Kabar fault (KKF), Karakoram fault (KF), Kaurik F System (KFS), Kishtwar F (KiF), Mangla fault (MF), Mahendragarh Dehra Dun F (MHDDDDN), Ropor F (RF), Sundarnagar F (SNF), Tso Morari F (TsoMF)
3.	Suture zones	2	ISZ, Shyok Suture (SS)
4.	Anticline	1	Mastgarh anticline (MA)
5.	Unnamed closed thrusts	7	T1, T2, T3, T4, T5, T6, T7
6.	Unnamed thrusts	20	TH 01, TH 02, TH 03, TH 04, TH 05, TH 06, TH 07, TH 08, TH 09, TH 10, TH 11, TH 12, TH 13, TH 14, TH 15, TH 16, TH 17, TH 18, TR 01, TR 02
7.	faults involving basement and cover	15	FG 01, FG 02, FG 03, FG 04, FG 05, FG 06, FG 07, FG 08, FG 09, FG 10, FG 11, FG 12, FG 13, FG 14, FG 15
8.	Neotectonic faults	16	FR 01, FR 02, FR 03, FR 04, FR 05, FR 06, FR 07, FR 08, FR 09, FR 10, FR 11, FR 12, FR 13, FR 14, FR 15, FR 16
9.	Gravity faults	3	GF 01, GF 02, GF 03
10.	Lineaments	28	L 01, L 02, L 03, L 04, L 05, L 06, L 07, L 08, L 09, L 10, L 11, L 12, L 13, L 14, L 15, L 16, L 17, L18, L19, L20, L21, L22, L23, L24, L25, L26, L27, L28
	<b>Total</b>	<b>118</b>	

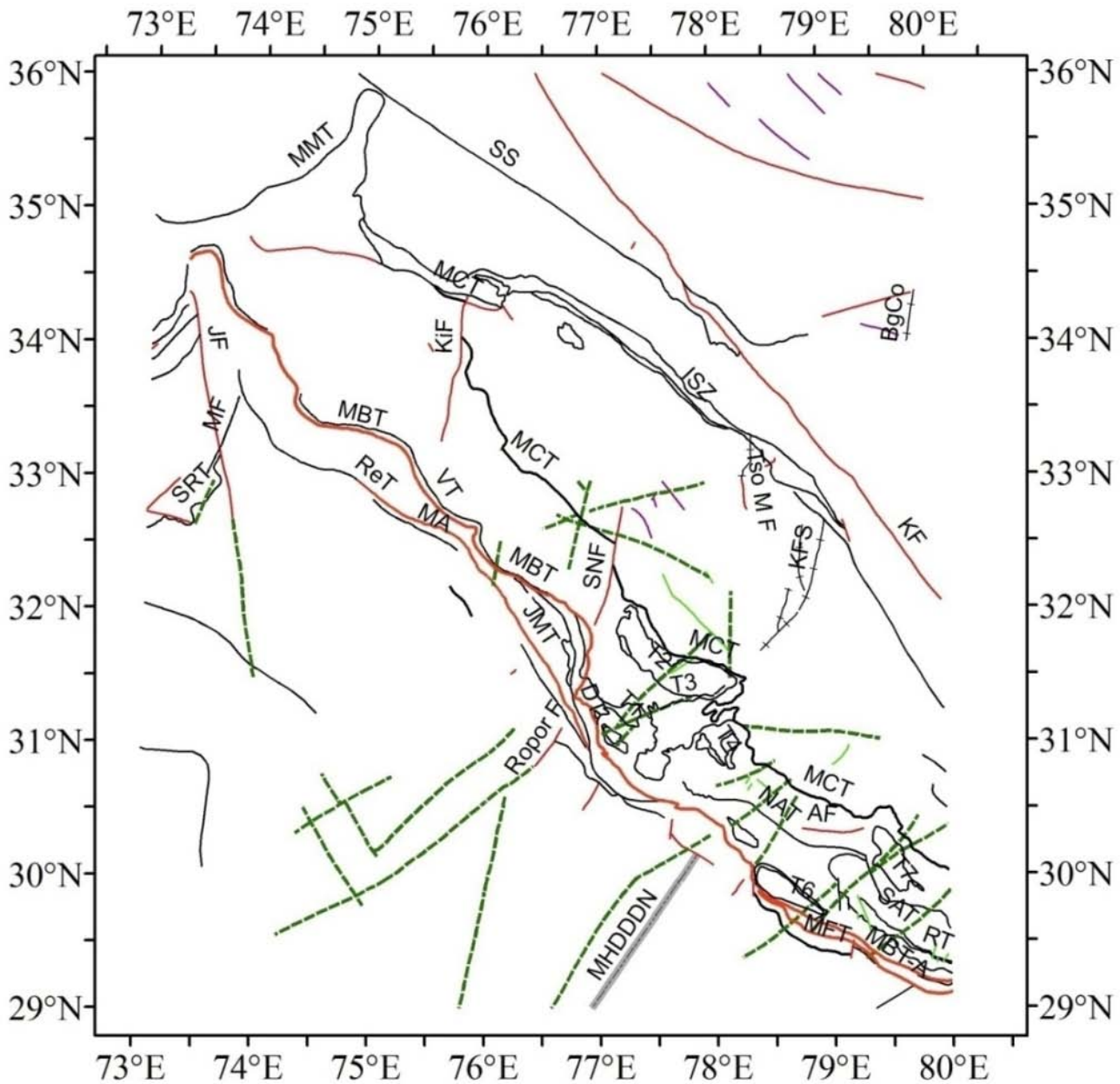


**Figure 2.10:** 118 tectonic units in the study area, where abbreviations of tectonic units are as per table 2.13. AF: Alaknanda fault; Bg Co: Beng Co fault; DT: Drang thrust; ISZ: Indus Suture Zone; JF: Jhelum fault; JMT: Jwalamukhi thrust; KF: Karakoram fault; KFS: Kaurik fault System; KiF: Kishtwar fault; MA: Mastgarh anticline; MBT: Main Boundary thrust; MCT: Main Central Trust; MF: Mangla fault; MHDDDN: Mahendragarh Dehradun fault; MMT: Main Mantle thrust; NAT: North Almora thrust; ReT: Reasi thrust; SAT: Saouth Almora thrust; SNF: Sundarnagar fault; SRT: Salt Range thrust; SS: Shyok Suture; T1, T2, ..., T7: Closed thrust between MBT and MCT; Tso M F: Tso Morari fault; VT: Vaikrita thrust.



#### 2.4.4 Tectonic units

After digitizing, correcting and joining the SEISAT sheets the following tectonic units were studied for the area for seismic hazard assessment. Some of these were very large features (MBT, MCT and ISZ) and some of them were comparably small features (Kishtwar fault, Sundarnagar Fault). Due to presence of small features in the map large features such as Main Boundary Thrust (MBT) and Main Central Thrust (MCT) were dislocated at several places by Kishtwar fault and Sundarnagar fault. MCT was a very complex feature at many places due to the presence of several closely spaced thrusts in the form of closed loops.

##### *Characterization of tectonic units for further analysis*

After preparation of the tectonic map the 118 tectonic units were assigned characteristics which were subsequently used for hazard assessment. This included naming and assigning an abbreviation to each unit and then assigning to each unit the following: its type, dip, strike, length, length that would rupture in an earthquake, maximum magnitude that the unit is capable of supporting and down dip rupture width. All tectonic units were classified into four types of faulting: strike slip, thrust, normal and unspecified type. Initially the SEISAT notation was used, then it was modified to meet the requirements of Wells and Coppersmith formulation and finally as per requirements of this study. Table 2.14 shows convergence between all these notations. Dip was assigned as given in Chapter 6, section 6.3. Strike was assigned as per the SEISAT sheets. Each tectonic unit was then characterized by its length,  $L$ , as per the tectonic map, measured by using software package ArcGIS-9.3. As the ISZ consists of three parallel lines and one closed curve in the area between longitude  $75^{\circ}\text{E}$  to  $79^{\circ}\text{E}$  and latitude  $33^{\circ}\text{N}$  to  $35^{\circ}\text{N}$ , it added up to be the longest unit in the study area, with a combined length of 1605 km. Length of each sliver was computed separately and was considered for further computations. The longest of the 3 slivers was 568 km and was retained for SHA. An entire fault does not rupture over its entire length,  $L$ , in a single earthquake, but it is assumed that only  $1/3$  to  $1/2$  of its length ruptures during an earthquake, (Mark, 1977) and therefore  $L$  was replaced by  $L/3$  for computation of maximum earthquake,  $M_w$  and then down dip rupture width, calculated as per Wells and Coppersmith (1994) formulation, as given in table 2.14. Table 2.15 gives a list of 118 tectonic units, type of faulting, length (computed from ArcGIS), computed  $M_w$  and down dip rupture width for each unit using Wells and Coppersmith (1994) formulation.

**Table 2.14:** Convergence between different notations used for fault type, as per SEISAT, Wells and Coppersmith, (1994) formulation (W&C) and this study. Relations (equations 2.4-2.6) for computing maximum magnitude are different for each type of fault and depend on rupture length.

SEISAT Notation for Fault Type	W & C Notation	Notation Present Study	W & C Relationship between Rupture Length and Maximum Magnitude
Strike slip	SS	SS	$M_w = 5.16 + 1.12 \log L$ (2.4)
Thrust	Reverse, R	thrust	$M_w = 5.00 + 1.22 \log L$ (2.5)
Gravity fault	Normal, N	GF	$M_w = 4.86 + 1.32 \log L$ (2.6)
Fault, lineament, anticline	All	F, L, anticline, unspecified	$M_w = 5.08 + 1.16 \log L$ (2.7)

#### 2.4.5 Use of tectonic data in this research work

The identified tectonic units were used for several aspects presented in this research work, viz. for identification of susceptible areas (Chapter 4), segmentation of longer tectonic units (Chapter 5) and for hazard assessment, DSHA (Chapter 6) and PSHA (Chapter 7)).

#### 2.4.6 Seismotectonics of the study area

The seismotectonic map, shown in figure 2.11 , emerged by overlaying the merged, homogenized and declustered MHD earthquake catalogue data, figure 2.4 on to the tectonic map figure 2.10 of the region. Seismo-tectonics of the region showed a very interesting pattern. Seven clusters of dense seismicity were observed, these were: around the western syntaxes, (epicenter of the Kashmir earthquake of 8<sup>th</sup> October, 2005;  $M_w = 7.6$  (MHD), was part of this cluster); along the Great Karakoram Range; in the area between the MBT in the south, the MCT in the north, Sundarnagar fault in the east and Kishtwar Fault in the west, epicenter of the great Kangra earthquake of 1905 in the vicinity of MBT is a part of this dense cluster; in the eastern part of the study area a prominent cluster of seismicity is observed, along the MCT. Uttarkashi earthquake of 20<sup>th</sup> October, 1991,  $M_w=6.8$  (MHD) and Chamoli earthquake of 28<sup>th</sup> March, 1999,  $M_w = 6.7$  (MHD), are part of this cluster. Another prominent cluster was observed transverse to the Himalayan trend, along the Kaurik Fault system. The Kinnaur earthquake of 19<sup>th</sup> January, 1975,  $M_w=6.6$  (MHD) is part of this cluster. Another cluster of dense seismicity is observed in the north eastern part of the study area along Beng Co fault and in the east of Karakoram fault and. Compared to these seven clusters, seismicity was observed to be sparse in three regions, viz. along ISZ,

Jhelum fault, region roughly defined between MCT, Shyok Suture, Kishtwar Fault and Tso Morari Fault and in a very large part of the study area, in Indi Gangetic plains, south of the MBT.

**Table 2.15:** List of 118 tectonic units, its length, (computed form ArcGIS), type of faulting, (strike slip: SS, thrust: T, Gravity fault: N, fault: F, Unspecified: U), computed maximum magnitude  $M_w$  and down dip rupture width RW, using Wells and Coppersmith (1994) formulation. \* longest sliver of the three parallel portions of ISZ was retained.

S. No.	Tectonic Unit	Length (km)	Type	Computed $M_w$	RW
1	Alaknanda F	50.32	F	6.50	11.75
2	Altyn Tagh	41.98	SS	6.44	9.54
3	Beng Co	42.69	N	6.38	12.41
4	Drang Thru	393.56	T	7.58	31.58
5	FG 01	11.33	F	5.75	6.76
6	FG 02	87.00	F	6.78	14.40
7	FG 03	23.79	F	6.12	8.90
8	FG 04	21.23	F	6.07	8.53
9	FG 05	5.70	F	5.40	5.24
10	FG 06	5.71	F	5.40	5.24
11	FG 07	16.74	F	5.95	7.81
12	FG 08	27.47	F	6.20	9.39
13	FG 09	15.66	F	5.91	7.62
14	FG 10	4.86	F	5.32	4.93
15	FG 11	32.16	F	6.27	9.95
16	FG 12	10.67	F	5.72	6.61
17	FG 13	3.30	F	5.13	4.28
18	FG 14	2.14	F	4.91	3.64
19	FG 15	3.40	F	5.14	4.33
20	FR 01	287.95	F	7.38	22.46
21	FR 02	5.63	F	5.40	5.21
22	FR 03	5.88	F	5.42	5.30
23	FR 04	7.10	F	5.51	5.68
24	FR 05	50.22	F	6.50	11.74
25	FR 06	74.91	F	6.70	13.62
26	FR 07	37.33	F	6.35	10.52
27	FR 08	16.83	F	5.95	7.83
28	FR 09	10.69	F	5.72	6.61
29	FR 10	18.99	F	6.01	8.19
30	FR 11	5.17	F	5.35	5.05
31	FR 12	27.04	F	6.19	9.33
32	FR 13	15.90	F	5.92	7.66
33	FR 14	25.85	F	6.17	9.18

S. No.	Tectonic Unit	Length (km)	Type	Computed $M_w$	RW
34	FR 15	14.73	F	5.88	7.45
35	FR 16	15.89	F	5.92	7.66
36	GF 01	39.35	N	6.34	11.95
37	GF 02	55.98	N	6.54	14.07
38	GF 03	37.60	N	6.31	11.70
39	Indus Suture Zone*	568.49	T	7.78	37.95
40	Jhelum F	235.66	SS	7.28	16.08
41	Jwalamukhi T	290.24	T	7.42	27.12
42	Kallar Kabbar F	37.15	F	6.30	10.14
43	Karakoram F	553.82	SS	7.70	20.82
44	Kaurik FS	123.19	N	6.99	20.25
45	Kishtwar F	123.11	SS	6.97	13.21
46	L 01	41.53	U	6.40	10.94
47	L 02	132.11	U	6.99	16.82
48	L 03	38.07	U	6.36	10.60
49	L 04	12.40	U	5.80	6.99
50	L 05	75.44	U	6.70	13.66
51	L 06	98.29	U	6.84	15.07
52	L 07	30.73	U	6.25	9.79
53	L 08	136.71	U	7.00	17.03
54	L 09	72.09	U	6.68	13.43
55	L 10	110.10	U	6.90	15.72
56	L 11	82.30	U	6.75	14.11
57	L 12	21.56	U	6.07	8.58
58	L 13	114.62	U	6.92	15.95
59	L 14	29.88	U	6.24	9.69
60	L 15	92.82	U	6.81	14.75
61	L 16	95.41	U	6.82	14.90
62	L 17	54.01	U	6.54	12.07
63	L 18	156.09	U	7.07	17.89
64	L 19	256.49	U	7.32	21.52
65	L 20	180.17	U	7.14	18.87
66	L 21	53.64	U	6.53	12.04
67	L 22	63.48	U	6.62	12.81
68	L 23	69.61	U	6.66	13.26
69	L 24	199.64	U	7.19	19.60
70	L 25	98.58	U	6.84	15.09
71	L 26	132.08	U	6.99	16.82
72	L 27	75.22	U	6.70	13.65
73	L 28	88.84	U	6.79	14.51

S. No.	Tectonic Unit	Length (km)	Type	Computed $M_w$	RW
74	Mangla fault	69.62	SS	6.69	11.12
75	Mastgarh anticline	115.28	U	6.92	15.99
76	MBT	997.43	T	8.08	50.28
77	MBT-A	190.26	T	7.20	21.95
78	MCT	800.45	T	7.96	45.04
79	MFT	134.48	T	7.01	18.45
80	MHDDDN F	154.47	F	7.07	17.82
81	MKT	20.56	T	6.02	7.21
82	MMT	416.33	T	7.61	32.48
83	NAT	277.69	T	7.40	26.52
84	Ramgarh T	114.69	T	6.93	17.04
85	Reasi T	17.70	T	5.94	6.69
86	Ropor F	38.05	SS	6.40	9.26
87	Salt Range T	117.81	T	6.90	0.00
88	SAT	96.59	T	6.84	15.64
89	Shyok Suture	385.43	T	7.57	31.25
90	Sundarnagar F	101.59	SS	6.87	12.47
91	T1	167.02	T	7.13	20.57
92	T2	316.80	T	7.47	28.33
93	T3	288.55	T	7.42	27.04
94	T4	79.46	T	6.74	14.18
95	T5	75.52	T	6.71	13.83
96	T6	245.03	T	7.33	24.91
97	T7	171.88	T	7.14	20.86
98	TH-02	45.44	T	6.44	10.73
99	TH-03	53.37	T	6.53	11.62
100	TH-04	57.29	T	6.56	12.04
101	TH-05	146.11	T	7.06	19.24
102	TH-06	68.77	T	6.66	13.20
103	TH-07, VT	665.24	T	7.43	41.06
104	TH-08	97.92	T	6.85	15.75
105	TH-09	13.78	T	5.81	5.90
106	TH-1	66.78	T	6.64	13.00
107	TH-10	75.89	T	6.71	13.86
108	TH-11	51.74	T	6.51	11.44
109	TH-12	25.09	T	6.13	7.97
110	TH-13	1.67	T	4.69	2.06
111	TH-14	24.17	T	6.11	7.82
112	TH-15	24.26	T	6.11	7.83
113	TH-16	64.35	T	6.62	12.76

<b>S. No.</b>	<b>Tectonic Unit</b>	<b>Length (km)</b>	<b>Type</b>	<b>Computed <math>M_w</math></b>	<b>RW</b>
114	TH-17	101.29	T	6.86	16.01
115	TH-18	108.72	T	6.90	16.59
116	TR-01	111.13	T	6.91	16.77
117	TR-02	45.03	T	6.44	10.68
118	Tso Morari F	24.87	N	6.07	9.67

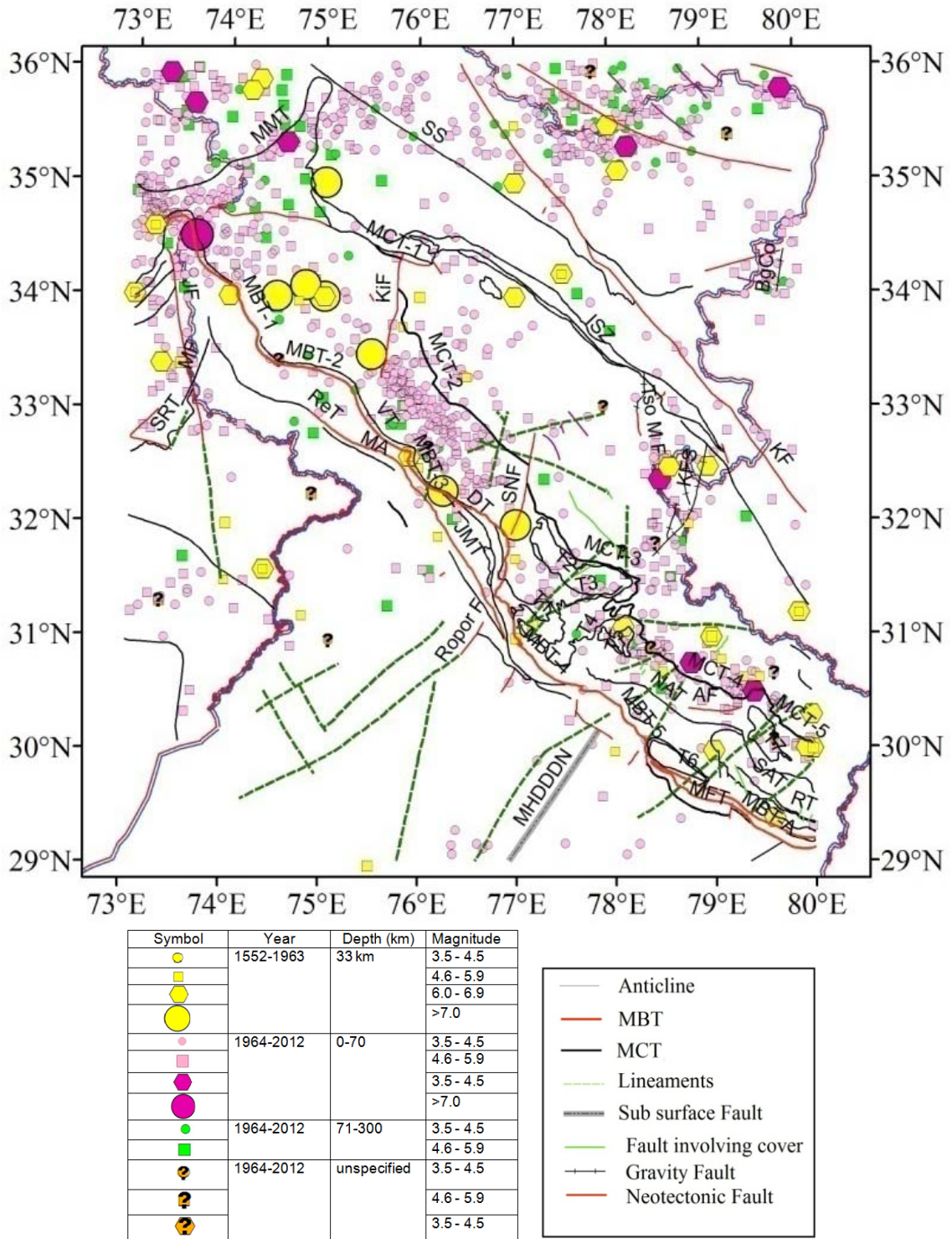


**Figure 2.11:** Seismotectonics of the study area in western Himalaya emerged by overlaying the figure 2.4 and figure 2.10.

### 2.4.7 Fault plane solutions

Mukhopadhyay (2015) listed fault plane solutions for 70 earthquakes (period 1980–2009) in the western Himalaya. This list contained aftershocks of several earthquakes. In MHD catalogue aftershocks were removed. Fault plane solutions of 27 mainshocks from MHD catalogue were studied. Strike dip and rake angles of these were considered from Mukhopadhyay (2015). Table 2.16 shows fault plane solutions of 27 earthquakes, i.e. strike, dip and rake. Beach ball presentation of these 27 earthquakes was prepared in ArcGIS. These are shown in figure 2.12. Fault plane solutions show thrust mechanism in the western syntaxis, along MBT. It showed strike slip mechanism along Main Mantle Thrust (MMT) in NW and along Karakoram fault in NE part of the study area. It also indicated normal faulting along Kaurik fault system. These faulting mechanisms were considered one of the important parameter while considering seismogenic source zones in Chapter 7.

### 2.4.8 MHD catalogue-2, for validation of results

For validation of various analyses carried out in this study a separate catalogue was prepared, which consisted of earthquakes which occurred after completion of the MHD catalogue. This catalogue was prepared by considering events for the period January 2013 to September 2015 from various agencies such as: USGS, IMD and ISC. The USGS catalogue contained 86 earthquakes in the magnitude range  $3.7 \leq m_b \leq 5.4$ , the IMD catalogue contained 3 earthquakes in the magnitude range between  $4.5 \leq M_L \leq 5.6$  and the ISC catalogue contained 4 earthquakes in the magnitude range  $4.4 \leq m_b \leq 4.7$  for the year 2013, table 2.17. These three catalogues were merged, homogenized and declustered as was done for the MHD catalogue, (section 2.3.2) to obtain a new catalogue, which was used for validation of results. This catalogue was named as MHD catalogue-2, for validation of results. This catalogue contained 80 earthquakes of magnitude range between  $4.5 \leq M_w \leq 5.7$ , for the time span 2013-2015 and space defined by longitude  $73^\circ\text{E} - 80^\circ\text{E}$  and latitude  $29^\circ\text{N} - 36^\circ\text{N}$ . Magnitude wise distribution of these earthquakes is: 6 earthquakes are of  $5.5 \leq M_w \leq 5.7$  and 74 earthquakes are of  $4.5 \leq M_w \leq 5.4$ .

Magnitude break up of epicenters from MHD catalogue-2 was considered in accordance with the classification criteria-II, discussed in section 3.5, which gave best results while identifying seismically susceptible areas, as given in Chapter 4. Magnitude wise breakup of these earthquakes is given in table 2.18. MHD catalogue-2 was prepared for validation of all results.



**Table 2.16:** Fault plane solutions of 27 earthquakes from MHD catalogue.

S.No.	YY	MM	DD	hour	min	long	lat	M <sub>w</sub>	Depth	Strike	Dip	Rake	Reference
1	1945	6	22	18.00	0.00	75.90	32.60	6.5	0.0	349	26	0	Narula <i>et al.</i> (2000)
2	1975	1	19	8.00	1.00	78.50	32.39	6.6	1.4	360	50	0	Khattri <i>et al.</i> (1978)
3	1980	8	23	9.00	36.00	75.75	32.96	5.5	3.2	293	10	63	Mukhopadhyay (2015)
4	1981	9	12	7.00	15.00	73.60	35.68	6.5	29.7	107	36	79	-do-
5	1986	4	26	7.00	35.00	76.40	32.15	5.8	33.0	299	19	58	-do-
6	1986	7	16	10.00	3.00	78.00	31.05	5.9	4.4	278	17	37	-do-
7	1991	10	20	9.00	23.00	78.79	30.77	6.8	13.2	317	14	0	Narula <i>et al.</i> (2000)
8	1992	1	24	5.00	4.00	74.55	35.50	5.6	85.5	268	86	0	Mukhopadhyay (2015)
9	1993	4	8	3.00	49.00	77.64	35.69	5.2	38.2	269	73	-14	-do-
10	1993	6	15	11.00	12.00	77.76	35.65	5.0	41.6	95	74	-13	-do-
11	1996	4	1	8.00	8.00	73.46	31.46	5.7	47.9	98	33	101	-do-
12	1999	3	29	7.00	5.00	79.42	30.51	6.7	22.9	282	9	0	USGS
13	2000	6	19	10.00	41.00	77.46	35.19	5.3	33.0	179	77	-179	Mukhopadhyay (2015)
14	2001	7	16	4.00	7.00	73.13	32.85	5.2	57.5	65	36	49	-do-
15	2001	9	28	4.00	37.00	75.83	33.30	5.3	27.1	323	32	105	-do-
16	2002	1	27	10.00	33.00	75.99	33.10	4.9	30.8	225	20	-11	-do-
17	2004	2	14	10.00	30.00	73.16	34.75	5.7	26.3	111	49	57	-do-
18	2004	10	31	6.00	2.00	74.42	35.32	5.8	12.6	247	22	-92	-do-
19	2004	10	31	3.00	49.00	74.87	35.46	4.3	10.0	39	74	-164	-do-
20	2004	10	31	8.00	5.00	75.13	35.47	4.2	5.6	253	36	-65	-do-
21	2005	10	8	3.00	50.00	73.64	34.52	7.2	7.9	338	50	0	EERI (2005)
22	2005	10	8	1.00	45.00	73.09	34.57	5.1	10.0	96	47	55	Mukhopadhyay (2015)
23	2006	4	4	11.00	40.00	75.86	33.18	4.1	43.3	98	44	57	-do-
24	2007	10	26	6.00	50.00	76.71	35.25	5.5	30.2	274	66	-10	-do-
25	2009	2	20	3.00	48.00	73.82	34.24	5.7	21.0	308	21	99	-do-
26	2009	7	27	6.00	23.00	73.24	34.93	5.3	32.5	338	34	130	-do-
27	2009	12	6	4.00	33.00	77.33	35.74	5.7	66.3	348	19	158	-do-

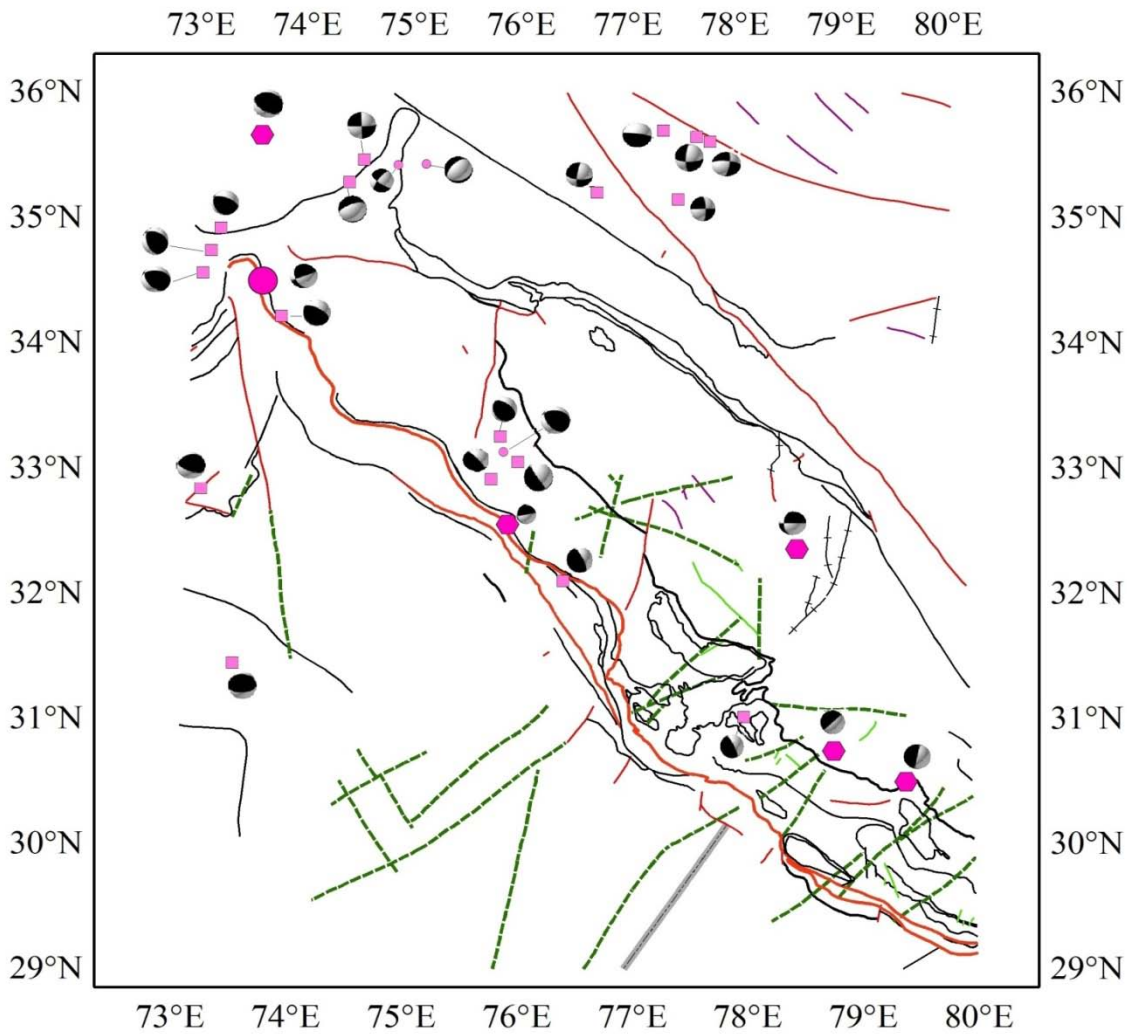


**Figure 2.12:** Fault plane solutions of 27 earthquakes listed in table 2.16.

**Table 2.17:** Salient features of earthquake catalogues used for compilation of MHD catalogue-2 for the study area.

S. No.	Catalogue	Time Period	Magnitude		No. of events considered
			Scale	Range	
1	IMD	2013-2015	$M_L$	$4.5 \leq M_L \leq 5.6$	3
2	ISC	2013-2015	$m_b$	$4.4 \leq m_b \leq 4.7$	4
3	USGS	2013-2015	$m_b$	$4.4 \leq m_b \leq 5.4$	86
<b>Total no. of events</b>					93

**Table 2.18:** Magnitude wise breakup of earthquakes from MHD catalogue-2 for validation of results.

Magnitude range	Number of earthquakes
$5.5 \leq M_w \leq 5.7$	6
$4.5 \leq M_w \leq 5.4$	74

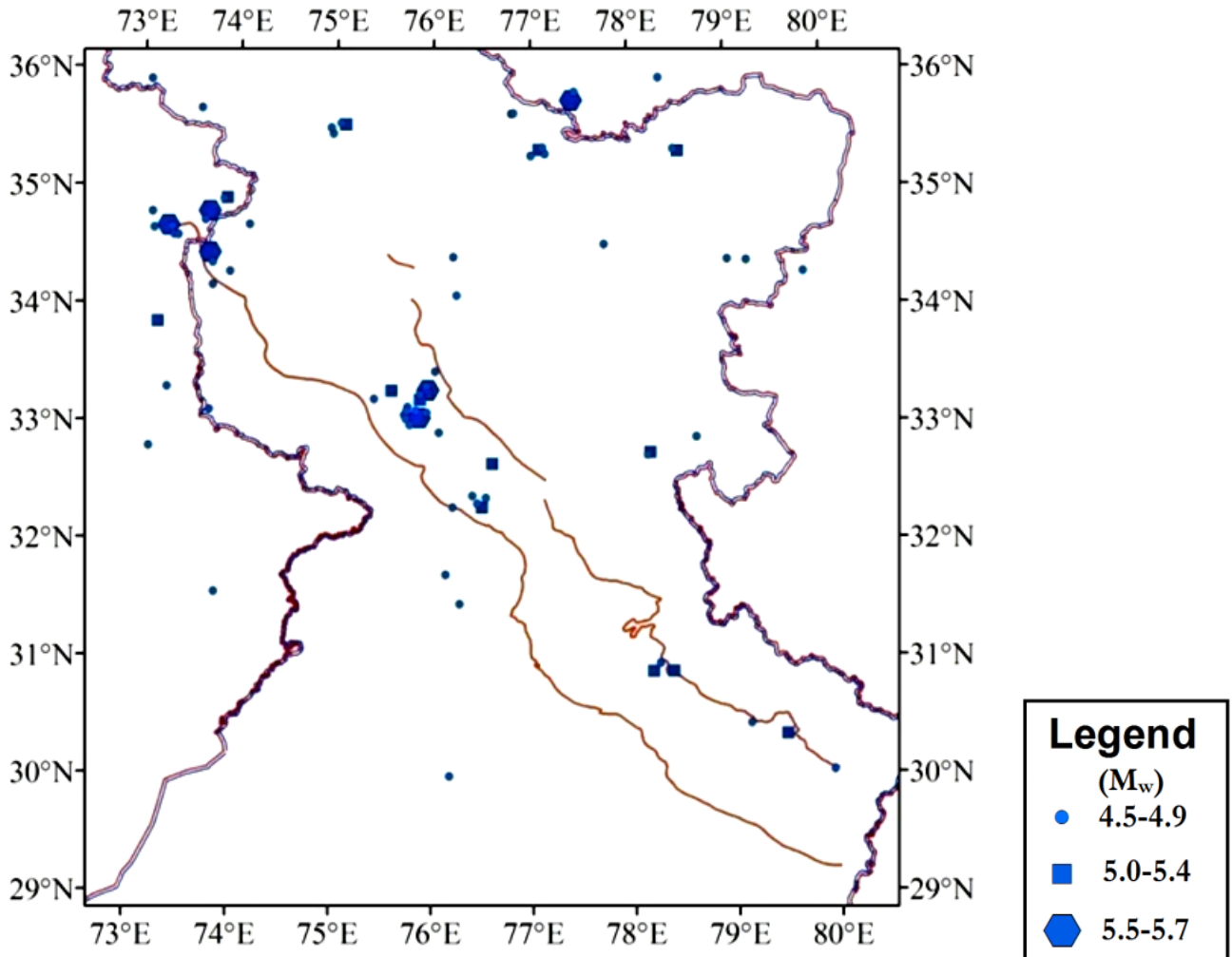


**Figure 2.13:** Seismicity as per MHD catalogue-2 for validation of results.

## 2.5 Conclusions

Study area was identified as  $7^\circ$  by  $7^\circ$  area with coordinates between longitude:  $73^\circ\text{E}$  to  $80^\circ\text{E}$  and latitude:  $29^\circ\text{N}$  to  $36^\circ\text{N}$ , in the western Himalaya for which several analyses were carried out. Seismicity data was compiled by merging, homogenization and declustering earthquake catalogues obtained from IMD, ISC and NEIC (USGS). Two different catalogues were compiled for the same space window with different objectives, viz. MHD catalogue and MHD catalogue-2 for validation of results. MHD earthquake catalogue contained 1172 earthquakes of magnitude  $M_w = 3.5$  and above for the time span 1552-2012 and was used for carrying out various analyses such as identification of susceptible areas, segmentation of longer lineaments and hazard assessment. MHD catalogue-2 contained 90 earthquakes of magnitude range between  $4.0 \leq M_w \leq 5.7$ , for the time span 2013-2015 and was used for validation of all results. Epicentral maps were prepared for these catalogues.

Tectonic data was prepared for the study area. Initially 21 prominent and named tectonic units were considered and later all tectonic units in the study area were considered. Tectonic map was prepared. Seismotectonic map for the study area was prepared by superimposing seismicity data and tectonic data. These data were used for identification of seismically susceptible areas in Chapter 4, segmentation of longer tectonic units in Chapter 5 and for hazard assessment in Chapters 6 and 7.

Identification of seismically susceptible areas and segmentation of longer tectonic units were identified resorting to pattern recognition technique, in which seismicity and tectonic data plays an important role. An introduction to major steps of pattern recognition technique is described in Chapter 3.



# CHAPTER 3

## PATTERN RECOGNITION

---

### 3.1 Introduction

Pattern recognition (PR) is the study which aims to recognize objects or patterns into different categories or classes based either on *a priori* knowledge or on statistical information extracted from the patterns (Robbert *et al.* 1992; Aguilar, 2004). Pattern recognition is the study that concerns either the description and/ or classification (recognition) of a set of events. It is the study of how machines can observe the environment, learns to distinguish patterns of interest from their background, and make sound and reasonable decisions about categories of patterns (Walt *et al.* 2007).

Humans have developed highly sophisticated skills for sensing their environment and taking actions according to what they observe, e.g., recognizing a face, understanding spoken words, reading handwriting, distinguishing fresh food from its smell, etc. However, making a computer to recognize these types of objects is a very challenging task (Duin *et al.* 2005). This chapter first presents major steps of PR technique, and then it goes on to deal with identification of seismically susceptible areas as a case study, which is further extended in Chapter 4. PR is also applied for segmentation of longer tectonic units, details of which are given in Chapter 5.

### 3.2 Major Steps of Pattern Recognition

The PR technique applied in this study consists of six major steps: identification and extraction of features, classification of the data set, discriminant analysis, i.e. training exercise, decision making based on results of training exercise and validation of results. These are shown in figure 3.1. These six steps of pattern recognition were used in this study for two different approaches: identification of seismically susceptible areas and segmentation of two longer lineaments (MBT and MCT) in the western Himalaya. These steps are shown in detail for one case study.

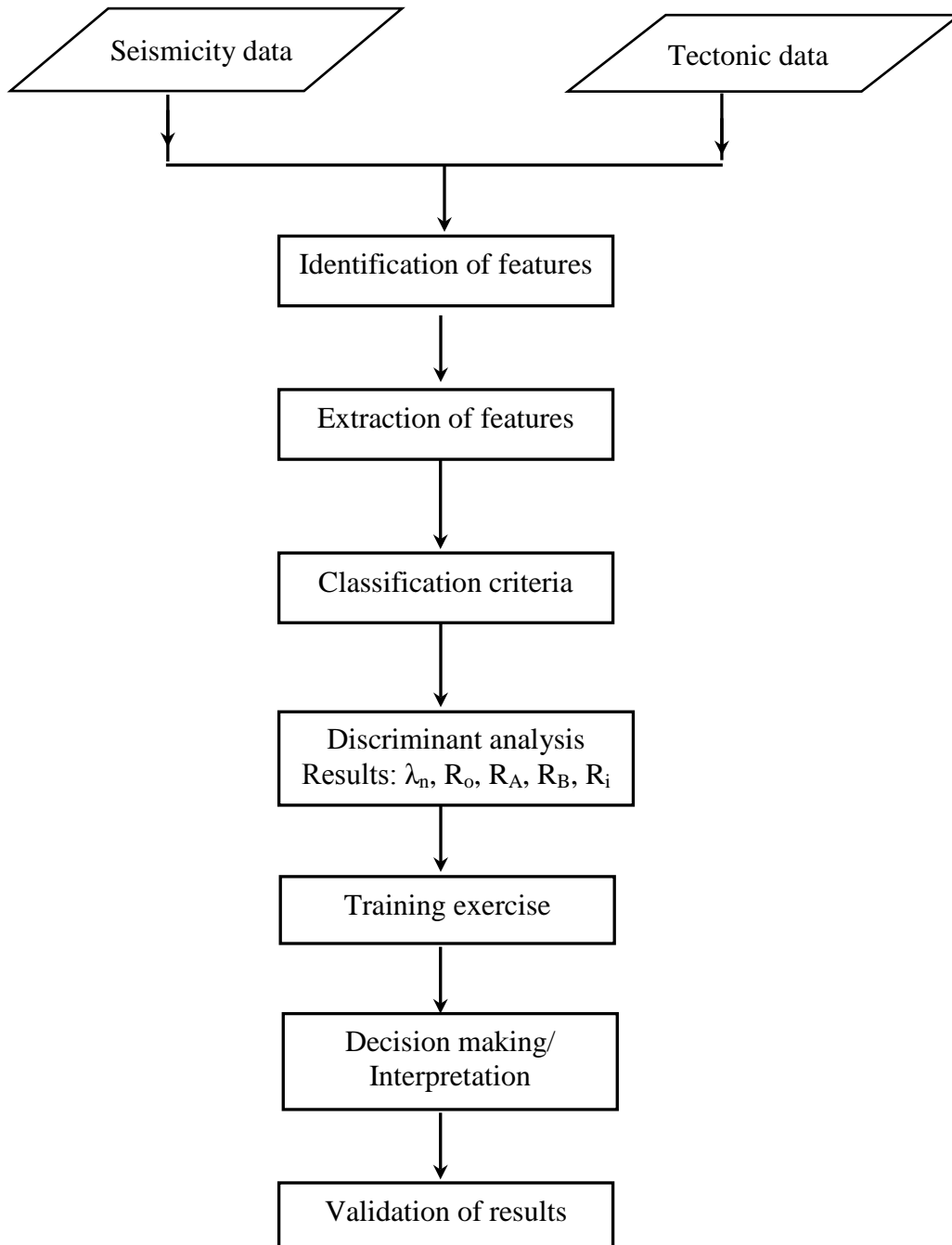


**Figure 3.1:** Major steps of Pattern Recognition (PR) technique.

### 3.3 Identification of Features

Feature identification is the process of choosing input to the pattern recognition system. It involves judgment of identifying features which can be identified from a given set of data and which are also extractable. Features may be qualitative, i.e. symbolic (like color). These may be represented by continuous or discrete-binary variables. Binary features may be used to represent

the presence or absence of a particular feature. On the other hand, features may be quantitative, i.e., numerical (example: weight). Features may also be represented by a combination of both qualitative and quantitative features. Feature identification needs to be addressed at the beginning of any pattern recognition exercise.

Features in the present study were identified from seismicity and tectonic data. Seismicity data was considered as per MHD catalogue, and tectonic data was considered from SEISAT Atlas. This data has been described in Chapter 2. A circle of 25 km radius was drawn around each earthquake of MHD catalogue. All features were identified and quantified within this radius. All 1172 epicenters of the MHD catalogue were considered and are referred to as central earthquakes henceforth.

Twelve features were identified from a circle of radius 25 km. These are: F1: magnitude of central earthquake ( $M_w$ ); F2: number of epicenters other than central earthquake; F3: number of tectonic units; F4: number of tectonic intersections; F5: number of intersections of tectonic units with river; F6: distance between central earthquake and nearest tectonic unit; F7: distance between central earthquake and nearest tectonic intersection; F8: Length of river; F9: addition of number of earthquakes and number of tectonic units (F2+F3). Three additional features were identified from Digital Elevation Models (DEM's).

Digital Elevation Model available on National Remote Sensing Centre (Indian Space Research Organization, ISRO) website has been studied for the study area. ISRO launched Cartosat-1 with the primary objective of providing high resolution satellite data of 2m in track stereo. DEM generated by Cartosat-1 facilitates large scale mapping and terrain modeling. A digital elevation model (DEM) is a digital model or 3 dimensional representation of a terrain's surface. A DEM can be represented as a raster (a grid of squares, also known as a height map when representing elevation) or as a vector-based triangular irregular network (TIN). DEM's were downloaded from the website ([http://bhuvan.nrsc.gov.in/bhuvan\\_links.php](http://bhuvan.nrsc.gov.in/bhuvan_links.php)) and elevation contours were generated at 50m interval in ArcGIS-9.3. Elevations were available for the colored areas shown in figure 3.2 and are not available for Nepal, Tibet, China and parts of India. Following features were extracted from DEM data. F10: Maximum elevation,  $E_{max}$ ; F11: Minimum elevation,  $E_{min}$  and F12: Difference in elevation ( $E_{max} - E_{min}$ ).



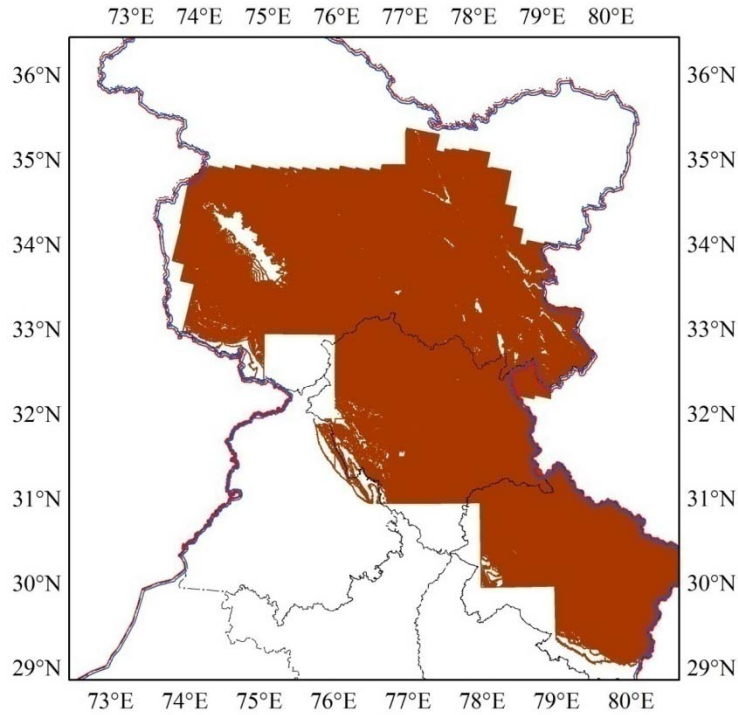


**Figure 3.2:** DEM data available for portions shown in brown, from ISRO website. Features F10, F11 and F12 were extractable in these areas only.

### 3.4 Extraction of Features

Feature extraction involves extraction of numeric or symbolic information from a set of observations. Features which are to be extracted must be able to fulfill the following conditions: it should be feasible to computationally extract these; lead to a good pattern recognition system success; and reduce the problem data into a manageable amount of information without discarding valuable information (Duda *et al.* 2001).

In this study features were extracted by considering an area within a radius of 25 km drawn around each epicenter of MHD catalogue. The reason for selecting this radius is given below. Two classification criteria based on magnitude of an earthquake were considered, discussed in section 3.5. As per Wells and Coppersmith (1994) formulation between magnitude and surface rupture length (SRL) for  $M_w = 5.5$ , SRL is 20.89 km. Therefore, minimum radius within which feature should be extracted is 20.89 km. A second classification criteria for magnitude  $M_w = 6.0$ , yields a length of 24.95 km. Moreover, Peresan *et al.* (2015) considered 25 km radius for identifying areas where earthquakes of magnitude  $M_w = 5.5$  can take place. Therefore, all features are extracted from

within a circle of radius 25 km. Taking these factors into account 25 km radius was considered for extraction of features.

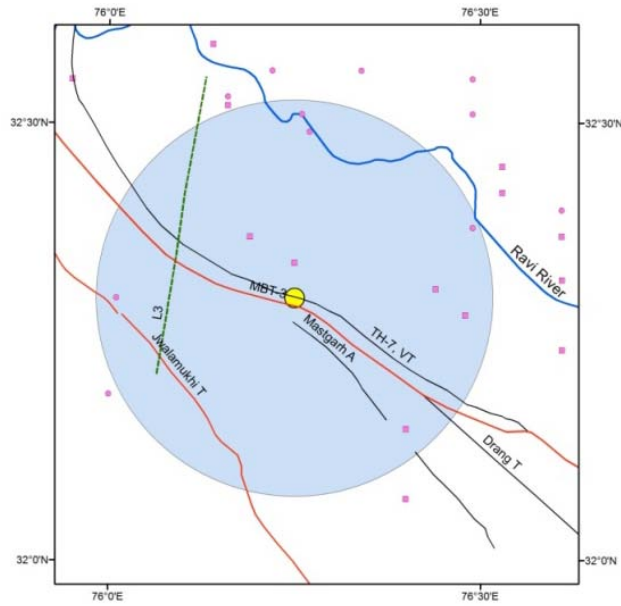
A set of features, F1-F12, which were identified for each central earthquake, were extracted from this circle and each has a numerical value. Out of twelve features, 11 features, i.e. from F2 to F12 were used for the identification of susceptible areas in Chapter 4 and four features F1, F2, F3 and F4 were used for segmentation of longer tectonic units MBT and MCT.

It was observed that in some cases features F6 and F7 do not lie within the circle. For feature F6, i.e. distance to the nearest tectonic unit, most of the time there was a tectonic unit within the 25 km radius but sometimes if there is no tectonic unit within the circle, nearest distance to tectonic unit was considered. Similarly, for feature F7, i.e., intersection between a tectonic unit with another tectonic unit outside the circle, nearest distance was considered.

Twelve features, F1- F12, extracted for the great Kangra earthquake of 4<sup>th</sup> April, 1905 ( $M_w= 8.0$ ) are shown in figures 3.3(a) and 3.3(b), and described here. F1: Magnitude of central earthquake is  $M_w=8.0$ ; F2: number of earthquake epicenters other than the central earthquake, i.e. epicenter of Kangra earthquake (shown by yellow circle at center) within the circle = 9; F3: number of tectonic units = 6, these are MBT, Mastgarh Anticline, Jwalamukhi thrust, Drang thrust, thrust TH07 and a lineament L3; F4: lineament L3 intersects MBT, TH 07 and JMT and Drang thrust is intersecting in MBT, therefore 4 tectonic intersections; F5: number of intersections between river and tectonic unit = 0; F6: distance between epicenter of central earthquake and nearest tectonic unit TH 07 is 0.14 km; F7: distance between central earthquake and nearest tectonic intersection is 15.75 km; F8: length of Ravi river within the circle is 25.68 km; F9: this is the addition of number of tectonic units and number of epicenters within the circle, (F2 + F3) which is equal to 15. F10: maximum elevation is 4850 m; F11: minimum elevation is 350 m; F12: difference in elevation is 4500 m. Minimum elevation is shown by green and maximum elevation is shown by red triangle in figure 3.3(b).

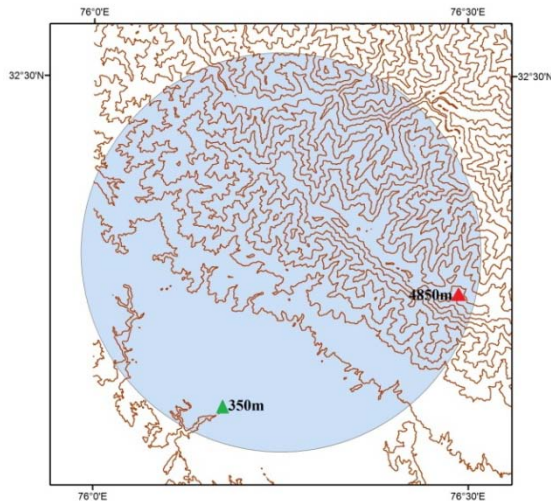
Similarly, feature extraction for several earthquakes of magnitude more than  $M_w$  5.5, such as Kashmir earthquake of 8<sup>th</sup> October, 2005, five historical earthquakes which had same epicenters in the Srinagar Baramula region, Uttarkashi earthquake of 20<sup>th</sup> October, 1991, Chamoli earthquake of 29<sup>th</sup> March, 1999, Kinnaur earthquake of 19<sup>th</sup> January, 1975, Chamba earthquake of

22<sup>nd</sup> June, 1945, and Dharamshala earthquake of 26<sup>th</sup> April, 1986 are shown in figures 3.4(a-g). Similar extraction for an earthquake of magnitude less than  $M_w$  5.5 is shown in figure 3.4(h).



(a)

Feature	Value
F1	8.0
F2	9
F3	6
F4	4
F5	0
F6	0.14Km
F7	15 Km
F8	25.68 Km
F9	15
F10	4850 M
F11	350 M
F12	4500 M



(b)

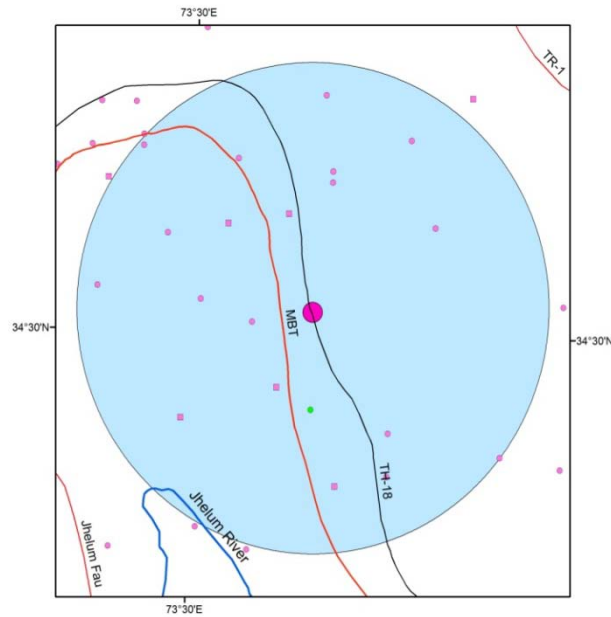
**Figure 3.3:** (a) An example of extracted features for the great Kangra earthquake of 4<sup>th</sup> April, 1905,  $M_w = 8.0$  (MHD catalogue); (b): Elevation contours as per ISRO website within the circle around the Great Kangra earthquake of 1905, at 500 m interval. Minimum elevation is shown by green and maximum elevation is shown by red triangle. Accompanying table shows the numerical values of the extracted features, F1, F2, F3,..., F12. These are described in section 3.4.

## Earthquake

### Kashmir earthquake of 8<sup>th</sup> October, 2005

$M_w$ : 7.2  
 Lat: 34.52°N  
 Long: 73.64°E

## Feature extraction (within 25 km radius)



## Features

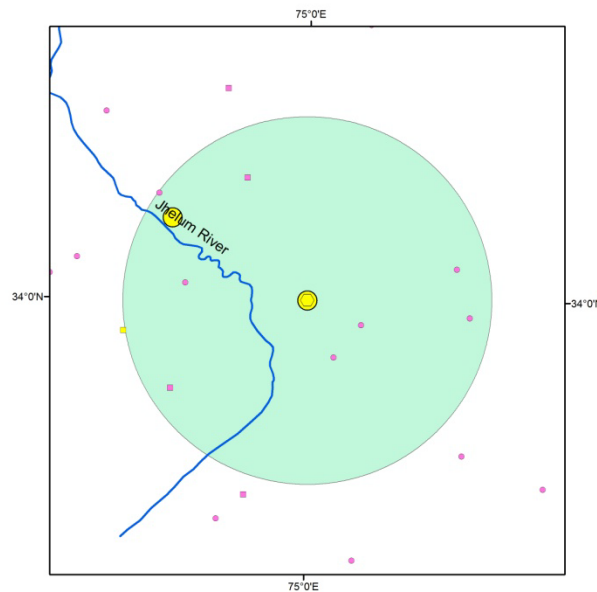
F2	20
F3	2
F4	0
F5	0
F6	0.12 km
F7	40.25 km
F8	8.47 km
F9	22
F10	4350 m
F11	50 m
F12	4300 m

(a)

YY	MM	DD	$M_w$
1778	-	-	7.7
1662	-	-	7.5
1735	-	-	7.5
1784	-	-	7.3
1803	-	-	6.5

Lat: 34.00°N  
 Long: 75.00°E

**Note:** Five historical earthquakes have same epicenter.

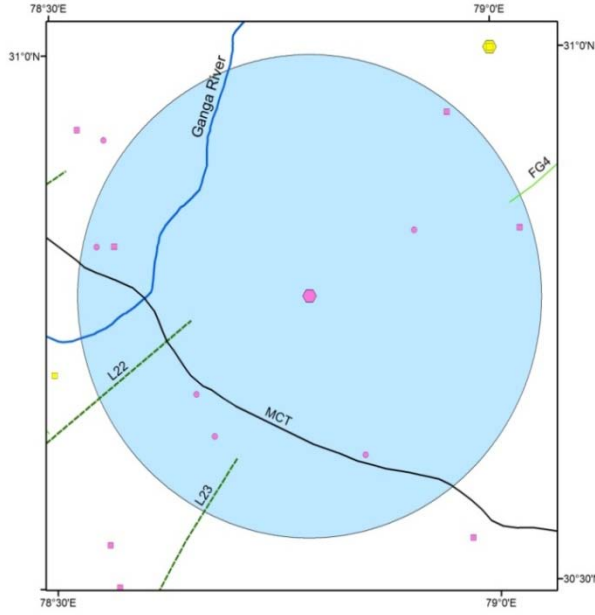


F2	14
F3	0
F4	0
F5	0
F6	44.14 km
F7	67.86 km
F8	50.19 km
F9	14
F10	4450 m
F11	50 m
F12	4400 m

(b)

**Uttarkashi earthquake of 20<sup>th</sup> October, 1991**

$M_w$ : 6.8  
 Lat: 30.77 °N  
 Long: 78.79 °E

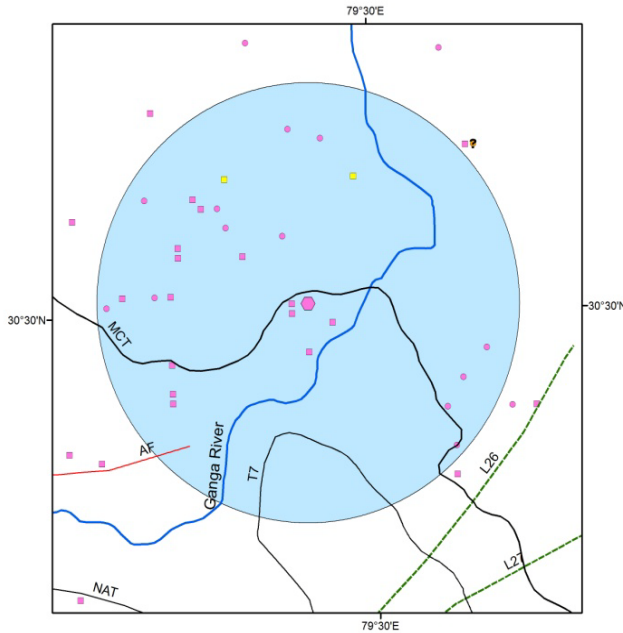


F2	8
F3	4
F4	1
F5	1
F6	13.02
F7	16.08
F8	34.32
F9	12
F10	6650 m
F11	1350 m
F12	5300 m

(c)

**Chamoli earthquake of 29<sup>th</sup> March, 1999**

$M_w$ : 6.7  
 Lat: 30.51 °N  
 Long: 79.42 °E

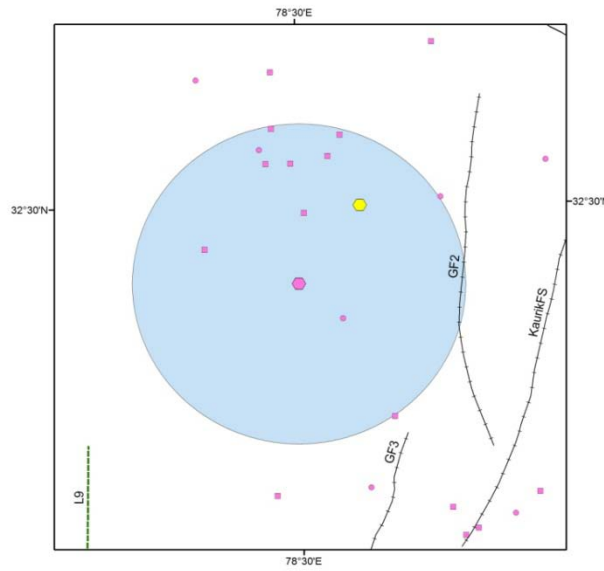


F2	28
F3	3
F4	0
F5	1
F6	1.35 km
F7	29.73 km
F8	65.07 km
F9	31
F10	6550 m
F11	850 m
F12	5700 m

(d)

**Kinnaur earthquake of  
19<sup>th</sup> January, 1975**

$M_w$ : **6.6**  
 Lat: 32.39°N  
 Long: 78.50°E

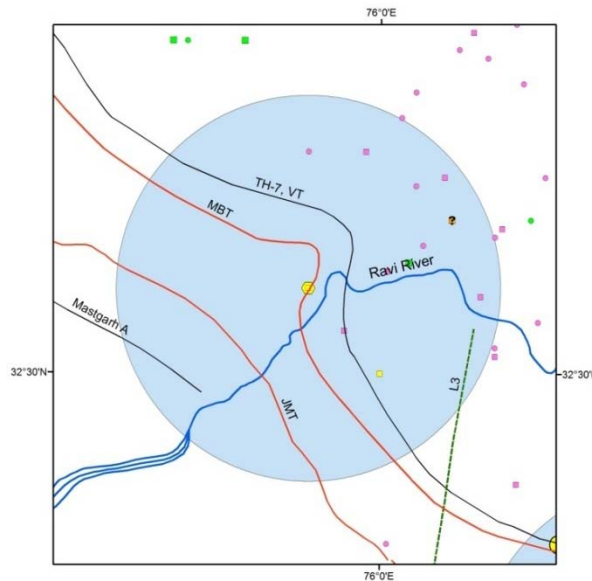


F2	10
F3	1
F4	0
F5	0
F6	24.27
F7	51.62
F8	0
F9	11
F10	6550 m
F11	250 m
F12	6300 m

(e)

**Chamba earthquake of  
22<sup>nd</sup> June, 1945**

$M_w$ : **6.5**  
 Lat: 32.60°N  
 Long: 75.90°E

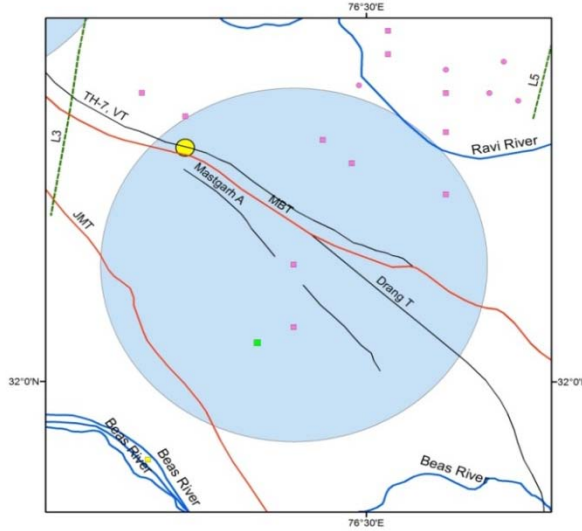


F2	14
F3	6
F4	0
F5	3
F6	0.18 km
F7	31.55 km
F8	57.4 km
F9	20
F10	3350 m
F11	750 m
F12	2600 m

(f)

**Dharamshala earthquake of 26<sup>th</sup> April, 1986**

$M_w$ : 5.8  
 Lat: 32.15°N  
 Long: 76.40°E

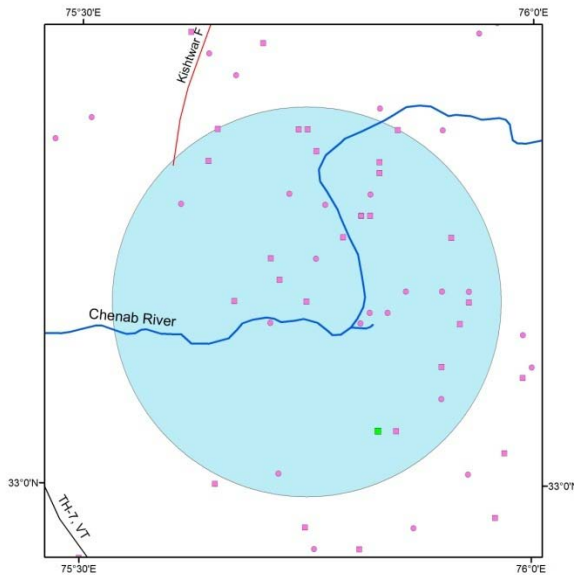


F2	6
F3	5
F4	2
F5	0
F6	2.72 km
F7	4.85 km
F8	6.59 km
F9	11
F10	4850 m
F11	250 m
F12	4600 m

(g)

**Class B earthquake**

$M_w$ : 4.6  
 Year: 1973  
 Month: 4  
 Day: 10  
 Lat: 33.17°N  
 Long: 75.75°E



F2	36
F3	1
F4	0
F5	0
F6	24.62 km
F7	37.47 km
F8	54.99 km
F9	37
F10	4450 m
F11	50 m
F12	4400 m

(h)

**Figure 3.4 (a-h):** Feature extraction shown for different earthquakes, where **F2**: number of earthquake epicenters other than central earthquake; **F3**: number of tectonic units; **F4**: number of intersections between two tectonic units; **F5**: number of intersections between tectonic unit and river; **F6**: distance of central earthquake from nearest tectonic feature (km); **F7**: distance of central earthquake from nearest tectonic intersection (km); **F8**: length of river (km); **F9**: combination of number of earthquakes and number of tectonic features (F2+F3); **F10**: maximum elevation,  $E_{max}$  (meters); **F11**: minimum elevation,  $E_{min}$  (meters) and **F12**: difference in elevation ( $E_{max} - E_{min}$ ) (meters).

### 3.5 Classification Criteria

Classification is an important step of any pattern recognition technique. Patterns of interest can be learnt or distinguished from their background. This involves formulating a classification criterion. The classification or description is usually based on the availability of a set of patterns that have already been classified or described. To recognize the patterns, it is important to train the classifier first by the training data set that is usually some data that have already been classified or described. Pattern recognition is generally categorized according to the type of learning procedure used to generate the output value.

In this study four different classification criteria were considered, two of these were based on seismicity data and two on tectonic data. In seismicity data, classification criteria was based on magnitude and all epicenters in the MHD catalogue were divided into two classes based on their magnitude. These classification criteria were applied in Chapter 4 for identification of susceptible areas. These classification criteria are:

- a) **Classification criteria-I:** Class I: epicenters having magnitude  $M_w \geq 6.0$ ; Class II: epicenters having  $4.5 \leq M_w \leq 5.9$ ; and
- b) **Classification criteria-II:** Class A: epicenters having magnitude  $M_w \geq 5.5$ ; Class B: epicenters having  $4.5 \leq M_w \leq 5.4$ .

In classification criteria based on tectonic data, distance from a long tectonic unit was considered to divide epicenters into two classes, based on the distance from either MBT or MCT. These classification criteria were used for segmentation of longer tectonic units MBT and MCT in Chapter 5. These classification criteria are:

- a) **Classification criteria-III:** Classification of epicenters with respect to distance from MBT, Class  $S_{B1}$ : epicenters within 25 km of MBT on either side; Class  $S_{B2}$ : epicenters outside 25 km of MBT on either side. A distance of 25 km south of MBT was considered in classification criteria-III because several tectonic units are south and parallel to trend of the MBT and may act as causative faults. Some of the prominent ones are MFT, Drang thrust and Jwalamukhi thrust shown in figure 2.10.
- b) **Classification criteria-IV:** Classification of epicenters with respect to distance from MCT, Class  $S_{C1}$ : epicenters within 25 km of MCT on either side;  $S_{C2}$ : epicenters outside 25 km of MCT on either side.



### 3.6 Discriminant Analysis

Discriminant analysis is a method used in pattern recognition to find a linear combination of features that characterizes or separates two or more classes of objects or events. This method is used to develop a linear combination of extracted features to maximize the difference between two or more classes. Discriminant function transforms the original set of features of an earthquake into a single seismic score which represents the specimen's position along a line defined by the linear discriminant function. Discriminant analysis is one of the most widely used multivariate procedures for analysis in earth sciences and the algorithm for two classes is detailed below (Davis, 2002).

Assume that there are two classes: Class P having  $n_p$  number of samples and Class Q having  $n_q$  number of samples. To compute the discriminant function, an equation of the form

$$S. \lambda = D \quad (3.1)$$

must be solved, where, S is an  $m \times m$  matrix of pooled variances and covariances of the  $m$  variables,  $\lambda$  is the coefficient of discriminant function and D is multivariate mean of the two classes. Following equations show step by step computations of these variables.

Vector mean of all features of each Class is given as

$$\text{Vector mean of features of Class P: } \bar{P}_j = \frac{\sum_{i=1}^{n_p} p_{ij}}{n_p} \quad (3.2)$$

$$\text{Vector mean of features of Class Q: } \bar{Q}_j = \frac{\sum_{i=1}^{n_q} q_{ij}}{n_q} \quad (3.3)$$

$p_{ij}$  is the  $i^{\text{th}}$  observation on variable  $j$  in Class P and  $\bar{P}_j$  is the mean of variable  $j$  in Class P, which is arithmetic average of the  $n_p$  observations of variable  $j$  in Class P. Same conventions apply to group Q.

Vector mean difference between two classes is simply given by:

$$d_j = \bar{P}_j - \bar{Q}_j \quad (3.4)$$

Multivariate means of the two classes is computed as:

$$D = \bar{P} - \bar{Q} \quad (3.5)$$

Expanding equation 3.4, we may write:

$$\begin{bmatrix} d_1 \\ d_2 \\ \vdots \\ d_m \end{bmatrix} = \begin{bmatrix} \bar{P}_1 \\ \bar{P}_2 \\ \vdots \\ \bar{P}_m \end{bmatrix} - \begin{bmatrix} \bar{Q}_1 \\ \bar{Q}_2 \\ \vdots \\ \bar{Q}_m \end{bmatrix} \quad (3.6)$$

where  $m$  is the number of features in each class.

To construct the matrix of pooled variances and covariances, a matrix of sum of squares and cross products of all variables in Class P and Class Q were computed.

Pooled variance covariance matrix of Class P is given by:

$$S_{Pjk} = \sum_{i=1}^{n_p} p_{ij} p_{ik} - \frac{\sum_{i=1}^{n_p} p_{ij} \sum_{i=1}^{n_p} p_{ik}}{n_p} \quad (3.7)$$

where,  $p_{ij}$  is the  $i^{\text{th}}$  observation on variable  $j$  in Class P, and  $p_{ik}$  is the  $i^{\text{th}}$  observation on variable  $k$  in Class P. Similarly, pooled variance covariance matrix of Class Q is given by:

$$S_{Qjk} = \sum_{i=1}^{n_q} q_{ij} q_{ik} - \frac{\sum_{i=1}^{n_q} q_{ij} \sum_{i=1}^{n_q} q_{ik}}{n_q} \quad (3.8)$$

Then pooled variance matrix is given by:

$$S = \frac{S_P + S_Q}{n_p + n_q - 2} \quad (3.9)$$

Now, solving the equation (3.1) using equations (3.5) and (3.9), coefficient of discriminant function,  $\lambda$ , is given as

$$S \cdot \lambda = D, \text{ i.e., } \lambda = S^{-1} D \quad (3.10)$$

Coefficients are found as  $\lambda_1, \lambda_2, \dots, \lambda_n$ . These coefficients are used to determine the seismic score of each earthquake epicenter which is the sum of products of  $\lambda$  of each feature to the numerical value of that feature given by expression 3.11:

$$R_i = \sum_{n=1}^n F_n \lambda_n \quad (3.11)$$

where  $F_1, F_2, \dots, F_n$  are extracted features and  $R_1, R_2, \dots, R_n$  are seismic scores of 1<sup>st</sup> epicenter, 2<sup>nd</sup> epicenter and so on up to  $n^{\text{th}}$  epicenter.

Multivariate mean of Class P is given as:

$$R_P = \lambda_1 p_{1i} + \lambda_2 p_{2i} + \dots + \lambda_n p_{ni} \quad (3.12)$$

Multivariate mean of Class Q is given as:

$$R_Q = \lambda_1 q_{1i} + \lambda_2 q_{2i} + \dots + \lambda_n q_{ni} \quad (3.13)$$

Discriminant index ( $R_0$ ), which is exactly halfway between the center of Class P and center of Class Q, i.e., midpoint between multivariate means of two classes is given as:

$$R_0 = (R_P + R_Q) / 2 \quad (3.14)$$

Percentage contribution of each feature gives the percentage a feature contributes in discriminating a class from another. This is given as:

$$[(D * \lambda) / D^2] * 100 \% \quad (3.15)$$

In this study, the discriminant analysis was used for achieving two objectives: identification of susceptible areas in the western Himalaya as shown in Chapter 4 and to determine the segments of longer lineaments MBT and MCT as shown in Chapter 5.

The following section shows an example of calculations of all steps of PR. In this example, out of 1172 earthquakes in the MHD catalogue 537 earthquakes of magnitude  $4.5 \leq M_w \leq 8.0$  were considered for the PR analysis. Since the magnitude of completeness of MHD catalogue was 4.3, as mentioned in Chapter 2 (section 2.4.8) the lower cut off value was considered close to this, as  $M_w = 4.5$ . A circle of 25 km radius was drawn around each epicenter and 11 features F2 to F12 were extracted for each of the 537 central earthquakes. F1, i.e., the magnitude of central earthquake was not considered as a feature in this exercise because the classification of epicenters was based on magnitude. The epicenters were then divided into two classes as per classification criteria I, i.e. Class I contained 45 epicenters of magnitude  $M_w \geq 6.0$ , and Class II contained 492 epicenters of magnitude range  $4.5 \leq M_w \leq 5.9$ . With this classification criterion and eleven features following discriminant analysis was carried out.

Vector mean of features of Class I, Class II, and vector of mean differences of both classes were calculated as per equations 3.2, 3.3 and 3.4, respectively. Coefficients of discriminant function, i.e.  $\lambda$  values, were calculated using equation 3.10. These values are given in table 3.1.

Multivariate means of Class I and II and discriminant index ( $R_0$ ) were calculated using equations 3.12, 3.13 and 3.14, respectively. The values of  $R_I$ ,  $R_{II}$ , and  $R_0$  are: multivariate mean of Class I,  $R_I = -3.73$ ; multivariate mean of Class II,  $R_{II} = -7.54$  and discriminant index,  $R_0 = -5.63$ . Seismic score for each of the 537 earthquakes was calculated by considering the numerical value of the feature and the corresponding  $\lambda$  value as per equation 3.11.

Discriminant index ( $R_0$ ) and seismic scores are shown in figure 3.5(a). Seismic scores greater than discriminant index,  $R_0 = -5.63$ , i.e., seismic score  $\geq -5.63$ , were classified as Class I epicenters and seismic scores  $\leq -5.63$  were classified as Class II epicenter, and used to determine whether it is properly classified or misclassified, i.e., if seismic score of any earthquake of Class I is located on Class I side then it is properly classified else the epicenter is said to be misclassified.

**Table 3.1:** Salient features of model PR1, classification criteria I was considered i.e. Class I: epicenters having magnitude  $M_w \geq 6.0$ , which contained 45 epicenters and Class II: epicenters having  $4.5 \leq M_w \leq 5.9$ , which contained 492 epicenters. Features F2-F12 were extracted for 537 epicenters of  $4.5 \leq M_w \leq 8$ . Vector mean of Class I, Vector mean of Class II, Vector of mean differences of both classes, coefficients of discriminant function i.e.  $\lambda$  values and percentage contribution computed for each feature are shown in the table.

Feature	Name of Feature	Vector Mean Class I	Vector Mean Class II	Vector Mean difference	Coefficients of Discriminant Function, $\lambda$	% Contribution of Feature
F2	Number of earthquake epicenters other than central earthquake	11.18	10.73	0.45	-0.94	22.28
F3	Number of tectonic units	2.16	1.79	0.37	3.25	34.72
F4	Number of intersections between two tectonic units	0.64	0.44	0.20	-4.07	-24.47
F5	Number of intersections between tectonic unit and river	21.43	16.24	5.18	0.22	23.43
F6	Distance of central earthquake from nearest tectonic feature (km)	58.80	61.84	-3.04	-0.05	4.26
F7	Distance of central earthquake from nearest tectonic intersection (km)	23.46	18.63	4.82	0.06	8.96
F8	Length of river (km)	0.27	0.37	-0.10	-9.59	4.79
F9	Combination of number of earthquakes and no of tectonic features (F2+F3)	13.33	12.51	0.82	0.63	14.31
F10	Maximum elevation, $E_{\max}$ (meters)	3.86	3.12	0.73	0.88	18.57
F11	Minimum elevation, $E_{\min}$ (meters)	0.36	0.48	-0.12	-4.13	14.89
F12	Difference in elevation ( $E_{\max} - E_{\min}$ ) (meters)	3.50	2.64	0.86	-0.88	-21.74

### 3.7 Interpretation of Results

Results are interpreted in terms of properly classified and misclassified epicenters in either Class, in percentage. A lower value of the percentage of misclassification indicates a better result of discriminant analysis. In the above exercise out of 45 seismic scores of Class I, 43 were on Class I side and 2 were on Class II side, i.e. 95% epicenters were appropriately classified. Similarly, for Class II epicenters out of 492 earthquakes 324 were on Class II side and 168 epicenters were on Class I side, i.e. it showed 66% appropriate classification. This is shown in figure 3.5(a).

This exercise was repeated by changing the classification criteria and varying number of features. 15 iterations were carried out and percentage of properly classified epicenters and percentage of misclassified epicenters were checked every time. Table 3.2 shows salient features of these 15 iterations, and the corresponding histograms plotted for seismic scores are shown in figures 3.5 (a-o). Each iteration was considered as a PR model and has been named as PR1-PR15. The model discussed above in sections 3.2 to 3.7 is PR1.

While carrying out of the many iterations of discriminant analysis the best combination of classification criteria and number of features was retained. The best combination can be determined by the best separation between the two classes achieved after discriminant analysis. The separation between both classes is shown by  $R_0$  in histograms. Row 4, PR4, of table 3.2 gives the best combination. This was retained for further applications for identifying seismically susceptible areas and is discussed in detail in Chapter 4.

**Table 3.2:** Percentage of classification of either Class by varying classification criteria and number of features, step wise exclusion of one feature out of 11 features are shown from row number 5 to 15. The combination of classification criteria and number of features at S.No. 4, model PR4, gives the best results, and model PR15 gives second best result.

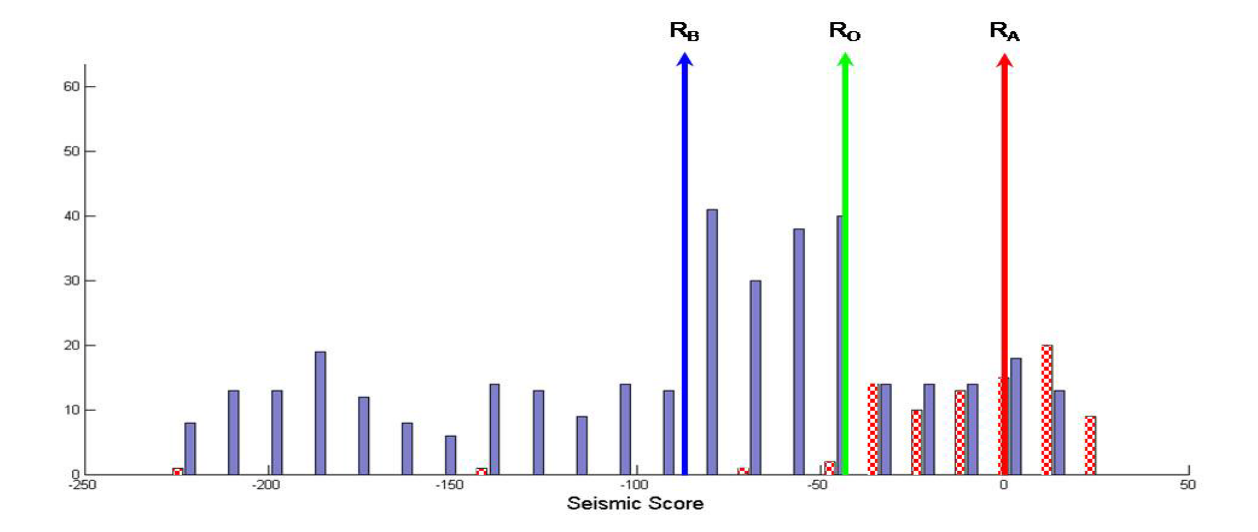
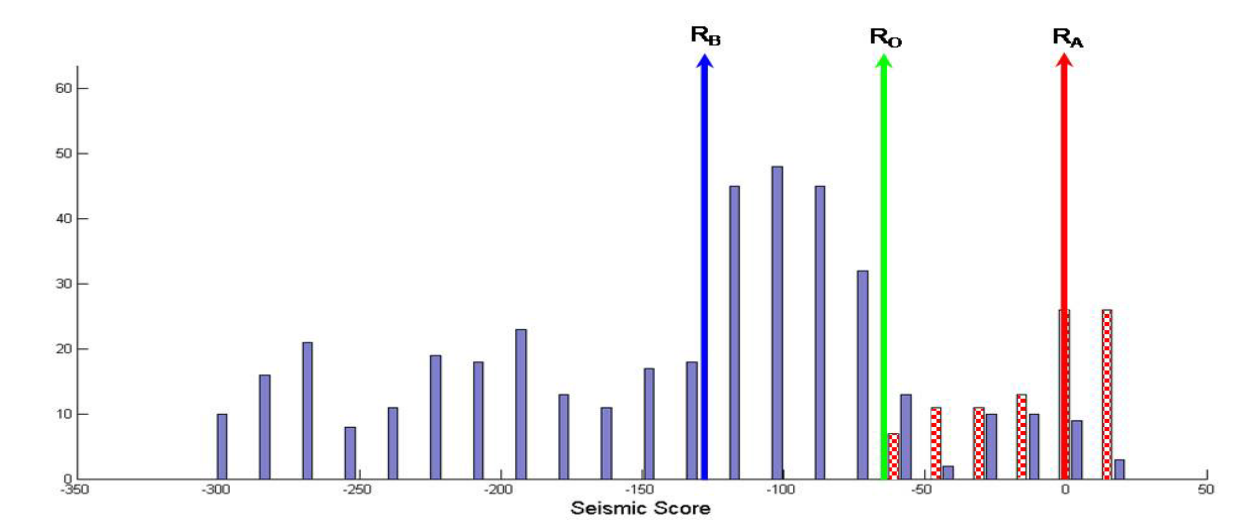
S. No.	Classification of Magnitude		No of Epicenters in Class A	No of Epicenters in Class B	Number of Features Used	% Classification of Class A	% Classification of Class B	PR Analysis
	Class A	Class B						
1.	$M_w \geq 6.0$	$4.5 \leq M_w \leq 5.9$	45	492	11 (F2-F12)	95	66	PR1
2.	$M_w \geq 5.5$	$4.5 \leq M_w \leq$	94	443	4 (F2, F3, F4,	92	85	PR2

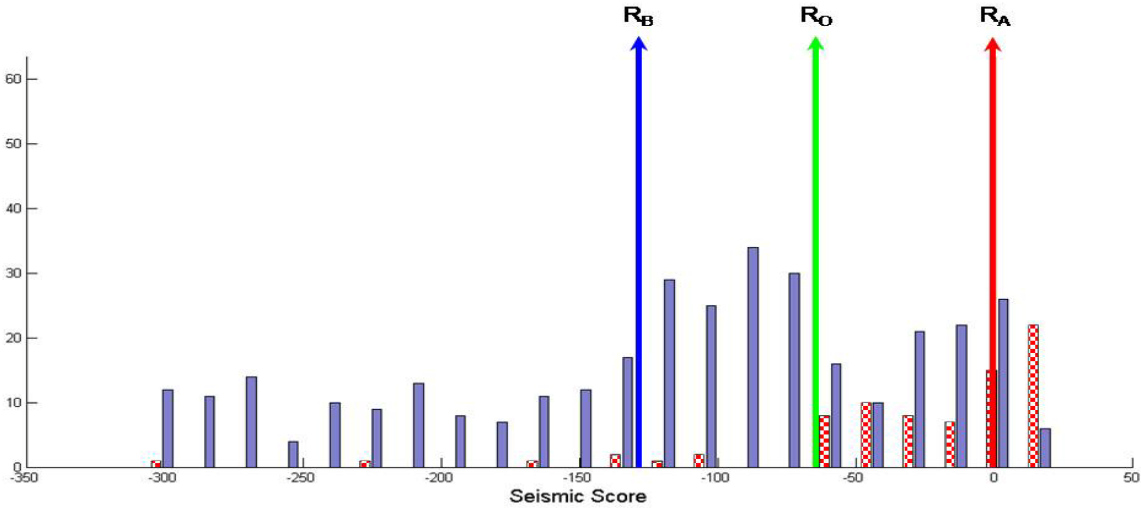
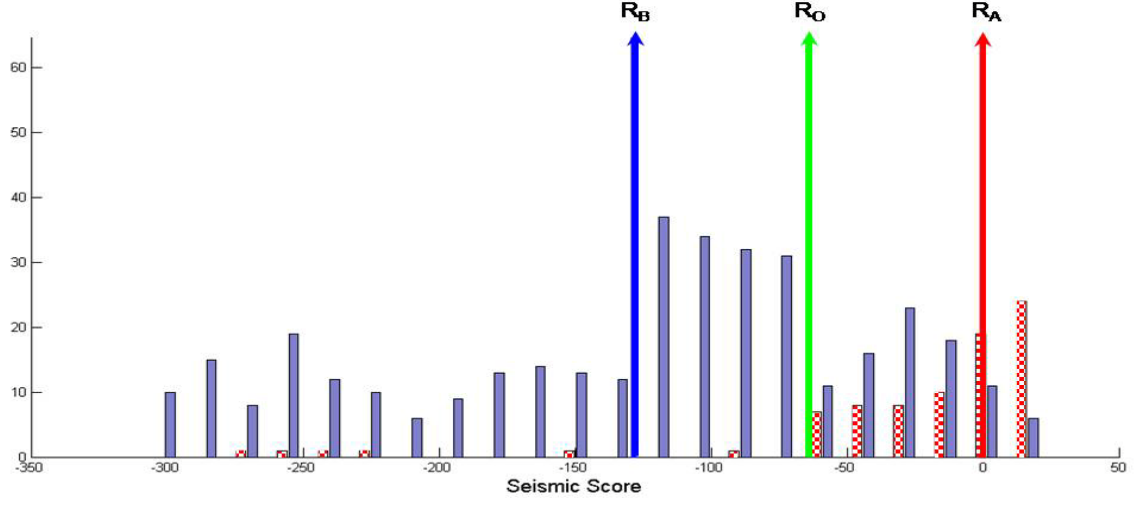
S. No.	Classification of Magnitude		No of Epicenters in Class A	No of Epicenters in Class B	Number of Features Used	% Classification of Class A	% Classification of Class B	PR Analysis
	Class A	Class B						
		5.4			F5)			
3.	$M_w \geq 5.5$	$4.5 \leq M_w \leq 5.4$	94	443	7 ( F2, F3, F4, F5 F6, F10, F11)	96	82	PR3
<b>4.</b>	<b><math>M_w \geq 5.5</math></b>	<b><math>4.5 \leq M_w \leq 5.4</math></b>	<b>94</b>	<b>443</b>	<b>11(F2-F12)</b>	<b>100</b>	<b>91</b>	<b>PR4</b>
5.	$M_w \geq 5.5$	$4.5 \leq M_w \leq 5.4$	94	443	F2 (No of earthquakes) excluded	92	78	PR5
6.	$M_w \geq 5.5$	$4.5 \leq M_w \leq 5.4$	94	443	F3 (Number of tectonic units) excluded	94	81	PR6
7.	$M_w \geq 5.5$	$4.5 \leq M_w \leq 5.4$	94	443	F4 (Number of tectonic intersections) excluded	97	93	PR7
8.	$M_w \geq 5.5$	$4.5 \leq M_w \leq 5.4$	94	443	F5 (Number of tectonic river intersections) excluded	100	89	PR8
9.	$M_w \geq 5.5$	$4.5 \leq M_w \leq 5.4$	94	443	F6 (Distance of central earthquake from nearest tectonic feature) excluded	98	88	PR9
10.	$M_w \geq 5.5$	$4.5 \leq M_w \leq 5.4$	94	443	F7 (Distance of central earthquake from nearest tectonic intersection) excluded	97	88	PR10
11.	$M_w \geq 5.5$	$4.5 \leq M_w \leq 5.4$	94	443	F8 (Length of river) excluded	99	86	PR11
12.	$M_w \geq 5.5$	$4.5 \leq$	94	443	F9 (Combination	96	85	PR12

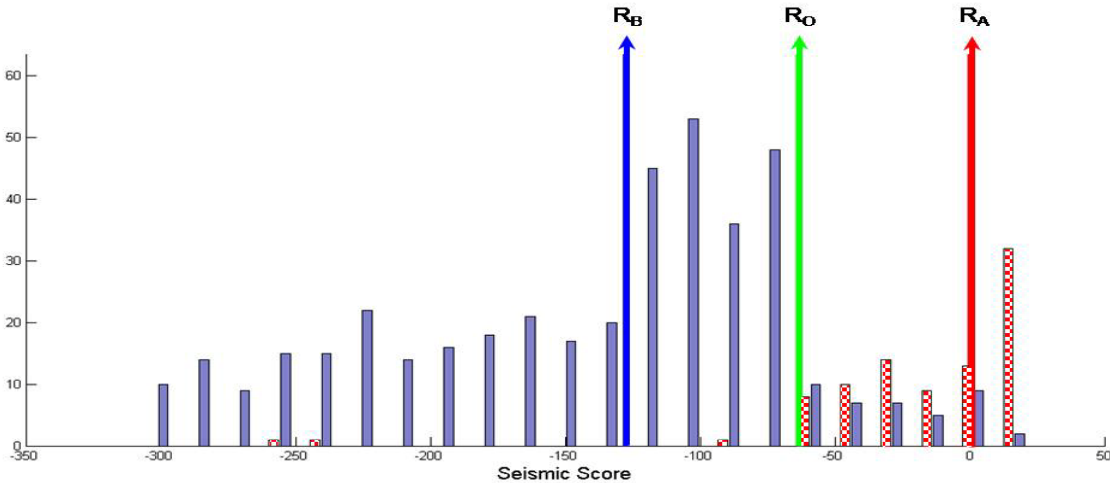
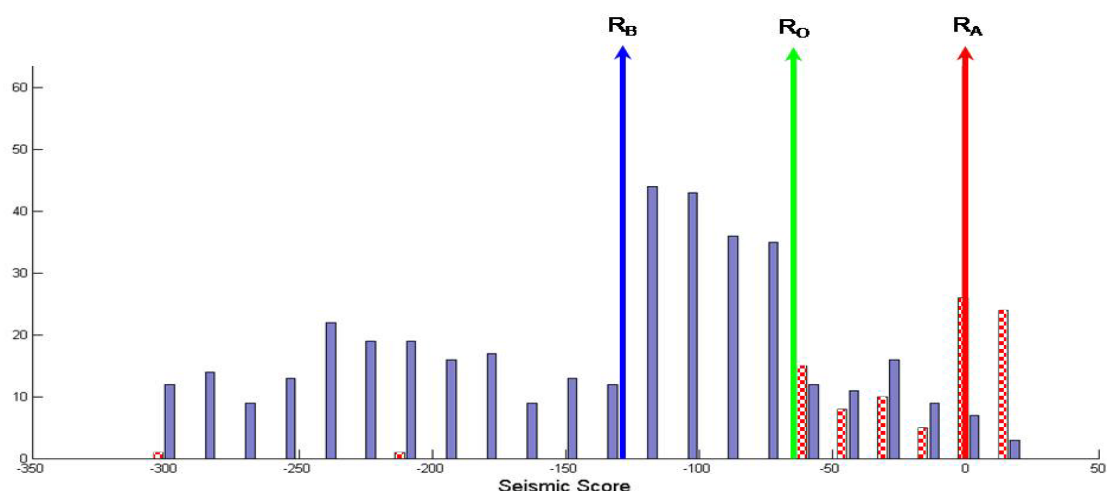
S. No.	Classification of Magnitude		No of Epicenters in Class A	No of Epicenters in Class B	Number of Features Used	% Classification of Class A	% Classification of Class B	PR Analysis
	Class A	Class B						
		$M_w \leq 5.4$			of no of earthquake and no of tectonic features) excluded			
13.	$M_w \geq 5.5$	$4.5 \leq M_w \leq 5.4$	94	443	F10 (Minimum elevation) excluded	96	92	PR13
14.	$M_w \geq 5.5$	$4.5 \leq M_w \leq 5.4$	94	443	F11 (Maximum elevation) excluded	97	92	PR14
15.	$M_w \geq 5.5$	$4.5 \leq M_w \leq 5.4$	94	443	F12 (Difference in elevation (Maximum elevation-minimum elevation)) excluded	100	90	PR15

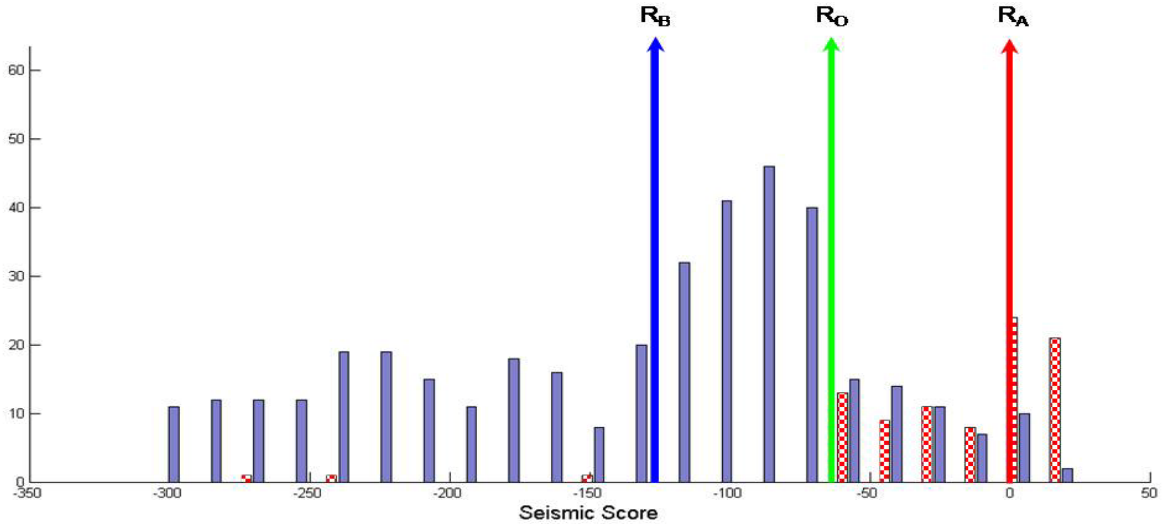
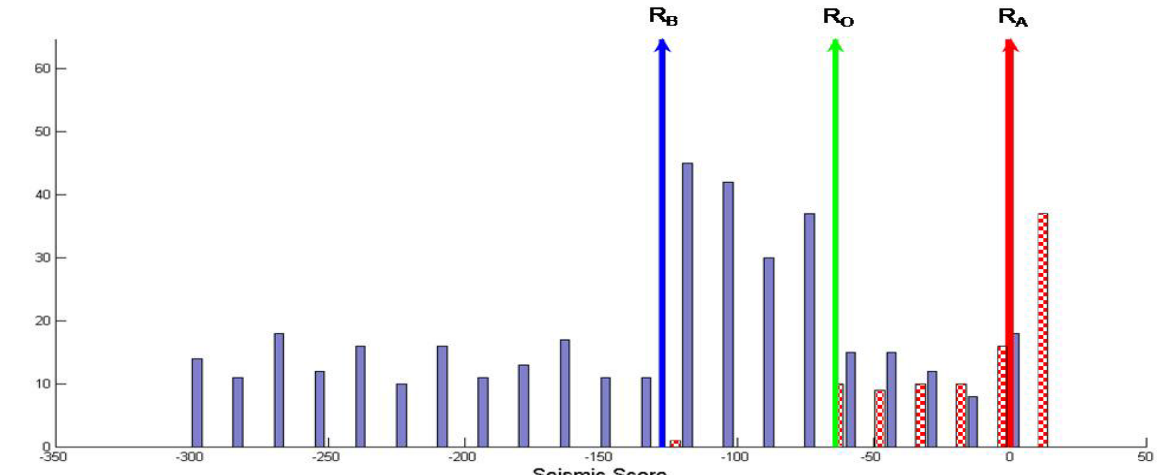
PR Model	$R_A$	$R_B$	$R_0$	Histogram	
PR1	-3.73	-7.54	-5.63		a.
PR2	0.09	-90.77	-45.34		b.



PR Model	$R_A$	$R_B$	$R_0$	Histogram	
PR3	0.01	-86.87	-43.43	 <p>The histogram for the PR3 model shows a distribution of seismic scores from -250 to 50. The y-axis represents frequency, ranging from 0 to 60. Three vertical arrows indicate specific values: <math>R_B</math> (blue arrow) at approximately -87, <math>R_0</math> (green arrow) at approximately -43, and <math>R_A</math> (red arrow) at 0. The distribution is roughly bell-shaped, centered around -100, with a tail extending to the right. Some bars are filled with a red checkered pattern, particularly those between <math>R_0</math> and <math>R_A</math>.</p>	c.
PR4	-0.55	-128.14	-64.34	 <p>The histogram for the PR4 model shows a distribution of seismic scores from -350 to 50. The y-axis represents frequency, ranging from 0 to 60. Three vertical arrows indicate specific values: <math>R_B</math> (blue arrow) at approximately -128, <math>R_0</math> (green arrow) at approximately -64, and <math>R_A</math> (red arrow) at 0. The distribution is roughly bell-shaped, centered around -150, with a tail extending to the right. Some bars are filled with a red checkered pattern, particularly those between <math>R_0</math> and <math>R_A</math>.</p>	d.

PR Model	$R_A$	$R_B$	$R_0$	Histogram	
PR5	-0.34	-128.29	-64.32	 <p>The histogram for the PR5 model shows a distribution of seismic scores from -350 to 50. The y-axis represents frequency, ranging from 0 to 60. Three vertical arrows indicate specific values: <math>R_B</math> (blue arrow) at approximately -128.29, <math>R_0</math> (green arrow) at approximately -64.32, and <math>R_A</math> (red arrow) at approximately -0.34. The distribution is roughly bell-shaped, centered around -100, with a tail extending to the right. There are some red checkered bars at the right end of the distribution.</p>	e.
PR6	-0.34	-128.29	-64.32	 <p>The histogram for the PR6 model shows a distribution of seismic scores from -350 to 50. The y-axis represents frequency, ranging from 0 to 60. Three vertical arrows indicate specific values: <math>R_B</math> (blue arrow) at approximately -128.29, <math>R_0</math> (green arrow) at approximately -64.32, and <math>R_A</math> (red arrow) at approximately -0.34. The distribution is roughly bell-shaped, centered around -100, with a tail extending to the right. There are some red checkered bars at the right end of the distribution.</p>	f.

PR Model	$R_A$	$R_B$	$R_0$	Histogram	
PR7	0.33	-127.45	-63.56	 <p>The histogram for PR7 shows the distribution of seismic scores. The x-axis is labeled 'Seismic Score' and ranges from -350 to 50. The y-axis represents frequency, ranging from 0 to 60. Three vertical arrows indicate specific values: <math>R_B</math> (blue arrow) at approximately -127.45, <math>R_0</math> (green arrow) at approximately -63.56, and <math>R_A</math> (red arrow) at 0. The distribution is roughly bell-shaped, centered around -100, with a tail extending to the right. The bars are blue, with some red checkered patterns near the <math>R_A</math> marker.</p>	g.
PR8	-0.25	-128.46	-64.35	 <p>The histogram for PR8 shows the distribution of seismic scores. The x-axis is labeled 'Seismic Score' and ranges from -350 to 50. The y-axis represents frequency, ranging from 0 to 60. Three vertical arrows indicate specific values: <math>R_B</math> (blue arrow) at approximately -128.46, <math>R_0</math> (green arrow) at approximately -64.35, and <math>R_A</math> (red arrow) at 0. The distribution is roughly bell-shaped, centered around -100, with a tail extending to the right. The bars are blue, with some red checkered patterns near the <math>R_A</math> marker.</p>	h.

PR Model	$R_A$	$R_B$	$R_0$	Histogram	
PR9	-0.33	-127.06	-63.69	 <p>The histogram for the PR9 model shows a distribution of seismic scores from -350 to 50. The y-axis represents frequency, ranging from 0 to 60. Three specific values are marked with vertical arrows: <math>R_B</math> (blue arrow) at approximately -127, <math>R_0</math> (green arrow) at approximately -64, and <math>R_A</math> (red arrow) at approximately -0.33. The distribution is roughly bell-shaped, centered around -100, with a tail extending to the left. The bars are blue, and the markers are colored to match their respective labels.</p>	i.
PR10	-0.43	-127.56	-63.99	 <p>The histogram for the PR10 model shows a distribution of seismic scores from -350 to 50. The y-axis represents frequency, ranging from 0 to 60. Three specific values are marked with vertical arrows: <math>R_B</math> (blue arrow) at approximately -128, <math>R_0</math> (green arrow) at approximately -64, and <math>R_A</math> (red arrow) at approximately -0.43. The distribution is roughly bell-shaped, centered around -100, with a tail extending to the left. The bars are blue, and the markers are colored to match their respective labels.</p>	j.

PR Model	$R_A$	$R_B$	$R_0$	Histogram	
PR11	0.49	-127.07	-63.29		k.
PR12	-0.34	-128.29	-64.32		l.

PR Model	$R_A$	$R_B$	$R_0$	Histogram	
PR13	0.03	-1.26	-0.62		m.
PR14	-0.84	-128.97	-64.91		n.

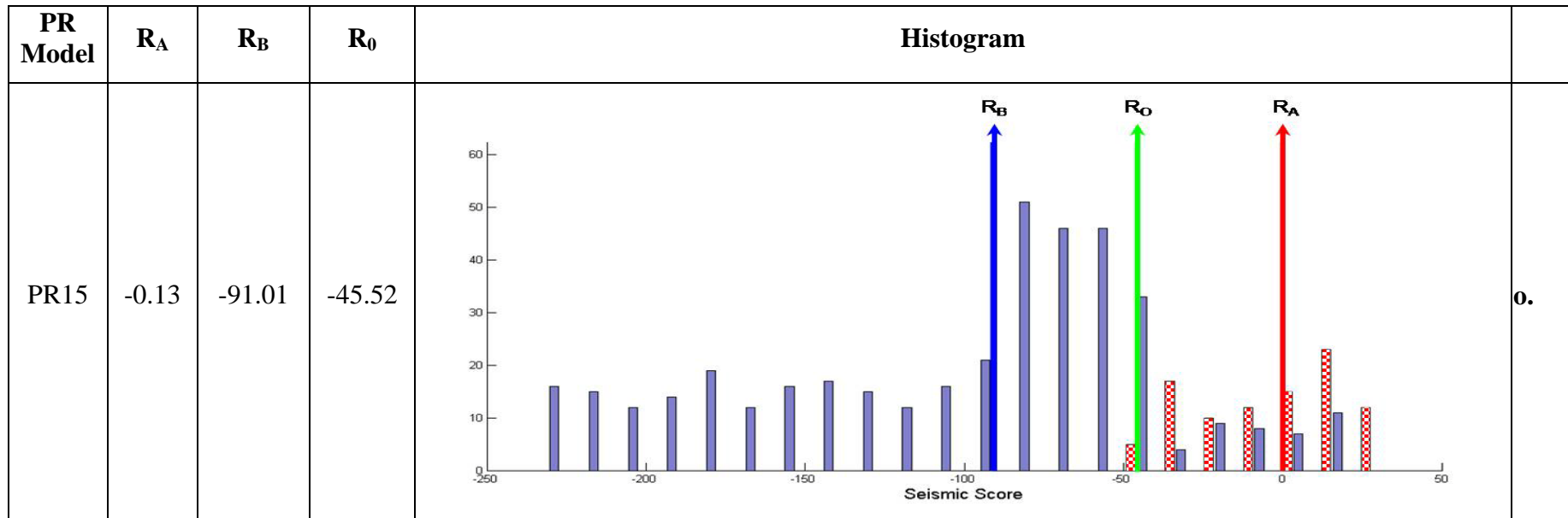


**Figure 3.5 (a-o):**  $R_A$ ,  $R_B$  and  $R_0$  values and histograms for different analysis carried out for identification of susceptible areas. Classification criteria and number of features selected for each PR model is as per table 3.2.

### **3.8 Validation of Results**

Validation of results for best analysis, model PR4, is discussed in detail in Chapter 4 for identification of seismically susceptible areas.

### **3.9 Segmentation of Long Tectonic Units**

With these major steps discussed above PR analysis was also tried for segmentation of long tectonic units with several iterations. Seismicity data was as per the MHD catalogue, and number of epicenters in each iteration varied as shown in table 3.3. Tectonic data considered was as per table 2.12 in which 26 prominent units in study area was part of the PR analysis initially. Further, 118 tectonic units were considered, as per table 2.13. Four features F1, F2, F3 and F4 were used, and classification criteria were based on tectonic data, criteria III referred to classification with respect to MBT in which 9 iterations were tried, and criteria IV referred to classification with respect to MCT in which 3 iterations were tried. These 12 iterations are shown graphically in figure 3.6(a-1) and were named as models PR16-PR27. MBT was segmented into 6 segments and MCT was segmented into 5 segments, and details are given in Chapter 5.

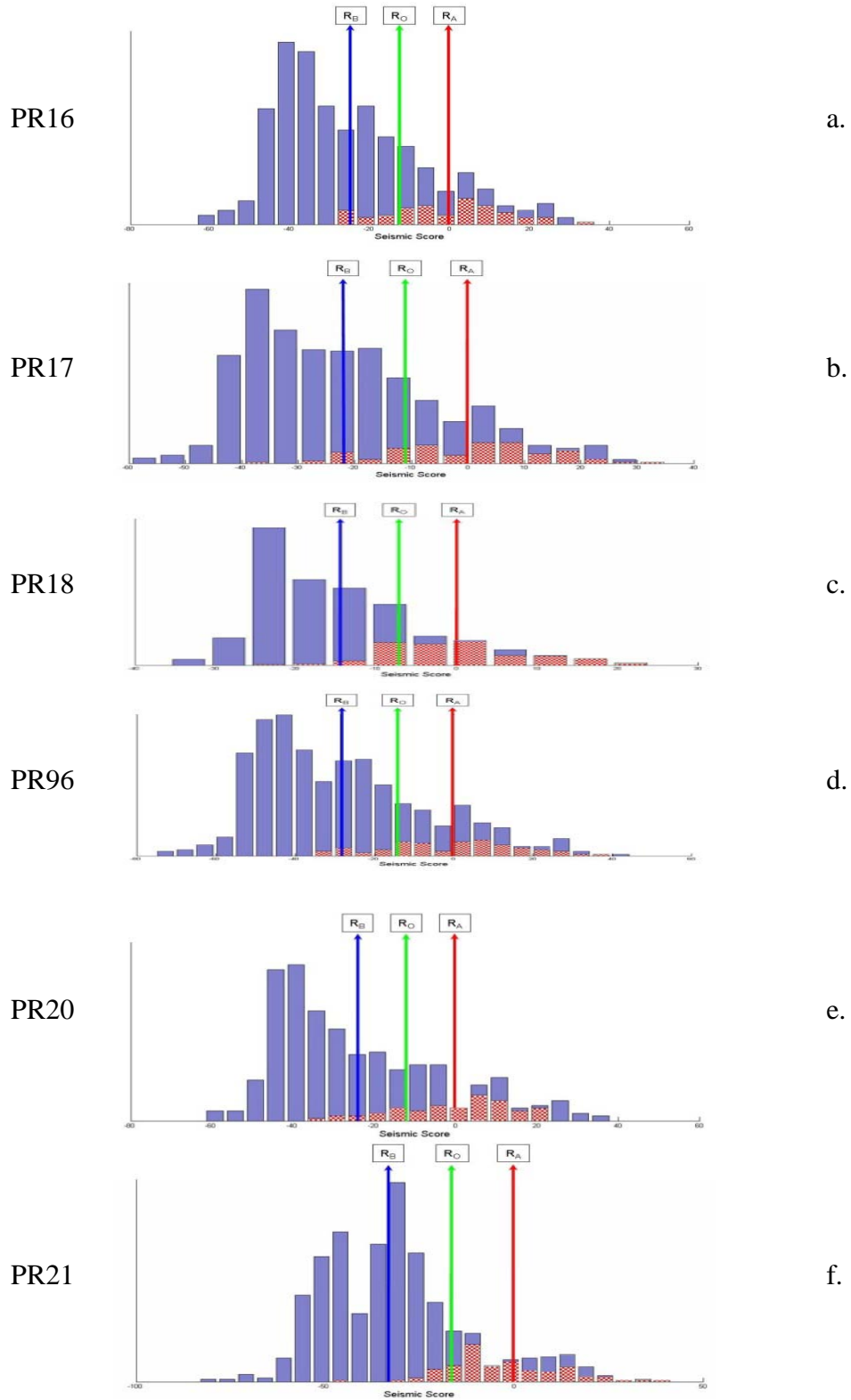


**Table 3.3:** Salient features of different PR models.  $\lambda$  values and percentage contribution of each feature by varying seismicity and number of tectonic units. Classification was done in terms of distance from either MBT of MCT. **F1:** magnitude of central earthquake; **F2:** Number of earthquake epicenters other than central earthquake; **F3:** Number of tectonic units; **F4:** Number of intersections between two tectonic units.

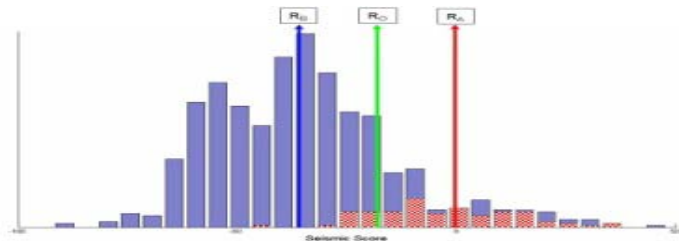
S. No	Seismicity		Class		No. of tectonic Units	classification wrt MBT/ MCT	F1	F2	F3	F4	PR analysis
	$\Sigma$	A	B	$\lambda_1/\%$			$\lambda_2/\%$	$\lambda_3/\%$	$\lambda_4/\%$		
1.	1137	158	979	26	MBT	-7.388/ -0.439	0.461/ 20.718	13.383/ 83.103	-3.695/ -3.382	PR16	
2.	1100	152	948	26	MBT	-7.469/ -1.2	0.476/ 21.036	13.389/ 83.488	-3.440/ -3.323	PR17	
3.	1000	125	875	26	MBT	-7.957/ -2.693	0.527/ 17.295	14.199/ 89.214	-3.377/ -3.816	PR18	
4.	900	97	803	26	MBT	-9.253/ -7.012	0.791/ 12.058	15.699/ 98.965	-2.911/ -2.911	PR19	
5.	800	76	724	26	MBT	-11.505/ -5.843	0.946/ 8.256	19.474/ 103.79 1	-5.531/ -6.204	PR20	
6.	594	66	528	26	MBT	-9.783/ -4.724	0.820/ 5.371	16.871/ 106.93 9	-6.344/ -7.586	PR21	
7.	900	159	741	26	MCT	-5.555/ -0.850	0.370/ 10.702	10.986/ 90.627	-3.593/ -0.478	PR22	
8.	455	55	400	26	MBT	-9.766/ -7.424	0.997/ 13.539	16.134/ 101.15 2	-5.688/ -7.267	PR23	
9.	455	55	400	26	MCT	-3.307/ -21.046	0.222/ 8.471	6.970/ 122.91 8	-2.877/ -10.342	PR24	
10.	1137	158	979	118	MBT	-11.813/ -0.542	0.298/ 7.515	17.488/ 96.264	-6.766/ -3.237	PR25	
11.	1172	164	1008	118	MBT	-13.319/ -6.187	0.608/ 5.638	18.605/ 106.46 4	-5.674/ -5.914	PR26	
12.	1172	199	973	118	MCT	-4.223/ -0.945	0.351/ 16.772	6.408/ 85.866	-0.497/ -1.693	PR27	

**PR  
Model**

**Histogram**

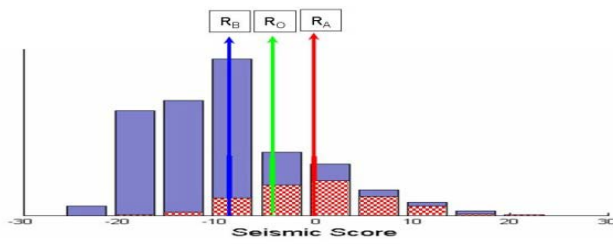


PR22



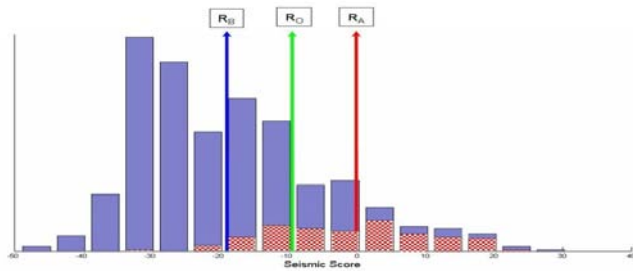
g.

PR23



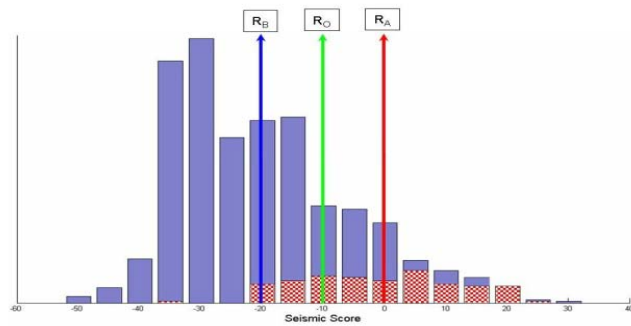
h.

PR24



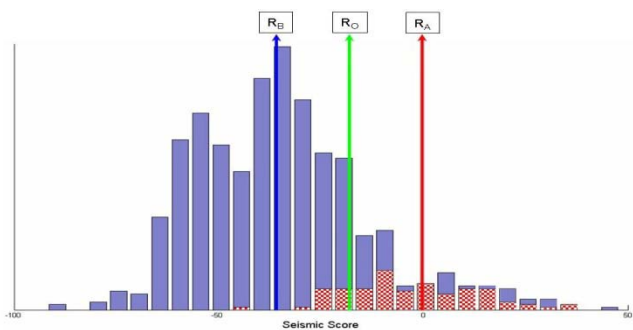
i.

PR25



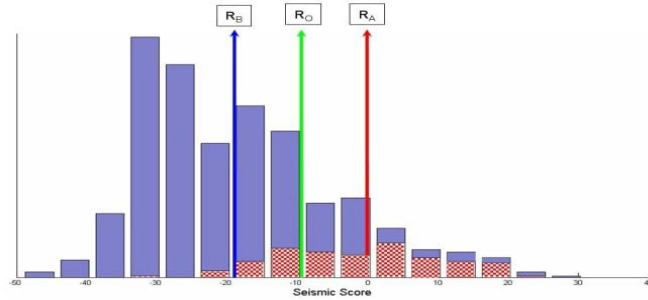
j.

PR26



k.

PR27



1.

**Figure 3.6 (a-1):** Histograms for different analysis carried out for segmentation of longer tectonic units. Classification criteria and number of earthquake epicenters in each class and number of tectonic units is as per table 3.3.

### 3.10 Conclusions

Six major steps of pattern recognition technique were explained in this Chapter. These steps are identification and extraction of features, classification of the data set, discriminant analysis, i.e. training exercise, decision making based on results of training exercise and validation of results. Twelve features which were subsequently used in different sets in different studies were introduced and explained. Four different classification criteria of which two were based on seismicity and two on tectonics were explained. The algorithm of discriminant analysis was explained in detail and a case study, PR1, was shown in this chapter.

Fifteen PR models, PR1-PR15, of discriminant analysis were tried for identification of seismically susceptible areas, and the best of all is explained in Chapter 4. Similarly, 12 PR models, PR16-PR27, were tried for segmentation of longer tectonics units, MBT and MCT and the best is further explained in detail in Chapter 5.



## CHAPTER 4

# IDENTIFICATION OF SEISMICALLY SUSCEPTIBLE AREAS IN WESTERN HIMALAYA

---

### 4.1 Introduction

In western Himalaya, different areas exhibit different patterns of seismicity, i.e., some parts of Himalaya show concentrated seismicity but some other parts show sparse seismicity. It is therefore necessary to differentiate between areas which can experience relatively high seismicity compared to other areas. The areas which experience high seismicity and complex tectonics are most likely to be prone to higher seismicity in future and are defined as seismically susceptible areas. Seismically susceptible areas in the study area were identified using PR technique, as explained in six steps in Chapter 3, figure 3.1.

For identifying susceptible areas, epicentral data in the study area was divided into two classes on the basis of magnitude of earthquakes. This step consists of classification of seismic data. Both classes were then subjected to discriminant analysis. The objective is to find a linear combination of extracted features that produces the maximum difference between the two previously defined classes. If we find a function that produces a significant difference, we can use it to allocate new specimens of unknown origin to one of the two classes of the training exercise. In this chapter the study area was considered as 196 specimens or as 196 sites. Linear combination of the features extracted for these 196 sites was estimated using the previously computed  $\lambda$  values. Seismic score was computed for each site. On the basis of seismic scores and multivariate means a decision was made about each site to assign it to a new class. All sites were divided into three classes. Envelopes were drawn around clusters of the same class, each class was interpreted in terms of a different susceptibility and the results were validated. The above discussed steps for training exercise and decision making exercise are shown by flowcharts in figures 4.1(a) and 4.1 (b). The detailed methodology for identification of susceptible areas using PR technique for model PR4 is given in the following sections.

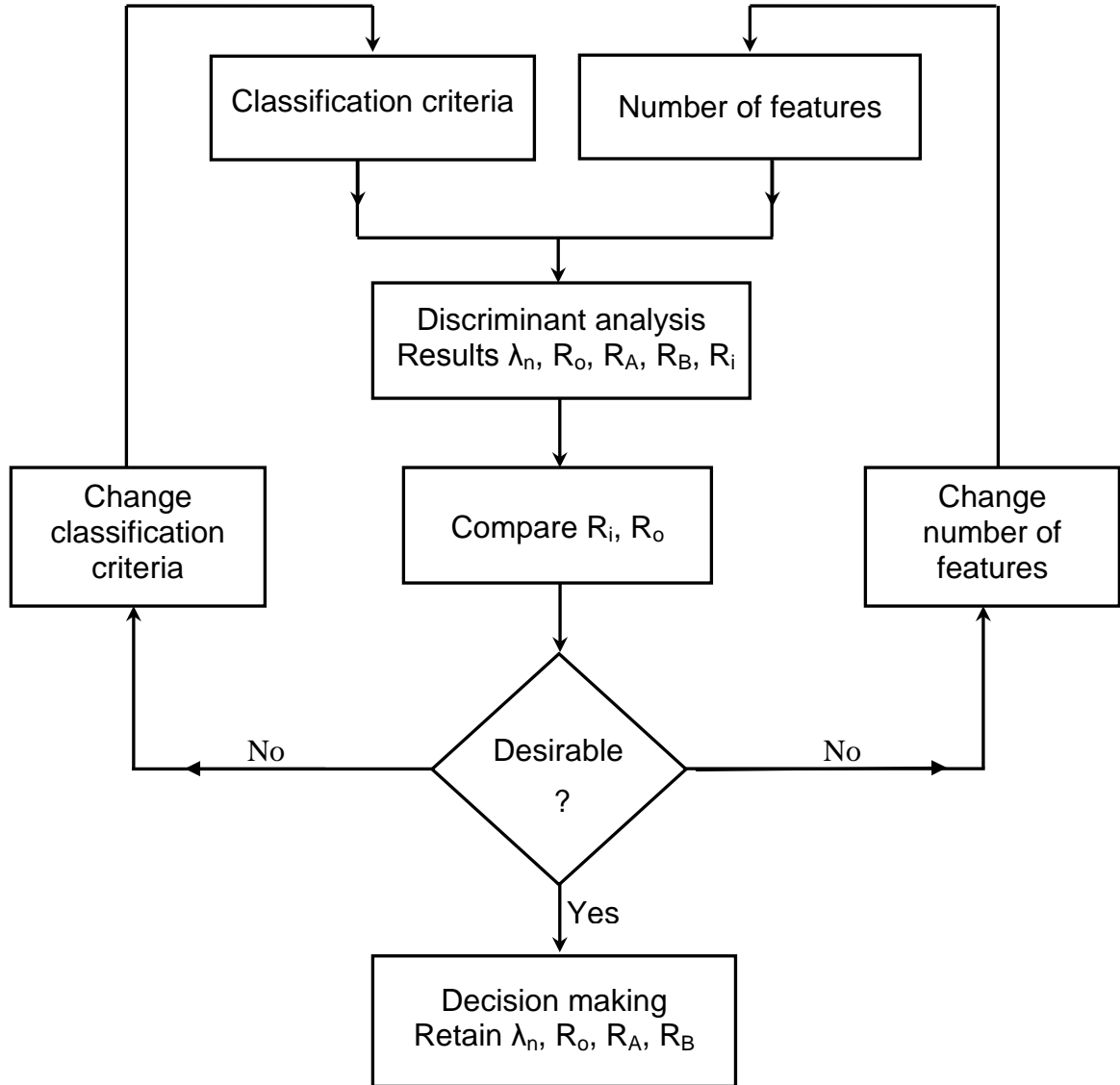


**Figure 4.1(a):** Steps used for training exercise for identification of seismically susceptible areas.

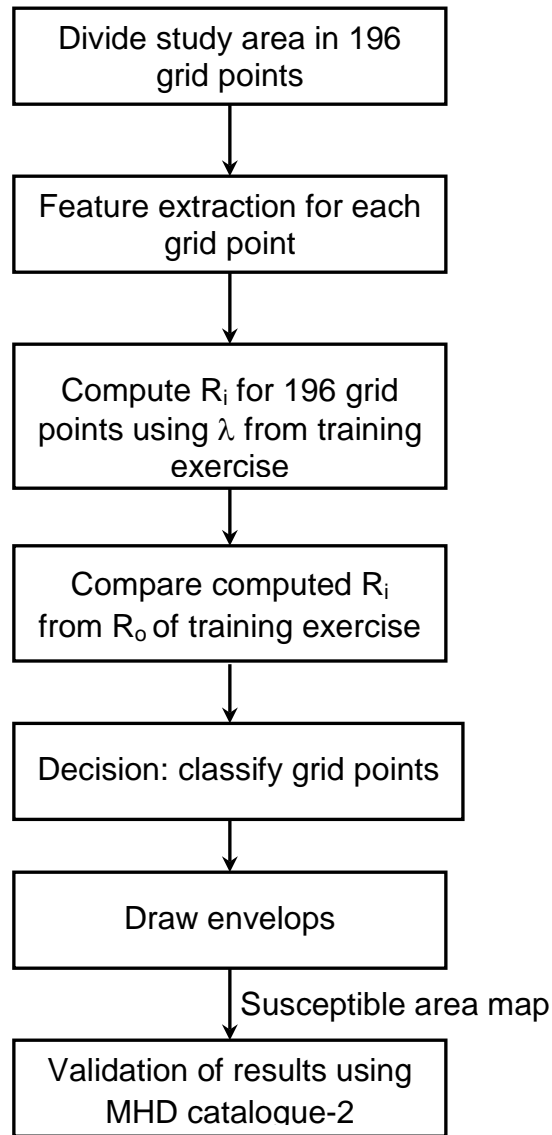


**Figure 4.1(b):** Decision making exercise.

## 4.2 Features Used for Discriminant Analysis in Model PR4

The eleven features considered for the present study are: F2: number of epicenters other than central earthquake, F3: number of tectonic units, F4: number of tectonic intersections, F5: number of intersections of tectonic units with river, F6: distance between central earthquake and nearest tectonic unit (km), F7: distance between central earthquake and nearest tectonic intersection (km), F8: Length of river (km), F9: number of earthquakes + number of tectonic units



(F2+F3), F10: maximum elevation ( $E_{\max}$ ), F11: minimum elevation ( $E_{\min}$ ) and F12: difference in elevation ( $E_{\max} - E_{\min}$ ).

### 4.3 Classification Criteria

All epicenters in the MHD catalogue were divided into two classes based on their magnitude. Classification criteria-I is defined as Class I: epicenters having magnitude  $M_w \geq 6.0$ ; and Class II: epicenters having  $4.5 \leq M_w \leq 5.9$ . PR analysis as per this classification criterion has been discussed in Chapter 3, results of which were given in row 1, and pertain to model PR1, of table 3.2. It was observed that out of 45 seismic scores of Class I, 43 had seismic scores  $\geq -5.63$ , i.e. 95% epicenters of Class I were desirably classified. However, for Class II out of 492 earthquakes 324 seismic scores were  $\leq -5.63$ , i.e. it showed 66% appropriate classification.

To improve appropriate classification in each class, i.e. to reduce misclassification and to increase the number of events in the higher magnitude range a second classification criterion, criteria-II, formulated and discussed in Chapter 3 section 3.5, was tested. In this a lower magnitude threshold was considered. Classification criteria-II is defined as Class A: epicenters having magnitude  $M_w \geq 5.5$ ; and Class B: epicenters having  $4.5 \leq M_w \leq 5.4$ . 537 epicenters of magnitude range  $4.5 \leq M_w \leq 8.0$  from MHD catalogue were re-classified into a different training exercise with these two classes. Class A contained 94 epicenters and Class B contained 443 epicenters, i.e. there were more than four times the epicenters in the lower magnitude range. Figure 4.2 shows the epicentral map of the study area with classification criteria-II.

Magnitudes in the MHD catalogue ranged between 3.5 and 8.0, and magnitudes lower than  $M_w = 4.5$  were retained in this study as these were part of a discriminant feature, F2, in discriminant analysis. However, these were neither part of Class A nor B.

With this classification criterion and with different combinations of features 14 iterations of discriminant analyses were carried out, and these have been named as PR models PR2 to PR15. Percentage of classification of epicenters was computed for all iterations, as shown in table 3.2. It was observed that a set of 11 features gave the most desirable result. Therefore, results obtained from a set of 11 features and classification criterion-II, i.e. model PR4 is discussed further in this chapter.

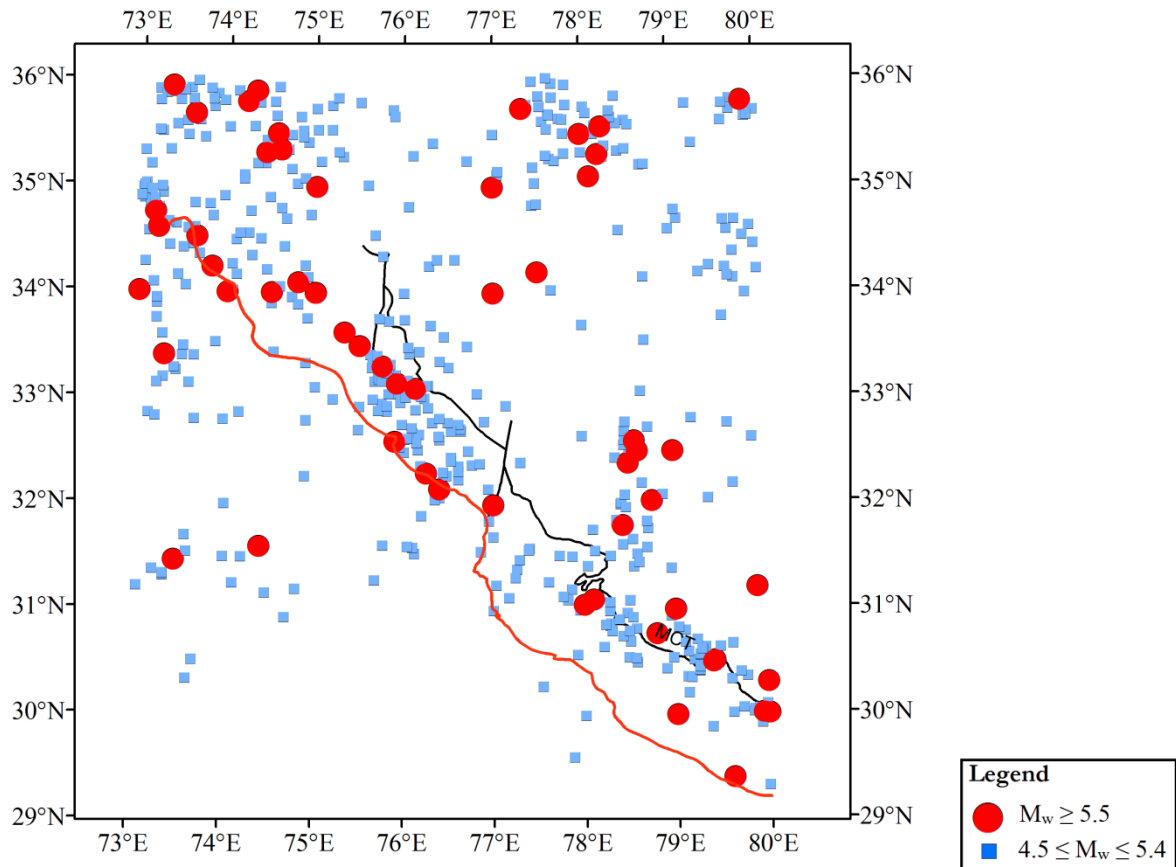


**Figure 4.2:** Epicentral map of the study area, showing classification of epicenters as per classification criteria-II, i.e., Class A:  $M_w \geq 5.5$ , shown in red and Class B:  $4.5 \leq M_w \leq 5.4$ , shown in blue.

#### 4.4 Discriminant Analysis

With classification criteria-II and a set of eleven features results of discriminant analysis, model PR4, are discussed here. Vector mean of each feature of Class A, Class B, and vector of mean differences of both classes were calculated as per equations 3.2, 3.3 and 3.4, respectively. Coefficients of discriminant function, i.e.  $\lambda$  values were calculated using equation 3.10, and are given in table 4.1. Multivariate means of Class A and B and discriminant index ( $R_0$ ) were calculated using equations 3.12, 3.13 and 3.14, respectively. Multivariate mean of Class A,  $R_A = -0.55$ ; multivariate mean of Class B,  $R_B = -128.14$  and discriminant index,  $R_0 = -64.34$ . Seismic score for each of the 537 epicenters was calculated as per equation 3.11.

**Table 4.1:** Salient features of model PR4, vector mean of Class A, vector mean of Class B, Vector of mean differences of both classes, discriminant function, i.e.  $\lambda$  values and percentage contribution of each feature, for model PR4.

Feature	Name of Feature	Vector Mean Class A	Vector Mean Class B	Vector Mean Difference	Discriminant Function, $\lambda$	Contribution of Each Feature (%)
F2	Number of earthquake epicenters other than central earthquake	13	10.28	2.72	-3.68	26.34
F3	Number of tectonic units	2.33	1.71	0.61	-3.70	33.58
F4	Number of intersections between two tectonic units	0.58	0.43	0.16	0.08	-23.67
F5	Number of intersections between tectonic unit and river	0.52	0.33	0.19	1.18	19.11
F6	Distance of central earthquake from nearest tectonic feature (km)	53.55	63.44	-9.89	-0.05	7.34
F7	Distance of central earthquake from nearest tectonic intersection (km)	16.25	16.82	-0.57	0.03	6.44
F8	Length of river	27.99	17.13	10.86	-0.10	8.56
F9	Addition of number of earthquakes and no of tectonic features (F2+F3)	15.33	11.99	3.33	3.56	15.52
F10	Maximum elevation, $E_{\max}$	3.69	30.89	-27.20	-4.55	16.9
F11	Minimum elevation, $E_{\min}$	0.40	0.49	-0.09	0.26	15.33
F12	Difference in elevation ( $E_{\max} - E_{\min}$ )	3.29	2.60	0.69	6.81	-25.45

In this exercise seismic scores of all 94 epicenters of Class A were  $\geq -0.55$ , i.e.  $\geq R_0$ , which is a desirable 100% classification. This can be attributed to the fact that Class A, representing a higher magnitude, is related to tectonics of the region and higher magnitudes will not occur all over the study area. However, Class B, representing lower magnitudes showed 9% misclassification of epicenters, i.e. out of 443 epicenters 42 which were originally in Class B were misclassified in Class A. Graphically, these are shown in figure 4.3. The list of these 42 earthquakes is given in table 4.2. It is pertinent to note that all aftershocks have been removed in the declustering exercise and all lower magnitudes considered in this study represent main events only. It may also be noted that several misclassified epicenters are located on sharp bends of MCT, and most are associated with the MBT– MCT region. Figure 4.4 shows the epicentral map drawn after discriminant analysis, and also misclassified epicenters.

**Table 4.2:** List of 42 epicenters of Class B which are misclassified as Class A after discriminant analysis.

S. No.	YR	MM	DD	HR	MN	Long	Lat	Mag	Depth	Source
1	1858	8	11	0	0	77.17	31.12	5.0	-	IMD
2	1871	4	1	0	0	76.00	34.00	5.0	-	IMD
3	1908	12	11	0	0	79.00	31.00	5.0	-	IMD
4	1962	8	2	15	32	73.50	33.40	5.0	-	IMD
5	1963	4	12	0	41	78.79	32.00	5.4	36.0	IMD
6	1966	3	16	12	8	75.91	33.23	4.9	33.0	ISC
7	1968	4	9	1	14	73.10	35.20	4.9	51.0	ISC
8	1970	3	5	6	34	76.61	32.32	4.9	33.0	ISC
9	1970	1	17	6	33	76.64	32.70	4.9	22.0	ISC
10	1971	12	21	9	54	74.28	35.57	5.2	15.0	ISC
11	1972	9	6	2	51	78.51	32.49	5.2	14.0	ISC
12	1973	1	16	9	31	75.83	33.29	5.3	39.2	ISC
13	1973	12	9	2	36	73.35	35.93	5.3	47.6	ISC
14	1974	11	22	6	51	76.71	33.50	4.8	48.6	ISC
15	1975	3	23	1	19	74.84	35.53	4.9	33.0	ISC
16	1975	4	23	9	7	73.42	35.81	4.9	59.6	ISC
17	1976	9	29	7	47	78.40	31.83	5.1	20.4	ISC
18	1976	10	1	11	27	77.45	36.00	5.3	82.1	ISC
19	1977	1	28	3	48	78.04	31.42	4.9	50.1	ISC
20	1977	6	22	3	53	76.04	33.18	5.1	47.0	ISC
21	1978	1	7	7	23	79.40	30.51	4.8	33.0	ISC
22	1978	5	7	10	32	73.63	33.40	5.2	25.4	ISC
23	1978	9	28	5	32	76.05	33.49	5.0	40.3	ISC

S. No.	YR	MM	DD	HR	MN	Long	Lat	Mag	Depth	Source
24	1979	12	28	1	59	78.57	30.82	5.2	23.0	ISC
25	1979	6	2	1	5	76.01	33.75	4.9	33.0	ISC
26	1980	5	1	5	43	75.97	33.03	5.1	18.1	ISC
27	1981	3	3	8	43	73.22	31.37	5.2	47.8	ISC
28	1981	7	12	8	45	76.09	32.73	4.9	35.9	ISC
29	1981	8	31	12	31	78.99	34.60	5.0	38.6	ISC
30	1981	1	26	10	11	77.71	35.25	4.7	43.2	ISC
31	1981	9	18	5	5	73.65	35.62	5.3	52.6	ISC
32	1985	5	22	1	57	73.34	31.31	5.3	0.0	ISC
33	1985	8	10	12	56	74.80	33.89	4.8	40.6	ISC
34	1987	6	6	11	2	79.12	30.36	5.1	36.0	ISC
35	1988	11	25	12	7	75.81	32.89	5.0	79.9	ISC
36	1991	4	22	8	48	79.72	30.06	4.9	35.8	ISC
37	1991	1	20	12	43	77.40	31.59	5.1	33.0	ISC
38	1998	7	18	6	21	78.43	35.34	4.9	41.4	ISC
39	1999	2	23	6	56	74.59	34.06	5.0	24.7	ISC
40	2002	1	27	10	33	75.99	33.10	4.9	30.8	ISC
41	2004	11	11	2	13	76.61	32.37	5.0	15.0	ISC
42	2012	2	20	13	59	79.72	35.72	5.3	10.0	USGS(NEIC)

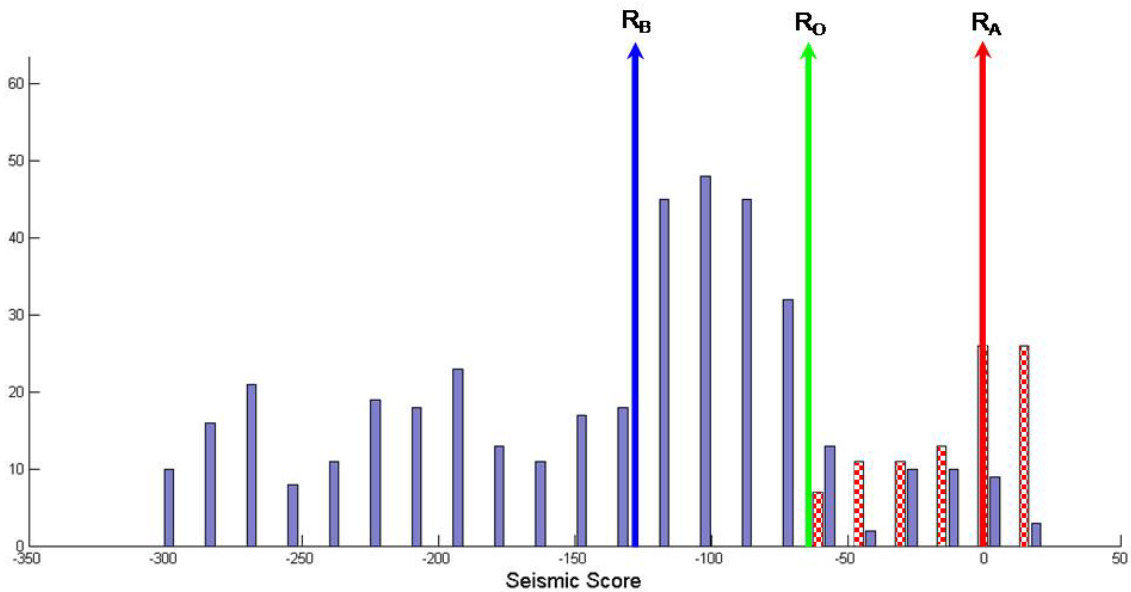


**Figure 4.3:** Plot of seismic scores,  $R_A$ ,  $R_B$  and  $R_0$  for the training exercise. Red represents Class A and blue represents Class B.

Model PR4 showed the best results of all the 15 training exercises and was retained for further consideration. The discriminant functions obtained from this training exercise was then applied for the decision making exercise to identify susceptible areas.

The study area was reconsidered. It was divided into a grid of  $0.5^\circ$  by  $0.5^\circ$  which resulted in 196 quadrangles. This grid was also used for computation of PGA in DSHA and PSHA as discussed in Chapters 6 and 7, respectively. The midpoint of each quadrangle was considered as a site and also the centre of a circle, of radius 25 km, as shown in figure 4.5. The radius around each site was 25 km as feature extraction was also within this radius. The same eleven features, as in the training exercise, F2 to F12, were extracted for each site. Features extracted for one site are shown in figure 4.6. Since the  $\lambda_2, \lambda_3, \dots, \lambda_{12}$ , values calculated from the training exercise were known *a priori*, these were used to compute the seismic score for each site. These seismic scores were compared to  $R_A, R_B$  and  $R_0$  values as obtained from the training exercise. Graphically this is shown in figure 4.7. Seismic score for each site was classified accordingly, and each site was assigned a class either A' or B'.

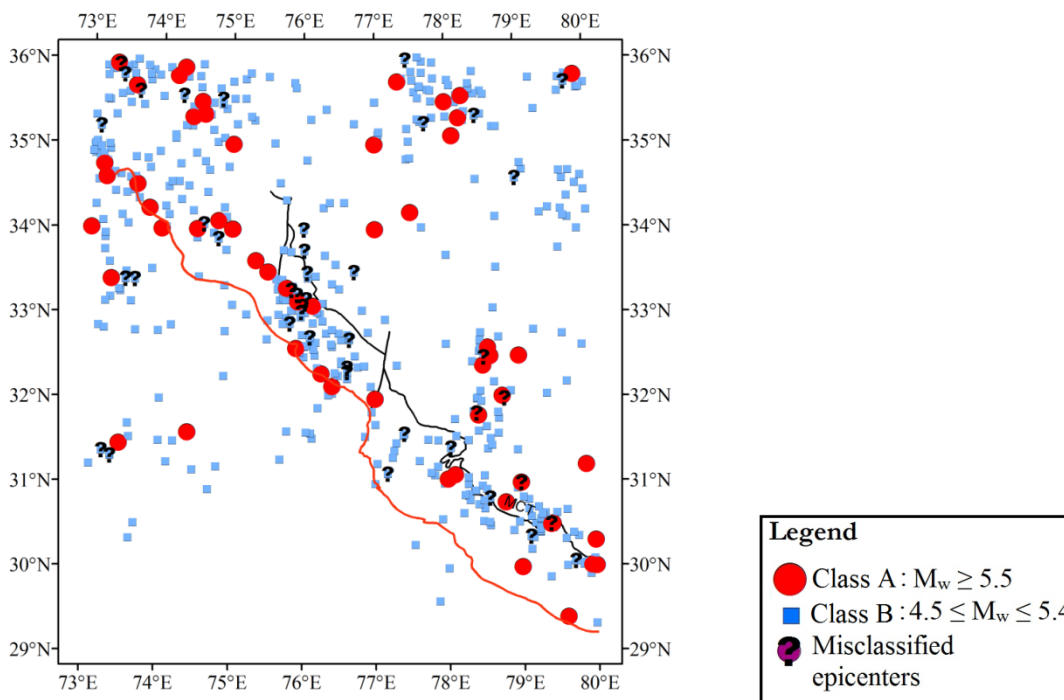


**Figure 4.4:** Epicentral map of the study area, after discriminant analysis. Epicenters in purple with question mark show 42 misclassified events, all from Class B. List of these 42 epicenters is given in table 4.2.

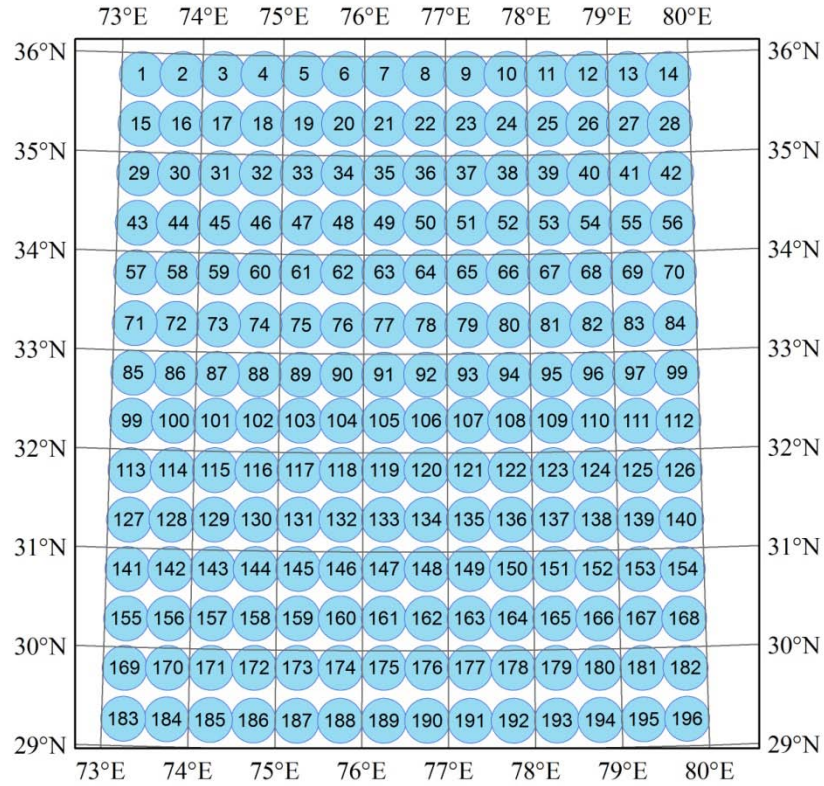


**Figure 4.5:** The study area is divided into a grid of  $0.5^\circ$  by  $0.5^\circ$ , which resulted in 196 quadrangles. Midpoint of every quadrangle was considered as a site. Circle represents an area of 25 km radius drawn around each site for extraction of features.

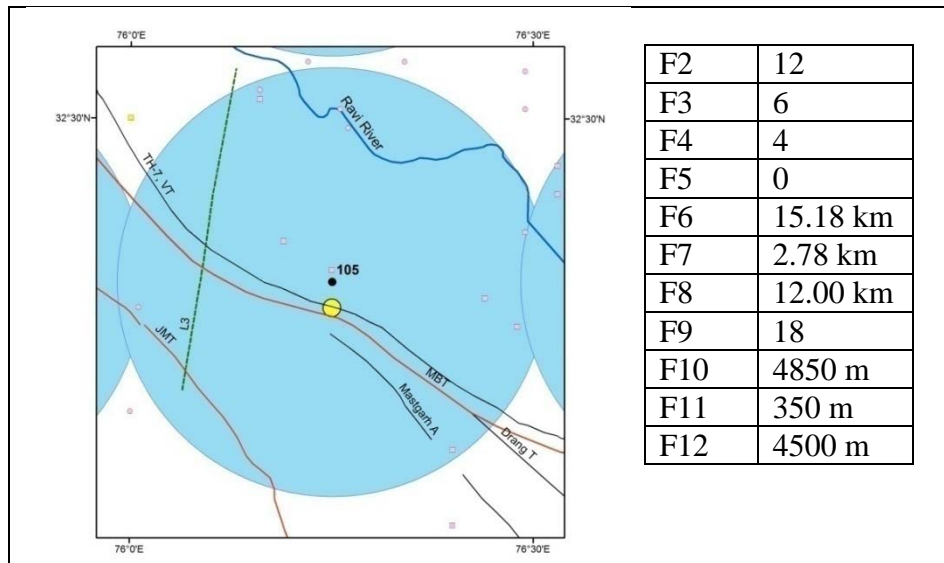


**Figure 4.6:** Eleven features F2-F12, extracted from within a circle of radius 25 km drawn around a site, Lat:  $32.32^\circ\text{N}$ , Long:  $76.25^\circ\text{E}$ . This is the nearest site to the great Kangra earthquake of 1905. Yellow represents the epicenter of 1905 Kangra earthquake.

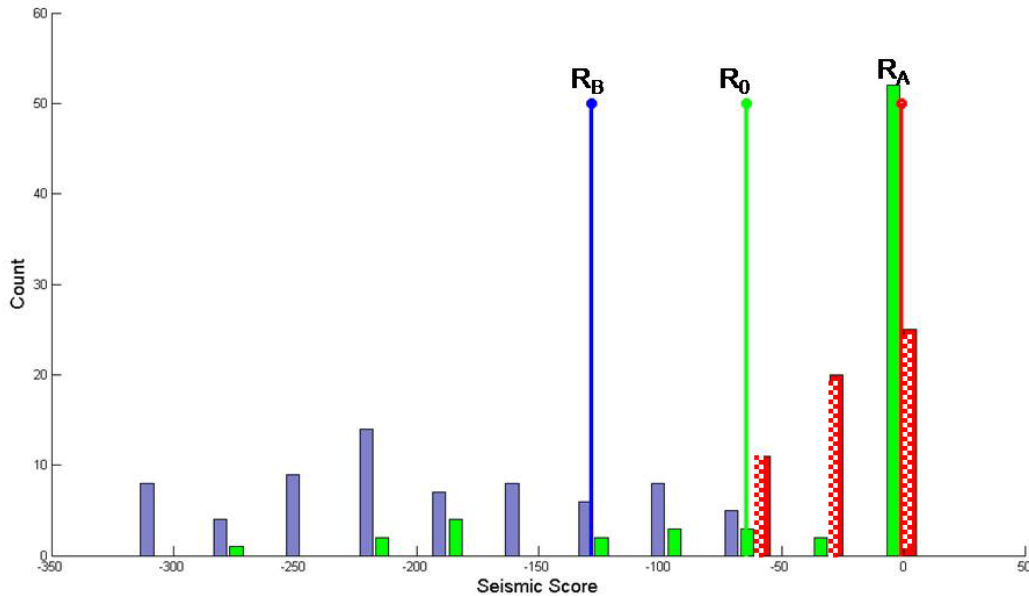


**Figure 4.7:** Plot of seismic scores,  $R_A$ ,  $R_B$  and  $R_0$  for sites for decision making exercise. Red represents Class A', blue represents Class B' and green represents Class C' that were considered neither in Class A' nor Class B'.

At some sites some of the 11 features were not extractable, due to sparse or absence of seismicity and tectonics. Also, elevations were not available for many areas as per ISRO data. Consequently these sites were reconsidered for classification. In this case the addition of number of tectonic units and number of epicenters, if  $\leq 3$ , i.e. if feature F9 was  $\leq 3$ , it was assigned a new Class C'. Also in case of absence of all features it was again assigned to Class C'. Therefore, the study area was re assigned into three classes, A', B', and C' and this is shown in figure 4.8.

#### 4.5 Interpretation and Decision Making

Out of the 196 grid points, 56 grid points were classified as Class A'; 71 as Class B' and 69 as Class C. Some sites formed clusters of a particular class. The largest cluster consisted of 38 sites and was of Class A'.



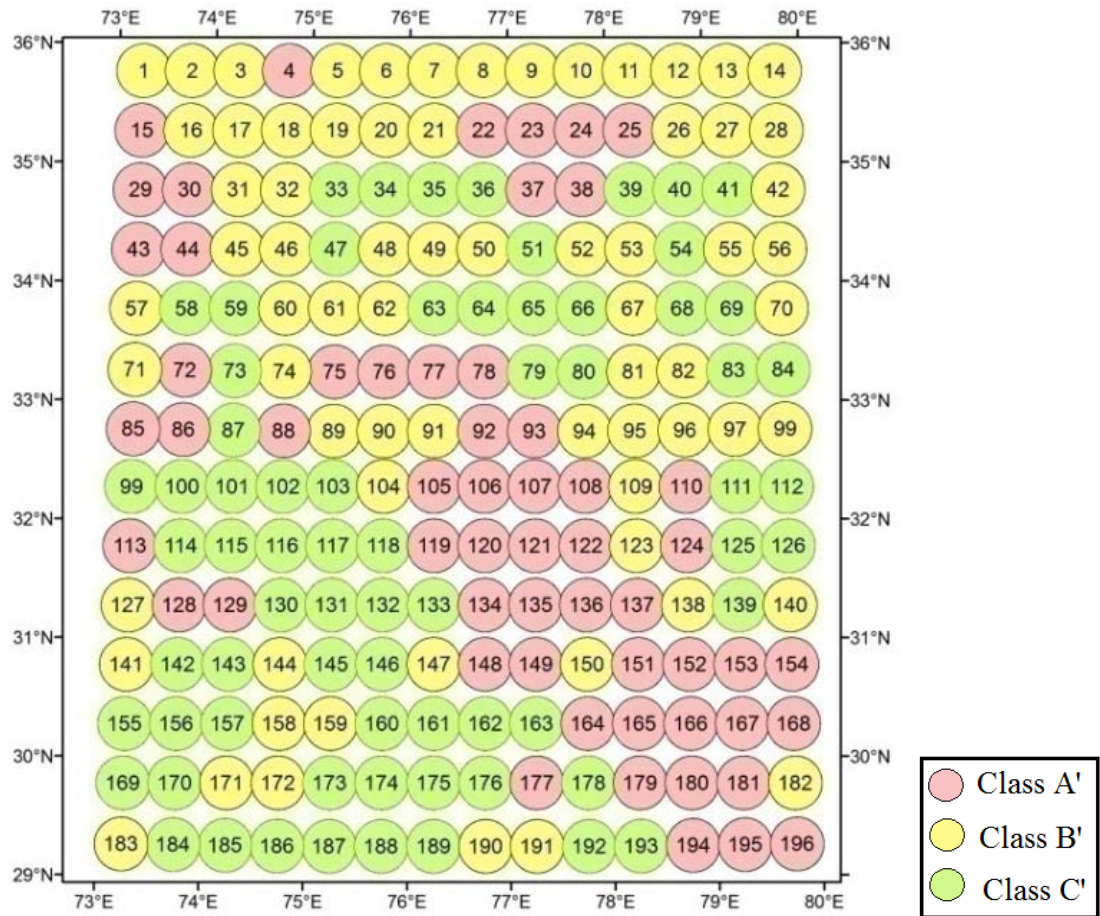


**Figure 4.8:** 196 sites divided into one of the three classes Class A', Class B' and Class C', identified after the training exercise and decision making exercise.

Envelopes were drawn around clusters of same class, using nearest neighbour interpolation tool given in ArcGIS-9.3, which approximates the value of a function for a non-given point when given the value of that function in points around (neighboring) that point. The nearest neighbour algorithm selects the value of the nearest point and does not consider the values of neighboring points at all, yielding a piecewise-constant interpolant. Three areas were identified from these clusters, and these were named according to their Class as A'', B'' or C''. The study area was divided into three types based on their seismic scores, viz. area A'', area B'': and area C''. Figure 4.9 shows these identified areas. This map is hereafter referred to as the susceptibility map of the study area. Red represents area A'', yellow represents area B'' and green represents area C''.

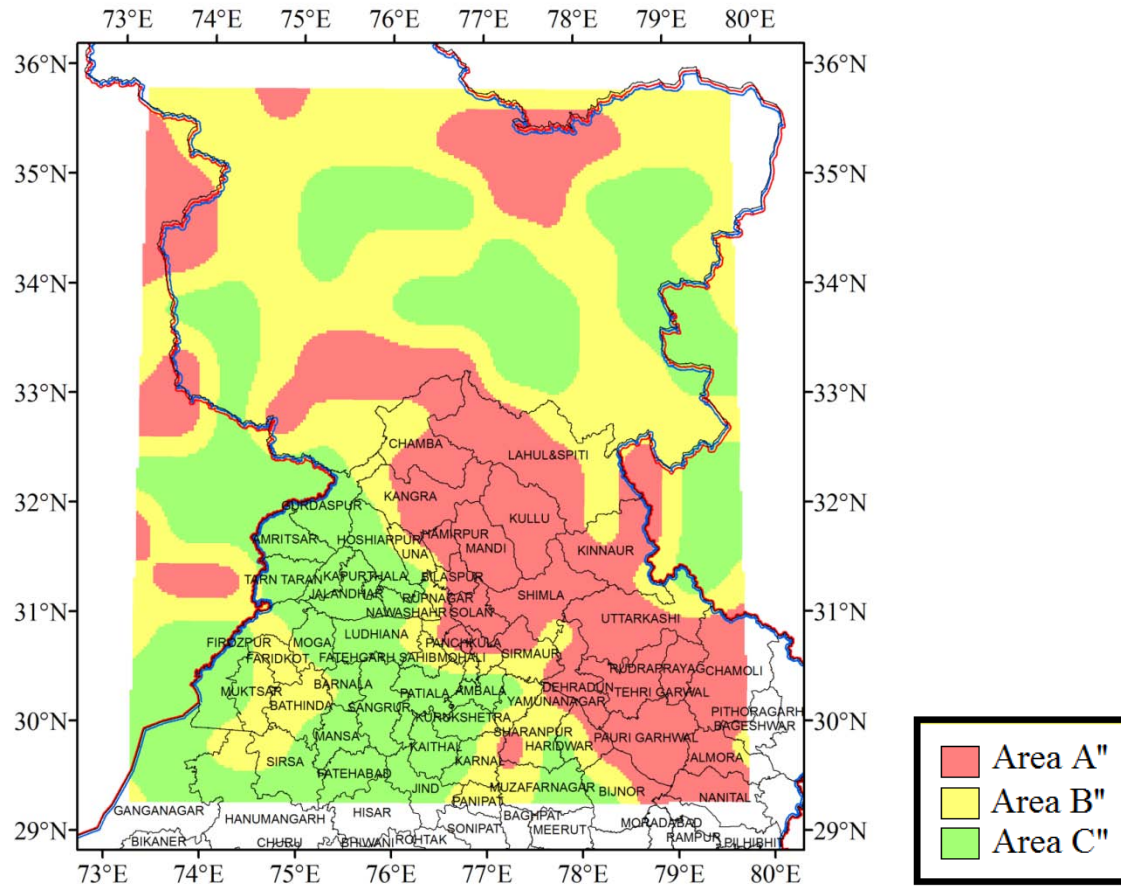


**Figure 4.9:** Three types of susceptible areas. Red represents area A'': Most susceptible area; Yellow represents area B'': Moderately susceptible area; and green represents area C'': Least susceptible area. This is obtained after making envelopes and smoothing the results of figure 4.8. Map also shows districts as per Survey of India, (2011).

Area A'' (susceptible area map) is continuous along the entire MCT, and extends north of MCT, sometimes as much as 50 km, and a prominent 50 km by 100 km finger cuts out along the Kaurik Fault system. Large portions of MBT are also included in area A'', which extends south of MBT also, and it also includes areas between MBT and MCT. Area A'' represents the area having  $M_w \geq 5.5$  as per training exercise; therefore, it may be considered as the most susceptible area. Seven islands of area A'' exist in the study area. Earthquakes of magnitude  $M_w \geq 5.5$  which were used in the training exercise (which was as per magnitude classification) also exist in the identified area A''. Some of the prominent earthquakes in A'' are Kashmir earthquake of 8<sup>th</sup> October, 2005, Kangra earthquake of 4<sup>th</sup> April, 1905, Dharamshala earthquake of 26<sup>th</sup> April, 1986, Kinnaur earthquake of 19<sup>th</sup> January, 1975, Uttarkashi earthquake of 20<sup>th</sup> October, 1991, Chamoli earthquake of 29<sup>th</sup> March, 1999, and three historical earthquakes in Srinagar-Baramula region of magnitude

7.7 in 1554, magnitude 7.5 in 1552 and magnitude 7.7 in 1778. Major tectonic units in area  $A'$  are: MBT, MCT, Main Mantle Thrust (MMT), Mahendragarh-Dehradun Fault, seven closed thrusts between MBT and MCT and neotectonic fault FR1.

Area  $B''$  represents earthquakes of magnitude  $4.5 \leq M_w \leq 5.4$  as per training exercise; therefore, it may be considered as an area less susceptible area than  $A'$ . Envelop  $B''$  was observed to enclose area  $A''$ . Major tectonic units in area  $B''$  are Indus Suture zone, Shyok suture, parts of MMT, several unnamed lineaments, unnamed faults and thrusts.

Area  $C''$  was observed mostly in the north eastern part of study area, i.e. in Tibet China region and in the Indo Gangetic plains. Sparse seismicity was observed in these areas, faults and thrusts were absent, only lineaments were present in area  $C''$ . Also, these areas have a deficiency of a combination of tectonic units and seismicity. This aspect was also obvious as part of the training exercise.

On the basis of two classes in the training exercise discriminant functions,  $\lambda$ , were obtained. It was decided that new specimens of unknown origin, i.e. the grid points, can now be allocated to one of these two classes by using  $\lambda$ . The entire study area was thus divided into two types of area. Later a new type of area was introduced at the decision making step in application of model PR4. Validation of these results is discussed in the next section.

#### **4.6 Validation of Results**

For validation of results obtained in section 4.5, MHD catalogue-2, given in Chapter 2, section 2.4.8 was considered. Out of 80 recent earthquakes of the MHD catalogue-2, which were not part of the training exercise, 6 had  $M_w \geq 5.5$ ; and 74 were in the range  $4.5 \leq M_w \leq 5.4$ . 57 out of the 80 epicenters were located in area  $A''$ . Six of these had  $M_w \geq 5.5$ . It is significant to note that all these 6 epicenters are located within area  $A''$ . Therefore, success rate for validation for area  $A'$  may be considered as 100%. Therefore, area  $A''$  is validated as the most susceptible area within the study area. This also implies that recent higher magnitude earthquakes are originating in identified susceptible area  $A''$ , and it can be considered as a source zone where future large earthquakes can be expected.

A similar exercise was carried out for validation of 'area  $B''$ '. 20 out of 74 earthquakes of magnitude  $4.5 \leq M_w \leq 5.4$  are in area  $B''$ . It may be noted that no earthquake of

magnitude  $M_w \geq 5.5$  occurred in area B". This implies that classification criteria-II is validated, and also identified areas are validated. Three earthquakes of magnitude  $4.5 \leq M_w \leq 5.4$  occurred in area C". Magnitude wise breakup of MHD catalogue-2 is given in table 4.3 and is shown in figure 4.10. Occurrence of smaller magnitude earthquakes together with higher magnitudes in area A implies that area A' is seismically most active compared to other areas. This implies the need of special attention for hazard assessment in area A. The study area is now divided into three types of susceptible areas viz. area A": most susceptible area, area B": moderately susceptible area and area C": least susceptible area.

Susceptible areas map was superimposed on the political map of India, Survey of India, (2011). It was observed that large parts of Himachal Pradesh, Uttarakhand and parts of Jammu and Kashmir are parts of the largest cluster of the most susceptible area, A. In Himachal Pradesh, this includes major parts of Bilaspur, Chamba, Kangra, Kullu, Lahaul & Spiti, Mandi, Shimla, Solan and Sirmaur. In Uttarakhand, parts of Almora, Chamoli, Dehradun, Haridwar, Nainital, Pauri Garhwal, Tehri Garhwal and Uttarkashi are in area A. District wise breakup of the three kinds of susceptible areas within the western Himalaya and the Indo Gangetic plains is given in table 4.4 and was shown in figure 4.9.

**Table 4.3:** Magnitude wise break up of 80 recent earthquakes from MHD catalogue-2 for validation of results of susceptible areas A", B" and C".

Magnitude Range↓	Area ↓			Total
	A"	B"	C"	
$M_w \geq 5.5$	6	0	0	6
$4.5 \leq M_w \leq 5.4$	51	20	3	74
	$\Sigma 57$	$\Sigma 20$	$\Sigma 3$	$\Sigma 80$

**Table 4.4:** States and districts identified in Areas A'', B'' and C''.

<b>Area</b>	<b>States</b>	<b>DISTRICTS</b>
<b>A''</b>	<b>Jammu &amp; Kashmir</b>	Anantnag, Doda, Jammu, Kishtwar, Kulgam, Reasi.
	<b>Himachal Pradesh</b>	Bilaspur, Chamba, Kangra, Kullu, Lahaul & Spiti, Mandi, Shimla, Solan and Sirmaur
	<b>Uttarakhand</b>	Almora, Chamoli, Dehradun, Haridwar, Nainital, Pauri Garhwal, Tehri Garhwal and Uttarkashi
	<b>Punjab</b>	Mohali
	<b>Uttar Pradesh</b>	Bijnor
	<b>Haryana</b>	Panipat and Sirsa
<b>B''</b>	<b>Jammu &amp; Kashmir</b>	Bandipora, Kargil, Kathua, Leh (Ladakh), Srinagar, Udhampur,
	<b>Himachal Pradesh</b>	Parts of Bilaspur, Chamba, Kinnaur, Kangra, Lahul & Spiti and Shimla, Sirmaur, Una
	<b>Uttarakhand</b>	Almora, Bageshwar, Dehradun, Haridwar, Uttarkashi
	<b>Punjab</b>	Bathinda, Faridkot, Gurdaspur and Ludhiana
	<b>Uttar Pradesh</b>	Muzaffarnagar
	<b>Haryana</b>	Ambala, Fatehabad, Hisar, Jind, Kaithal, Karnal and Yamunanagar
	<b>Rajasthan</b>	Ganganagar, Hanumangarh
<b>C''</b>	<b>Jammu &amp; Kashmir</b>	Kargil, Leh (Ladakh),
	<b>Himachal Pradesh</b>	Una
	<b>Uttar Pradesh</b>	Bijnor, Muzaffarnagar and Sharanpur
	<b>Punjab</b>	Amritsar, Ferozpur, Gurdaspur, Hoshiarpur, Kapurthala, Ludhiana, Mansa, Moga, Patiala, Sangrur and Tarn Taran
	<b>Rajasthan</b>	Ganganagar and Hanumangarh

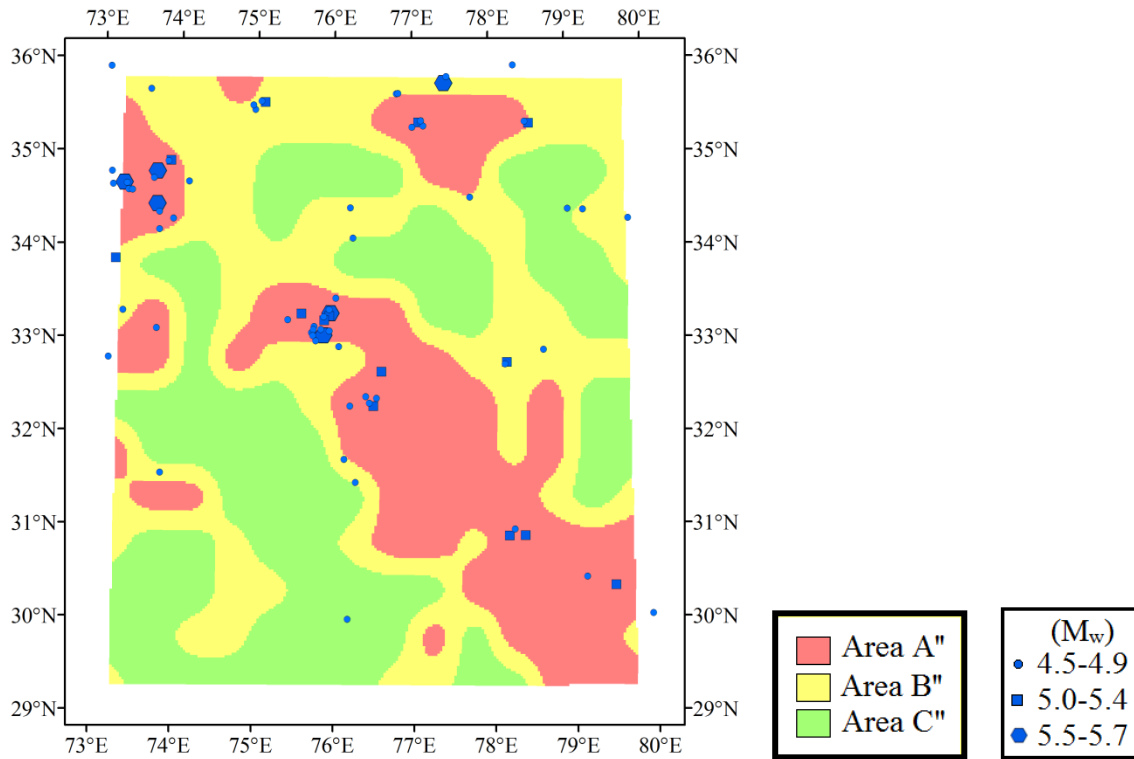


**Figure 4.10:** Seismicity as per MHD catalogue-2 superposed on susceptible areas for validation of results.

#### 4.7 Comparisons

The qualitative study carried out by Bhatia *et al.* (1992) identifies potential areas where strong earthquakes may occur as dangerous knots in the Himalayan arc. The quantitative approach of the present study has identified three kinds of seismically susceptible areas in western Himalayas where area A'' is the most susceptible. The susceptible area map of this study was superimposed on the map of dangerous knots for earthquakes  $M_w \geq 6.5$ , identified by Bhatia *et al.* (1992), and is shown in figure 4.11. Several dangerous knots #10, 18, 19, 23, 24, 25, and 34 are located totally within area A'', and major parts of several other knots partially overlap area A''. Similarly, for map of potential knots for earthquakes  $M_w \geq 7.0$ , two knots #16 and #19, between 76°E to 78°E, and knot #23 between 78°E to 70°E are completely within area A'', as shown in figure 4.12. Other knots also partially overlap some parts of area A''. Dangerous knots identified by Bhatia *et al.* (1992) are either within area A'' or are at boundary of A'', which implies a similarity in identification of almost same areas by different methods. In addition, area A'' is much larger than the area encompassed by knots.



Gorshkov *et al.* (2012) reconsidered and validated Bhatia *et al.* (1992) maps 20 years after their publication, in that time period several high magnitude and destructive earthquakes had occurred. It was observed that the Uttarkashi earthquake of 1991,  $M_w = 6.8$  (MHD) occurred within knot #24, Chamoli earthquake of 1999,  $M_w = 6.7$  (MHD) occurred within knot #35 and the Kashmir earthquake of 2005,  $M_w = 7.2$  (MHD) occurred within knot #5. It is significant to note that these three knots, #24, 35, 5 are totally within area A" of the present study. Two knots, i.e. #24 and 35 are within the largest area "A and #5 is in a different island of area A". For the present study data taken for validation of results is for three years, 2013-2015, and the largest magnitude earthquake within this period in the study area was  $M_w = 5.7$ .

The significance of area A was also observed while carrying out PSHA studies for the same study area. Area A" is overlapped by large parts of Kangra seismogenic source zone (SSZ) and Uttarakhand SSZ. Kangra SSZ was identified as the most vulnerable zone in terms of hazard parameters, viz. magnitude, return periods and PGA. Implications of this overlap are discussed in Chapter 7.

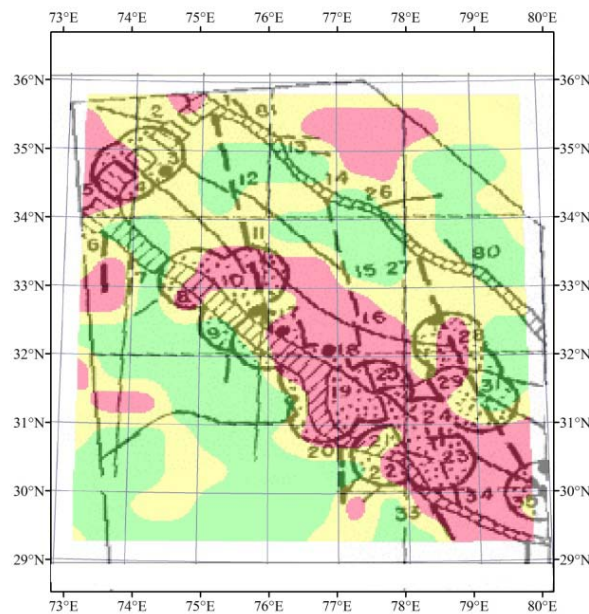


**Figure 4.11:** Susceptible area map (as per figure 4.9) superimposed on the map of potential knots of  $M_w \geq 6.5$  nodes of Bhatia *et al.* (1992).

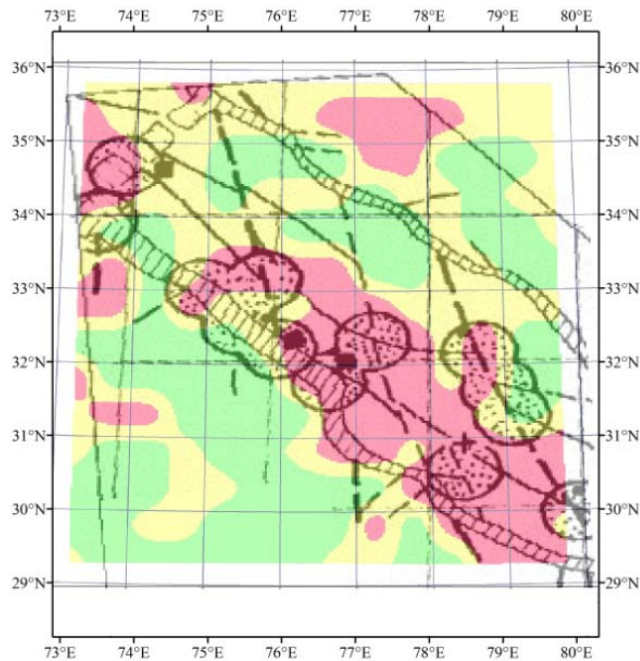


**Figure 4.12:** Susceptible area map (as per figure 4.9) superimposed on the map of potential knots of  $M_w \geq 7.0$  nodes of Bhatia *et al.* (1992).

#### 4.8 Conclusions

This study is an attempt to identify seismically susceptible areas in the northwest Himalayas, using pattern recognition technique. Pattern recognition started with identification, selection and extraction of features from seismotectonic data. These features were then subjected to discriminant analysis which consists of training exercise. The discriminant functions obtained from this training exercise was then applied for the decision making exercise to identify susceptible areas. The northwest Himalaya was classified into three types of area. The study was validated by testing earthquake data which occurred after completion of the MHD catalogue and was not part of the training exercise, i.e., for the years 2013 to 2015. It was found that 6 out of 80 earthquakes were of magnitude  $M_w \geq 5.5$ , and all 6 occurred in area A'', which has been assigned as the most susceptible area. Similar analysis was carried out for assigning moderately and least susceptible areas. Therefore, the study area was divided into three types of susceptible areas viz. area A'': most susceptible area, area B'': moderately susceptible area and area C'': least susceptible area. Results show that almost the entire states of Himachal Pradesh and Uttarakhand and a portion of Jammu & Kashmir are classified as area A'', while most of Jammu & Kashmir is classified as area B'' and the Indo-Gangetic plains are classified as area C''.



After identifying the three types of seismically susceptible areas, the next step is to assign Peak Ground Acceleration (PGA) to these areas, either by the deterministic seismic hazard assessment (DHSa) or probabilistic seismic hazard assessment (PSHA) method. The next chapter deals with segmentation of the main boundary thrust and the main central thrust in western Himalaya for assessment of seismic hazard.

## **CHAPTER 5**

# **SEGMENTATION OF MAIN BOUNDARY THRUST AND MAIN CENTRAL THRUST IN WESTERN HIMALAYA**

---

### **5.1 Introduction**

Many seismic sources are present in western Himalaya in the form of faults, thrusts and lineaments, which are capable of producing an earthquake of varying magnitude. These sources can either be small features or these may be mega thrusts like the Main Boundary Thrust (MBT) and Main Central Thrust (MCT). During an earthquake a long fault may not rupture over its entire length, but a small segment may rupture, depending on some physical boundary in the fault that controls and defines the location and extent of rupture, which in turn may be governed by several factors such as presence of transverse tectonic features, change in seismicity pattern along the fault, difference in slip rates, occurrence of significant lithologic changes, or strike of fault etc (Schwartz and Coppersmith, 1986). Moreover, the entire fault is not active; rather it is active in segments. Therefore, long tectonic features need to be segmented into smaller segments and then used in hazard assessment.

Segmentation of long tectonic units was carried out in several steps. Initially, six prominent tectonic units were segmented into equal portions, which were more than 294 km in length and hazard was assessed for the study area. After this exercise it was felt that the two longest and most prominent tectonic units, the MBT and the MCT be segmented as per a combination of seismicity and tectonic data. The objective of this study was to identify segments of the MBT and the MCT by using seismicity and tectonic data described in Chapter 2 and by resorting to Pattern Recognition (PR) technique as outlined in Chapter 3. The steps involved in segmentation are discussed in detail in this chapter. These segments along with other tectonic features and seismicity of the region were then included in assessment of hazard.

### **5.2 Equal Segmentation of Long Tectonic Units**

Twenty one prominent tectonic units were considered for the initial study. These are in alphabetical order: Alaknanda Fault (AF), Drang thrust (DT), Indus Suture Zone (ISZ), Jhelum fault, Jwalamukhi thrust (JMT), Karakoram fault, Kishtwar fault, Mahendragarh-Dehradun Fault (MHD-DDN F), Mastgarh Anticline, Main Boundary Thrust (MBT), MBT-A, Main Central Thrust (MCT), Main Frontal Thrust (MFT), Main Mantle Thrust (MMT), North Almora Thrust (NAT), Ramgarh Thrust, Reasi Thrust, Ropor Fault, Shyok Suture, South

Almora Thrust (SAT) and Sundarnagar fault (SNF). In addition, 5 closed unnamed thrusts, which are in between the MBT and MCT, were also considered, and salient features of all 26 tectonic units are given in table 2.12.

From seismicity data as given in Chapter 2, section 2.3.2, the MHD catalogue revealed the presence of one earthquake of magnitude  $M_w = 8.0$  (the great Kangra earthquake of 1905) in the entire study area. This earthquake posed the largest seismic hazard in the entire study area. It yields a rupture length of 151.35 km (Wells and Coppersmith, 1994) and a corresponding surface length of 454.06 km (Mark, 1977). The same exercise was repeated for the next largest earthquake which in the MHD catalogue was  $M_w = 7.7$ . Since this magnitude was repeated twice (1554, 1778) in the Srinagar Baramula region alone, it posed a repeated seismic hazard. Surface rupture length and surface length of fault due to this magnitude was computed as 98 km and 294 km, respectively. Therefore, it was considered that any feature longer than 294 km may support an earthquake of magnitude larger than 7.7 and was segmented. Length of each tectonic unit was measured in ARCGIS -9.3 and is given in table 2.12. It was observed that 9 tectonic units were longer than 294 km. These are: the Karakoram fault, 644 km; MBT, 997 km; MCT, 847 km; the closed thrust T2, 608 km; Drang thrust, 394 km; MMT, 407 km; Shyok Suture, 385 km; ISZ 1, 485 km and ISZ 2, 568 km.

In an initial attempt, the Karakoram fault, Drang thrust, MMT and Shyok Suture were segmented into two equal portions. Each segment of the longest of these faults, the Karakoram fault is 322 km, which is in approximate agreement with the 294 km length computed for a 7.7 magnitude earthquake. Moreover, as observed in the seismotectonic map, figure 2.11, the maximum earthquake each segment seems to support is 6.0 and 6.5 which is substantially lower than 7.7. Also, it is at a very large distance from both the MBT (267 km) and MCT (200 km). Therefore, this unit was not further segmented. When Drang thrust, MMT and Shyok suture were segmented into two equal portions, each segment was less than 294 km in length, and, therefore, these segments were retained. If a segment was substantially longer than 294 km, then it was further segmented. MBT and MCT were segmented into five equal segments. These segments of MBT were named, from west to east, as MBT-A, MBT-B, MBT-C, MBT-D and MBT-E. Similarly for MCT, segments were named as MCT-A, MCT-B, MCT-C, MCT-D and MCT-E.

Salient features of these six tectonic units and their equal segments are given in table 5.1 and are shown in figure 5.1 (a). However, as T2 which is a very complex tectonic unit and sometimes seemed to merge with the MCT, was difficult to trace on SEISAT 05 and 06, and

was not segmented. ISZ consists of three closely spaced parallel features; therefore, each sliver was considered separately in hazard assessment and was not further segmented. After considering equal segments the tectonic units increased from 26 to 40, and this increased number was considered for hazard assessment using deterministic seismic hazard assessment (DSHA) approach and this is discussed in Chapter 6.

**Table 5.1:** List of tectonic units, longer than 294 km that were segmented into equal portions, shown in figure 5.1.

S No.	Tectonic units	Length (km)	Segments	Length (km)
1.	Drang Thrust	394	Drang Thrust 1	197
			Drang Thrust 2	197
2.	Karakoram Fault	644	Karakoram Fault 1	322
			Karakoram Fault 2	322
3.	MBT	997	MBT-A	199
			MBT-B	199
			MBT-C	199
			MBT-D	199
			MBT-E	199
4.	MCT	847	MCT-A	169
			MCT-B	169
			MCT-C	169
			MCT-D	169
			MCT-E	169
5.	MMT	407	MMT 1	203
			MMT 2	203
6.	Shyok Suture	385	Shyok Suture 1	192
			Shyok Suture 2	192

After this exercise it was felt that equal segmentation needs to be reconsidered because of the following reasons pertaining to MBT and MCT. When equal segments of MBT were superimposed on the seismicity map, figure 5.1(b), it was observed that different segments showed different levels of seismicity. MBT-C was the most active of all segments and supported the highest magnitudes,  $M_w$  8.0 and 7.0; followed by MBT-A. Moreover, MBT-B indicates non uniform activity; the eastern portion is more active than the western portion; MBT-D and E indicate sparse seismicity. This implies that the entire MBT is not uniformly active but needs to be re-segmented as per seismicity and tectonics of the region.

Similarly, when segments of MCT were superimposed on the seismicity map, figure 5.1(b), it was observed that different segments showed different levels of seismicity. A dense

cluster of seismicity was observed between eastern portion of MCT-A and western portion of MCT-B, while western portion of MCT-A showed sparse seismicity. MCT-C shows an almost equal distribution of seismicity north and south of it. MCT-D and MCT-E are active segments with seismicity north of MCT. This implies that the entire MCT is not uniformly active but needs to be re-segmented as per seismicity and tectonics of the region. Moreover, MCT was considered as a continuous tectonic unit, prominent dislocations due to Kishtwar fault and Sundarnagar fault were ignored, these were added in the length of MCT, and needs to be reconsidered.

In a further exercise the most prominent and seismically active tectonic units, the MBT and MCT, were segmented once again using seismicity as per MHD catalogue and tectonics as per SEISAT using the PR technique.

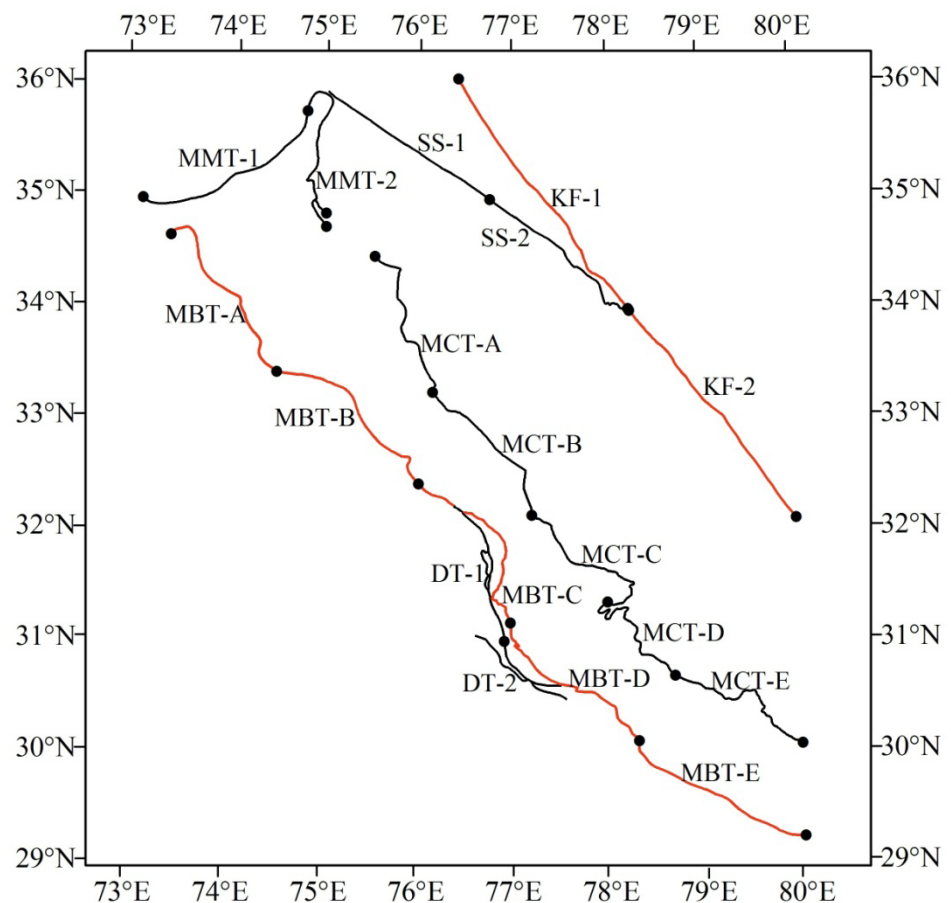


**Figure 5.1(a):** Segmentation of Karakoram fault (KF), Drang thrust (DT), Main Mantle Thrust (MMT), Shyok Suture (SS), Main Boundary Thrust (MBT) and Main Central Thrust (MCT) into equal segments.

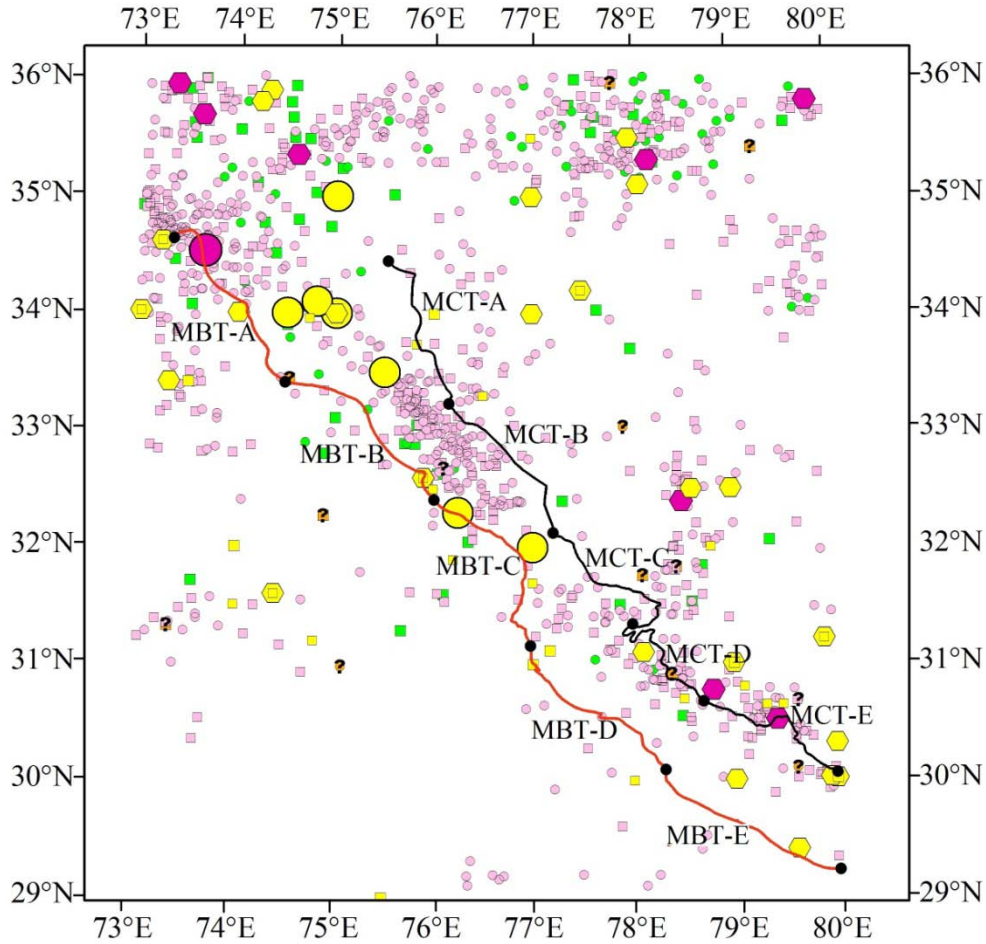


**Figure 5.1(b):** Seismicity of the study area as per MHD catalogue superimposed on the equal segments of MBT and MCT.

### 5.3 Segmentation of Main Boundary Thrust (MBT)

A second attempt was made to identify different segments of the MBT and the MCT, and these were used later for assessing seismic hazard by DSHA and PSHA. A combination of several features associated with seismicity and tectonics were subjected to the PR technique, to segment the MBT and the MCT in western Himalaya. The following discussion pertains to segmentation of the MBT. Initially four segments were identified. Later the two longest segments were further segmented to fulfill the Wells and Coppersmith criteria of relation between magnitude and surface rupture length.

#### 5.3.1 Features used

Four features were considered, two each from seismicity and tectonic data. These features are: F1: magnitude of central earthquake ( $M_w$ ); F2: number of epicenters other than

central earthquake; F3: number of tectonic units and F4: number of tectonic intersections. In the previous exercises for identification of susceptible areas, (models PR1-PR15), it was observed model PR4 showed the best discrimination and features F2 and F3 made the best contributions in discrimination. F1 was not considered as a feature in those exercises because the classification was magnitude wise. F4 is associated with tectonics and so it is considered for this study. Method of extraction of these features was shown in Chapter 3.

### 5.3.2 Classification criteria

Strike of the highly contorted MBT varies in the Himalayan arc and it is mostly a north dipping thrust in the entire study area. Of the 1172 epicenters in the MHD catalogue 91% have shallow depths. If dip of the MBT is assumed to be about  $30^\circ$ , and most shallow focus earthquakes originate at depths of approximately 15 km, then surface distance of these earthquakes from the MBT is about 25 km. This aspect was formulated as a classification criterion of epicentres. All epicenters in the MHD catalogue were divided into two classes based on their distance from MBT; this classification criteria discussed in Chapter 3, classification criteria-III was used for this analysis. Nine iterations of discriminant analysis were performed for segmentation of MBT and results are given in Chapter 3, table 3.3. The pattern of misclassification of epicenters was similar in all iterations. Therefore, the iteration which used the maximum amount of data, i.e. model PR26, which considered the entire MHD catalogue and 118 tectonic units of the study area is discussed here. Class  $S_{B1}$  contained 164 epicenters which are within a belt defined by a distance of 25 km on either side of MBT, and Class  $S_{B2}$  contained 1008 epicenters outside this belt. This classification is shown in figure 5.2.

### 5.3.3 Discriminant analysis

With classification criteria-III and a set of four features results of discriminant analysis, model PR26, are discussed here. Vector mean of each feature of Class  $S_{B1}$ , Class  $S_{B2}$ , and vector of mean differences of both classes were calculated as per equations 3.2, 3.3 and 3.4, respectively. Discriminant function, i.e.  $\lambda$  values were calculated using equation 3.10. These values are given in table 5.2. Multivariate means of Classes  $S_{B1}$  and  $S_{B2}$  and discriminant index ( $R_0$ ) were calculated using equations 3.12, 3.13 and 3.14, respectively. Multivariate mean of Class  $S_{B1}$ ,  $R_{SB1} = -0.225$ ; multivariate mean of Class B,  $R_{SB2} = -35.786$  and discriminant index,  $R_0 = -17.997$ . Seismic score for all epicenters in the MHD catalogue were calculated as per equation 3.11. In this exercise, 144 out of 164 seismic scores of Class  $S_{B1}$  were  $\geq -17.997$ , i.e.  $\geq R_0$ , i.e. 144 epicenters were desirably classified and 22 were crossover epicenters. However, for

Class  $S_{B2}$ , 816 out of 1008 seismic scores were  $\leq -17.997$ , i.e. 192 were crossover epicenters. Graphically, these are shown in figure 5.3.

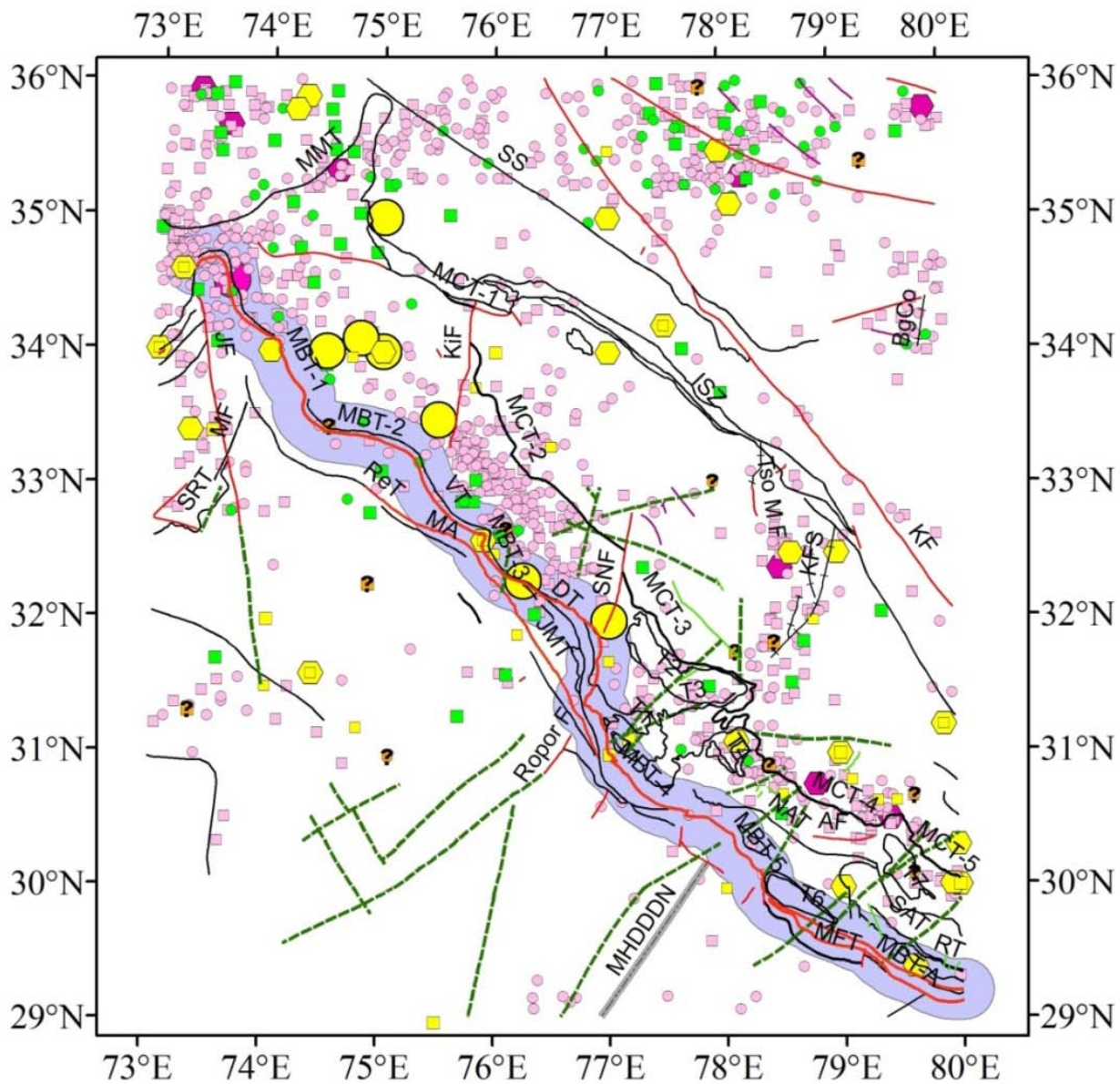


**Figure 5.2:** Classification of epicenters of MHD catalogue as per classification criteria-III. Purple belt indicates area 25 km on either side of MBT, epicenters within this belt are classified as Class  $S_{B1}$  and Class  $S_{B2}$  defines epicenters outside this belt. Legend for seismicity and tectonics is as per figure 2.11.



**Table 5.2:** Salient features of model PR26: classification criteria-III was considered, i.e., Class  $S_{B1}$  contained 164 epicenters which are within a 25 km belt on either side of MBT, and Class  $S_{B2}$  contained 1008 epicenters outside this belt. Features used were F1-F4. Vector means of Classes  $S_{B1}$ ,  $S_{B2}$ , difference of both Classes, discriminant function, i.e.,  $\lambda$  values and percentage contribution computed for each feature is shown in the table.

Feature	Name	Vector Mean Class $S_{B1}$	Vector Mean Class $S_{B2}$	Vector Mean difference	Discriminant Function, $\lambda$	Contribution of Each Feature (%)
F1	Magnitude of central earthquake	4.76	4.59	0.17	-13.32	-6.19
F2	Number of earthquake epicenters other than central earthquake	15.81	12.52	3.30	0.61	5.64
F3	Number of tectonic units	3.04	1.01	2.03	18.61	106.46
F4	Number of intersections between two tectonic units	0.54	0.17	0.37	-5.67	-5.91

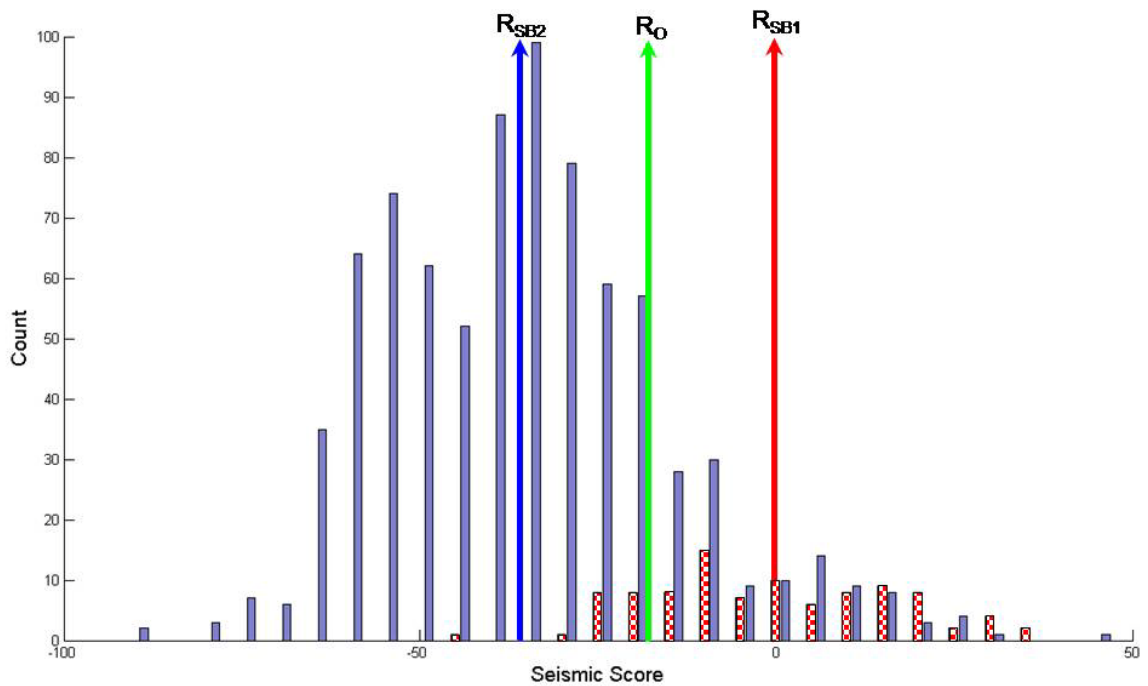


**Figure 5.3:** Seismic scores for the 1172 epicenters in the study area, model PR26. Blue represents Class  $S_{B1}$  and red represents Class  $S_{B2}$  epicenters.  $R_{SB1}$ ,  $R_{SB2}$  and  $R_0$ , are also plotted to show the separation between the two classes of epicenters.  $R_{SB1} = -0.225$ ,  $R_{SB2} = -35.768$  and  $R_0 = -17.997$ .

### 5.3.4 Results and decision making

Crossover epicenters were located on the seismo-tectonic map, shown in figure 5.4. It was observed that five distinct clusters of cross over epicenters were present in the study area. These were concentrated in the following regions: (1) around the western syntaxis; (2) Near Nanga Parbat; (3) the largest cluster was between Kishtwar and Sundernagar faults; (4) between Sundernagar fault and northward extension of Mahendragarh- Dehradun fault, north of MBT; (5) between northward extension of Mahendragarh - Dehradun fault and 80°E, i.e. Kumaon region in Uttarakhand, south east end of the study area. Most epicenters in cross over clusters (3), (4), and (5), were located south of the MCT, on the hanging wall of the MBT. Considering the dip of MBT and MCT this can be construed as epicenters which are more likely to be associated with MBT than MCT.

These crossover epicenters were in the magnitude range,  $M_w$  4.6-5.9 and are at shallow depths. The crossover epicenters were used in segmentation of the mega lineament MBT, model PR26. Four segments, MBT-1, 2, 3 and 4 were identified, and their salient features are given in the table 5.3.

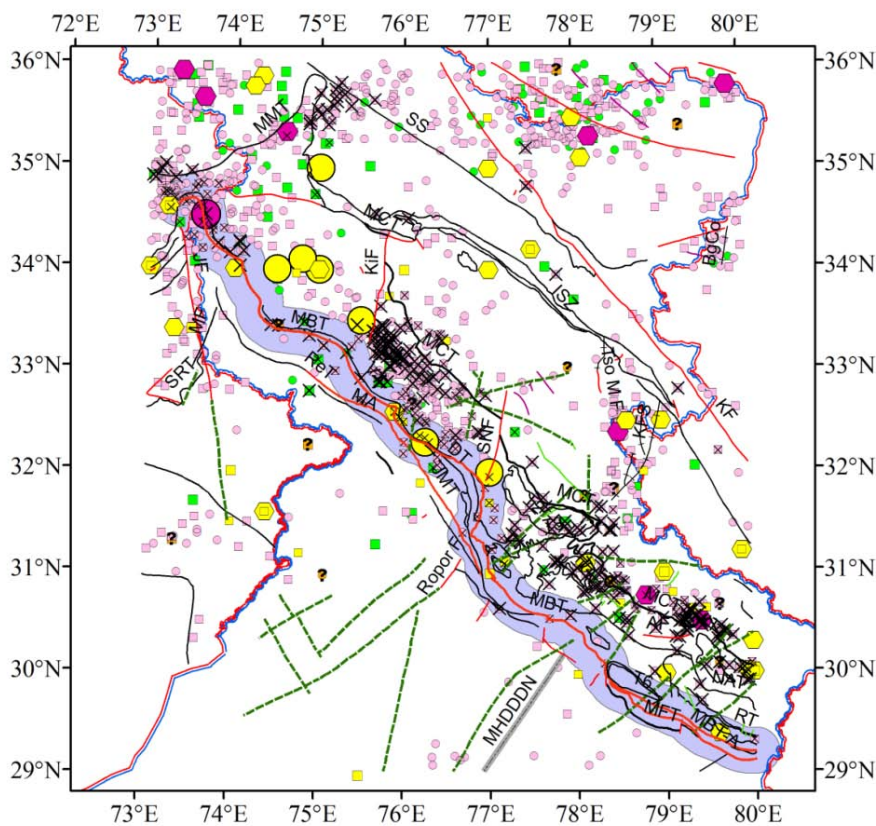


**Figure 5.4:** X shows cross over epicenters after discriminant analysis, and are significant while segmentation.

**Table 5.3** Initial four segments of MBT.

<b>Segment</b>	<b>Length (km)</b>	<b>Extent of segmented MBT</b>
MBT-1	317	N-W end of MBT to Kishtwar Fault
MBT-2	189	Between Kishtwar Fault to Sundernagar fault
MBT-3	241	East of Sundernagar F to northward extension of Mahendragarh Dehradun Fault into Kaurik F
MBT-4	249	Rest of MBT upto 80° E.

The 317 km long MBT-1 is the most westerly segment of MBT and extends from the northwest end of MBT in the study area to the intersection of the point where MBT intersects the southward extension of the transverse Kishtwar fault. A dense cluster of seismicity was observed in the western part of MBT-1, around the western syntaxis. However, there is an abrupt change in seismicity, including historical seismicity of large magnitude earthquakes, in the eastern part of MBT-1, about 170 km from the syntaxial bend. It was observed that most changes in the well defined pattern of seismicity were accompanied by prominent changes in strike of the MBT tectonic environment. The 317 km long segment was therefore further segmented, on account of change in strike of the highly contorted MBT, accompanied with sharp bends.

There is a prominent L shaped bend in the MBT, in the vicinity of South Kashmir, Punch and Reasi regions, corresponding to the Pir Panjal Pass in the Pir Panjal range. Coordinates of Pir Panjal Pass are 74°32'E, 33°38'N, as noted from Survey of India Toposheet 43K, scale 1:250,000 km. It was observed that seismicity changed abruptly at this L shaped prominent bend where large historical earthquakes were separated from smaller magnitude earthquakes, and seismicity was sparse at the bend and continued to be sparse till the eastern end of this segment. Therefore, the Pir Panjal pass was chosen as the region at which the MBT-1 was further segmented. This factor decided the length of the most westerly segment of the MBT, which extends from Muzaffarabad to Pir Panjal Pass. The eastern segment of MBT-1 extends from Pir Panjal Pass to intersection of the point where MBT intersects southward extension of the Kishtwar fault.

A large and dense cluster of seismicity between the two faults transverse to the MBT, Kishtwar fault in west, Sundarnagar fault in east, MBT in south and MCT in north was observed along MBT-2. This is the region where the largest and densest cluster of crossover epicenters was observed. It extends from intersection of the point where MBT intersects southward extension of the Kishtwar fault in west to intersection of Sundarnagar fault and

Ropor fault with MBT in the east, and has a length of 189 km. Similarly, a distinct concentration of crossover epicenters is nestled in a C shaped bend convex towards the Indo Gangetic plains, between the 25 km MBT belt and south of MCT. MBT-3 extends from intersection of Sundarnagar fault and Ropor fault, with MBT in west to northward extension of L24 towards MBT with its continuity as L22 in east. Length of MBT-3 is 241. Sparse seismicity was observed along MBT-4 which is the most easterly segment of the MBT, which is 249 km long. MBT-4 extends from intersection of transverse tectonic lineaments L24 and L22 with MBT in west to 80°E, i.e. eastern extremity of the study area. This segment was further divided into two segments by a point where a transverse lineament L26 intersects MBT. Transverse tectonic units which were used for segmentation of MBT are shown in figure 5.5.

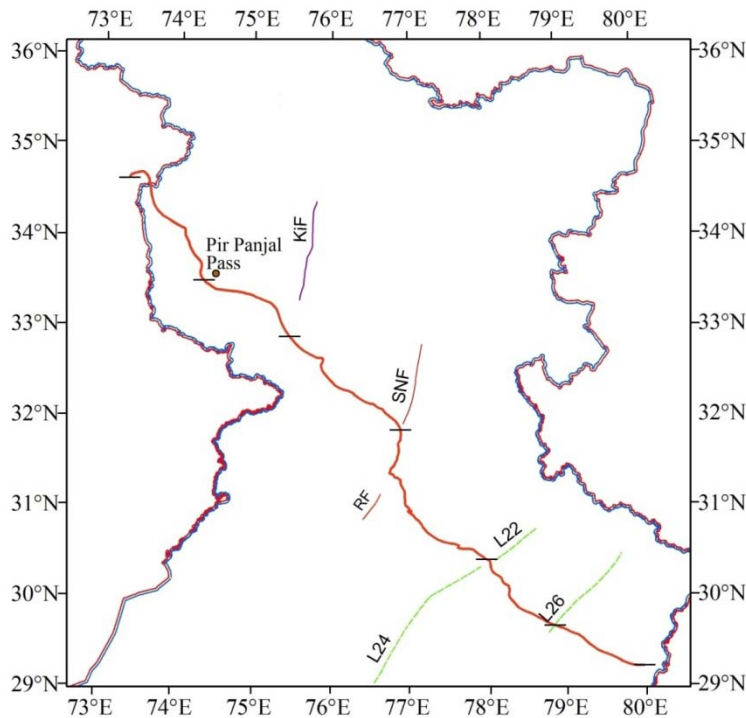


**Figure 5.5:** Figure shows MBT in red and tectonic units transverse to it which were used for segmentation. These are Kishtwar fault (KiF), Ropor fault (RF), Sundarnagar fault (SNF) and lineaments L22, L24 and L26.

This resulted in six segments of MBT, which were then renamed as MBT-1, MBT-2, MBT-3, MBT-4, MBT-5 and MBT-6 starting from west to east. Nomenclature of these segments was given based on the place they passed through. Salient features of these segments are given in table 5.4. MBT-1 is the Poonch segment which is 182 km long and it extends from north of Muzaffarabad to Pir Panjal Pass. MBT-2 is the 135 km long Udampur segment and it extends from Pir Panjal Pass to South of Doda. MBT-3 is Kangra segment, 190 km long and

extends from South of Doda to Mandi (Chachyot taluka). MBT-4 is Solan segment, 241 km long, and extends from Chachyot taluka to northern border of Vikasnagar and Dehradun. East of this is the MBT-5, which is the 125 km long Dehradun segment, and extends upto south of Lansdowne. MBT-6 is the 124 km long Nainital segment extending from south of Lansdowne to Purnagiri. These six segments of MBT are shown in figure 5.6.

**Table 5.4:** Six segments of MBT, from west to east, its given name, length (L), tectonic units demarcating the segment and places that define its extent and coordinates.

S. No.	Segment	Name	Length (km)	Demarcation of MBT on basis of intersection of Tectonic Unit	Place names (W-E)		Coordinates	
					From	To	From	To
1	MBT-1	Poonch segment	182	NW end of MBT in study area to Pir Panjal Pass	North of Muzaffarabad	Extension of Pir Panjal Pass	73.3°E, 34.61°N	74.33 °E, 33.50 °N
2	MBT-2	Udhampur segment	135	From Pir Panjal pass to south of Punch	Extension of Pir Panjal Pass	South of Doda	74.33 °E, 33.50 °N	75.47 °E, 32.89 °N
3	MBT-3	Kangra segment	190	Between Kishtwar fault and Sundernagar fault	South of Doda	Dist Mandi, Chachyot Taluka ,HP	75.47 °E, 32.89 °N	76.92 °E, 31.86 °N
4	MBT-4	Solan segment	241	South of Sundernagar and extension of Mahendragar h Dehradun Fault into Kaurik F	Chachyot taluka, HP	North of Dehradun, Border of Vikasnagar and Dehradun	76.92 °E, 31.86 °N	78.02 °E, 30.42 °N
5	MBT-5	Dehradun segment	125	South extension of Mahendragar h Dehradun Fault to lineament cutting MBT	North of Dehradun	South of Lansdowne	78.02 °E, 30.42 °N	78.87 °E, 29.67 °N
6	MBT-6	Nainital segment	124	Rest of MBT in the study area upto 80°E	South of Lansdowne	Purnagiri	78.87 °E, 29.67 °N	80 °E, 29.21 °N

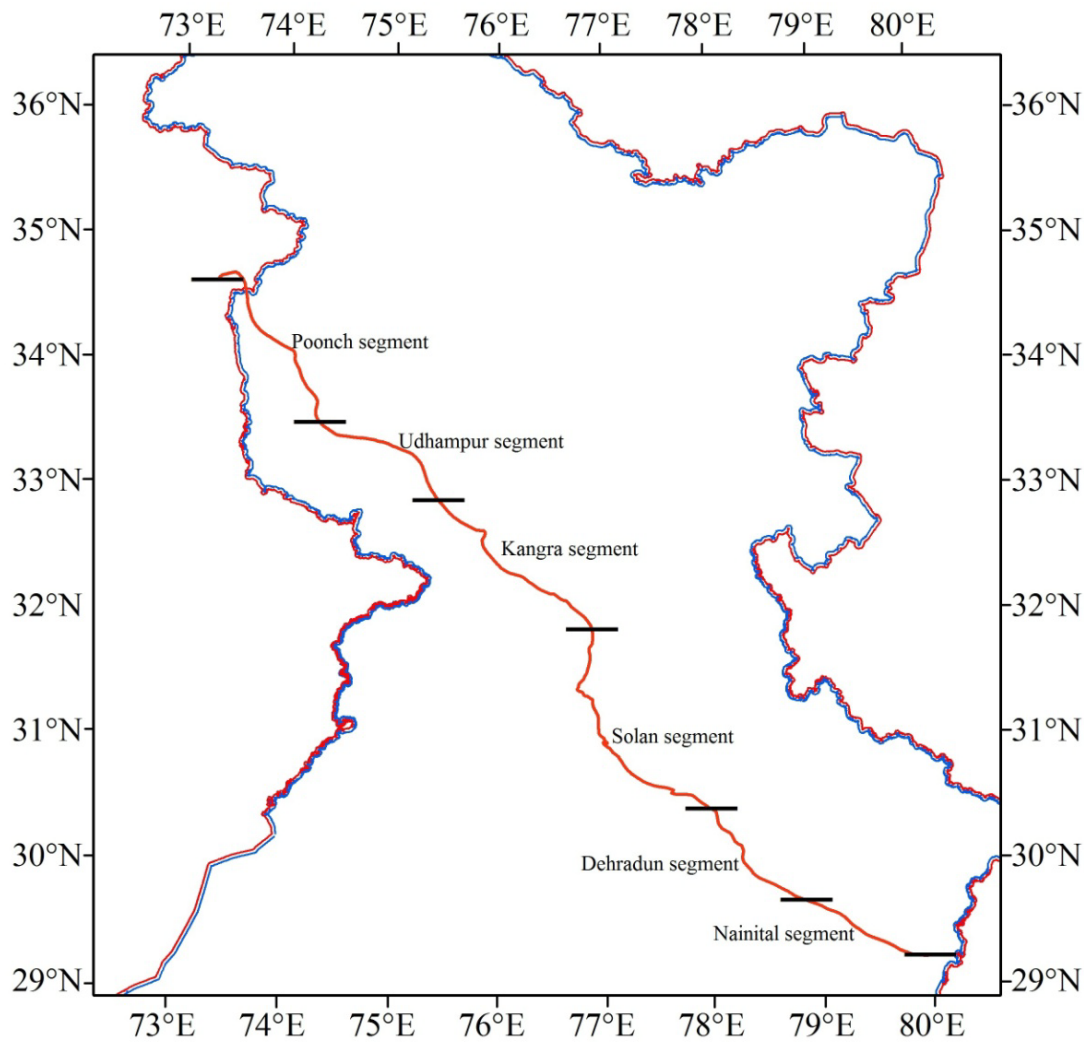


**Figure 5.6:** Six segments of MBT in western Himalaya.

#### 5.4 Segmentation of Main Central Thrust (MCT)

A similar exercise was carried out for the MCT. Four features (F1-F4) were used for discriminant analysis. A classification criteria, similar to the one used for MBT was formulated with respect to MCT by considering a distance of 25 km on either side of MCT. The 1172 epicenters of MHD catalogue were divided into two classes with respect to the MCT: Class  $S_{C1}$  contained 199 epicenters which are within a belt defined by a distance of 25 km on either side of MCT, and Class  $S_{C2}$  contained epicenters 973 outside this belt. These are shown in figure 5.7.

Discriminant analysis was carried out and, vector mean of Class  $S_{C1}$ , vector mean of Class  $S_{C2}$ , vector of mean differences of both classes, discriminant function, i.e.,  $\lambda$  values and

percentage contribution computed for each feature are shown in the table 5.5. The values obtained for  $R_{SC1}$ ,  $R_{SC2}$  and  $R_0$  were - 0.027, -8.748 and -4.387 respectively. Graphically these are shown in figure 5.8. These values were used for identifying cross over epicenters. These, when located on the seismo-tectonic map, shown in figure 5.9, show four distinct clusters of crossover epicenters. These were concentrated in the following regions: (1) Near Nanga Parbat; (2) near Muzaffarabad (3) Between Kishtwar and Sundernagar faults (mostly south of MCT); (4) east of Sundernagar fault upto  $80^{\circ}E$ . These observations were used for segmentation of the MCT. Clusters of crossover epicenters almost coincided with identification of segments confirmed by reexamining the tectonic environment, mainly two abrupt dislocations in MCT and presence of transverse tectonic units cutting across MCT.

Kishtwar fault dislocated a segment of MCT in the northwest part of the study area. This was identified as one small segment, MCT-1. MCT-2 was identified between Kishtwar and Sundernagar faults. South east of Sundernagar fault there exists a 'w' shaped contortion of MCT. Southward extension of Kaurik fault system seems to intersect this 'w' shaped contortion of MCT. The intersection point of this 'w' was considered as a discontinuity and MCT-3 was identified. MCT- 4 was identified between the 'w' shaped contortion and a lineament L26 cutting MCT. MCT-5 is rest of the MCT upto  $80^{\circ}E$  of the study area. Therefore, MCT was divided into five segments and salient features are given in table 5.6. Transverse tectonic units which were used for segmentation of MCT are shown in figure 5.10.

MCT-1 is 29 km long Mashko segment, which is a small segment NW of Kishtwar fault in Jammu and Kashmir. MCT-2 is 235 km long Chenab segment which extends between Jammu and Kashmir and Kyelang. MCT-3 is 229 km long Kinnaur segment which extends between Kyelang and Chirgaon. MCT-4 is 257 km long Uttarkashi segment which extends between Chirgaon and Chamoli. MCT-5 is 48 km long Bageshwar segment between Chamoli and Kapkot, Uttarakhand. Various segments of MCT are shown in figure 5.11.

These segments of MBT and MCT resulted in 127 tectonic units in the study area. The list of these 127 tectonic units is given in Chapter 6, table 6.3. These segments were then further used for hazard assessment in DSHA in Chapter 6 and PSHA in Chapter 7.



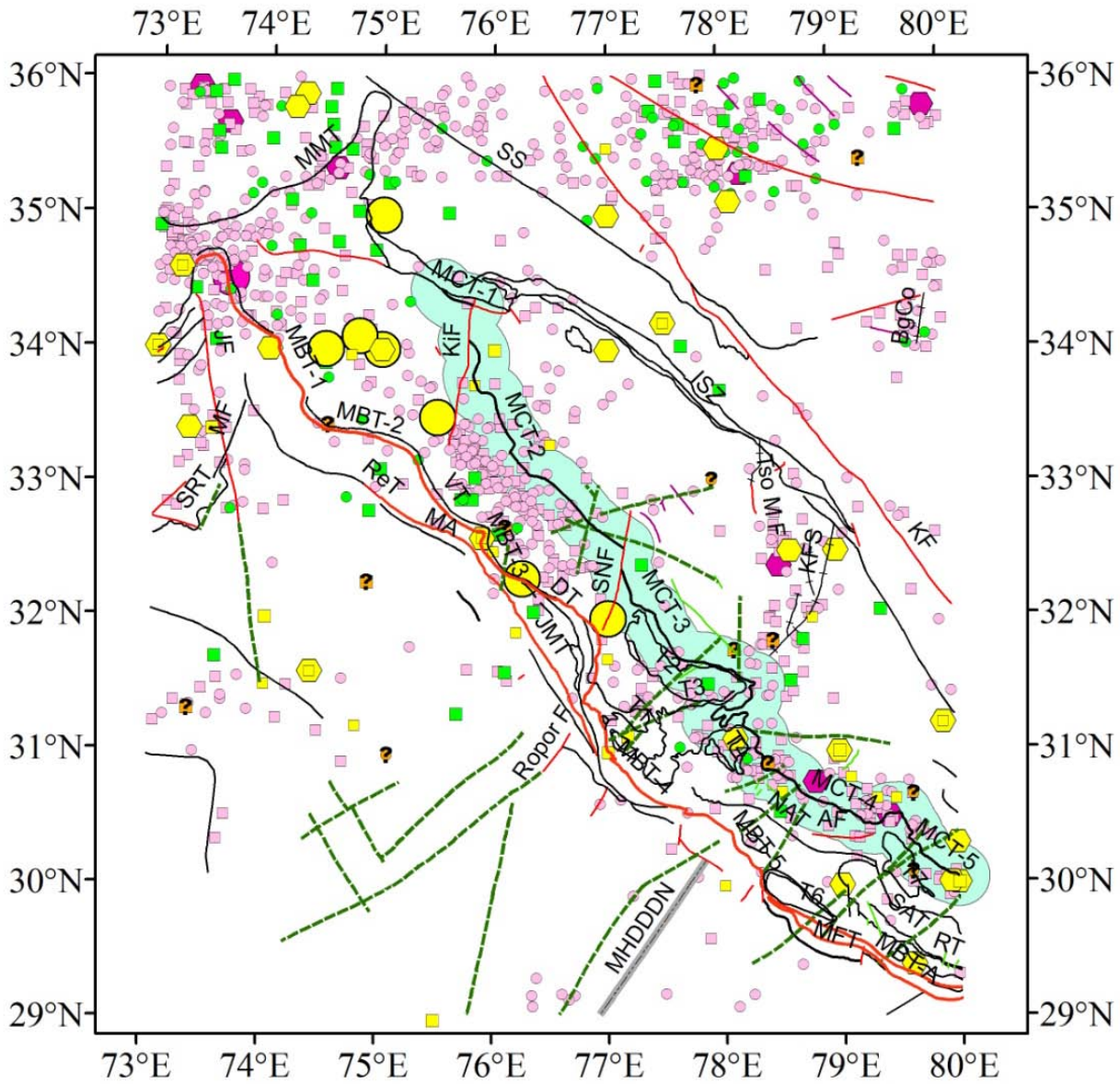


**Figure 5.7:** Classification of epicenters of MHD catalogue as per classification criteria-IV. Green belt indicates area 25 km on either side of MCT, epicenters within this belt are classified as Class  $S_{C1}$  and Class  $S_{C2}$  defines epicenters outside this belt. Legend for seismicity and tectonics is as per figure 2.11.



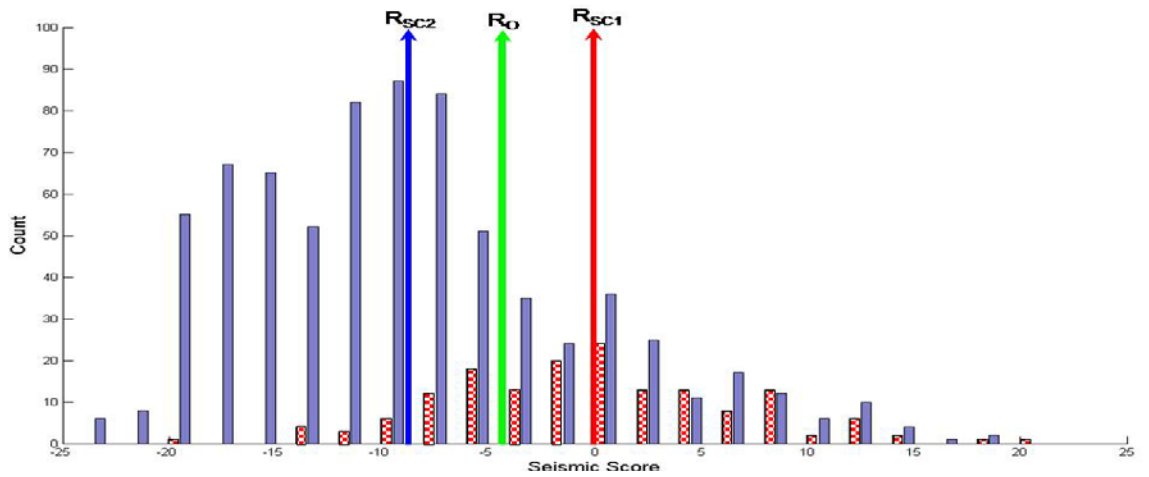


**Figure 5.8:** Seismic scores for the 1172 epicenters in the study area. Blue represents Class  $S_{C1}$  and red represents Class  $S_{C2}$  epicenters.  $R_{SC1}$ ,  $R_{SC2}$  and  $R_0$ , are also plotted to show the separation between the two classes of epicenters.  $R_{SC1} = -0.027$ ,  $R_{SC2} = -8.748$  and  $R_0 = -4.387$ .

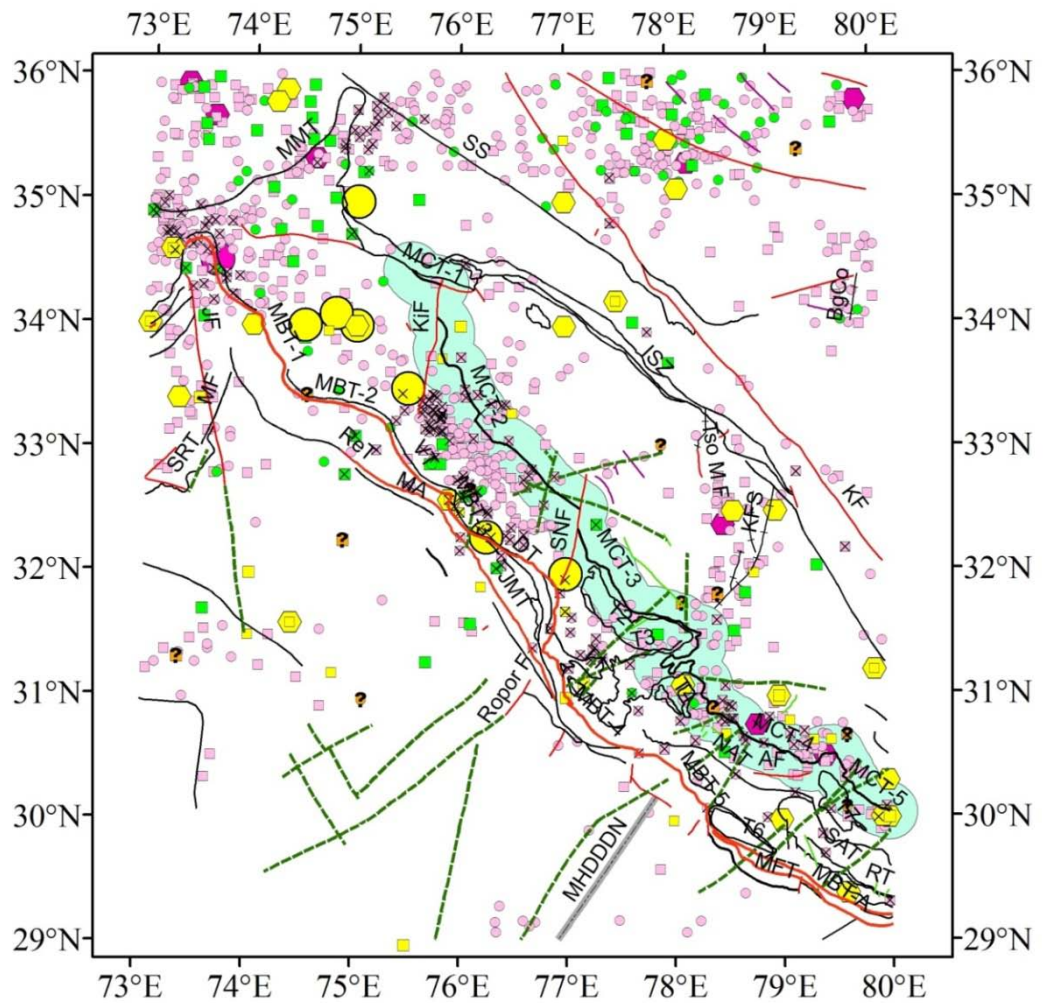


**Figure 5.9:** X shows cross over epicenters after discriminant analysis, and are significant while segmentation.

**Table 5.5:** Salient features of model PR27: classification criteria-IV was considered i.e. Class  $S_{C1}$  contained 199 epicenters which are within a belt defined by a distance of 25 km on either side of MCT, and Class  $S_{C2}$  contained epicenters 973 outside this belt. Features used were F1-F4. Vector means of class  $S_{C1}$ ,  $S_{C2}$ , difference of both classes, discriminant function i.e.  $\lambda$  values and percentage contribution computed for each feature is shown in the table.

Feature	Name	Vector Mean class $S_{C1}$	Vector Mean Class $S_{C2}$	Vector Mean difference	Discriminant Function, $\lambda$	% Contribution of Each Feature
F1	Magnitude of central earthquake	4.63	4.61	0.02	-4.22	-0.95
F2	Number of earthquake epicenters other than central earthquake	16.30	12.13	4.17	0.35	16.77
F3	Number of tectonic units	2.19	1.02	1.17	6.41	85.87
F4	Number of intersections between two tectonic units	0.45	0.15	0.30	-0.50	-1.69

**Table 5.6:** Five segments of MCT, from west to east, its given name, length (L), tectonic units demarcating the segment and places that define its extent and coordinates.

S. No.	Name	Name	Length (km)	Demarcation of MCT on basis of intersection of Tectonic Unit	Place names (W-E)		Coordinates	
					From	To	From	To
1.	MCT-1	Mashko segment	29	A small segment NW to Kishtwar fault	J&K	J&K	75.53°E, 34.45°N	75.80°E, 34.33°N
2.	MCT-2	Chenab segment	235	Between Kishtwar fault and Sundernagar fault	J&K	Kyelang	75.77°E, 34.07°N	77.15°E, 32.52°N
3.	MCT-3	Kinnaur segment	229	South of Sundernagar fault and w-shaped bend	Kyelang	Chirgaon	77.12°E, 32.37°N	78.01°E, 31.27°N
4.	MCT-4	Uttarkashi segment	257	W-shaped bend to lineament cutting MCT	Chirgaon	Chamoli	78.01°E, 31.27°N	79.62°E, 30.30°N
5.	MCT-5	Bageshwar segment	48	Rest of MCT in the study area upto 80°E	Chamoli	Kapkot	79.62°E, 30.30°N	80°E, 30.04°N

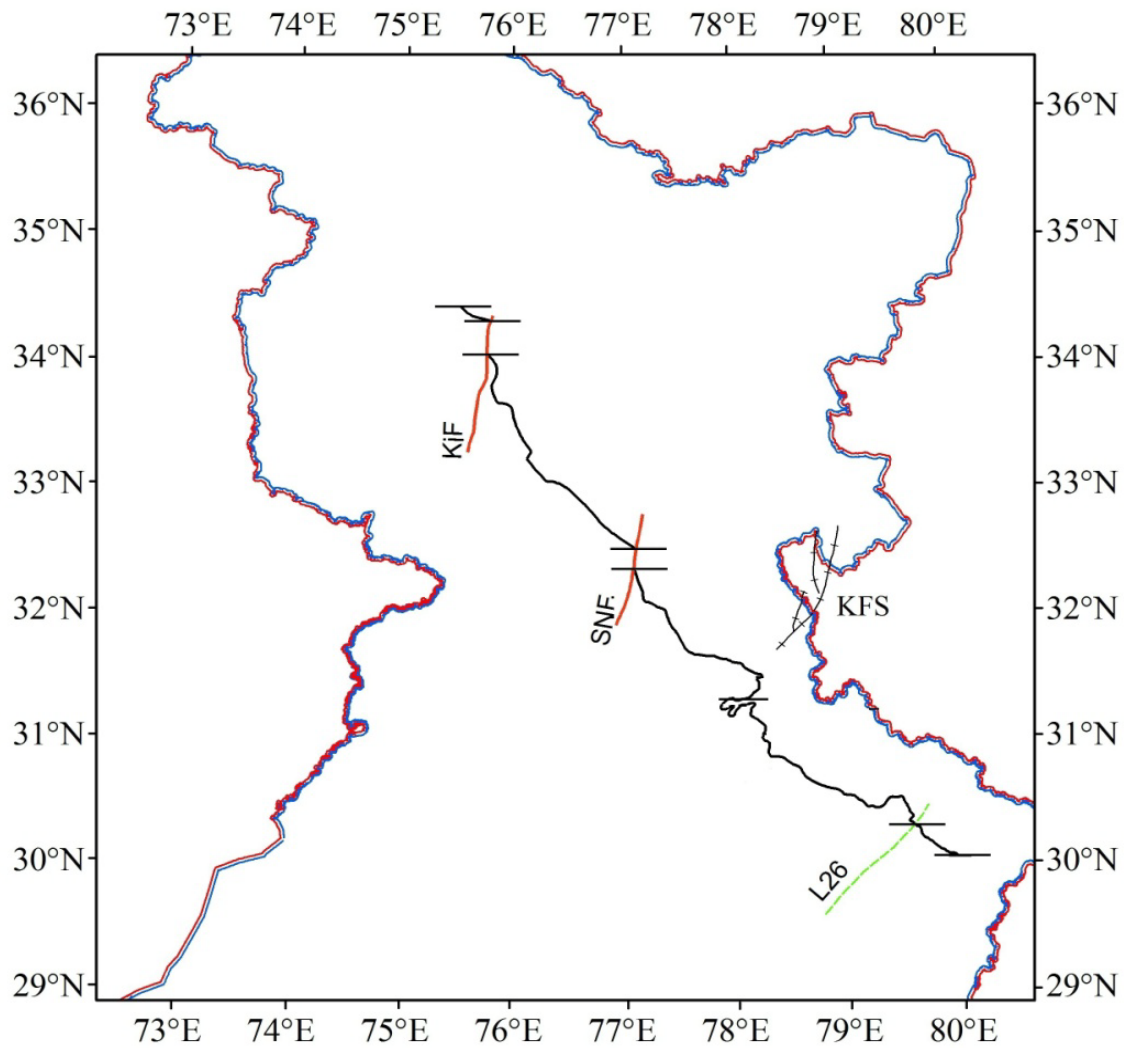


**Figure 5.10:** Figure shows MCT in black and tectonic units transverse to it which were used for segmentation. These are Kishtwar fault (KiF), Sundarnagar fault (SNF), Kaurik fault system (KFS) and lineaments L26.

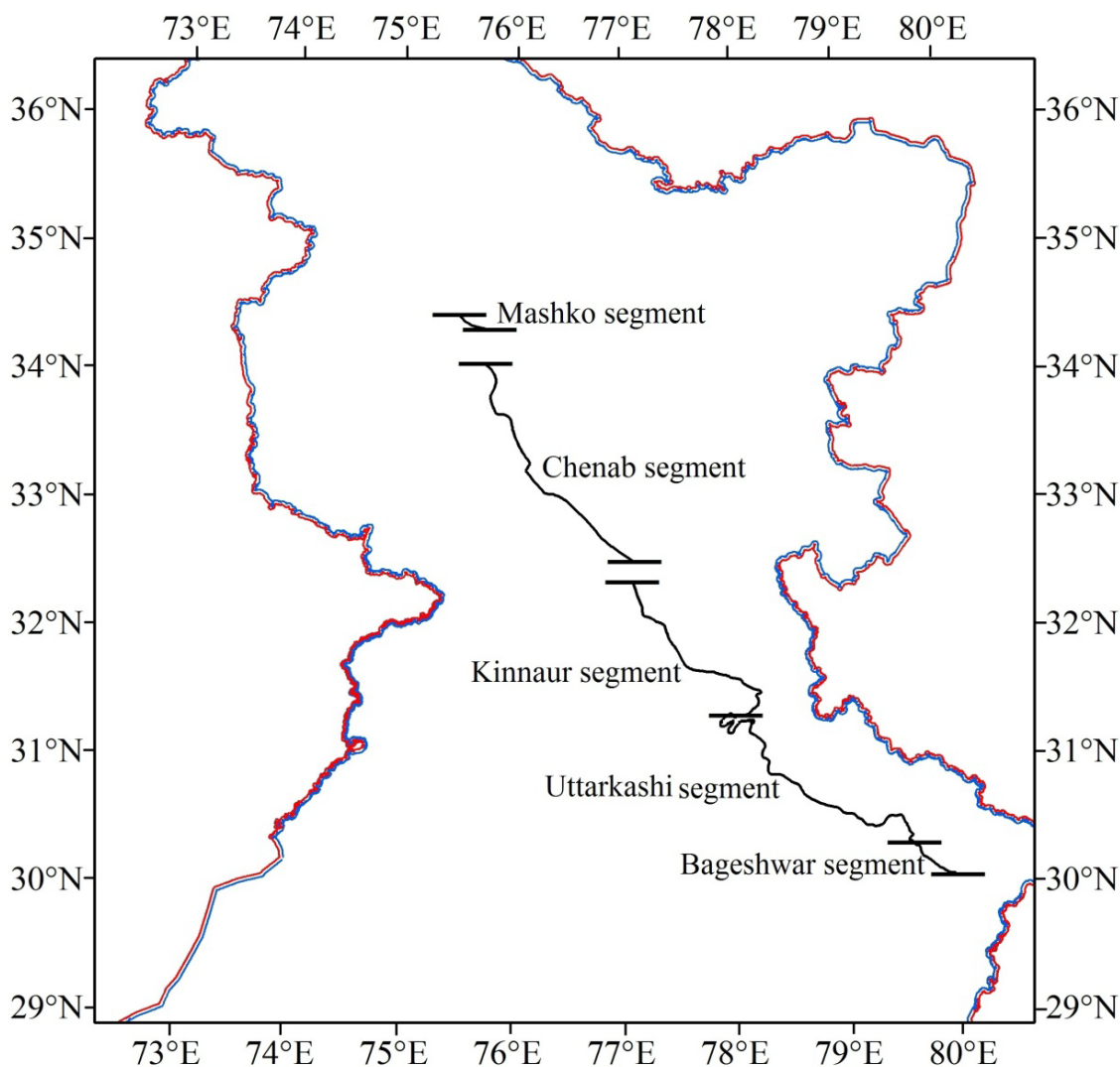


**Figure 5.11:** Five segments of MCT in western Himalaya.

## 5.5 Validation of Results of Segmentation

For validation of results obtained in sections 5.3 and 5.4, MHD catalogue-2 for validation of results, given in Chapter 2, section 2.4.8, figure 2.13 was considered. These epicenters were plotted on segmented MBT and MCT, as shown in figure 5.12, it showed that 45 epicenters out of 80 are associated with the MBT and MCT. 15 epicenters, 3 of which are within magnitude range  $5.5 \leq M_w \leq 5.7$ , 1 between  $5.0 \leq M_w \leq 5.4$  and 11 earthquakes between  $4.5 \leq M_w \leq 4.9$  are associated with Poonch segment of MBT. 24 epicenters, 2 of which are in magnitude range  $5.5 \leq M_w \leq 5.7$ ; 5 between  $5.0 \leq M_w \leq 5.4$  and 17 earthquakes between  $4.5 \leq M_w \leq 4.9$  are associated within the area demarcated by the Chenab segment of MCT, and Udhampur and Kangra segments of MBT. Six epicenters of lower magnitude range (3 between

$5.0 \leq M_w \leq 5.4$  and 3 earthquakes between  $4.5 \leq M_w \leq 4.9$ ) are associated with Uttarkashi and Bageshwar segments of MCT. This validates the assumption that the MBT and MCT are not uniformly seismically active over their entire length but certain segments are more active than other segments. MBT is active in the western part of the study area, whereas MCT is active in eastern part of the study area. Moreover, in central portion of the study area recent seismic activity is concentrated between the MBT and MCT.

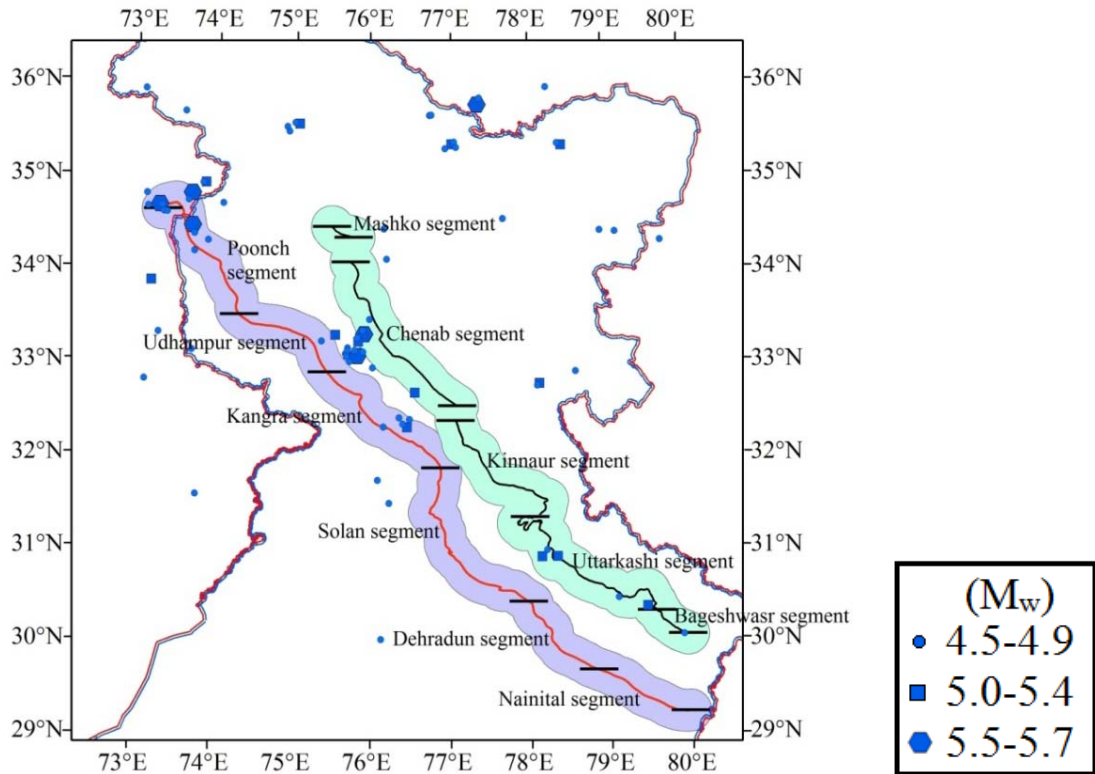


**Figure 5.12:** Recent epicenters from MHD catalogue-2, plotted on segments of MBT and MCT. These were used for validation of seismicity of these segments.

## 5.6 Conclusions

Since very long tectonic units cannot be considered as such for assessment of seismic hazard, it is necessary to segment these. This study makes an attempt of segmenting longer tectonic units. By resorting to PR technique the MBT and MCT were segmented. In the learning exercise crossover epicenters were identified and, crossover epicenters when plotted on seismotectonic map, which led to a decision making. Using these and several other factors such as presence of transverse tectonic features, change in seismicity pattern along the fault, strike of fault, six segments of MBT and five segments of MCT were identified. These segments were used while assessing seismic hazard of the area by two different methods: Deterministic Seismic Hazard Assessment (DSHA), as discussed in Chapter 6 and Probabilistic Seismic Hazard Assessment (PSHA), as discussed in Chapter 7.

## CHAPTER 6

# **DETERMINISTIC SEISMIC HAZARD ASSESSMENT (DSHA)**

---

### **6.1 Introduction**

Deterministic Seismic Hazard Assessment (DSHA) involves the development of particular earthquake scenario upon which a ground motion hazard evaluation is based (Kramer, 2009). Deterministic seismic hazard assessment is called “deterministic” because it is based on facts, data and physical models, describing the behavior of earthquakes (Klügel, 2008). DSHA involves the estimation of ground motion at any particular site where the earthquake scenario has been assumed. DSHA is a four step process (Reiter, 1990): identification and characterization of seismogenic sources; calculation of source to site distances; identification of maximum earthquake and calculating Peak Ground Acceleration (PGA) using Ground Motion Prediction Equation (GMPE). These four steps are described briefly in the following section and are illustrated in figure 6.1.

Earthquake sources which are capable of producing significant ground motion are identified as seismogenic sources. These sources can range from clearly understood and defined faults to less well understood hypothetical seismotectonic sources. Seismogenic sources are characterized as either point source or line source or area or volume source. The characterization of seismogenic sources involves quantifying three physical parameters of a potential seismic source: geometry and location of source, (where do earthquakes occur?); rate of earthquake recurrence (how often do earthquakes occur?) and maximum magnitude, (how big can we expect these earthquakes to be?), (Reiter, 1990). An additional characteristic is based on type of faulting i.e. whether it is a reverse fault, a strike slip fault, a normal fault and sometimes may be an unspecified type of fault.

The source to site distance is mostly measured as the shortest distance between the site and seismogenic source. Various types of distance measures are in vogue, like hypocentral, epicentral, distance to the zone of maximum energy release, closest distance to zone of rupture, and the closest horizontal distance to vertical projection of the rupture i.e. the Joyner-Boore distance. These distances are shown in figure 6.2.



## Steps in Deterministic Seismic Hazard Analysis

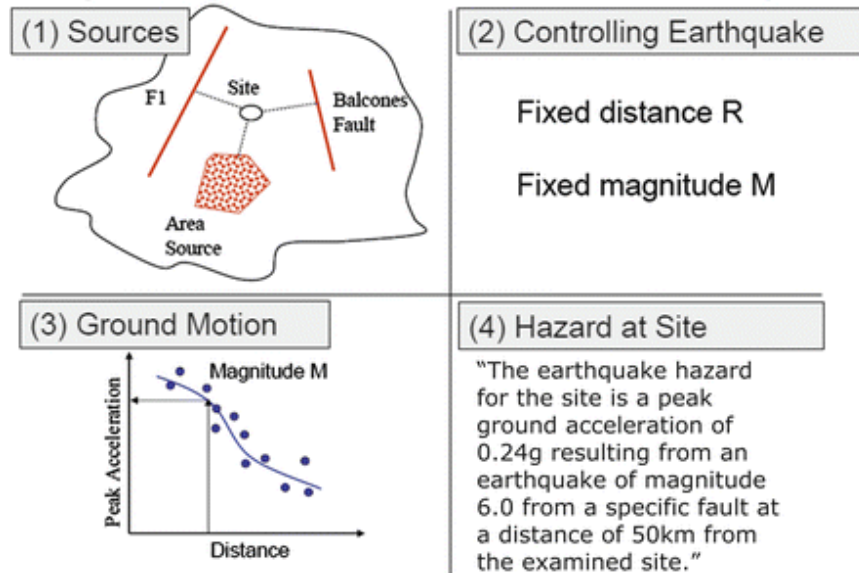


**Figure 6.1:** Major steps in Deterministic Seismic Hazard Assessment (DSHA) approach (after Reiter, 1990).

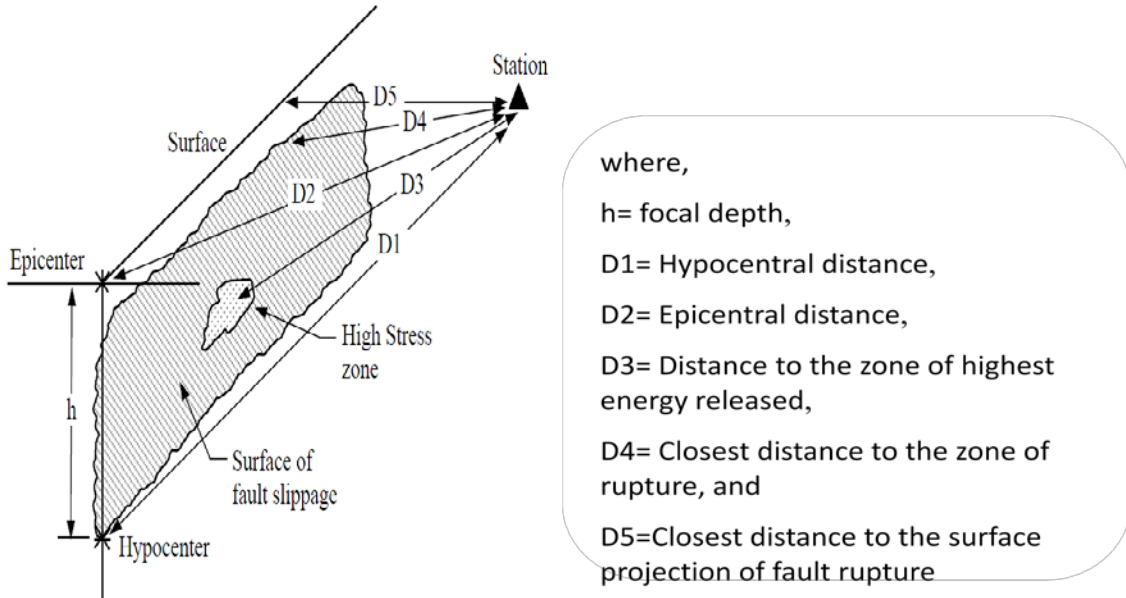


**Figure 6.2:** Various measures of distance used in strong-ground predictive relationships (After Shakal and Bernreuter, 1980).

The maximum earthquake is identified as the earthquake capable of producing maximum ground motion at a particular site. The maximum earthquake is expressed in terms of its size (magnitude) and distance from the site. There are two methods of assigning maximum earthquake to any fault. a) Based on past seismicity: i.e. observed maximum magnitude in the vicinity of seismogenic source. This method has the disadvantage that there may be several tectonic units which do not have any significant earthquake present around them but these may be responsible for generating future earthquakes. Moreover, a small tectonic unit in the vicinity of a large tectonic unit may be assigned the same magnitude as observed for the large tectonic unit. b) Based on dimensions of surface rupture length the maximum magnitude earthquake the fault can support is calculated using Wells and Coppersmith, (1994) formulation. The first approach was used in DSHA-1 analysis and the second approach was used in DSHA-2 analysis.

Seismic hazard is then calculated in terms of ground motion produced at the site by the maximum earthquake. Ground motion is usually expressed using predictive relations which express ground motion parameter as a function of magnitude and distance and in some cases, other variables i.e.

$$Y = f(M, R, Pi) \quad (6.1)$$

where  $Y$  is the ground motion parameter,  $M$  is the magnitude of earthquake,  $R$  is a measure of distance from the source to the site being considered and  $Pi$  are other parameters (which may be used to characterize the earthquake source, wave propagation path, and/or local site conditions). The ground motion parameters are calculated using one of the many available ground motion prediction equations (GMPE). Different attenuation relationships have been developed for different regions worldwide in the past for estimation of peak ground acceleration (McGuire, 1976, 1977, 2004; Joyner and Boore, 1981, 1988; Campbell, 1981, 1985; Boore and Joyner, 1982; Abrahamson and Litehiser, 1989; Fukushima and Tanaka, 1990; Singh *et al.* 1996; Boore *et al.* 1997; Youngs *et al.* 1997; Sharma, 1998; Atkinson and Boore, 2006; Zhao *et al.* 2006; Boore and Atkinson, 2008; Nath *et al.* 2008; Chiou and Yongs, 2008; Sharma *et al.* 2009; Joshi *et al.* 2013a etc.). A list of attenuation relations developed between 1969 and 2000 has been listed by Douglas (2001) which has been revised in 2010 by Douglas (2011). Abrahamson and Litehiser (1989), attenuation relation was considered in DSHA-1 analysis and Boore and Atkinson (2008) was considered in DSHA-2 analysis.



This Chapter deals with assessment of seismic hazard using deterministic approach by using seismicity and tectonic data as discussed in Chapter 2. Initially, 26 named and major tectonic units, as described in section 2.4.2 were considered as seismogenic sources. This exercise is termed as DSHA-1, and is discussed in section 6.2. Later all tectonic units, 127, in the study area were considered as seismogenic sources. This exercise is termed as DSHA-2, and is discussed in section 6.3. For both studies 196 grid points as per section 2.2 were considered.

## 6.2 Deterministic Seismic Hazard Assessment (DSHA-1)

For the first deterministic seismic hazard assessment study 26 tectonic units as listed in table 2.12, were considered, six of these were segmented into equal portions as described in section 5.2. After segmenting into equal portions, a total of 40 tectonic units emerged for the study area, salient features of these are given in table 6.1. Each of these 40 tectonic units was considered as a seismogenic line source for computation of source to site distances. The next step was to assign maximum magnitude to each seismogenic source. In this study maximum earthquake to each tectonic unit was assigned on the basis of past seismicity i.e. observed seismicity from the MHD catalogue. The earthquake which was of largest magnitude within 100 km of a tectonic unit was assigned as maximum earthquake to that tectonic unit. To assess the worst case scenario it was assumed that the maximum magnitude earthquake identified for each tectonic unit will occur at the closest possible distance from site. Closest distance to the zone of energy release was calculated. For calculation of peak ground acceleration (PGA) ground motion prediction equation (GMPE), developed by Abrahamson and Litehiser (1989) was considered. This relationship takes into account fault characteristics and plate environment, and gives horizontal, ( $a_H$ ), and vertical, ( $a_v$ ), components of peak ground acceleration (PGA) at each site as given in equations 6.2 and 6.3.

$$\log_{10} a_H (g) = -0.62 + 0.177M - 0.982 \log_{10} (r + e^{0.284M}) + 0.132F - 0.0008 Er \quad (6.2)$$

$$\log_{10} a_v (g) = -1.15 + 0.245M - 1.096 \log_{10} (r + e^{0.256M}) + 0.096F - 0.0011 Er \quad (6.3)$$

where,  $M$  is the moment magnitude,  $r$  is the distance in km to the closest approach of the zone of energy release,  $F$  is a dummy variable that is 1 for reverse or reverse oblique events and 0 otherwise, and  $E$  is a dummy variable that is 1 for interplate events and 0 for intraplate events. The Himalayan arc is at the boundary between the Indian and Eurasian plates. The MBT and the MCT are reverse thrusts, with prominent crustal shortening across both, and can be considered to represent an inter-plate environment. Using this GMPE, PGA was calculated for all 196 sites. At

each site PGA due to all 40 tectonic units were calculated. Highest PGA obtained from magnitude-distance combination was retained at each site. Table 6.2 shows the highest PGA obtained at each site, its causative tectonic unit and epicentral distance.

**Table 6.1:** Salient features of 40 tectonic units considered in DSHA-1, (in alphabetical order) including segments of the larger units are shown in this table. Column 2: Tectonic unit, column 3: its length, column 4: maximum earthquake,  $M_w$ , assigned to each tectonic unit, column 5 and 6: epicenter (Longitude °E, latitude °N), column 7: depth (km) and column 8: descriptive identifier of earthquake.

1	2	3	4	5	6	7	8
1.	Alaknanda Fault	50	6.8	78.79	30.77	13.2	Uttarkashi earthquake of 1991
2.	Drang Thrust-1	197	8.0	76.30	32.30	35.0	Kangra Earthquake 1905
3.	Drang Thrust-2	197	6.1	77.00	31.70	33.0	Earthquake of 1930
4.	ISZ 1	485	7.7	75.00	35.00	33.0	Earthquake of 1554
5.	ISZ 2	568	6.1	77.50	34.20	33.0	Earthquake of 1917
6.	ISZ 3	203	6.6	78.50	32.30	14.0	Earthquake of 1975
7.	Jhelum Fault	201	6.5	73.30	33.40	33.0	Earthquake of 1669
8.	Jwalamukhi Thrust	290	8.0	76.30	32.30	35.0	Kangra Earthquake 1905
9.	Karakoram fault Fault-1	322	6.6	78.50	32.30	14.0	Earthquake of 1975
10.	Karakoram fault Fault-2	322	6.5	73.30	33.40	33.0	Earthquake of 1669
11.	Kishtwar Fault	123	7.5	75.00	34.00	33.0	Earthquake of 1662
12.	Mahendragarh Dehradun Fault	154	5.0	77.87	29.60	15.8	Earthquake of 1975
13.	Mastgarh Anticline	115	5.8	76.40	32.15	33.0	Dharamshala Earthquake of 1986
14.	MBT-A	199	7.2	73.64	34.54	7.9	Kashmir Earthquake of 2005
15.	MBT-B	199	8.0	76.30	32.30	35.0	Kangra Earthquake of 1905
16.	MBT-C	199	8.0	76.30	32.30	35.0	Kangra Earthquake of 1905
17.	MBT-D	199	6.8	78.79	30.77	13.2	Uttarkashi Earthquake of 1991
18.	MBT-E	199	6.7	79.42	30.51	22.9	Chamoli earthquake of 1999
19.	MBT-a	196	6.7	79.42	30.51	22.9	Chamoli earthquake of 1999
20.	MCT-A	160	7.5	75.00	34.00	33.0	Earthquake of 1662
21.	MCT-B	160	8.0	76.30	32.30	35.0	Kangra Earthquake of 1905
22.	MCT-C	160	8.0	76.30	32.30	35.0	Kangra Earthquake of 1905
23.	MCT-D	160	6.8	78.79	30.77	13.2	Uttarkashi Earthquake of 1991
24.	MCT-E	160	6.7	79.42	30.51	22.9	Chamoli Earthquake of 1999
25.	MFT	134	6.2	79.90	30.00	33.0	Earthquake of 1958
26.	MMT-1	203	7.9	73.64	34.54	7.2	Kashmir Earthquake of 2005
27.	MMT-2	203	7.7	75.00	35.00	33.0	Earthquake of 1554
28.	North Almora	278	6.8	78.79	30.77	13.2	Uttarkashi Earthquake of 1991

1	2	3	4	5	6	7	8
	Thrust						
29.	Ramgarh Thrust	120	6.7	79.42	30.51	22.9	Chamoli Earthquake of 1999
30.	Reasi Thrust	18	4.7	75.00	33.11	35.0	Earthquake of 1970
31.	Ropor Fault	38	6.2	77.00	31.70	33.0	Earthquake of 1930
32.	Shyok Suture-1	192	7.7	75.00	35.00	33.0	Earthquake of 1554
33.	Shyok Suture-2	192	6.5	73.30	33.40	33.0	Earthquake of 1669
34.	South Almora Thrust	96	6.8	78.79	30.77	13.2	Uttarkashi Earthquake of 1991
35.	Sundarnagar Fault	101	8.0	76.30	32.30	35.0	Kangra Earthquake of 1905
36.	T1	246	6.2	77.00	31.70	33.0	Earthquake of 1930
37.	T2	608	6.2	77.00	31.70	33.0	Earthquake of 1930
38.	T3	155	5.9	78.00	31.05	4.4	Earthquake of 1986
39.	T4	320	6.8	78.79	30.77	13.2	Uttarkashi Earthquake of 1991
40.	T5	285	6.7	79.42	30.51	22.9	Chamoli Earthquake of 1999

**Table 6.2:** Table shows computed PGA for 196 sites as per DSHA-1 study. Column 1: site number, column 2: tectonic unit nearest to site, column 3: epicentral distance, column 4: PGA (g) as per Abrahamson and Litehiser (1989) formulation. Length and maximum magnitude are given in table 6.1.

Site number	Tectonic unit	Epicentral Distance (km)	PGA (g)
1	2	3	4
1	MMT-1	95.4	0.06
2	MMT-1	72.8	0.07
3	MMT-1	48.1	0.11
4	MMT-1	3.9	0.34
5	SS-1	3.4	0.18
6	SS-1	28.9	0.14
7	KF-1	26.3	0.10
8	KF-1	12.4	0.11
9	KF-1	50.5	0.07
10	KF-1	87.8	0.06
11	KF-1	122.5	0.05
12	KF-1	156.1	0.05
13	KF-1	190.1	0.04
14	KF-1	227.1	0.04
15	MMT-1	43.2	0.12
16	MMT-1	25.0	0.18
17	MMT-1	7.6	0.34
18	MMT-1	13.5	0.20
19	MMT-1	31.8	0.14
20	SS-1	17.4	0.16

Site number	Tectonic unit	Epicentral Distance (km)	PGA (g)
21	SS-1	7.4	0.18
22	KF-1	17.9	0.14
23	KF-1	18.9	0.10
24	KF-1	52.5	0.07
25	KF-1	85.9	0.06
26	KF-1	122.2	0.05
27	KF-1	162.1	0.04
28	KF-1	196.7	0.04
29	MMT-1	11.5	0.29
30	MMT-1	20.6	0.21
31	MMT-1	44.9	0.11
32	MMT-1	12.1	0.17
33	ISZ2	9.6	0.18
34	ISZ2	31.3	0.14
35	ISZ2	32.2	0.13
36	SS-1	13.3	0.17
37	SS-1	13.0	0.11
38	KF-1	16.5	0.13
39	KF-1	56.9	0.10
40	KF-1	92.7	0.07
41	KF-2	127.9	0.07
42	KF-2	163.5	0.05
43	Jhelum Fault	11.9	0.14
44	MBT-A	5.4	0.40
45	MBT-B	30.9	0.16
46	ISZ3	41.8	0.12
47	ISZ3	26.8	0.14
48	MCT-A	3.2	0.18
49	ISZ3	8.7	0.18
50	ISZ3	0.3	0.18
51	ISZ2	17.0	0.14
52	SS-1	1.2	0.17
53	KF-1	22.9	0.17
54	KF-1	58.1	0.14
55	KF-2	93.9	0.12
56	KF-2	126.2	0.07
57	Jhelum Fault	19.9	0.10
58	Jhelum Fault	25.8	0.14
59	MBT-A	4.8	0.40
60	MBT-A	43.8	0.14
61	Kishtwar F	41.9	0.12
62	Kishtwar F	1.0	0.17
63	MCT-A	29.9	0.13
64	ISZ3	41.7	0.11

Site number	Tectonic unit	Epicentral Distance (km)	PGA (g)
65	ISZ3	11.9	0.20
66	ISZ2	5.7	0.18
67	KF-2	10.5	0.20
68	KF-2	23.0	0.15
69	KF-2	57.7	0.11
70	KF-2	95.0	0.07
71	Jhelum Fault	32.7	0.45
72	Jhelum Fault	12.6	0.16
73	MBT-A	23.8	0.15
74	MBT-B	11.0	0.18
75	MBT-B	4.1	0.19
76	Kishtwar Fault	13.7	0.17
77	MCT-A	6.2	0.37
78	MCT-B	37.9	0.23
79	SNF	53.9	0.23
80	ISZ3	25.3	0.19
81	ISZ3	6.3	0.14
82	KF-2	12.9	0.11
83	KF-2	23.7	0.09
84	KF-2	55.2	0.07
85	Jhelum Fault	45.9	0.24
86	Jhelum Fault	0.3	0.39
87	Jhelum Fault	46.4	0.18
88	Reasi Thrust	24.4	0.13
89	Jwalamukhi T	3.6	0.19
90	MBT-B	9.6	0.19
91	MCT-B	31.4	0.21
92	MCT-B	1.2	0.47
93	SNF	4.4	0.21
94	SNF	50.8	0.22
95	ISZ3	36.9	0.12
96	ISZ3	15.1	0.19
97	KF-2	13.0	0.07
98	KF-2	25.5	0.14
99	Jhelum Fault	65.6	0.05
100	Jhelum Fault	43.9	0.07
101	Jhelum Fault	62.8	0.07
102	Mastgarh A	60.3	0.09
103	Mastgarh A	37.6	0.13
104	MFT	14.2	0.24
105	MBT-C	3.9	0.47
106	MBT-C	26.2	0.23
107	MCT-B	9.7	0.39
108	MCT-C	45.1	0.15

Site number	Tectonic unit	Epicentral Distance (km)	PGA (g)
109	MCT-C	79.2	0.09
110	ISZ3	50.8	0.09
111	ISZ3	35.4	0.24
112	KF-2	4.4	0.23
113	Jhelum Fault	111.0	0.03
114	Jhelum Fault	99.0	0.04
115	Jhelum Fault	108.2	0.05
116	MFT	97.9	0.06
117	MFT	58.3	0.08
118	MFT	21.2	0.12
119	Jwalamukhi T	9.3	0.19
120	Drang T-1	0.7	0.31
121	T2	2.5	0.26
122	MCT-C	15.8	0.31
123	MCT-C	27.8	0.22
124	MCT-C	55.8	0.12
125	KF-2	73.7	0.12
126	KF-2	39.1	0.20
127	Jhelum Fault	162.6	0.02
128	Jhelum Fault	154.1	0.03
129	Jhelum Fault	159.9	0.03
130	MFT	129.5	0.04
131	MFT	94.0	0.06
132	MFT	73.4	0.08
133	Jwalamukhi T	39.6	0.13
134	Drang T-1	2.4	0.42
135	T1	0.4	0.21
136	T3	2.3	0.24
137	MCT-D	5.5	0.40
138	MCT-D	48.5	0.14
139	MCT-E	83.2	0.07
140	MCT-E	87.3	0.17
141	Jhelum Fault	215.9	0.02
142	Jhelum Fault	209.2	0.02
143	MFT	201.4	0.03
144	Ropor F	160.5	0.03
145	Ropor F	113.0	0.04
146	Ropor F	65.4	0.07
147	Ropor F	17.9	0.11
148	Drang T-1	10.7	0.17
149	T3	5.5	0.36
150	NAT	9.6	0.22
151	T5	8.4	0.28
152	MCT-D	14.1	0.24

Site number	Tectonic unit	Epicentral Distance (km)	PGA (g)
153	MCT-E	32.7	0.11
154	MCT-E	37.2	0.10
155	Jhelum Fault	269.9	0.02
156	Ropor F	263.7	0.02
157	Ropor F	217.4	0.02
158	Ropor F	171.8	0.03
159	Ropor F	128.0	0.04
160	Ropor F	88.4	0.05
161	Ropor F	61.7	0.07
162	Drang T-2	47.8	0.08
163	Drang T-2	25.0	0.12
164	MHD-DDN	16.1	0.17
165	MBT-D	12.0	0.27
166	NAT	4.2	0.26
167	Alaknanda F	6.7	0.24
168	MCT-E	8.1	0.17
169	Jhelum Fault	324.3	0.01
170	Ropor F	282.5	0.02
171	Ropor F	239.3	0.02
172	Ropor F	198.4	0.03
173	Ropor F	161.5	0.03
174	Ropor F	131.9	0.04
175	MHD-DDN	102.0	0.05
176	MHD-DDN	62.4	0.05
177	MHD-DDN	23.0	0.11
178	MHD-DDN	16.8	0.13
179	MFT	10.3	0.18
180	T6	2.9	0.26
181	SAT	2.8	0.26
182	NAT	1.7	0.27
183	Ropor F	352.4	0.02
184	MHD-DDN	308.0	0.03
185	MHD-DDN	259.9	0.04
186	MHD-DDN	211.8	0.09
187	MHD-DDN	163.9	0.15
188	MHD-DDN	116.5	0.06
189	MHD-DDN	70.0	0.07
190	MHD-DDN	28.7	0.02
191	MHD-DDN	10.8	0.10
192	MHD-DDN	50.6	0.02
193	MFT	48.7	0.01
194	MFT	23.1	0.16
195	MBT-a	13.2	0.01
196	MBT-E	2.3	0.18

### ***Hazard map, DSHA-1***

PGA in the study area varied between 0.012 - 0.470 g. Contour maps, with contour intervals of 0.01 g and 0.1 g are shown in figures 6.3(a) and (b), respectively. Figure 6.3(b) is the hazard map for the study area.

It was observed that maximum PGA, 0.470g, at site #105, was due to the great Kangra earthquake of 1905 which was at an epicentral distance of 3.9 km from MBT-C. PGA greater than 0.40g was observed in large parts of Bilaspur, Chamba, Kangra and Lahaul & Spiti districts of Himachal Pradesh. PGA in the range 0.30 g - 0.39g was observed in parts of Bilaspur, Chamba, Hamirpur, Kangra, Kinnaur, Kullu, Lahaul & Spiti, Mandi, Shimla, Sirmaur and Solan districts of HP; parts of Jammu & Kashmir and in Uttarkashi district of Uttarakhand. This range 0.30 g - 0.39g, was observed as several islands on the MBT and MCT, in the Nanga Parbat region of MMT and in the Jhelum region. PGA in the range 0.20-0.29g was observed in parts of Bilaspur, Chamba, Hamirpur, Kangra, Kinnaur, Kullu, Lahaul & Spiti, Mandi, Shimla, Sirmaur, Solan and Una districts of HP; parts of Jammu & Kashmir; Almora, Bageshwar, Chamoli, Dehradun, Pauri Garhwal, Rudraprayag, Tehri Garhwal and Uttarkashi districts of Uttarakhand. PGA in the range 0.10-0.19g was observed in small parts of Bilaspur, Kinnaur, Lahaul & Spiti, Sirmaur, Solan and Una districts of HP and a large part of Jammu and Kashmir; and parts of Almora, Chamoli, Dehradun, Nainital, Pauri Garhwal, Rudraprayag, Tehri Garhwal, Udham Singh Nagar and Uttarkashi districts of Uttarakhand. PGA less than 0.1g was observed in large parts of Indo Gangetic plains, in the north eastern part of the study area near Leh (Laddakh) and in Tibet region.



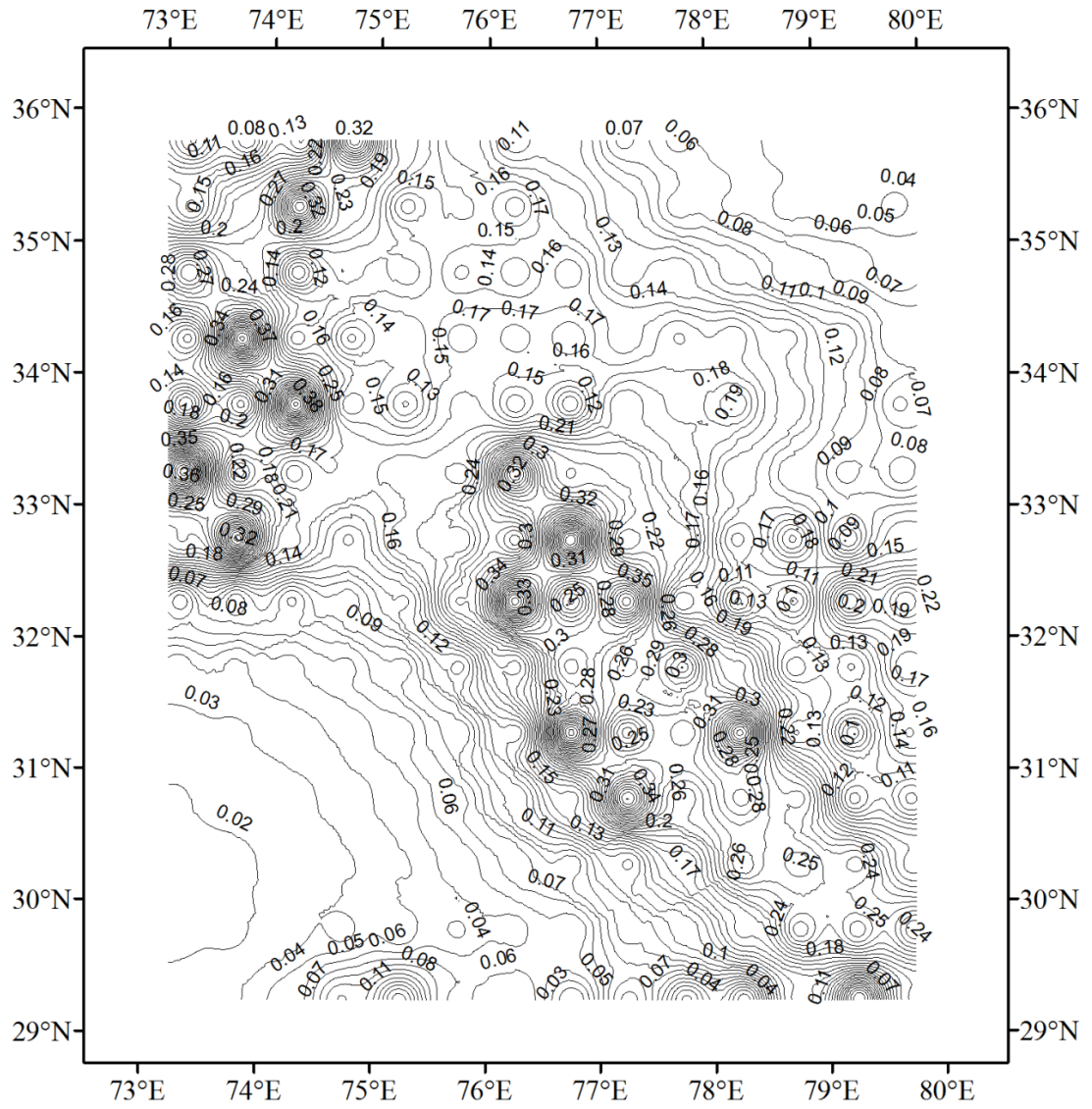


**Figure 6.3 (a):** Contour map for PGA as per DSHA-1, at contour interval 0.01 g.

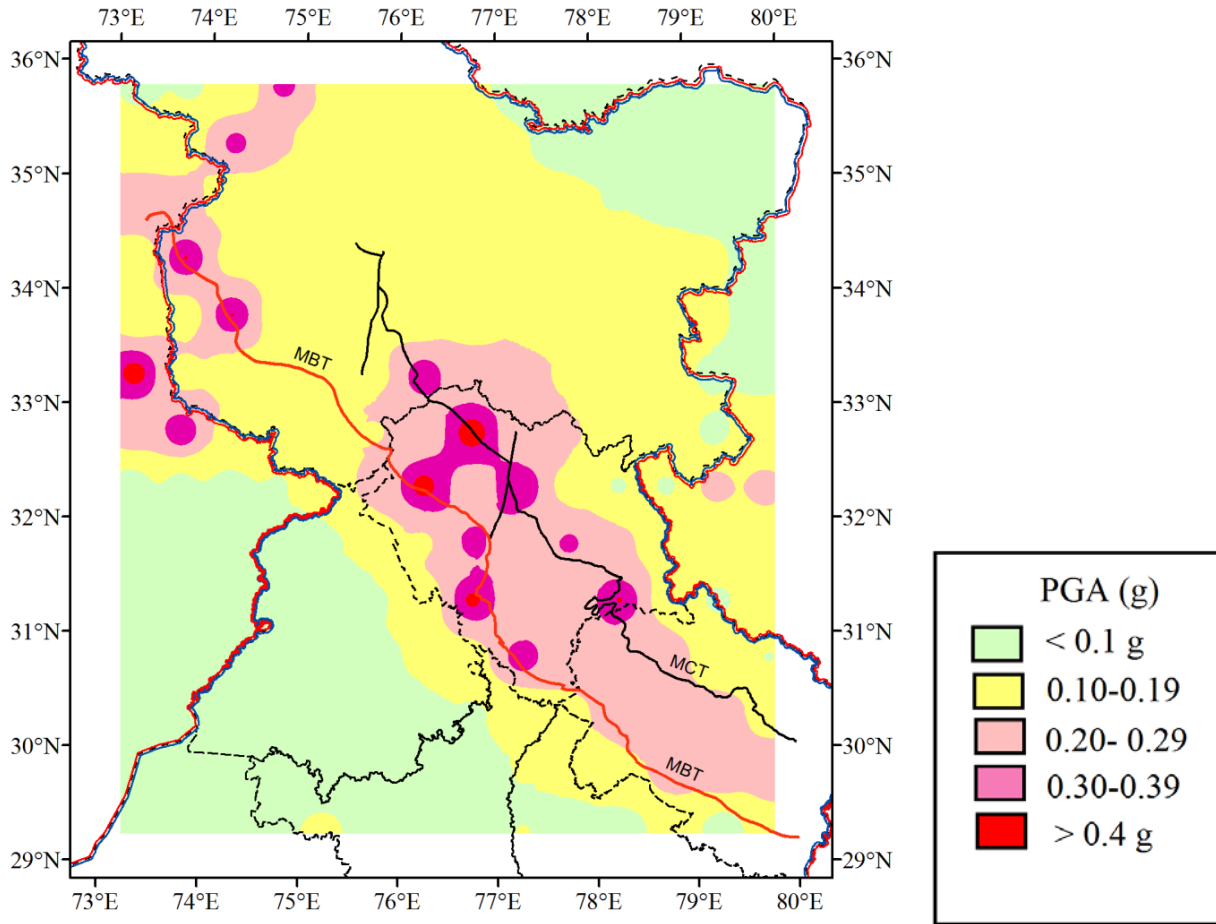


**Figure 6.3 (b):** Hazard map for PGA as per DSHA-1. Map also shows state boundaries as per Survey of India, 2011, MBT and MCT.

### 6.3 Deterministic Seismic Hazard Assessment (DSHA-2)

The above study, DSHA-1, was refined by considering the following aspects:

1. 26 tectonic units were considered as seismogenic sources in DSHA-1. This aspect was reconsidered by taking into account all tectonic units which were in the SEISAT in the study area, i.e. 118 tectonic units, as per table 2.13.
2. Equal segments of six tectonic units were considered in DSHA-1. This was reconsidered by considering segments of MBT and MCT as discussed in Chapter 5, sections 5.3 and 5.4. This resulted in 127 tectonic units in the study area, each of which was characterized on the basis of type of faulting as per SEISAT. Salient features of these are given in table 6.3.

3. Assigning maximum magnitude from observed seismicity leads to some ambiguity as two closely spaced tectonic units of significantly different lengths may not be capable of producing an earthquake of the same magnitude. For example in DSHA-1, MBT-C and Sundarnagar fault have different lengths, 199 km and 101 km, respectively, but both were assigned the same maximum magnitude,  $M_w = 8.0$ . This situation was observed in many cases and is shown in table 6.1. To circumvent this situation the maximum magnitude a tectonic unit can support was therefore computed as per Wells and Coppersmith, (1994) formulation, as given in equation 2.4 -2.6.
4. Each site was classified on the basis of shear-wave velocity in the top 30 m of rock type, three site classes were defined: firm to hard rock,  $V_{s30} = 700$  m/sec-1600 m/sec; soft to firm rock,  $V_{s30} = 375$  m/sec-700 m/sec; and soil (alluvium, slope wash material, Aeolian),  $V_{s30} = 200$  m/sec-375 m/sec, as per Mittal *et al.*, (2012). This classification is shown in figure 6.4 (a) and (b). Figure 6.4(a) shows the classification as per Mittal *et al.* (2012) and figure 6.4 (b) shows classification of sites. In this study  $V_{s30}$  was considered as 1100 m/sec for firm to hard rock sites, 500 m/sec for soft to firm rock sites and 300 for soil sites.
5. PGA was computed by using Abrahamson and Litehiser (1989) in DSHA-1. A more recent GMPE, Boore and Atkinson (2008), was considered for DSHA-2 which takes into account additional factors like fault type, its dip, rupture width, closest distance to surface projection of rupture, i.e.  $R_{JB}$  distance, and site amplification. The general attenuation model is described by equation 6.4:

$$\ln Y = F_M(M) + F_D(R_{JB}, M) + F_S(V_{S30}, R_{JB}, M) + \varepsilon\sigma_T \quad (6.4)$$

where,  $Y$  is the peak ground acceleration,  $F_M$  is the magnitude scaling function,  $F_D$  is the distance function,  $R_{JB}$  is the closest distance to surface projection of rupture, the Joyner–Boore distance in km,  $M$  is moment magnitude,  $F_S$  is site amplification function,  $V_{S30}$  is shear-wave velocity in m/s in the top 30 m.  $\varepsilon$  is standard deviation of a single predicted value of  $\ln Y$  from the mean value of  $\ln Y$ .  $\sigma_T$  is the intra-event aleatory uncertainty. This model is applicable for magnitude range 5 to 8, with  $R_{JB} < 200$  km and  $V_{S30} = 180$  to 1300 m/s. This attenuation model was used to compute PGA.

6. Down dip rupture width (RW) was calculated from maximum magnitude, given in step 3 above, using Wells and Coppersmith (1994) formulation, given in equations 6.5, 6.6,

6.7 and 6.8.  $RW \cdot \cos(\delta)$  is surface projection of  $RW$ , which was used for calculation of  $R_{JB}$ .

$$\text{Strike Slip} \quad \log(RW) = -0.76 + 0.27 \cdot M \quad (6.5)$$

$$\text{Reverse} \quad \log(RW) = -1.61 + 0.41 \cdot M \quad (6.6)$$

$$\text{Normal} \quad \log(RW) = -1.14 + 0.35 \cdot M \quad (6.7)$$

$$\text{All} \quad \log(RW) = -1.01 + 0.32 \cdot M \quad (6.8)$$

7. A fault model shown in figure 6.5 was prepared for calculation of  $R_{JB}$  distance to be used further in PGA computation. Figure 6.6 (a-d) shows computation of  $R_{JB}$  distance with respect to type of fault and also position of site with respect to dip of fault. For a strike slip fault dip is considered as  $90^\circ$ , (Ni and Barazangi, 1984; Kumar *et al*, 2015).  $R_{JB}$  is measured as closest horizontal distance between site and vertical projection of rupture, figure 6.6 (a). For thrust/reverse faults the dip angle ( $\delta$ ) was assumed as  $15^\circ$ , and for normal faults it was assumed as  $50^\circ$ , (Ni and Barazangi, 1984; Kumar *et al*, 2015). On down-dip side or up-dip side of a dipping fault,  $R_{JB}$  is measured as horizontal distance of the site from the surface projection of the rupture plane; figure 6.6 (b) and (c). However, if the site is within surface projection of the reverse fault,  $R_{JB}$  considered as 0, figure 6.6 (d).

The above discussed parameters are listed in table 6.4 and were used for computation of PGA using Boore and Atkinson (2008) GMPE model, through the Pacific Earthquake Engineering Research Center (PEER) software, 'ba\_progs'. This software requires input in the form of T: Time period, M: Magnitude ( $M_w$ ); R:  $R_{JB}$ , v30:  $V_{s30}$  and imech: Focal Plane Mechanism (-1: Unknown, 0: Strike Slip, 1: Normal, 2: Thrust). PGA was calculated for all 196 sites. At each site PGA due to all 127 tectonic units were calculated. Maximum PGA obtained at each site was retained. Table 6.4 shows the maximum PGA obtained at each site.

**Table 6.3:** Salient features of 127 tectonic units, its type (F: Fault; SS: Strike Slip; GF: Gravity Fault, as per SEISAT), surface length, (computed from ARCGIS), computed  $M_w$  (Wells and Coppersmith, 1994). \* longest sliver of the three was retained. This tectonic data was used for DSHA-2 study.

S. No	Tectonic Unit	Type of Fault	Length of Tectonic unit	Computed $M_w$
1.	Alaknanda Fault	F	50.32	6.5
2.	Altyn Tagh Fault	SS	41.98	6.4
3.	Beng Co Fault	GF	42.69	6.4
4.	Drang Thrust	Thrust	393.56	7.6
5.	FG 01	F	11.33	5.6
6.	FG 02	F	87.00	6.8
7.	FG 03	F	23.79	6
8.	FG 04	F	21.23	6
9.	FG 05	F	5.70	5.2
10.	FG 06	F	5.71	5.2
11.	FG 07	F	16.74	5.8
12.	FG 08	F	27.47	6.1
13.	FG 09	F	15.66	5.8
14.	FG 10	F	4.86	5.1
15.	FG 11	F	32.16	6.2
16.	FG 12	F	10.67	5.6
17.	FG 13	F	3.30	4.9
18.	FG 14	F	2.14	4.7
19.	FG 15	F	3.40	4.9
20.	FR 01	F	287.95	7.5
21.	FR 02	F	5.63	5.2
22.	FR 03	F	5.88	5.2
23.	FR 04	F	7.10	5.4
24.	FR 05	F	50.22	6.5
25.	FR 06	F	74.91	6.7
26.	FR 07	F	37.33	6.3
27.	FR 08	F	16.83	5.8
28.	FR 09	F	10.69	5.6
29.	FR 10	F	18.99	5.9
30.	FR 11	F	5.17	5.2
31.	FR 12	F	27.04	6.1
32.	FR 13	F	15.90	5.8
33.	FR 14	F	25.85	6.1
34.	FR 15	F	14.73	5.8
35.	FR 16	F	15.89	5.8
36.	GF 01	GF	39.35	6.3

<b>S. No</b>	<b>Tectonic Unit</b>	<b>Type of Fault</b>	<b>Length of Tectonic unit</b>	<b>Computed <math>M_w</math></b>
37.	GF 02	GF	55.98	6.5
38.	GF 03	GF	37.60	6.3
39.	Indus Suture Zone*	Thrust	568.00	7.8
40.	Jhelum Fault	SS	235.66	7.3
41.	Jwalamukhi Thrust	Thrust	290.24	7.4
42.	Kallar Kabbar Fault	Fault	37.18	6.3
43.	Karakoram fault	SS	553.82	7.7
44.	Kaurik FS	GF	123.19	7
45.	Kishtwar Fault	SS	123.11	7
46.	L 01	F	41.53	6.4
47.	L 02	F	132.11	7
48.	L 03	F	38.07	6.3
49.	L 04	F	12.40	5.7
50.	L 05	F	75.44	6.7
51.	L 06	F	98.29	6.9
52.	L 07	F	30.73	6.2
53.	L 08	F	136.71	7
54.	L 09	F	72.09	6.7
55.	L 10	F	110.10	6.9
56.	L 11	F	82.30	6.8
57.	L 12	F	21.56	6
58.	L 13	F	114.62	6.9
59.	L 14	F	29.88	6.2
60.	L 15	F	92.82	6.8
61.	L 16	F	95.41	6.8
62.	L 17	F	54.01	6.5
63.	L 18	F	156.09	7.1
64.	L 19	F	256.49	7.4
65.	L 20	F	180.17	7.2
66.	L 21	F	53.64	6.5
67.	L 22	F	63.48	6.6
68.	L 23	F	69.61	6.7
69.	L 24	F	199.64	7.3
70.	L 25	F	98.58	6.9
71.	L 26	F	132.08	7
72.	L 27	F	75.22	6.7
73.	L 28	F	88.84	6.8
74.	MHD-DDN F	F	154.47	7.1
75.	Mangla Fault	SS	69.62	6.7
76.	Mastgarh Anticline	Thrust	115.28	6.9

<b>S. No</b>	<b>Tectonic Unit</b>	<b>Type of Fault</b>	<b>Length of Tectonic unit</b>	<b>Computed <math>M_w</math></b>
77.	MBT-1	Thrust	181.84	7.2
78.	MBT-2	Thrust	135.76	7
79.	MBT-3	Thrust	189.71	7.2
80.	MBT-4	Thrust	241.42	7.3
81.	MBT-5	Thrust	126.19	7
82.	MBT-6	Thrust	122.00	7
83.	MBT-a	Thrust	190.26	7.2
84.	MCT-1	Thrust	29.68	6.2
85.	MCT-2	Thrust	235.53	7.3
86.	MCT-3	Thrust	229.01	7.3
87.	MCT-4	Thrust	257.19	7.4
88.	MCT-5	Thrust	48.97	6.5
89.	MFT	Thrust	134.48	7
90.	MKT	Thrust	20.56	6
91.	MMT	Thrust	416.33	7.6
92.	NAT	Thrust	277.69	7.4
93.	Ramgarh Thrust	Thrust	114.69	6.9
94.	Reasi Thrust	Thrust	17.70	5.9
95.	Ropor Fault	F	38.05	6.3
96.	Salt Range Thrust	Thrust	117.81	6.9
97.	SAT	Thrust	96.59	6.8
98.	Shyok Suture	Thrust	385.43	7.6
99.	Sundarnagar Fault	SS	101.59	6.9
100.	T1	Thrust	167.02	7.1
101.	T2	Thrust	316.80	7.5
102.	T3	Thrust	288.55	7.4
103.	T4	Thrust	79.46	6.7
104.	T5	Thrust	75.52	6.7
105.	T6	Thrust	245.03	7.3
106.	T7	Thrust	171.88	7.1
107.	TH 01	Thrust	66.78	6.6
108.	TH 02	Thrust	45.44	6.4
109.	TH 03	Thrust	53.37	6.5
110.	TH 04	Thrust	57.29	6.6
111.	TH 05	Thrust	146.11	7.1
112.	TH 06	Thrust	68.77	6.7
113.	TH 07, VT	Thrust	665.24	7.9
114.	TH 08	Thrust	97.92	6.8
115.	TH 09	Thrust	13.78	5.8
116.	TH 10	Thrust	75.89	6.7

S. No	Tectonic Unit	Type of Fault	Length of Tectonic unit	Computed $M_w$
117.	TH 11	Thrust	51.74	6.5
118.	TH 12	Thrust	25.09	6.1
119.	TH 13	Thrust	1.67	4.7
120.	TH 14	Thrust	24.17	6.1
121.	TH 15	Thrust	24.26	6.1
122.	TH 16	Thrust	64.35	6.6
123.	TH 17	Thrust	101.29	6.9
124.	TH 18	Thrust	108.72	6.9
125.	TR 01	Thrust	111.13	6.9
126.	TR 02	Thrust	45.03	6.4
127.	Tso Morari Fault	GF	24.87	6.1

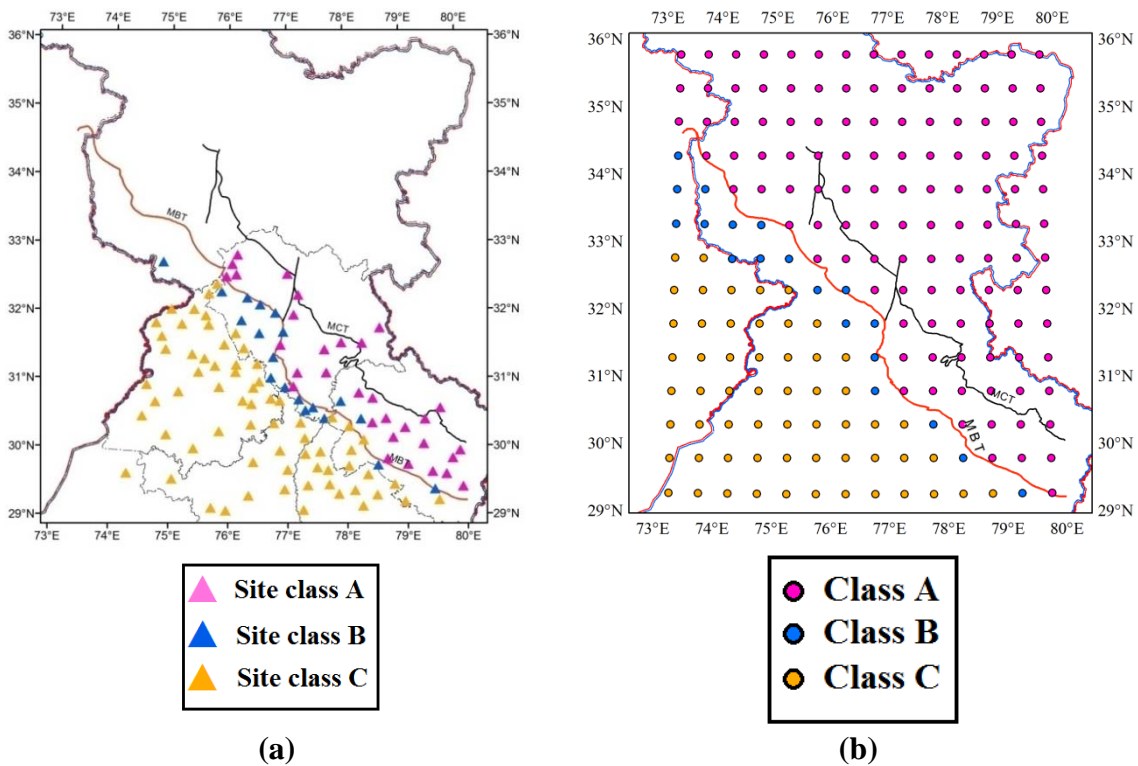


**Figure 6.4:** (a) Site characteristics of strong ground motion accelerograph stations, redrawn after Mittal *et al.*, 2012. Site class A, B and C are defined in section 6.3 (b) Site class considered for grid points in the present study.



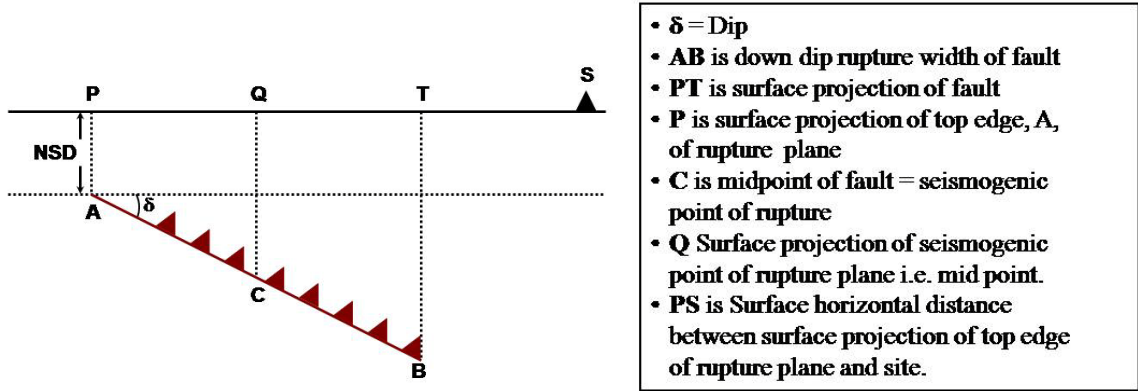
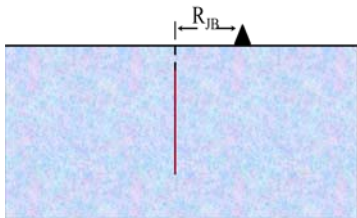
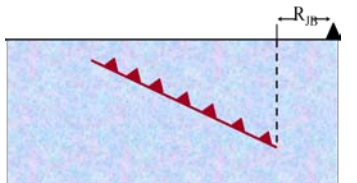


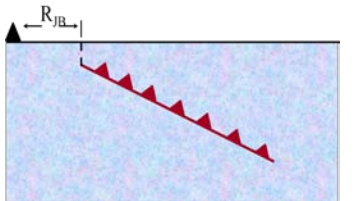
**Figure 6.5:** Fault model prepared for calculation of Joyner and Boore  $R_{JB}$  distance, as shown in figure 6.6. Box showing various distances used for computations. **NSD:** non seismogenic depth.



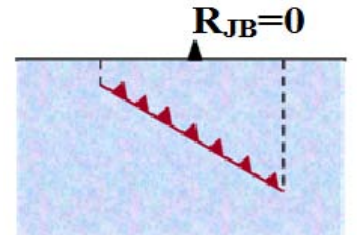
(a) for strike-slip fault



(b) for dipping fault, site on down-dip side of fault



(c) for dipping fault, site on up-dip side of fault



(d) for dipping fault, site within surface projection of fault

**Figure 6.6:** Illustration showing  $R_{JB}$  considered for different fault types (a-d).

### ***Hazard map, DSHA-2***

PGA in the study area varied between 0.039 g - 0.581g. Contour maps, with contour intervals of 0.01 g and 0.1 g are shown in figures 6.7(a) and (b), respectively. Figure 6.7(b) is the hazard map for the study area. PGA in the highest range 0.50-0.581g was observed as several islands on the MBT, at 14 sites. This was in parts of Bilaspur, Chamba, Hamirpur, Kangra, Kullu, Mandi, Solan and Una districts of HP, parts of Jammu and Kashmir near syntaxis and Dehradun and Haridwar districts of Uttarakhand. This was observed along five segments of MBT.

The highest PGA, 0.581g, was observed at site number #105 in Kangra district, reasons for this are given here. The nearest tectonic unit to this site was at a surface distance of 2.78km. This 665.24 km long Vaikrita thrust (VT) yields  $M_w=7.9$  as per equation 2.5, which in turn yields a down dip rupture width (RW) of 41.06km using equation 6.6. Surface projection,  $RW \cdot \cos(\delta)$ , of this fault rupture, with a dip of  $15^\circ$  is 39.66 km. Since the site is within the surface projection of fault, therefore,  $R_{JB}$  is 0. As the site was assigned soft to firm rock, with  $V_{s30}= 500$  m/sec, therefore there was considerable amplification of PGA at site, hence PGA estimated was as high as 0.581g. If the same site was considered as hard to firm rock, then PGA will decrease considerably, to 0.490g. This implies that rock type at site plays an important role while estimating PGA, as per Boore and Atkinson (2008) formulation.

The effect of site can also be seen at Haridwar (site #179) and Dehradun (site #164) districts in which PGA was substantially higher. This is explained for site #179 here. PGA of 0.547g was computed at site #179 in Haridwar district. The nearest tectonic unit to it was at a surface distance of 17.91km. This 245.03 km long MBT-a yields  $M_w=7.3$  as per equation 2.5, which in turn yields a down dip rupture width (RW) of 24.91km using equation 6.6. Surface projection,  $RW \cdot \cos(\delta)$ , of this fault rupture, with a dip of  $15^\circ$  is 24.06km. Since the site is within the surface projection of fault, therefore,  $R_{JB}$  is 0. As the site was assigned as soft to firm rock, with  $V_{s30}= 500$  m/sec, therefore there was considerable amplification of PGA at site, hence PGA estimated was as high as 0.547g. A similar explanation is valid for Dehradun district. These observations imply that high accelerations are due to the combined effect of maximum magnitude computed from length of fault, distance  $R_{JB}$  and site amplification factor.

PGA in the range 0.40 - 0.49g was observed encompassing the highest PGA range along parts of MBT, MCT, region between MBT and MCT, MMT, ISZ and parts of Shyok suture. This

includes Bilaspur, Chamba, Hamirpur, Kangra, Kinnaur, Kullu, Lahaul & Spiti, Mandi, Shimla, Sirmaur, Solan and Una districts of HP, parts of Almora, Bageshwar, Chamoli, Dehradun, Haridwar, Nainital, Pauri Garhwal, Rudraprayag, Tehri Garhwal and Uttarkashi districts of Uttarakhand and large parts of Jammu and Kashmir.

PGA in the range 0.30 – 0.39g was observed in parts of Bilaspur, Chamba, Kinnaur, Lahaul & Spiti, Sirmaur, Solan and Una districts of HP, parts of Almora, Chamoli, Haridwar, Nainital, Rudraprayag, Tehri Garhwal, Udham Singh Nagar, Uttarkashi and Pauri Garhwal districts of Uttarakhand and parts of Jammu and Kashmir. PGA in the range 0.20 - 0.29g was observed in parts of Chamba, Kinnaur, Lahaul & Spiti, Sirmaur and Solan districts of HP, parts of Chamoli, Haridwar, Nainital, Rudraprayag, Udham Singh Nagar and Uttarkashi in Uttarakhand and a large part of Jammu and Kashmir.

PGA in the range 0.10-0.19g was observed in small parts of Kinnaur and Lahaul & Spiti districts of HP, small parts of Haridwar, Nainital and Uttarkashi districts in Uttarakhand, parts of Jammu and Kashmir, in large parts of Indo Gangetic plains and in north eastern part of the study area between ISZ and Shyok suture in Laddakh and in Tibet. PGA less than 0.1 g was observed in small parts of Indo Gangetic plains and in Tibet.

**Table 6.4:** Calculation of PGA for DSHA-2, site wise. Column 1: site number; 2: Nearest tectonic unit to site; 3: Fault type (from SIESAT); 4: length of tectonic unit in km, length from ArcGIS-9.3; 5: Estimated  $M_w$  W&C94; 6: Calculated Rupture Width (RW), from W&C94; 7: Dip ( $\delta$ ) (Assumed,  $15^\circ$  for thrust/reverse sources,  $50^\circ$  for normal and  $90^\circ$  for strike slip sources (Ni and Barazangi, 1984)); 8: surface projection of fault rupture km ( $RW \cdot \cos\delta$ ); 9: Epicentral Distance; 10: Joyner and Boore Distance ( $R_{jb}$ ); 11: Site classification (Mittal et al., 2012); 12:  $V_{s,30}$ ; 13: Focal Plane Mechanism (as per BA08: - 1: Unknown, 0: Strike Slip, 1: Normal, 2: Thrust); 14: PGA (g) as per BA08.

1	2	3	4	5	6	7	8	9	10	11	12	13	14
1	MMT	T	416.33	7.6	32.48	15	31.37	95.40	64.03	A	1100	2	0.076
2	MMT	T	416.33	7.6	32.48	15	31.37	72.77	41.4	A	1100	2	0.112
3	MMT	T	416.33	7.6	32.48	15	31.37	48.08	16.71	A	1100	2	0.194
4	Shyok Suture	T	385.43	7.6	31.25	15	30.18	25.83	0	A	1100	2	0.480
5	Shyok Suture	T	385.43	7.6	31.25	15	30.18	3.35	0	A	1100	2	0.480
6	Shyok Suture	T	385.43	7.6	31.25	15	30.18	28.88	0	A	1100	2	0.480
7	Shyok Suture	T	385.43	7.6	31.25	15	30.18	53.44	23.26	A	1100	2	0.164
8	Karakoram F	SS	553.82	7.7	20.82	90	0	12.40	12.4	A	1100	0	0.230
9	FR01	F	287.95	7.4	22.46	50	14.44	11.34	0	A	1100	-1	0.463
10	FR01	F	287.95	7.4	22.46	50	14.44	12.10	0	A	1100	-1	0.463
11	FR01	F	287.95	7.4	22.46	50	14.44	34.36	19.92	A	1100	-1	0.161
12	FR01	F	287.95	7.4	22.46	50	14.44	52.69	38.25	A	1100	-1	0.106
13	FR01	F	287.95	7.4	22.46	50	14.44	65.55	51.11	A	1100	-1	0.084
14	Altyn Tagh F	SS	41.98	6.4	9.54	90	0	19.17	19.17	A	1100	0	0.107
15	MMT	T	416.33	7.6	32.48	15	31.37	43.17	11.8	A	1100	2	0.227
16	MMT	T	416.33	7.6	32.48	15	31.37	25.02	0	A	1100	2	0.480
17	MMT	T	416.33	7.6	32.48	15	31.37	7.60	0	A	1100	2	0.480
18	MMT	T	416.33	7.6	32.48	15	31.37	13.49	0	A	1100	2	0.480
19	MMT	T	416.33	7.6	32.48	15	31.37	31.80	0.43	A	1100	2	0.473
20	Shyok Suture	T	385.43	7.6	31.25	15	30.18	17.36	0	A	1100	2	0.480
21	Shyok Suture	T	385.43	7.6	31.25	15	30.18	7.40	0	A	1100	2	0.480
22	Shyok Suture	T	385.43	7.6	31.25	15	30.18	31.32	1.14	A	1100	2	0.442

1	2	3	4	5	6	7	8	9	10	11	12	13	14
23	Karakoram fault	SS	553.82	7.7	20.82	90	0	18.90	18.9	A	1100	0	0.190
24	FR01	F	287.95	7.4	22.46	50	14.44	35.67	21.23	A	1100	-1	0.155
25	FR01	F	287.95	7.4	22.46	50	14.44	14.67	0.23	A	1100	-1	0.461
26	FR01	F	287.95	7.4	22.46	50	14.44	0.33	0	A	1100	-1	0.463
27	FR01	F	287.95	7.4	22.46	50	14.44	12.18	0	A	1100	-1	0.463
28	FR01	F	287.95	7.4	22.46	50	14.44	19.91	5.47	A	1100	-1	0.282
29	MMT	T	416.33	7.6	32.48	15	31.37	11.48	0	A	1100	2	0.480
30	MMT	T	416.33	7.6	32.48	15	31.37	20.63	0	A	1100	2	0.480
31	TR-01	T	111.13	6.9	16.77	15	16.2	9.44	0	A	1100	2	0.468
32	ISZ3	T	568.49	7.8	37.95	15	36.66	25.57	0	A	1100	2	0.484
33	ISZ3	T	568.49	7.8	37.95	15	36.66	25.54	0	A	1100	2	0.484
34	ISZ3	T	568.49	7.8	37.95	15	36.66	34.29	0	A	1100	2	0.484
35	ISZ3	T	568.49	7.8	37.95	15	36.66	38.51	1.85	A	1100	2	0.416
36	Shyok Suture	T	385.43	7.6	31.25	15	30.18	13.29	0	A	1100	2	0.480
37	Shyok Suture	T	385.43	7.6	31.25	15	30.18	13.02	0	A	1100	2	0.480
38	Shyok Suture	T	385.43	7.6	31.25	15	30.18	37.96	7.78	A	1100	2	0.267
39	Shyok Suture	T	385.43	7.6	31.25	15	30.18	69.96	39.78	A	1100	2	0.116
40	FR01	F	287.95	7.4	22.46	50	14.44	52.26	37.82	A	1100	-1	0.107
41	FR01	F	287.95	7.4	22.46	50	14.44	42.05	27.61	A	1100	-1	0.133
42	FR01	F	287.95	7.4	22.46	50	14.44	34.23	19.79	A	1100	-1	0.161
43	TH-1	T	66.78	6.6	13.00	15	12.56	3.74	0	B	500	2	0.535
44	MBT-1	T	181.84	7.2	21.46	15	20.73	5.41	0	A	1100	2	0.473
45	MBT-1	T	181.84	7.2	21.46	15	20.73	30.88	10.15	A	1100	2	0.216
46	ISZ3	T	568.49	7.8	37.95	15	36.66	41.84	5.18	A	1100	2	0.320
47	ISZ3	T	568.49	7.8	37.95	15	36.66	26.84	0	A	1100	2	0.484
48	ISZ3	T	568.49	7.8	37.95	15	36.66	8.12	0	A	1100	2	0.484
49	ISZ3	T	568.49	7.8	37.95	15	36.66	8.66	0	A	1100	2	0.484

1	2	3	4	5	6	7	8	9	10	11	12	13	14
50	ISZ3	T	568.49	7.8	37.95	15	36.66	0.34	0	A	1100	2	0.484
51	ISZ3	T	568.49	7.8	37.95	15	36.66	26.76	0	A	1100	2	0.484
52	Shyok Suture	T	385.43	7.6	31.25	15	30.18	1.20	0	A	1100	2	0.480
53	Shyok Suture	T	385.43	7.6	31.25	15	30.18	30.97	0.79	A	1100	2	0.459
54	Shyok Suture	T	385.43	7.6	31.25	15	30.18	58.67	28.49	A	1100	2	0.145
55	FR06	F	74.91	6.7	13.62	50	8.76	4.09	0	A	1100	-1	0.445
56	FR06	F	74.91	6.7	13.62	50	8.76	8.04	0	A	1100	-1	0.445
57	TH-04	T	57.29	6.6	12.04	15	11.63	4.17	0	B	500	2	0.535
58	TH-05	T	146.11	7.1	19.24	15	18.58	3.28	0	B	500	2	0.565
59	TH-07, VT	T	665.24	7.9	41.06	15	39.66	20.69	0	A	1100	2	0.485
60	TH-07, VT	T	665.24	7.9	41.06	15	39.66	42.57	2.91	A	1100	2	0.382
61	TH-07, VT	T	665.24	7.9	41.06	15	39.66	53.17	13.51	A	1100	2	0.235
62	MCT-2	T	235.53	7.3	24.43	15	23.59	6.09	0	A	1100	2	0.475
63	MCT-2	T	235.53	7.3	24.43	15	23.59	29.95	6.36	A	1100	2	0.268
64	ISZ3	T	568.49	7.8	37.95	15	36.66	44.91	8.25	A	1100	2	0.275
65	ISZ3	T	568.49	7.8	37.95	15	36.66	15.58	0	A	1100	2	0.484
66	ISZ3	T	568.49	7.8	37.95	15	36.66	11.88	0	A	1100	2	0.484
67	Shyok Suture	T	385.43	7.6	31.25	15	30.18	12.24	0	A	1100	2	0.480
68	Shyok Suture	T	385.43	7.6	31.25	15	30.18	47.41	17.23	A	1100	2	0.191
69	Karakoram F	SS	553.82	7.7	20.82	90	0	57.67	57.67	A	1100	0	0.089
70	Beng Co F	N	42.69	6.4	12.41	50	7.98	24.74	16.76	A	1100	1	0.090
71	Jhelum Fault	SS	235.66	7.3	16.08	90	0	32.66	32.66	B	500	0	0.157
72	TH-05	T	146.11	7.1	19.24	15	18.58	27.99	9.41	B	500	2	0.272
73	TH-07, VT	T	665.24	7.9	41.06	15	39.66	28.09	0	B	500	2	0.579
74	TH-07, VT	T	665.24	7.9	41.06	15	39.66	13.98	0	B	500	2	0.579
75	TH-07, VT	T	665.24	7.9	41.06	15	39.66	0.63	0	A	1100	2	0.485
76	TH-07, VT	T	665.24	7.9	41.06	15	39.66	38.73	0	A	1100	2	0.485
77	MCT-2	T	235.53	7.3	24.43	15	23.59	6.16	0	A	1100	2	0.475

1	2	3	4	5	6	7	8	9	10	11	12	13	14
78	MCT-2	T	235.53	7.3	24.43	15	23.59	37.92	14.33	A	1100	2	0.189
79	ISZ3	T	568.49	7.8	37.95	15	36.66	61.54	24.88	A	1100	2	0.170
80	ISZ3	T	568.49	7.8	37.95	15	36.66	28.00	0	A	1100	2	0.484
81	ISZ3	T	568.49	7.8	37.95	15	36.66	6.31	0	A	1100	2	0.484
82	ISZ3	T	568.49	7.8	37.95	15	36.66	28.04	0	A	1100	2	0.484
83	ISZ3	T	568.49	7.8	37.95	15	36.66	54.64	17.98	A	1100	2	0.201
84	ISZ3	T	568.49	7.8	37.95	15	36.66	87.79	51.13	A	1100	2	0.104
85	Kalla Kabar F	F	37.15	6.3	10.14	50	6.52	9.11	2.59	C	300	0	0.175
86	Jhelum Fault	SS	235.66	7.3	16.08	90	0	0.27	0.27	C	300	0	0.302
87	TH-07, VT	T	665.24	7.9	41.06	15	39.66	76.59	36.93	B	500	2	0.186
88	Jwalamukhi T	T	290.24	7.4	27.12	15	26.19	26.62	0.43	B	500	2	0.562
89	TH-07, VT	T	665.24	7.9	41.06	15	39.66	28.91	0	B	500	2	0.579
90	TH-07, VT	T	665.24	7.9	41.06	15	39.66	5.47	0	A	1100	2	0.485
91	TH-07, VT	T	665.24	7.9	41.06	15	39.66	30.65	0	A	1100	2	0.485
92	MCT-2	T	235.53	7.3	24.43	15	23.59	1.15	0	A	1100	2	0.475
93	L06	U	98.29	6.8	15.07	50	9.69	6.60	0	A	1100	-1	0.454
94	L06	U	98.29	6.8	15.07	50	9.69	16.50	6.81	A	1100	-1	0.226
95	ISZ3	T	568.49	7.8	37.95	15	36.66	36.87	0.21	A	1100	2	0.482
96	ISZ3	T	568.49	7.8	37.95	15	36.66	15.12	0	A	1100	2	0.484
97	ISZ3	T	568.49	7.8	37.95	15	36.66	18.99	0	A	1100	2	0.484
98	ISZ3	T	568.49	7.8	37.95	15	36.66	56.47	19.81	A	1100	2	0.191
99	Salt Range T	T	117.81	6.9	0.00	15	0	39.23	39.23	C	300	2	0.142
100	L02	U	132.11	7.0	16.82	50	10.81	8.40	0	C	300	-1	0.229
101	L02	U	132.11	7.0	16.82	50	10.81	38.13	27.32	C	300	-1	0.179
102	Jwalamukhi T	T	290.24	7.4	27.12	15	26.19	65.54	39.35	C	300	2	0.175
103	TH-07, VT	T	665.24	7.9	41.06	15	39.66	63.28	23.62	C	300	2	0.280
104	TH-07, VT	T	665.24	7.9	41.06	15	39.66	28.17	0	A	1100	2	0.565
105	TH-07, VT	T	665.24	7.9	41.06	15	39.66	2.78	0	B	500	2	0.581

1	2	3	4	5	6	7	8	9	10	11	12	13	14
106	TH-07, VT	T	665.24	7.9	41.06	15	39.66	26.20	0	A	1100	2	0.485
107	MCT-3	T	229.01	7.3	24.08	15	23.26	9.73	0	A	1100	2	0.475
108	L08	U	136.71	7.0	17.03	50	10.95	5.41	0	A	1100	-1	0.457
109	L09	U	72.09	6.7	13.43	50	8.63	18.73	10.1	A	1100	-1	0.180
110	Kaurik FS	N	123.19	7.0	20.25	50	13.02	12.45	0	A	1100	1	0.368
111	ISZ3	T	568.49	7.8	37.95	15	36.66	35.41	0	A	1100	2	0.484
112	Karakoram F	SS	553.82	7.7	20.82	90	0	4.39	4.39	A	1100	0	0.333
113	L02	U	132.11	7.0	16.82	50	10.81	61.43	50.62	C	300	-1	0.118
114	L02	U	132.11	7.0	16.82	50	10.81	14.93	4.12	C	300	-1	0.099
115	L02	U	132.11	7.0	16.82	50	10.81	31.38	20.57	C	300	-1	0.207
116	TH-07, VT	T	665.24	7.9	41.06	15	39.66	135.93	96.27	C	300	2	0.095
117	TH-07, VT	T	665.24	7.9	41.06	15	39.66	98.77	59.11	C	300	2	0.163
118	MFT	T	134.48	7.0	18.45	15	17.83	21.20	3.37	C	300	2	0.420
119	Jwalamukhi T	T	290.24	7.4	27.12	15	26.19	9.34	0	B	500	2	0.571
120	TH-07, VT	T	665.24	7.9	41.06	15	39.66	8.69	0	B	500	2	0.579
121	TH-07, VT	T	665.24	7.9	41.06	15	39.66	36.91	0	A	1100	2	0.485
122	T2	T	316.80	7.5	28.33	15	27.36	19.03	0	A	1100	2	0.478
123	L09	U	72.09	6.7	13.43	50	8.63	9.95	1.32	A	1100	-1	0.387
124	Kaurik FS	N	123.19	7.0	20.25	50	13.02	15.43	2.41	A	1100	1	0.279
125	ISZ3	T	568.49	7.8	37.95	15	36.66	90.10	53.44	A	1100	2	0.100
126	Karakoram F	SS	553.82	7.7	20.82	90	0	39.05	39.05	A	1100	0	0.124
127	L02	U	132.11	7.0	16.82	50	10.81	72.51	61.7	C	300	-1	0.098
128	L02	U	132.11	7.0	16.82	50	10.81	31.14	20.33	C	300	-1	0.208
129	L02	U	132.11	7.0	16.82	50	10.81	34.19	23.38	C	300	-1	0.194
130	L02	U	132.11	7.0	16.82	50	10.81	76.49	65.68	C	300	-1	0.091
131	L15	U	92.82	6.8	14.75	50	9.48	60.25	50.77	C	300	-1	0.107
132	L18	U	156.09	7.1	17.89	50	11.5	48.24	36.74	C	300	-1	0.156
133	L18	U	156.09	7.1	17.89	50	11.5	19.31	7.81	C	300	-1	0.317



1	2	3	4	5	6	7	8	9	10	11	12	13	14
134	TH-07, VT	T	665.24	7.9	41.06	15	39.66	23.52	0	B	500	2	0.579
135	T3	T	288.55	7.4	27.04	15	26.12	16.33	0	A	1100	2	0.477
136	T2	T	316.80	7.5	28.33	15	27.36	6.78	0	A	1100	2	0.478
137	T2	T	316.80	7.5	28.33	15	27.36	16.66	0	A	1100	2	0.478
138	L13	U	114.62	6.9	15.95	50	10.26	22.65	12.39	A	1100	-1	0.175
139	L13	U	114.62	6.9	15.95	50	10.26	24.62	14.36	A	1100	-1	0.162
140	L13	U	114.62	6.9	15.95	50	10.26	40.38	30.12	A	1100	-1	0.103
141	L02	U	132.11	7.0	16.82	50	10.81	104.84	94.03	C	300	-1	0.058
142	L16	U	95.41	6.8	14.90	50	9.58	70.24	60.66	C	300	-1	0.090
143	L16	U	95.41	6.8	14.90	50	9.58	33.92	24.34	C	300	-1	0.178
144	L15	U	92.82	6.8	14.75	50	9.48	23.81	14.33	C	300	-1	0.131
145	L15	U	92.82	6.8	14.75	50	9.48	7.40	0	C	300	-1	0.196
146	L18	U	156.09	7.1	17.89	50	11.5	3.61	0	C	300	-1	0.197
147	L19	U	256.49	7.3	21.52	50	13.83	7.03	0	C	300	-1	0.201
148	Drang thrust	T	393.56	7.6	31.58	15	30.5	10.65	0	B	500	2	0.190
149	Drang thrust	T	393.56	7.6	31.58	15	30.5	20.83	0	A	1100	2	0.480
150	NAT	T	277.69	7.4	26.52	15	25.62	9.55	0	A	1100	2	0.477
151	NAT	T	277.69	7.4	26.52	15	25.62	24.62	0	A	1100	2	0.477
152	NAT	T	277.69	7.4	26.52	15	25.62	24.62	0	A	1100	2	0.477
153	MCT-4	T	257.19	7.4	25.52	15	24.65	32.68	8.03	A	1100	2	0.251
154	MCT-4	T	257.19	7.4	25.52	15	24.65	37.16	12.51	A	1100	2	0.208
155	L19	U	256.49	7.3	21.52	50	13.83	120.59	106.76	C	300	-1	0.057
156	L15	U	92.82	6.8	14.75	50	9.48	58.50	49.02	C	300	-1	0.111
157	L15	U	92.82	6.8	14.75	50	9.48	11.15	1.67	C	300	-1	0.202
158	L16	U	95.41	6.8	14.90	50	9.58	14.70	5.12	C	300	-1	0.162
159	L18	U	156.09	7.1	17.89	50	11.5	4.24	0	C	300	-1	0.197
160	L19	U	256.49	7.3	21.52	50	13.83	6.93	0	C	300	-1	0.201
161	L20	U	180.17	7.1	18.87	50	12.13	14.41	2.28	C	300	-1	0.276

1	2	3	4	5	6	7	8	9	10	11	12	13	14
162	Drang thrust	T	393.56	7.6	31.58	15	30.5	47.78	17.28	C	300	2	0.284
163	L19	U	256.49	7.3	21.52	50	13.83	94.92	81.09	C	300	-1	0.183
164	Drang thrust	T	393.56	7.6	31.58	15	30.5	24.61	0	B	500	2	0.545
165	NAT	T	277.69	7.4	26.52	15	25.62	24.11	0	A	1100	2	0.477
166	NAT	T	277.69	7.4	26.52	15	25.62	4.20	0	A	1100	2	0.477
167	MCT-4	T	257.19	7.3	25.52	15	24.65	12.80	0	A	1100	2	0.426
168	MCT-4	T	257.19	7.3	25.52	15	24.65	12.80	0	A	1100	2	0.426
169	L19	U	256.49	7.3	21.52	50	13.83	94.92	81.09	C	300	-1	0.083
170	L19	U	256.49	7.3	21.52	50	13.83	50.22	36.39	C	300	-1	0.171
171	L19	U	256.49	7.3	21.52	50	13.83	20.11	6.28	C	300	-1	0.123
172	L19	U	256.49	7.3	21.52	50	13.83	0.26	0	C	300	-1	0.192
173	L19	U	256.49	7.3	21.52	50	13.83	22.21	8.38	C	300	-1	0.192
174	L20	U	180.17	7.1	18.87	50	12.13	21.72	9.59	C	300	-1	0.295
175	L20	U	180.17	7.1	18.87	50	12.13	25.67	13.54	C	300	-1	0.124
176	L24	U	199.64	7.2	19.60	50	12.6	28.96	16.36	C	300	-1	0.146
177	L24	U	199.64	7.2	19.60	50	12.6	9.63	0	C	300	-1	0.159
178	MHDDDN	F	154.47	7.1	17.82	50	11.46	16.75	5.29	C	300	-1	0.076
179	MBT-a	T	245.03	7.3	24.91	15	24.06	17.91	0	B	500	2	0.547
180	T6	T	240.03	7.2	24.91	15	24.06	2.89	0	A	1100	2	0.475
181	NAT	T	277.69	7.4	26.52	15	25.62	16.32	0	A	1100	2	0.477
182	NAT	T	277.69	7.4	26.52	15	25.62	1.75	0	A	1100	2	0.477
183	L19	U	256.49	7.3	21.52	50	13.83	98.29	84.46	C	300	-1	0.079
184	L19	U	256.49	7.3	21.52	50	13.83	55.09	41.26	C	300	-1	0.158
185	L19	U	256.49	7.3	21.52	50	13.83	32.92	19.09	C	300	-1	0.105
186	L19	U	256.49	7.3	21.52	50	13.83	53.18	39.35	C	300	-1	0.163
187	L20	U	180.17	7.1	18.87	50	12.13	56.70	44.57	C	300	-1	0.137
188	L20	U	180.17	7.1	18.87	50	12.13	9.42	0	C	300	-1	0.197
189	L20	U	180.17	7.1	18.87	50	12.13	38.27	26.14	C	300	-1	0.190

<b>1</b>	<b>2</b>	<b>3</b>	<b>4</b>	<b>5</b>	<b>6</b>	<b>7</b>	<b>8</b>	<b>9</b>	<b>10</b>	<b>11</b>	<b>12</b>	<b>13</b>	<b>14</b>
190	L24	U	199.64	7.2	19.60	50	12.6	1.37	0	C	300	-1	0.199
191	MHDDDN	F	154.47	7.1	17.82	50	11.46	10.80	0	C	300	-1	0.197
192	MHDDDN	F	154.47	7.1	17.82	50	11.46	50.60	39.14	C	300	-1	0.150
193	L25	U	98.58	6.8	15.09	50	9.7	14.93	5.23	C	300	-1	0.345
194	MFT	T	134.48	7.0	18.45	15	17.83	23.13	5.3	C	300	2	0.364
195	MBT-a	T	190.26	7.2	21.95	15	21.2	13.24	0	B	500	2	0.182
196	MBT-a	T	190.26	7.2	21.95	15	21.2	12.42	0	A	1100	2	0.473

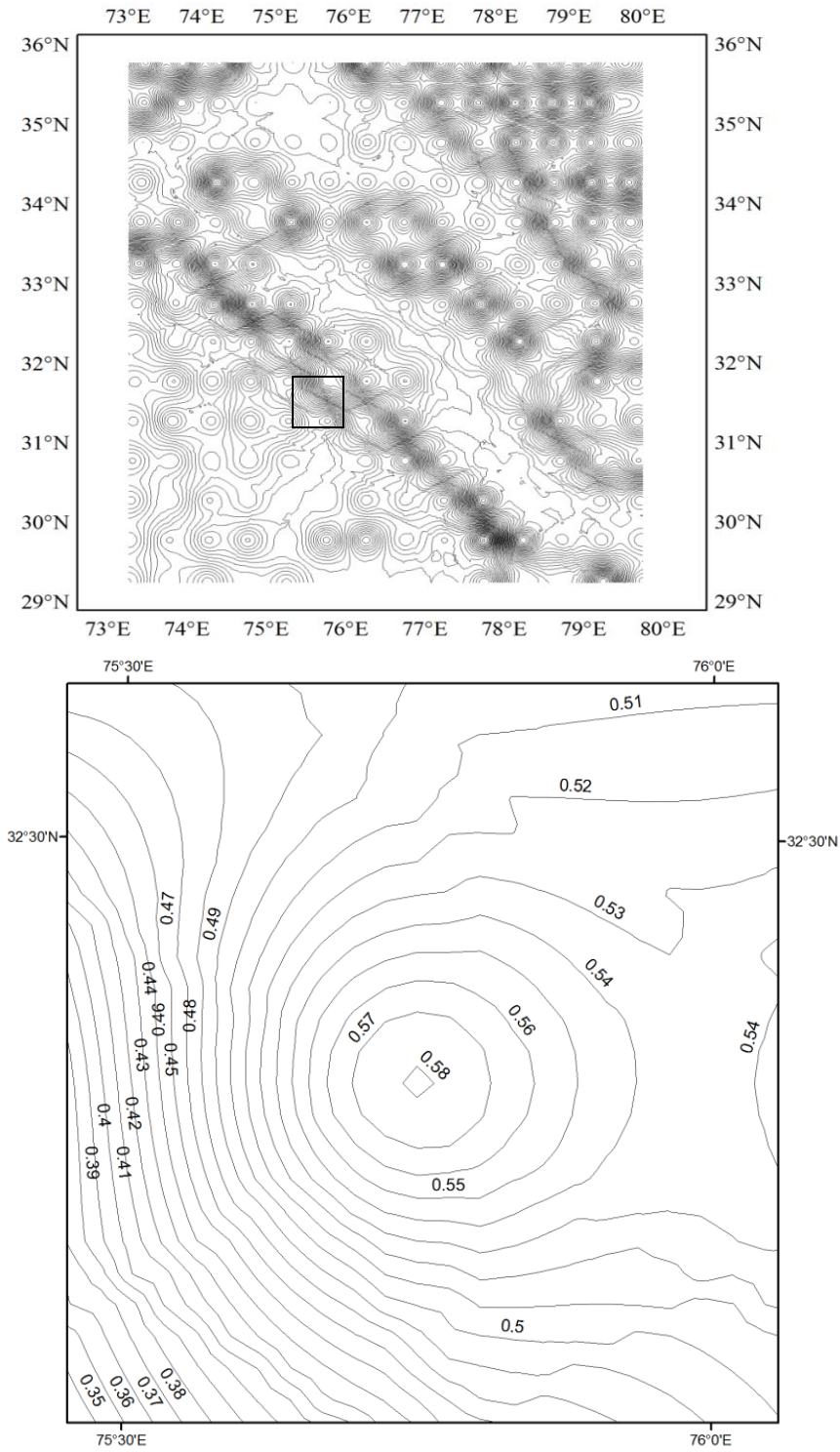


**Figure 6.7(a):** Contour map for PGA as per DSHA-2 at contour interval 0.01 g. Box shows contour intervals around the highest PGA in the study area.

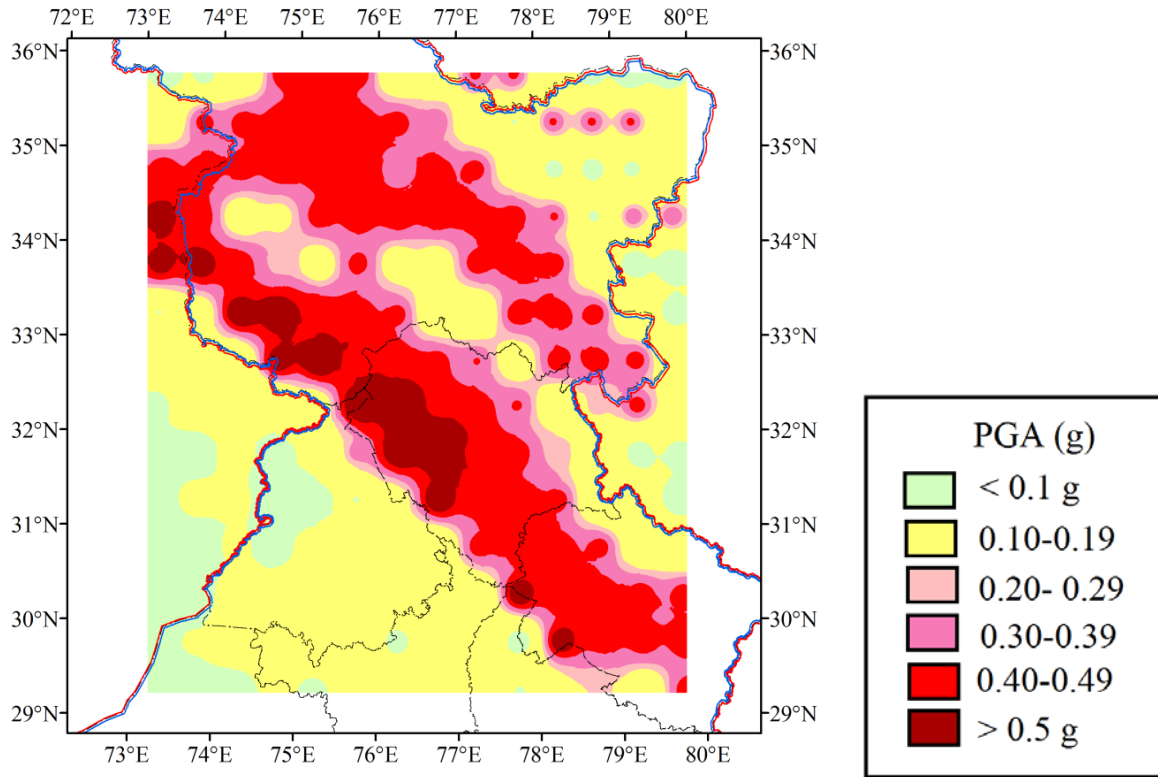


**Figure 6.7(b):** Hazard map as per DSHA-2. State boundaries are as per Survey of India (2011). This map is referred to as DSHA hazard map.

#### 6.4 Discussion

PGA was computed through DSHA approach in the entire study area, by two different methods, by varying all factors simultaneously: method of assigning maximum magnitude, source to site distance and GMPE. These are discussed as DSHA 1 and DSHA-2, as given in sections 6.2 and 6.3, respectively. In these methods different ranges of PGA emerged, in DSHA-1, highest PGA emerged as 0.470g whereas in DSHA-2 highest PGA emerged as 0.581 g. In both cases maximum PGA was observed at site #105 in Kangra district of HP. Reason for this is that maximum magnitude assigned for DSHA-1 study was the highest magnitude observed in the entire study area,  $M_w = 8.0$ . Likewise, for DSHA-2 study the highest magnitude computed was 7.9 in the entire study area. This unique situation does not exist at any other site.

Nearest tectonic unit to site #105 in case of DSHA-1 was MBT-C at an epicentral distance of 3.9km and for DSHA-2 the nearest tectonic unit was Vaikrita Thrust at an

epicentral distance of 2.8 km. Likewise for several other sites (#5, 21, 44, 49, 50, 52, 75, 77, 81, 86, 92, 93, 105, 107, 122, 119, 120, 166, 180, 182 and 191) epicentral distance in both analyses was of the same order. This is evident in tables 6.2 and 6.4, where the data is arranged site wise, epicentral distance and nearest tectonic unit can be seen at corresponding site numbers.

The methodology adopted for computing PGA in DSHA-2 study was refined at several stages, as explained in section 6.3. Also, it yields a higher PGA as compared to DSHA-1 study. Higher PGA indicates higher seismic hazard and can be of tremendous engineering significance. For these reasons results of DSHA-2 study were preferred over that of DSHA-1 study. The hazard map obtained for DSHA-2 is henceforth referred as DSHA hazard map, and is given in figure 6.7 (b).

The hazard map, figure 6.7(b), can be used to assign Peak Ground Acceleration (PGA) to any place within the entire study area. It was observed that areas with the highest PGA and the most susceptible area  $A'$  are along the MBT, and coincident most of the time. This includes several districts of Himachal Pradesh, Uttarakhand and J&K. This implies that the most susceptible area  $A''$  can be assigned PGA using DSHA hazard map. More than 90% of the area  $A''$  has PGA more than 0.30g. In areas of coincidence of the two maps confidence of assigning PGA is enhanced. Likewise for areas  $B''$  and  $C''$ , PGA's can be assigned by superimposing PGA contours on to the susceptible area map.

PGA computed in the present study was also compared with the PGA recorded at near field for several recent earthquakes. Maximum PGA for the Dharamshala earthquake of 26<sup>th</sup> April 1986, 0.244g, was recorded at Dharamshala station, at an epicentral distance of 10 km (Chandrasekaran, 1988). In the present study PGA was checked at the site nearest to the recording station as per hazard map given in figure 6.7(a). This was 0.581g at site #105, due to an earthquake of magnitude  $M_w=7.9$  originating at an epicentral distance of 2.78 km on the 665km long Vaikrita thrust, see table 6.4, row 105. The recording station is at a distance of 15km from site #105 and the PGA at recording station is 0.55g, as per figure 6.8(a). Therefore, for Dharamshala earthquake, calculated PGA is higher than the recorded PGA due to a higher assigned magnitude and length and closeness of the causative fault.

Maximum PGA, 0.313g, for Uttarkashi earthquake of 20<sup>th</sup> October 1991, was recorded at Uttarkashi station, at epicentral distance of 34 km (Chandrasekaran and Das, 1991; 1992). In the present study PGA was checked at the site nearest to the recording station as per hazard map given in figure 6.7(a). This was 0.476g at site #151, due to an earthquake of magnitude  $M_w = 7.4$  originating at an epicentral distance of 25.62 km on the 278 km long North Almora Thrust, see table 6.4, row 151. The recording station is at a distance of 20 km from site #151 and the PGA computed at recording station is 0.46g, as per figure 6.8(b). Therefore, for Uttarkashi earthquake, calculated PGA is higher than the recorded PGA.

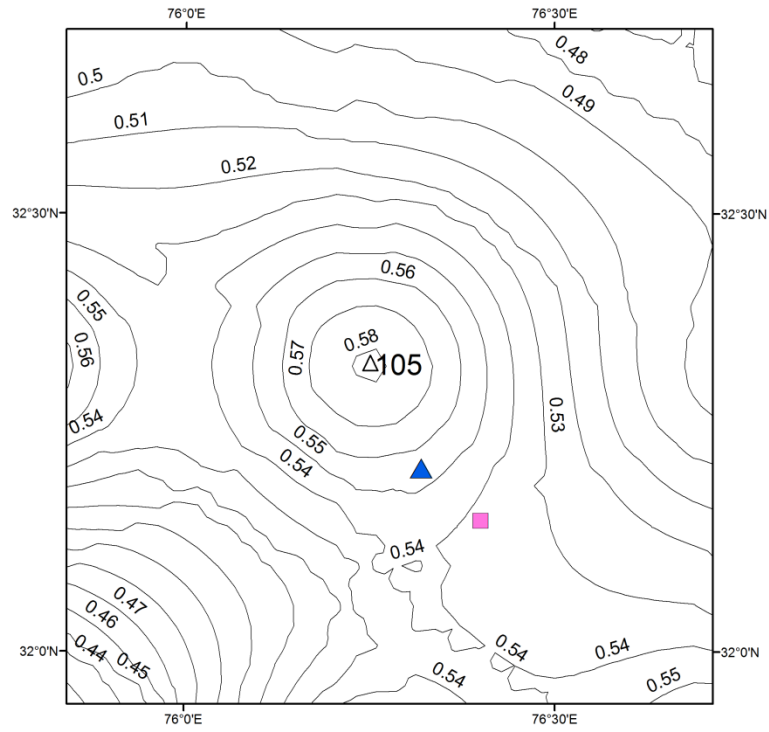
Maximum PGA, 0.359 g, for Chamoli earthquake of 28<sup>th</sup> March 1999, was recorded at Chamoli station, at epicentral distance of 14 km (DEQ report, 2000). In the present study PGA was checked at the site nearest to the recording station. This was 0.426g at site #167, due to an earthquake of magnitude  $M_w = 7.3$  originating at an epicentral distance of 24.65 km on the 257 km long MCT-4, see table 6.4, row 167. The recording station is at a distance of 14 km from site #167 and the PGA at recording station is 0.39g, as per figure 6.8(c). Therefore, for Chamoli earthquake, calculated PGA is comparable with the recorded PGA. Computed magnitude is larger in all three earthquakes. These comparisons are given in table 6.5.

Seismic zoning map of India (BIS, 2002) superimposed on the DSHA hazard map is shown in figure 6.9. Zone V of BIS is the most seismically active zone. Zone V can expect destruction of the built environment from earthquakes with magnitude greater than 7.0, and MM intensity greater than or equal to IX, with accelerations varying between 0.24g to 0.36g. In the DSHA hazard map it was observed that 0.24g exceeded at 95 sites in the study area, out of this 84 are within India. This covers almost the entire area between MBT and MCT, along ISZ in Leh (Laddakh), near Nanga Parbat along MMT, along neotectonic fault, FR1, around western syntaxis and along Kaurik fault system.

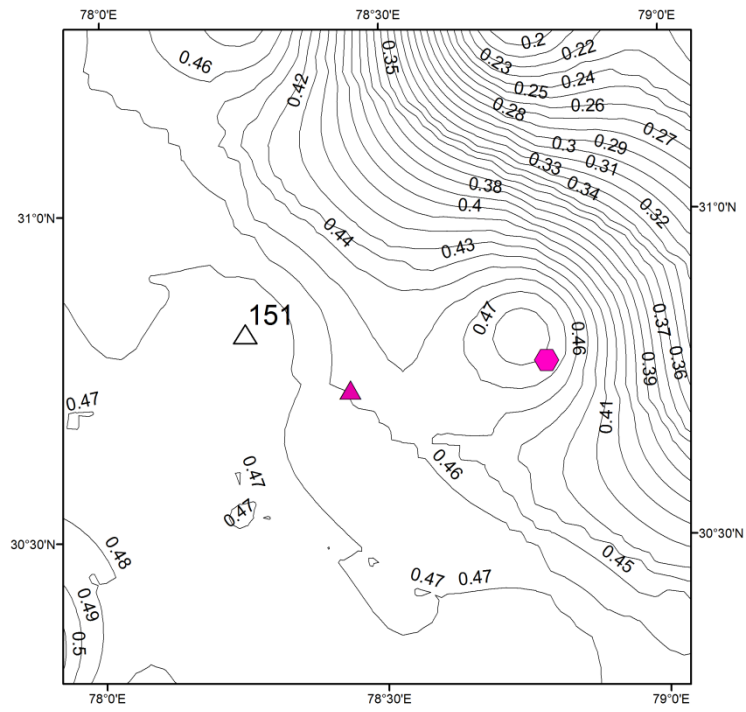
**Table 6.5:** PGA values computed in this study compared with observed PGA, from DSHA hazard map for Dharamshala earthquake, Uttarkashi earthquake and Chamoli earthquake. Computed Maximum magnitude, causative fault, fault length and epicentral distance for the nearest site are given in table 6.4. (<sup>1</sup>Chandrasekaran, 1988; <sup>2</sup>Chandrasekaran and Das, 1991, 1992; <sup>3</sup>DEQ report, 2000).

<b>Earthquake parameters as per MHD catalogue</b>	<b>PGA at station, Computed</b>	<b>Maximum PGA at nearest site, Computed</b>	<b>Station coordinates</b>	<b>Recorded PGA/ epicentral distance , <math>\Delta</math></b>
Dharamshala earthquake, 26 <sup>th</sup> April, 1986, $M_w = 5.8$ , 32.15 °N, 76.40 °E	0.55g	0.581 g at site #105	Dharamshala station <sup>1</sup> 32.21 °N, 76.32 °E	0.244g <sup>1</sup> $\Delta = 10$ km
Uttarkashi earthquake, 20 <sup>th</sup> October, 1991 , $M_w = 6.8$ , 30.77 °N, 78.79 °E	0.46 g	0.476 g at site # 151	Uttarkashi Station <sup>2</sup> 30.73 °N, 78.44 °E	0.313g <sup>2</sup> $\Delta = 34$ km
Chamoli earthquake, 28 <sup>th</sup> March 1999, $M_w = 6.7$ , 30.51 °N, 79.42 °E	0.39 g	0.426 g at site # 167	Chamoli station <sup>3</sup> 30.41°N, 79.32°E	0.359g <sup>3</sup> $\Delta = 14$ km

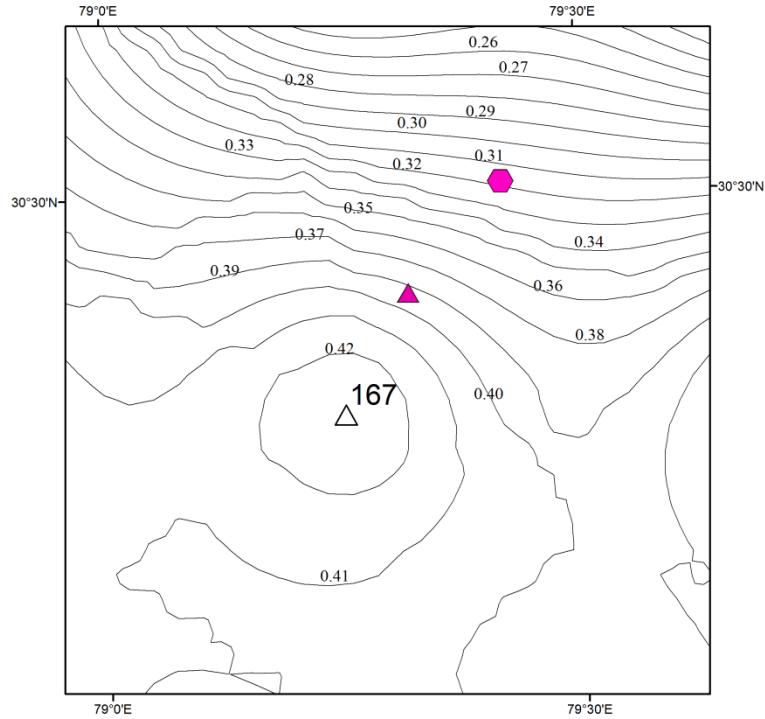




(a)



(b)



(c)

**Figure 6.8** Comparison of PGA computed in the present study, shown in figure 6.7(a), with the PGA recorded at near field stations for several recent earthquakes. Recording station is shown by colored triangle, color of station is as per site classification given in figure 6.4 (b), magnitude of epicenter is as per seismicity map (figure 2.4), and site at which maximum PGA obtained in this study is shown by hollow triangle. (a) Dharamshala earthquake of 26th April, 1986,  $M_w = 5.8$ , (b) Uttarkashi earthquake of 20<sup>th</sup> October, 1991,  $M_w = 6.8$ , (c) Chamoli earthquake of 28<sup>th</sup> March 1999,  $M_w = 6.7$ .

This indicates that 84 sites within India seem to be prone to PGA values as assigned in zone V in the Indian Standards (IS) code (BIS 1893: 2002). Sixteen of these are in Himachal Pradesh. These are in Bilaspur (site #134), Chamba (site #91, 106), Kangra (site #105, 119), Kinnaur (site #123), Kullu (site #107, 121, 122), Lahaul & Spiti (site #92, 93, 108), Mandi (site #120, 135) and Shimla (site #136,150) districts. Thirteen sites are in Uttarakhand. These are in Almora (site #181), Bageshwar (site #182), Chamoli (site #167, 168), Dehradun (site #150, 164), Haridwar (site #179), Nainital (site #196), Pauri Garhwal (site #180), Tehri Garhwal (site #165, 166), and Uttarkashi (site #151, 152) districts. Fifty five sites are in Jammu and Kashmir. District wise breakup for J&K cannot be given because district boundaries were not available for J&K in Survey of India map.

Island of zone V in Jammu and Kashmir encompasses the PGA range of 0.10-0.19g. This is in the Srinagar-Baramula region of J&K. Reason for low PGA value is given here. Seven historical earthquakes were present in the area. Since the earthquakes are historical epicentral location was approximate. Magnitude assigned in DSHA study was on the basis of length of tectonic unit. There is lack of tectonics in zone V. Maximum magnitude was assigned on the basis of length of tectonic unit. Nearest tectonic unit to this region was Poonch segment of MBT which is at surface distance 45.78km and thus, the PGA is low. It implies that PGA ranges of BIS may be revised downwards in these areas. Moreover, during Kashmir earthquake of 2005, ground damage and human tragedy was more on westward of zone V this implies that the island of zone V in J&K needs to be shifted westwards towards syntaxis.

It was observed that the island of zone V of BIS in Himachal Pradesh encompasses almost the entire area in the PGA range  $> 0.5g$ . It comprises of 6 sites (site #104, 105, 106, 119, 120 and 121). It implies that PGA calculated in the present study is much higher than that assigned to zone V in BIS. Since parts of the study area are undergoing a rapid phase of techno-economic development and hydro electric potential is tremendous in this area due to the presence of rivers and many tributaries more extensive studies in these areas is required for large civil structures. It is also recommended that PGA ranges of BIS be revised upwards in these areas.

In Uttarakhand, highest PGA, 0.547g, emerged at Haridwar and Dehradun districts. These two districts are in zone IV of BIS, but the PGA computed is much higher to that assigned to Zone V. Zone V of BIS in Uttarakhand comprises of Bageshwar, Chamoli, Champawat, Pithoragarh, Pauri Garhwal, Rudraprayag and Tehri districts. In the present study PGA of range 0.40 g to 0.49g was observed in Zone V of BIS, which is higher than that assigned to Zone V. This implies that PGA ranges of BIS be revised upwards in these areas.

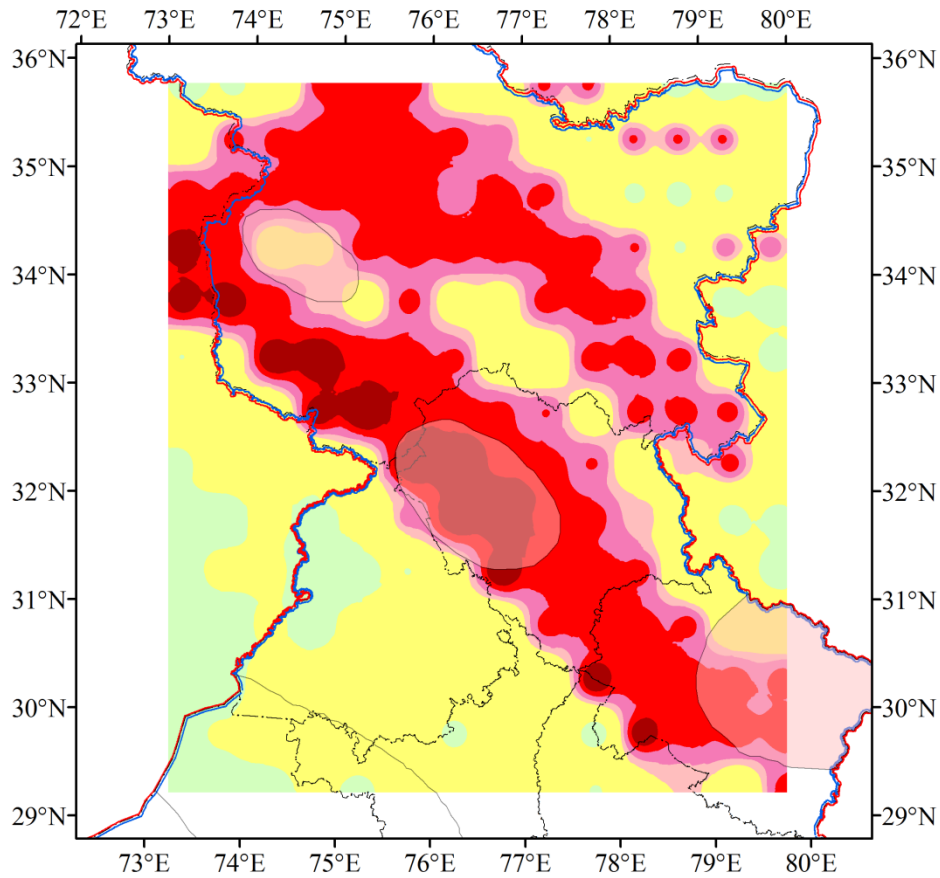


**Figure 6.9:** Hazard map as shown in figure 6.7(b) superimposed on seismic zoning map of India (BIS, 2002) as shown in figure 1.1.

DSHA attempts are few in western Himalaya, and are limited to Uttarakhand or even smaller areas within Uttarakhand, like Dehradun and are discussed in section 1.2.3. In the present study, DSHA has been carried out for a large area encompassing northwest India (including the states of Himachal Pradesh (HP) Jammu & Kashmir (J&K), Uttarakhand (UK), Punjab, Haryana, Uttar Pradesh (UP) Rajasthan and union territory of Chandigarh), and parts of neighboring countries like Pakistan, Afghanistan, China and Tibet. In the present study, PGA varied between 0.180g to 0.547g for Uttarakhand state. The comparison of maximum PGA or PGA range for different studies with the present study is shown in table 6.6. As different authors choose different data inputs and attenuation relationships to compute hazard PGA values vary significantly. The Boore and Atkinson (2008) relationship

yields the highest PGA ranges followed by Abrahamson and Litehiser (1989) relationship, and Sharma (2000) yields the lowest PGA values.

**Table 6.6:** PGA values computed by different authors compared with this study.

Author(s)	Study Area	Maximum PGA/ PGA Range	GMPE
Mohan <i>et al.</i> (2008)	Uttarakhand Himalayas	550 cm/sec <sup>2</sup>	Abrahamson & Litehiser (1989)
Kumar <i>et al.</i> (2011)	Uttarakhand	0.06 g - 0.5g	Abrahamson & Litehiser (1989)
Kumar <i>et al.</i> (2013)	Uttarakhand	0.475g	Abrahamson and Litehiser (1989)
Kumar <i>et al.</i> (2013)	Uttarakhand	0.334 g	Sharma (2000)
Kumar <i>et al.</i> (2014)	Uttarakhand	0.07 g - 0.605 g	Boore and Atkinson (2008)
This study	North west Himalaya, 7° by 7° area longitude:73°E - 80°E latitude: 29°N - 36°N	0.012g-0.470g	Abrahamson and Litehiser (1989), DSHA-1
		0.039g - 0.581g	Boore and Atkinson (2008), DSHA-2

## 6.5 Conclusions

Two different approaches for computation of seismic hazard using deterministic approach were attempted and are discussed in this chapter. PGA obtained for DSHA-1 ranged between 0.012 g - 0.470g, when equal segments of long tectonic units were considered, maximum earthquake assigned was on the basis of observed seismicity from MHD catalogue and Abrahamson and Litehiser (1989) GMPE was considered. PGA in the study area increased considerably for DSHA-2 study and ranged between 0.039 g - 0.581 g, when segments of MBT and MCT were considered as discussed in Chapter 5, maximum earthquake was assigned as per Wells and Coppersmith (1994) relation for maximum magnitude and surface rupture length of a tectonic unit and Boore and Atkinson (2008) GMPE was considered. For both studies hazard maps were prepared at 0.1 g contour interval. For both studies it was concluded that maximum PGA was obtained at same site #105. Also, higher range of PGA was observed in the vicinity of MBT and MCT and in the region

between MBT and MCT. Out of all the seismogenic sources considered, most dominant sources which contributed to hazard were the MBT and the MCT.

The hazard map obtained for DSHA-2 was preferred over that obtained for DSHA-1 study and results were validated using recent epicenters from MHD catalogue-2. This hazard map was compared with the map obtained for identification of seismically susceptible areas. By using this hazard map PGA can be assigned to the seismically susceptible areas. PGA computed in the present study was also compared with the PGA recorded at near field for several recent earthquakes. This hazard map has the potential for being used further for assessment of vulnerability of structures and populations at risk. This hazard map is used for comparison purposes in Chapter 8.

In spite of being used by several researchers DSHA suffers from various disadvantages (Krinitzsky, 2003). This method is dependent on choice of source, maximum earthquake, distance between source and site and the GMPE used. While calculating source to site distance the transmission path is assumed to be homogeneous. Moreover, different GMPE's give different PGA's at the same site. The deterministic approach provides no information about the time of occurrence of the maximum earthquake, the level of shaking that might be expected during a finite period of time and the likelihood of assuming where it is assumed to occur. It does not account for the effect of uncertainties in various steps required to compute the resulting ground motion. To overcome some of these disadvantages the application of Probabilistic Seismic Hazard Analysis (PSHA) came into vogue. PSHA was carried out for the entire study area and details are given in Chapter 7.



## CHAPTER 7

# **PROBABILISTIC SEISMIC HAZARD ASSESSMENT (PSHA)**

---

### **7.1 Introduction**

The objective of probabilistic seismic hazard assessment (PSHA) is to quantify the probability of exceeding various ground-motion levels at a site given all possible earthquakes. The numerical approach to PSHA was first formalized by Cornell (1968). The main advantage of PSHA is that it allows uncertainties in size, location, and rate of recurrence of earthquakes. The variation of ground motion characteristics is explicitly considered in the evaluation of seismic hazard (Cornell, 1968; Reiter, 1990). The probability distribution is defined in terms of the annual rate of exceeding the ground motion level at a site, due to all possible pairs of magnitude and distance of the maximum earthquake, (M, R), considering the nature of its statistical distribution (Reiter, 1990).

There are two types of uncertainties associated with most PSHA studies namely epistemic uncertainty and aleatory uncertainty. Epistemic uncertainty is associated with the imperfect knowledge about the process of generation of earthquake. This can be reduced by collecting additional seismic source data. Aleatory uncertainty is also known as randomness or variability of natural physical processes such as the location, time and size of the next earthquake. This uncertainty is irreducible even with the collection of additional data, as these parameters cannot be predicted.

Like DSHA, PSHA is also a four step process (Reiter, 1990): identification and characterization of seismogenic source zones; seismicity recurrence characteristics; strong ground motion prediction; probability estimation of ground motion. Major steps of PSHA approach are shown in figure 7.1.

On the basis of combination of seismicity and tectonics, seismogenic source zones are identified for the region. Unlike DSHA the sources in PSHA are explicitly defined to have uniform probability distribution, i.e., earthquakes of a given size are equally likely to occur at any point within the source zone. Spatial uncertainty and size uncertainty are associated with seismogenic sources. Spatial uncertainty deals with the uncertainty in geometries of earthquake sources. Sources can be characterized as a point source, areal source or volumetric source. Once the seismogenic source is identified and characterized the next step is to estimate the



magnitude of earthquakes expected to be produced by that source zone. All source zones can generate an earthquake with a maximum magnitude that cannot be exceeded. This pertains to size uncertainty of a seismogenic source.

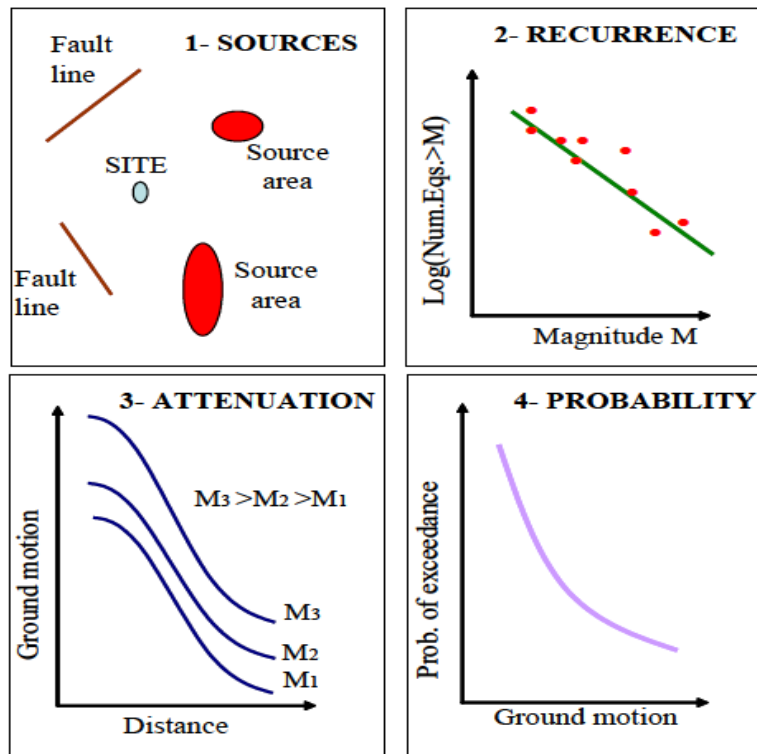


**Figure 7.1:** Major steps of probabilistic seismic hazard assessment approach (Reiter, 1990).

The next step is the characterization of temporal distribution of earthquake recurrence. A recurrence relationship is used to characterize the seismicity, of each source zone, which specifies the average rate at which an earthquake of some size will be exceeded. This step is different from step 2 of the DSHA. Instead of picking the maximum earthquake for each source, here each seismogenic source is characterized by a recurrence relationship or a probability distribution of occurrence of earthquakes. The distribution of the rate of occurrence of earthquakes for each source has to be explained as a function of magnitude.

The activity of each source zone is defined by the frequency-magnitude empirical relationship introduced by Gutenberg and Richter (1944) given in equation 7.1.

$$\log_{10}N = a - bM \quad (7.1)$$

where,  $N$  is the number of events per year having magnitude greater than  $M$  and  $a$  and  $b$  are constants. The regression parameter ' $a$ ' signifies seismic activity and  $10^a$  is the mean yearly number of earthquakes of magnitude greater than or equal to zero. ' $b$ ' value indicates the ratio

of relative likelihood of occurrence of large and small magnitude earthquakes. Frequent occurrence of large magnitude earthquakes is indicated by a low 'b' value whereas frequent occurrence of small magnitude earthquakes is indicated by a high 'b' value.

When logarithm of mean annual rate of exceedance versus magnitude is plotted, a linear relationship is observed, which is commonly known as Gutenberg-Richter recurrence law (1944) and is given as

$$\log_{10}\lambda_m = a - bM \text{ or } \lambda_m = 10^{a-bM} \quad (7.2)$$

$$\text{return period, } T=1/\lambda_m \quad (7.3)$$

where,  $\lambda_m$  is the mean annual rate of exceedance of an earthquake of magnitude greater than or equal to M. T is the return period of an earthquake of magnitude M.

The next step is to calculate PGA by considering all possible pairs of magnitude and distance of the maximum earthquake using ground motion prediction equations. The uncertainty associated with the ground motion prediction equation (GMPE) is also considered in PSHA. GMPE's given by Abrahamson and Litehiser (1989), Boore and Atkinson (2008) and Chiou and Youngs (2008) were used in this study. The relationships given by Abrahamson and Litehiser (1989) and Boore and Atkinson (2008) were described in Chapter 6, sections 6.2 and 6.3, respectively.

Chiou and Youngs (2008) developed an attenuation model for active shallow crustal regions, which gives spectral acceleration and horizontal component of PGA. This predictive model provides average horizontal component of ground motion along with peak acceleration, peak velocity and 5 % damped pseudo-spectral acceleration for spectral periods of 0.01–10 sec. The model includes improved magnitude and distance scaling factors along also with hanging-wall effects. The model is applicable for magnitude ranging between 4 to 8.5,  $R_{JB} < 200$  km and average shear-wave velocity range from 150 m/sec to 1500 m/sec.

The uncertainties involved in determining the location of an earthquake along with the calculation of earthquake size, ground motion prediction parameter is integrated to calculate the probability of exceeding of different levels of ground motion during a specified time period. Seismic hazard curves can be obtained for individual source zones and combined to express the aggregate hazard at particular site.

$$[Y > y^*] = \iint P[Y > y^* | m, r] f_M(m) f_R(r) dm dr \quad (7.4)$$

where  $f_M(m)$  and  $f_R(r)$  are the probability density functions for magnitude and distance, respectively (Kramer, 2009). Hazard maps were plotted for different probabilities of exceedance at contour interval of 0.1g.

## 7.2 Methodology

In assessment of seismic hazard using the probabilistic approach the first step is to identify and demarcate seismogenic source zones (SSZ). For this 1172 earthquake as per MHD catalogue (section 2.3.2) and 127 tectonic units (section 2.4.4) were used. Seismic hazard parameters were calculated for each SSZ. These parameters are minimum magnitude of completeness, ( $M_c$ ), ' $a$ ', ' $b$ ' values,  $\lambda_m$ , maximum observed magnitude ( $M_{\max,obs}$ ), maximum calculated magnitude ( $M_{\max,cal}$ ) and return period for different magnitudes,  $M_w = 5.0, 6.0, 7.0$  and 8.0.

The study area was divided into a grid of  $0.5^\circ$ , as per section 2.2 and peak ground acceleration was calculated at each grid point. Input parameters to compute PGA were the hazard parameters  $M_c$ , ' $a$ ', ' $b$ ',  $\lambda_m$ ,  $M_{\max,cal}$ , and distance. Hazard maps were prepared for the study area for different probabilities of exceedance at given return periods. These were for: (1) 10% probability of exceedance in 50 years, for a return period of 475 years, and (2) 2% probability of exceedance in 50 years, for a return period of 2,475 years. In addition, from the first hazard map districts affected in Himachal Pradesh and Uttarakhand by different PGA values were also identified. District wise breakup for Jammu & Kashmir could not be given as district boundaries were not available for J&K in Survey of India (2011) map.

### 7.2.1 Identification of seismogenic source zones

The  $7^\circ$  by  $7^\circ$  study area was divided into several seismogenic source zones (SSZ), step wise. Both seismicity and tectonics were taken into consideration. Seismicity as per MHD catalogue was used for demarcation of SSZ. The initial criteria for identification of boundaries of these zones were based on several factors such as distribution of seismicity, identification of seismic clusters, and its density in the region. These were further demarcated by considering the prominent tectonic elements around these clusters, including segments of MBT and MCT as discussed in Chapter 5. Fault plane solutions of 27 earthquakes in the study area, discussed in section 2.4.7 and shown in figure 2.12 were also considered while considering the boundaries of seismogenic source zones. This resulted into nine seismogenic source zones in the study area and is named as SSZ1 to SSZ9 and is listed in table 7.1.

SSZ1 is the area demarcated by four prominent tectonic units: in south the Kangra segment of MBT, in north the Chenab segment of MCT, in east the Sundarnagar fault and in west the Kishtwar fault. This SSZ has a dense cluster of earthquakes, and it consists of the great Kangra earthquake of 1905. This SSZ is referred to as the **Kangra seismogenic source zone**.

SSZ2 is the area demarcated by three segments of the MBT in south, viz. Solan segment, Dehradun segment and Nainital segment, and three segments of the MCT in north viz. Kinnaur segment, Uttarkashi segment and Bageshwar segment, in west the Sundarnagar Fault and in east the eastern extremity of the study area, i.e., 80°E longitude. This SSZ is referred to as **Uttarakhand seismogenic source zone**. Most epicenters are either close to or north of the various segments of MCT viz. MCT-3, MCT-4 and MCT-5. Uttarkashi earthquake of 20<sup>th</sup> October, 1991 and Chamoli earthquake of 29<sup>th</sup> March, 1999 are within this SSZ.

SSZ3 is referred to as **Kashmir syntaxis seismogenic source zone**. This zone has a dense cluster in north of Pooch segment and Udampur segment of MBT and around the Main Mantle Thrust (MMT). The 8<sup>th</sup> October, 2005, Kashmir earthquake is a part of this dense cluster. Five historical earthquakes of magnitude  $M_w > 7.0$ , given in table 2.8, are within this SSZ.

A prominent cluster of earthquakes, transverse to the trend of Himalayan arc, was observed along the Kaurik fault system. Seismicity is sparse on east and west side of this prominent cluster. This area is referred to as **Kaurik seismogenic source zone**. Its southern boundary is delineated by the Kinnaur segment of MCT, northern boundary by the Karakoram fault, eastern boundary is delineated by considering extension of the Tso Morari Fault in north-south direction and the western boundary is delineated by the north-south extension of a gravity fault which separates the dense seismicity from sparse seismicity. The 19<sup>th</sup> January, 1975, Kinnaur earthquake, is part of this dense cluster.

SSZ5 is referred to as **Kargil Laddakh seismogenic source zone** and it has sparse seismicity when compared to SSZ1 to SSZ4. In south this zone is demarcated by the Chenab segment and part of Kinnaur segment, in north by the Shyok suture, in west northward extension of the Kishtwar fault, and in east north-south extension of the Tso Morari Fault. SSZ6 has the least number of epicenters of all zones and is referred to as **Western Tibet seismogenic source zone**. It is delineated by the Uttarkashi segment and the Bageshwar segment in the south, the Karakoram fault in the north, and the eastern extremity of the study area, i.e., longitude 80°E in the east and boundary of SSZ4 marks its western boundary. SSZ7

occupies a large part in the north eastern corner of the study area and is referred to as the **Karakoram seismogenic source zone**. The Shyok suture which continues into the Karakoram Fault marks its southern boundary, northern extremity of the study area, i.e. 36°N, latitude demarcates its northern boundary, and eastern extremity of the study area, i.e., 80°E, longitude marks its eastern boundary. The smallest (area wise) of all zones is the **Jhelum seismogenic source zone**, SSZ8. This zone is demarcated around a cluster of earthquakes which is distributed along the Jhelum fault. The **Indo Gangetic seismogenic source zone** is the largest zone in terms of area and shows sparse seismicity. The identified seismogenic source zones are shown in figures 7.2(a, b, c) and table 7.1 shows salient features of nine seismogenic source zones which includes area of the SSZ, magnitude wise distribution of earthquakes within zone and tectonic units present in the zone. Figure 7.2(d) shows districts of Himachal Pradesh and Uttarakhand superimposed on SSZ.

### **7.2.2 Validation of SSZ as per MHD catalogue-2**

Earthquakes from MHD catalogue-2 for validation of results, as per section 2.4.8, were plotted on the seismogenic source zones and are shown in figure 7.3. Magnitude wise breakup of these earthquakes for each SSZ is given in table 7.2. Out of 80 earthquakes maximum, i.e. 24 are within SSZ1, out of which 2 are of magnitude greater than equal to 5.5. SSZ2 has earthquakes of lower magnitude range. The next highest number of earthquakes, 23, was in SSZ3, out of which 3 are of magnitude greater than equal to 5.5. SSZ4, SSZ5, SSZ8 and SSZ9 showed sparse seismicity. SSZ6 has no recent earthquakes. SSZ7 also showed more seismicity, i.e. 16 out of 80 are within this zone, out of which 1 is of magnitude greater than equal to 5.5.

The pattern of seismicity clusters as was observed from MHD catalogue in each SSZ is almost replicated as per MHD catalogue-2 for validation. The SSZ which had a dense cluster of seismicity (as per MHD catalogue) is showing a larger number of epicenters (as per MHD catalogue-2 for validation). It is pertinent to note that the MHD catalogue spans a time range of 460 years whereas the MHD catalogue-2 for validation spans a much shorter time range of 2 years 9 months only.

**Table 7.1:** Seismicity and tectonic distribution within each seismogenic source zone are shown in this table. This includes area (km<sup>2</sup>), magnitude wise distribution of earthquakes, total number of earthquakes and prominent tectonic units in each SSZ.

Source zone	Name of zone	Area (km <sup>2</sup> )	Seismicity of region (No. of events)					Total No. of events	Prominent Tectonic units
			≤ 4.9	5-5.9	6-6.9	7-7.9	≥ 8		
SSZ 1	Kangra source zone	24,013	143	34	2	1	1	181	<ul style="list-style-type: none"> <li>• MBT</li> <li>• MCT</li> <li>• Sundernagar F</li> <li>• Kistwar F</li> <li>• Jwalamukhi Thrust</li> <li>• Vaikrita Thrust</li> <li>• Drang Thrust</li> </ul>
SSZ 2	Uttarakhand source zone	49,310	123	27	8	0	0	158	<ul style="list-style-type: none"> <li>• MBT</li> <li>• MCT</li> <li>• MFT</li> <li>• Alaknanda F</li> <li>• NAT</li> <li>• SAT</li> <li>• Other tectonic units in the form of closed loops</li> </ul>
SSZ 3	Kashmir syntaxis source zone	75,638	310	32	8	11	0	361	<ul style="list-style-type: none"> <li>• MBT</li> <li>• MCT</li> <li>• MMT</li> <li>• Kishtwar F</li> </ul>
SSZ 4	Kaurik source zone	20,085	46	12	3	0	0	61	<ul style="list-style-type: none"> <li>• Kaurik fault System</li> <li>• Indus Suture Zone</li> </ul>
SSZ 5	Kargil Laddakh source zone	50,363	47	5	1	0	0	53	<ul style="list-style-type: none"> <li>• Indus Suture Zone</li> </ul>
SSZ 6	Western Tibet source zone	19,664	10	4	2	0	0	16	<ul style="list-style-type: none"> <li>• Indus Suture Zone</li> </ul>
SSZ 7	Karakoram source zone	82,364	203	27	5	0	0	235	<ul style="list-style-type: none"> <li>• Karakoram F</li> <li>• Shyok Suture</li> </ul>
SSZ 8	Jhelum source zone	15,733	41	8	2	0	0	51	<ul style="list-style-type: none"> <li>• Jhelum Fault</li> </ul>
SSZ 9	Indo Gangetic source zone	168,215	46	9	1	0	0	56	<ul style="list-style-type: none"> <li>• Mahendragarh-Dehradun fault</li> </ul>

Total number of events = 1172

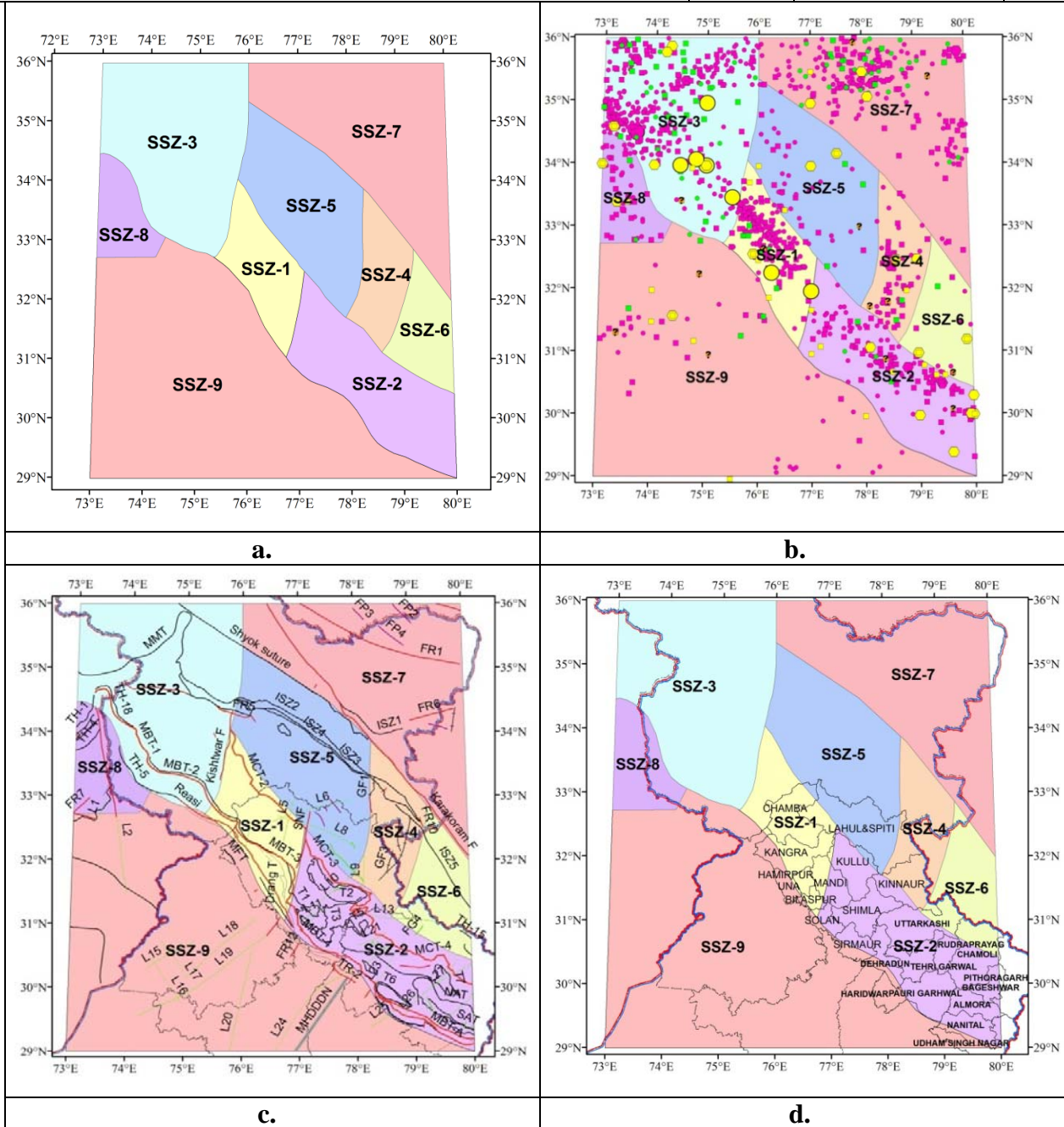


**Figure 7.2:** a. Seismogenic source zones delineated in the study area, where SSZ1: Kangra source zone; SSZ2: Uttarakhand source zone; SSZ3: Kashmir syntaxis source zone; SSZ4: Kaurik source zone; SSZ5: Kargil Laddakh source zone; SSZ6: Western Tibet source zone; SSZ7: Karakoram source zone; SSZ8: Jhelum source zone; SSZ9: Indo Gangetic source zone.  
b. Seismicity as per figure 2.4, superposed on seismogenic source zones.  
c. Tectonics as per figure 2.10, superposed on seismogenic source zones.  
d. Districts of Himachal Pradesh and Uttarakhand as per Survey of India (2011) superimposed on SSZ map.

**Table 7.2:** Magnitude wise break up of recent epicenters from MHD catalogue-2 for validation of seismic zones and return periods in each SSZ.

SSZ	Magnitude	
	$M_w \geq 5.5$	$4.5 \leq M_w \leq 5.4$
SSZ 1	2	22
SSZ 2	0	6
SSZ 3	3	20
SSZ 4	0	1
SSZ 5	0	2
SSZ 6	0	0
SSZ 7	1	15
SSZ 8	0	4
SSZ 9	0	4
<b>Total</b>	<b>6</b>	<b>74</b>

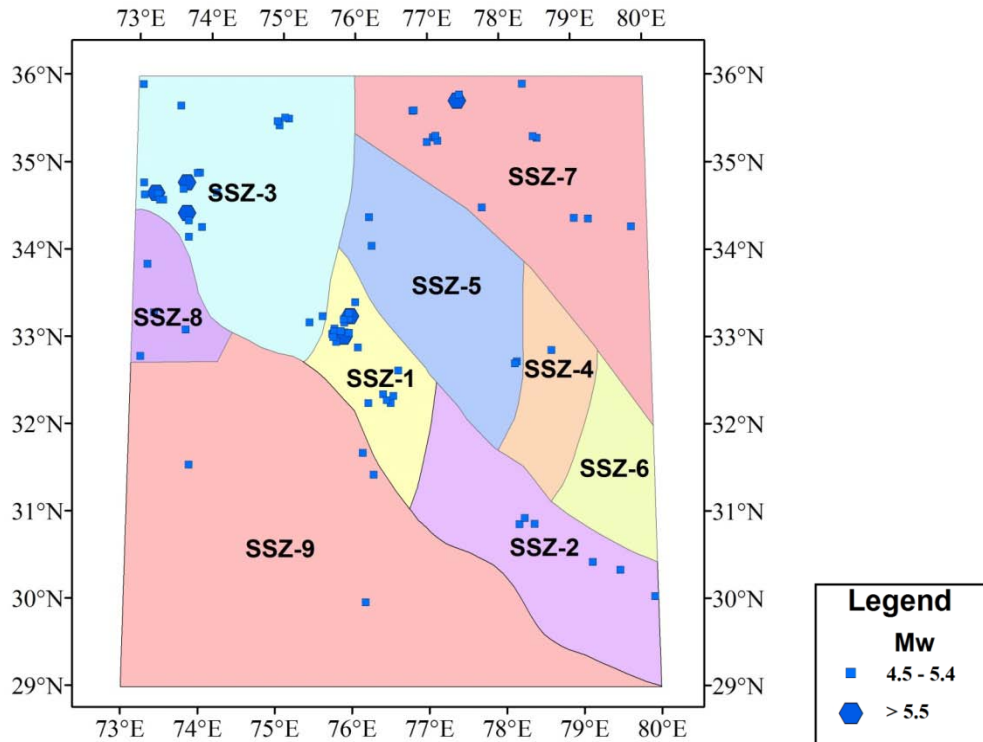


**Figure 7.3:** Epicenters of MHD catalogue-2 for validation of results plotted on SSZ map.

### 7.2.3 Seismic hazard parameters

The earthquake from MHD catalogue which had the maximum magnitude in the SSZ is identified as the maximum observed magnitude ( $M_{\max, \text{obs}}$ ). Nearest prominent tectonic unit to  $M_{\max, \text{obs}}$  was also identified, as it was assumed that this earthquake is generated in the vicinity of that tectonic unit. For example the maximum magnitude in Kangra SSZ is the great Kangra



earthquake of 1905, and the nearest tectonic unit to it is MBT. Table 7.3 gives maximum observed magnitude ( $M_{\max, \text{obs}}$ ), its epicenter, depth and prominent tectonic unit nearest to it.

In the present study, seismic hazard parameters,  $M_c$ , ' $a$ ', ' $b$ ' values were computed for each source zone using Z-MAP software (Wiemer, 2001). Magnitude of completeness,  $M_c$  was computed as 4.3 for the entire MHD catalogue in Chapter 2, section 2.3.2.1. MHD catalogue has 1172 epicenters. These epicenters are now divided into nine SSZ and  $M_c$  was estimated for each SSZ. Seismicity becomes sparse in some SSZ. Since EMR method is applicable only for dense seismicity, maximum curvature method (Wiemer and Wyss, 2000) was used for calculating  $M_c$  for SSZ where seismicity is sparse. Maximum curvature method is a reliable and fast method but it slightly underestimates the magnitude of completeness (Woessner and Wiemer, 2005).  $M_c$  was estimated by EMR method for all seismogenic source zones, except for SSZ6, due to sparse seismicity.  $M_c$  for all SSZ is listed in table 7.4.

Values of regression parameters, ' $a$ ' and ' $b$ ' were estimated by plotting magnitude versus log of cumulative number of earthquakes divided by number of years. Slope of the best fit line yields the ' $b$ ' value and intersection of this line with the y-axis yields the ' $a$ ' value. These ' $a$ ' and ' $b$ ' values were used to estimate mean annual rate of exceedance of an earthquake of magnitude greater than or equal to  $M$ ,  $\lambda_m$ , as per equation 7.2. Return periods were computed for  $M_w = 5.0, 6.0, 7.0$  and  $8.0$  for each SSZ using equation 7.3. Frequency magnitude distribution for estimation of  $M_c$ , ' $a$ ' value and ' $b$ ' value in each SSZ are shown in figure 7.4.

Since historical seismicity data is too sparse and is not able to reflect the full seismic potential of tectonic units, estimation of maximum magnitude becomes an important parameter. For a given source zone, maximum calculated magnitude,  $M_{\max, \text{cal}}$ , is defined as the upper limit, such that no earthquake of magnitude exceeding  $M_{\max, \text{cal}}$  is expected in that zone. For estimating  $M_{\max, \text{cal}}$ , doubly truncated Gutenberg-Richter relationship, programmed in Matlab (Kijko, 2004) was used.

Seismic hazard parameters  $M_{\max, \text{obs}}$ ,  $M_c$ ,  $a$ ,  $b$  value,  $\lambda_m$ , and  $M_{\max, \text{cal}}$ , and return period for earthquakes of magnitude  $M_w = 5.5, 6.0, 7.0$  and  $8.0$  were computed for nine seismogenic source zones and are given in table 7.4.

**Table 7.3:** Salient features of maximum observed earthquake, ( $M_{\max, \text{obs}}$ ), in each SSZ as per MHD catalogue. YYYY: Year, MM: month, DD: Day, Long: Longitude, Lat: Latitude, D: Depth,  $M_{\max, \text{obs}}$ : Maximum observed magnitude, district / place where it was observed, and its nearest prominent tectonic unit.

SSZ	YYY Y	M M	DD	Long (°E)	Lat (°N)	D (km)	$M_{\max, \text{obs}}$ ( $M_w$ )	District/ Place	Nearest Prominent Tectonic Unit
SSZ 1	1905	04	04	76.25	32.30	-	8.0	Kangra	MBT
SSZ 2	1991	10	19	78.79	30.77	13.2	6.8	Uttarkashi	MCT
SSZ 3	1554	-	-	75.00	35.00	-	7.7	Nanga Parbat	MMT
	1778	-	-	75.00	34.00	-	7.7	Near Muzaffarabad	MBT
SSZ 4	1975	01	19	78.50	32.39	1.40	6.6	Lahaul Spiti	Kaurik fault system
SSZ 5	1917	05	17	77.50	34.20	-	6.0	Leh Laddakh	Indus Suture Zone
SSZ 6	1902	06	16	79.00	31.00	-	6.0	Uttarkashi	MCT
SSZ 7	1669	06	22	77.00	35.00	-	6.5	Leh Laddakh	Karakoram Fault
	1996	11	19	78.20	35.31	35.50	6.5	Leh Laddakh	Neotectonic Fault
SSZ 8	1669	06	04	73.30	33.40	-	6.5	Pakistan	Jhelum fault
SSZ 9	1827	09	24	74.40	31.60	-	6.5	Pakistan	Southern tip of Jhelum fault

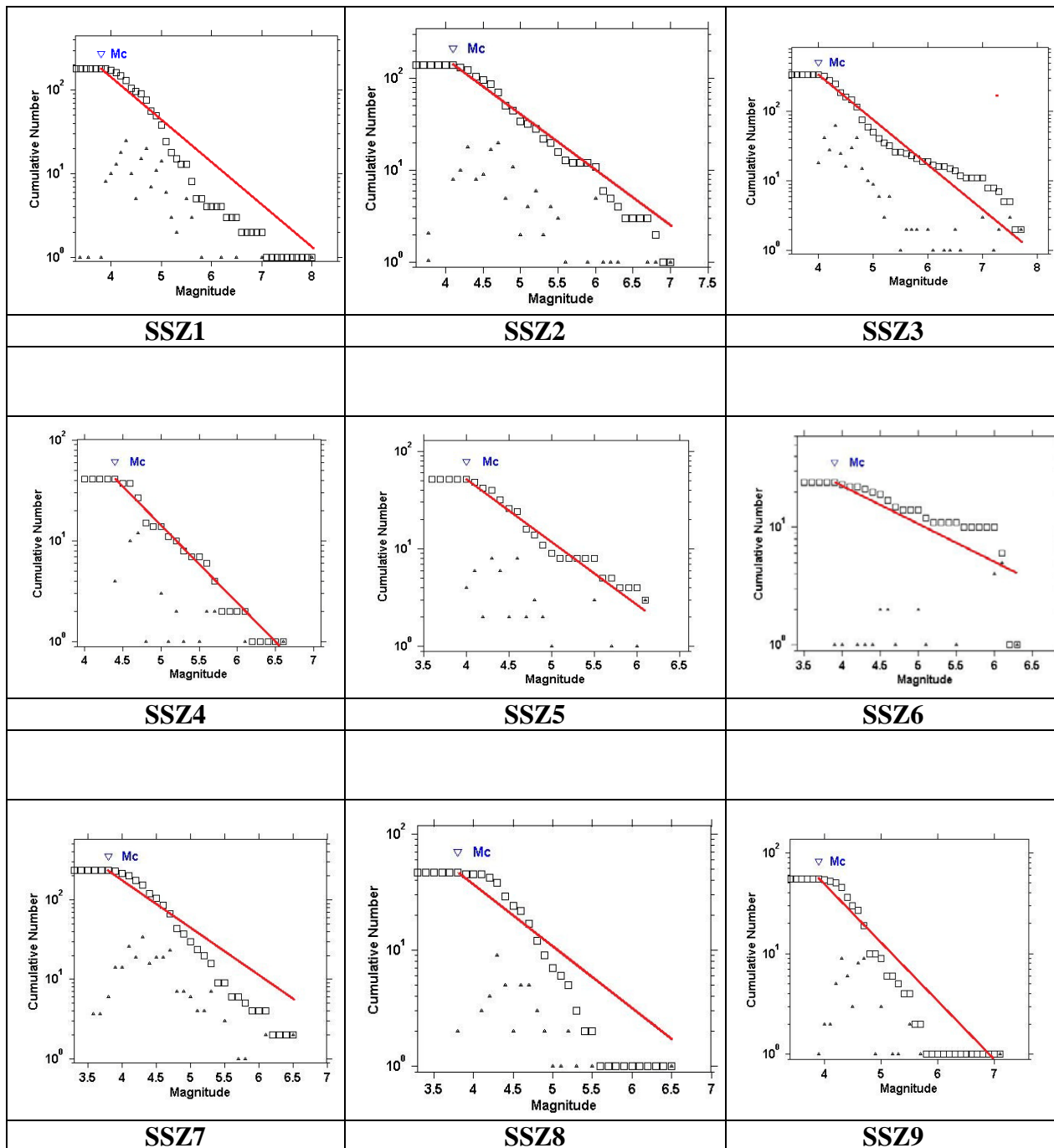


**Figure 7.4:** Frequency magnitude distribution plotted for estimation of seismic hazard parameters  $M_c$ , ' $a$ ' and ' $b$ ' value for all nine SSZ.

### 7.2.4 Significance of ' $a$ ' and ' $b$ ' values in different SSZs

' $a$ ' value signifies seismic activity, and is related to mean yearly number of earthquakes of magnitude greater than or equal to zero. A high value of ' $a$ ' indicates high seismic activity in terms of number of earthquakes and magnitude and a low value of ' $a$ ' indicates low seismic

activity in terms of number of earthquakes and magnitude. ‘*b*’ value describes the relative likelihood of large and small earthquakes. A low value of ‘*b*’ indicates frequent occurrence of high magnitude earthquakes and a high value of ‘*b*’ indicates frequent occurrence of low magnitude earthquakes. ‘*a*’ and ‘*b*’ values for the 9 SSZs are given in table 7.4.

**Table 7.4:** Seismic hazard parameters computed for each seismogenic source zone.  $M_c$ : magnitude of completeness, *a* value, *b* value and error in *b* value,  $\delta b$ , mean annual rate of exceedance,  $\lambda_m$ , and maximum magnitude computed with standard deviation,  $M_{max,cal} \pm s.d.$ , range of return period for earthquakes of magnitude 5.5, 6, 7 and 8.

Source Zone	$M_c$ ( $M_w$ )	‘ <i>a</i> ’	‘ <i>b</i> ’	$\pm \delta b$	$\lambda_m$	$M_{max,cal}$ $\pm s.d.$	Range of return period (years)			
							$M_w=5.5$	$M_w=6$	$M_w=7$	$M_w=8$
Kangra SSZ	3.8	1.93	0.51	0.02	0.982	8.71 $\pm 0.87$	6 - 10	10 -18	32 -60	98 - 204
Uttarakhand SSZ	4.1	2.31	0.61	0.04	0.675	6.94 $\pm 0.52$	7 - 18	13 - 39	48 -174	178 -776
Kashmir syntaxes SSZ	4.0	2.47	0.65	0.04	0.728	7.78 $\pm 0.51$	8 - 21	15 -47	63 -229	257-1122
Kaurik SSZ	4.4	3.17	0.74	0.01	0.812	6.85 $\pm 0.56$	7 - 9	16 -21	87 -120	468- 676
Kargil Laddakh SSZ	3.8	1.81	0.59	0.05	0.376	6.19 $\pm 0.54$	14 - 51	27 -107	93 -468	324-2042
Western Tibet SSZ	4.2	1.42	0.55	0.10	0.131	6.18 $\pm 0.53$	11 -143	19 -302	54 -1349	151-6026
Karakoram SSZ	3.8	2.07	0.59	0.03	0.685	6.63 $\pm 0.52$	10 - 22	19-45	71 -186	257- 776
Jhelum SSZ	3.8	1.09	0.50	0.04	0.151	6.89 $\pm 0.63$	28 - 76	47 -141	135 -490	389-1698
Indo Gangetic SSZ	4.1	2.43	0.72	0.08	0.292	6.96 $\pm 0.68$	12 -93	26 -234	112-1479	490-9333

For the Kangra SSZ, ‘*a*’ value obtained was 1.93. One of the lower ‘*b*’ values, 0.51, was estimated for this zone. This zone has 34 earthquakes of magnitude range 5.0 to 5.9, i.e. the lower magnitude. The slope of the best fit line tends to decrease and hence low ‘*a*’ and ‘*b*’ values are yielded. This can be interpreted as a zone which is liable to witness frequent strong and moderated magnitude earthquakes. For the Uttarakhand SSZ, ‘*a*’ value was estimated as 2.31, which indicates high seismic activity in this zone. ‘*b*’ value estimated was 0.61 which indicates both high and low magnitude earthquakes in this zone. Kashmir syntaxis SSZ has the maximum number of earthquakes of all SSZs. 19 out of 361 earthquakes in this zone have

magnitude greater than 6.0. This decreases the slope of the best fit line, therefore, 'a' value and the 'b' value also decreased slightly. This can be interpreted as a zone which is liable to witness frequent moderate magnitude earthquakes. The highest 'a' and 'b' value was obtained for the Kaurik SSZ which was also one of the smaller zones in the entire study area. The slope of best fit line was steep, figure 7.4(SSZ4), therefore, both 'a' and 'b' values increased simultaneously although this zone had sparse seismicity. This can be interpreted as the zone which is liable will witness very low magnitude earthquakes. Lowest 'a' and 'b' values are estimated for the Jhelum SSZ. The Indo Gangetic SSZ, which is the largest SZZ, showed high 'a' value. Since 'a' value is high but when compared to the area it indicates low seismic activity in the SSZ. 'b' value is high which indicates low magnitude earthquakes in the SSZ.

### 7.2.5 Return periods

A range of return periods were computed for different magnitudes for each SSZ. For each SSZ, the year when  $M_{\max, \text{obs}}$  occurred and the temporal range in which the next probable earthquake of same magnitude can be expected is given in table 7.5. The significance of this is discussed for the Kangra zone, SSZ1 as given below.

In SSZ1, 181 earthquakes occurred within an area of 24,013 km<sup>2</sup>. The great Kangra earthquake of 1905, as per MHD catalogue, was the maximum observed earthquake ( $M_{\max, \text{obs}}$ ) in the entire study area and also in the Kangra zone. The return period, for an 8.0 magnitude earthquake ranges between 98 and 204 years. Accordingly, the next such earthquake can be expected in the years between 2003 and 2109AD. However, the maximum calculated magnitude ( $M_{\max, \text{cal}}$ ) was in the range  $8.71 \pm 0.87$ , which means that the lower limit of magnitude can be 7.84 and the upper limit can be as high as 9.58.

An earthquake of magnitude 7.0 occurred in 1906 for which the estimated return period was in the range 32 to 60 years. Therefore, the next such earthquake was expected in the years between 1938 and 1966 AD. Also, the return period for the Chamba earthquake of 1945 ( $M_w = 6.5$ ) was estimated to be 18 to 33 years. Therefore, the next such earthquake was expected in the years between 1963 and 1978 AD. This implies that an earthquake of magnitude  $M_w = 6.5$  and an even higher magnitude 7.0 is overdue in this SSZ.

A similar interpretation was carried out for the other eight seismogenic source zones, (Mridula *et al.*, 2014). For return periods of maximum observed magnitude and  $M_w$  greater than equal to 5.0 results are given in table 7.5.

**Table 7.5:** Temporal range in years computed for  $M_{\max, \text{obs}}$  and other large earthquakes observed in the same SSZ for each SSZ, and predictive implications of the same. T1: Temporal range for  $M_{\max, \text{obs}}$ , T2: Temporal range for other large earthquakes observed in the same SSZ, Implications:  $T_{\text{overdue}}$  : overdue for the relevant  $M_w$ . (-) indicates no other large earthquake of magnitude  $M_w > 6.0$  is present on the SSZ.

SSZ			T1	Other large earthquakes observed			
	$M_{\max, \text{obs}}$	Year		$M_w$	Year	T2	Implication
SSZ1	8.0	1905	2003 to 2109	7.0	1906	1938 to 1966	$T_{\text{overdue}}$
SSZ2	6.8	1991	2028 to 2120	6.7	1999	2031 to 2110	-
SSZ3	7.7	1778	1947 to 2475	7.2	2005	2089 to 2320	-
				7.0	1885	1948 to 2114	-
				6.0	2002	2017 to 2049	-
SSZ4	6.6	1975	2019 to 2035	6.0	1955	1971 to 1976	$T_{\text{overdue}}$
SSZ5	6.0	1917	1944 to 2024	-	-	-	-
SSZ6	6.5	1906	1950 to 2038	-	-	-	-
SSZ7	6.5	1996	2028 to 2102	6.0	1975	1992 to 2026	-
SSZ8	6.5	1669	1748 to 1932	6.0	1852	1899 to 1993	$T_{\text{overdue}}$
SSZ9	6.5	1827	1925 to 2151	-	-	-	-

### 7.2.6 Validation of return periods in terms of MHD catalogue-2

80 earthquakes from MHD catalogue-2 for validation of results (Chapter 2, section 2.4.8) were plotted on the seismogenic source zones as shown in figure 7.3. Magnitude wise breakup of these earthquakes is given in table 2.18 and magnitude wise breakup of these earthquakes for each SSZ was given in table 7.2. Those zones in which earthquakes of higher magnitude,  $M_w \geq 5.5$ , occurred are considered significant and are discussed below. This includes SSZ1, SSZ3 and SSZ7.

It was observed that out of 80 earthquakes 24 were in SSZ1, 2 of which have  $M_w \geq 5.5$ , and the others have  $M_w \leq 5.4$ . Using 'a' and 'b' values for SSZ1 from table 7.4, and as per equations 7.2 and 7.3, return period of magnitude  $M_w = 5.7$ , ranges between 7 to 12 years. No earthquake of magnitude 5.7 occurred in SSZ1 as per MHD catalogue. However, 3 earthquakes of magnitude 5.6 occurred in the years 1973, 1975 and 1990 in this zone. The return period of  $M_w = 5.6$  ranges between 7 to 11 years. The next earthquake of this magnitude was expected in the temporal range between the years 1997 to 2001. However, no such earthquake occurred in this zone upto 2012, i.e. till the completion of MHD catalogue. This implies that an earthquake of magnitude 5.6 was overdue in this SSZ. Moreover, two earthquakes of higher magnitude, 5.7, occurred within three years, i.e. between the years 2013-2015. This indicates that after 2013 earthquakes of magnitude  $M_w = 5.7$  were recurring faster than expected.

Also, 22 earthquakes in the lower magnitude range  $M_w \leq 5.4$  occurred in SSZ1 within three years. Return periods of magnitude 4.5 and 5.4 ranges between 2 to 3 years and 5 to 9 years, respectively. This implies that earthquakes of magnitude,  $M_w \leq 5.7$ , are occurring more frequently than expected as per computations of return periods. It is interesting to note that the return period for Dharamshala earthquake of 1986,  $M_w=5.8$ , is in the range 8 to 14 years, i.e. the next earthquake of same magnitude was expected in the temporal range of 1992 to 2000 and is again overdue.

For SSZ3 the return period of magnitude  $M_w = 5.7$  ranges between 10 to 29 years. The last earthquake of this magnitude occurred in 2009. Therefore the next earthquake can be expected between the temporal ranges of 2019 to 2038. One earthquake of magnitude  $M_w=5.7$  occurred in 2013 in this SSZ, as per MHD catalogue-2. Moreover, two earthquakes of magnitude  $M_w=5.6$ , also occurred within one year of 2013. This implies that earthquakes of comparable magnitude,  $M_w = 5.7$ , are recurring faster than expected. 20 earthquakes of magnitude in the range  $M_w \leq 5.4$  occurred in this zone within three years. Return periods of magnitude 4.5 and 5.4 are 2 to 4 years and 7 to 18 years, respectively. This implies that earthquakes of magnitude,  $M_w \leq 5.7$ , are occurring more frequently than expected as per computations of return periods, for this zone too.

One earthquake of higher magnitude i.e.  $M_w = 5.7$  occurred in SSZ7 as per MHD catalogue-2. Return period of this magnitude ranges between 12 and 32 years. The last earthquake of magnitude 5.7 occurred in 2009. Therefore the next earthquake was expected between the temporal ranges of 2021 to 2041, i.e. earlier than expected. 15 earthquakes of  $M_w \leq 5.4$  are present on this zone as per MHD catalogue-2. This implies that earthquakes of magnitude,  $M_w \leq 5.7$ , are occurring more frequently than expected as per computations of return periods, for this zone too. Lower magnitude earthquakes in the range  $M_w \leq 5.4$  have occurred in SSZ2, SSZ4, SSZ5, SSZ8 and SSZ9.

Computation of return periods of all SSZ and validation by MHD catalogue-2, leads to the conclusion that the Kangra seismogenic source zone is the most vulnerable zone in the entire study area, followed by the Syntaxis source zone and Kaurik source zone, followed by the Uttarakhand SSZ.

### 7.2.7 Hazard maps

All nine seismogenic source zones, shown in figure 7.2(a), were considered as an area source for preparing a hazard map. Hazard parameters  $M_c$ ,  $a$ ,  $b$ ,  $\lambda_m$ ,  $M_{\max,cal}$ , as computed in section 7.2.3, and ground motion prediction equation (GMPE's) were input parameters to software CRISIS-2012 (Ordaz *et al.*, 2012) for computing PGA. Pseudo Spectral Acceleration (PSA) for ten structural periods, ranging between 0.03 sec (corresponding to short period structures) and 4 sec (corresponding to long period structures) were computed. The periods considered were 0.03, 0.05, 0.1, 0.2, 0.3, 0.5, 1, 2, 3 and 4 seconds. PGA was computed from PSA for 0.03 sec, as per equation 7.5, given in General Principles and Design Criteria, IS: 1893 Part I, 2002, page 16.

$$\frac{S_a}{g} = 1 + 15T, \quad 0.00 \leq T \leq 0.10 \quad (7.5)$$

where,  $S_a$  is spectral acceleration,  $g$  is PGA (g) and  $T$  is the time period in seconds.

PGA was computed for each SSZ in the entire study area. Three different GMPE's were used in two different combinations. Initially attenuation models given by Abrahamson and Litehiser (1989), (abbreviated to AL89), and Boore and Atkinson (2008), (abbreviated to BA08) were used to calculate PGA, as per justification given in sections 6.2 and 6.3. For estimation of PGA in the study area due to combination of both relationships the logic tree approach introduced by (Kulkarni *et al.*, 1984) was used. Assuming that both attenuation relations are correct, each was assigned an equal weightage. This case study is termed as PSHA-1. Later, to study the effect of varying GMPE's on PGA a New Generation Attenuation (NGA) relationship was introduced, Chiou and Youngs (2008), (abbreviated to CY08), while retaining BA08. This exercise is referred to as PSHA-2. Seismogenic source zones and hazard parameters remained the same for both studies, whereas, GMPE's were varied. For both studies PGA's were computed for 10% probability of exceedance in 50 years for return period of 475 years and for 2% probability of exceedance in 50 years for return period of 2,475 years. These are discussed as PSHA-1 and PSHA-2, in following sections.

#### ***Hazard map, PSHA-1***

PGA estimated by Abrahamson and Litehiser (1989) relationship varied between 0.084 - 0.373 g for 10% probability of exceedance in 50 years for a return period of 475 years. PGA estimated by Boore and Atkinson (2008) relationship varied between 0.014 – 0.190 g for 10% probability of exceedance in 50 years for a return period of 475 years. For 2 % probability of exceedance in 50 years for a return period of 2,475 years, PGA estimated by Abrahamson and



Litehiser (1989) relationship and Boore and Atkinson (2008) relationship was 0.129-0.863g and 0.030-0.519g, respectively. It was observed that Abrahamson and Litehiser (1989) relationship gave higher values of PGA compared to Boore and Atkinson (2008) relationship.

After subjecting the AL89 and BA08 models to the logic tree approach PGA varied between 0.022g - 0.289g for 10% probability of exceedance in 50 years, for a return period of 475 years and between 0.038 - 0.723g for 2% probability of exceedance in 50 years, for a return period of 2,475 years. These PGA's are given in table 7.6. Hazard maps were developed at a contour interval of 0.1g for the entire study area. Figure 7.5(a) is the hazard map for 10% probability of exceedance in 50 years, for a return period of 475 years and Figure 7.5(b) is the hazard map for 2% probability of exceedance in 50 years, for a return period of 2,475 years.

### ***Hazard map, PSHA-2***

For 10% probability of exceedance in 50 years, PGA estimated using Chiou and Youngs (2008) relationship ranged between 0.010 - 0.446g. For 2% probability of exceedance in 50 years, PGA varied between 0.022-0.889g for the study area. It was observed that Chiou and Youngs (2008) relationship gave the highest values of PGA followed by Abrahamson and Litehiser (1989) relationship and Boore and Atkinson (2008) relationship, respectively. After subjecting BA08 and CY08 attenuation models to the logic tree approach, it was observed that PGA in the study area varied between 0.013 to 0.315 g for 10% probability of exceedance in 50 years, and between 0.024 to 0.780 g for 2% probability of exceedance in 50 years. Hazard maps at contour interval 0.1g were developed and are shown in figures 7.6(a) and (b), respectively. Table 7.6 gives PGA ranges estimated by all three attenuation relationships separately and by the combination of AL89 with BA08 and BA08 with CY08. Of the four hazard maps prepared, PGA values estimated by the combination BA08 and CY08 relationship yielded higher results for both 10% and 2% probabilities of exceedance in 50 years.

A comparison of highest PGA obtained in both PSHA studies is shown in table 7.7. As economic considerations for most projects consider hazard maps for 10% probability of exceedance in 50 years, figure 7.6(a), is discussed further here. This hazard map is henceforth referred to as PSHA hazard map. The following section deals with interpretation of PSHA hazard map in terms of PGA, SSZ, affected districts and tectonic units.

**Table 7.6:** Range of PGA values for 10% and 2% probability of exceedance in 50 years, calculated using different attenuation relationships. AL89: Abrahamson and Litehiser (1989), BA08: Boore and Atkinson (2008), CY08: Chiou and Youngs (2008). BA08+AL89 and BA08+CY08: PGA value computed by subjecting attenuation relations to logic tree.

Probability of Exceedance (%)	Return Period	AL89	BA08	CY08	BA08 + AL89	BA08 + CY08
10	475	0.085-0.373g	0.014-0.190g	0.010-0.446g	0.022 - 0.289g	0.013-0.315g
2	2475	0.129-0.863g	0.030-0.519g	0.022-0.889g	0.038 - 0.723g	0.044-0.780g

**Table 7.7:** Comparison of highest PGA values obtained in PSHA-1 and PSHA-2, for 10% and 2% probabilities of exceedance in 50 years.

Study→	PSHA-1		PSHA-2	
	10%, 475 y	2%, 2475 y	10%, 475 y	2%, 2475 y
Highest PGA	0.289g	0.723 g	0.315 g	0.780 g
District at which highest PGA was computed	Kangra and Chamba, HP SSZ1	Kangra and Chamba HP, SSZ1	Kangra and Chamba HP, SSZ1	Kangra and Chamba HP, SSZ1

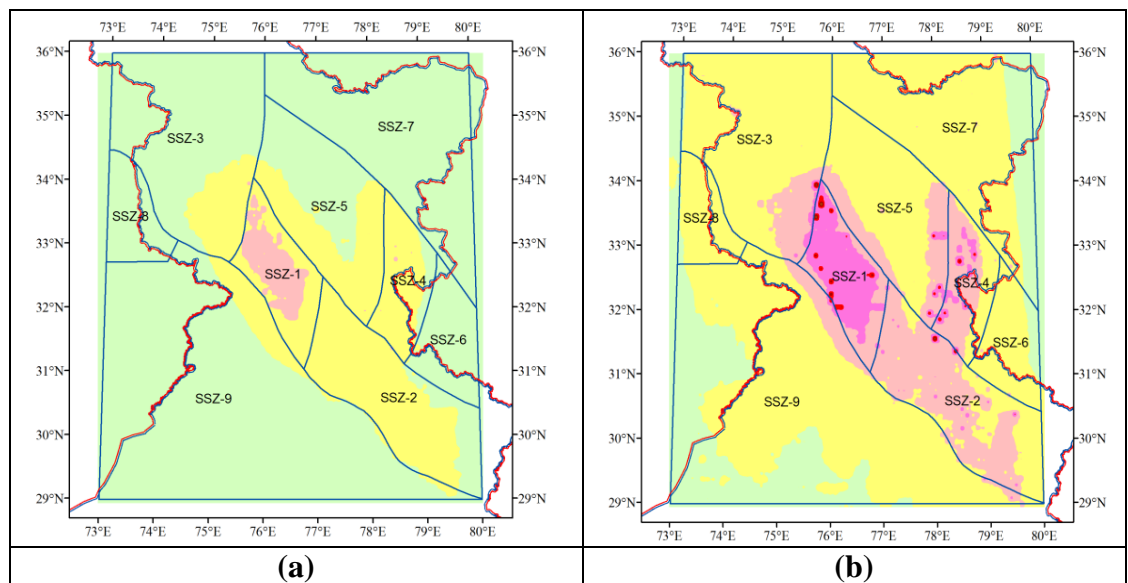


**Figure 7.5** Hazard maps as per PSHA-1 for (a) 10% probability of exceedance in 50 years for a return period of 475 years, (b) 2% probability of exceedance in 50 years for a return period of 2,475 years.

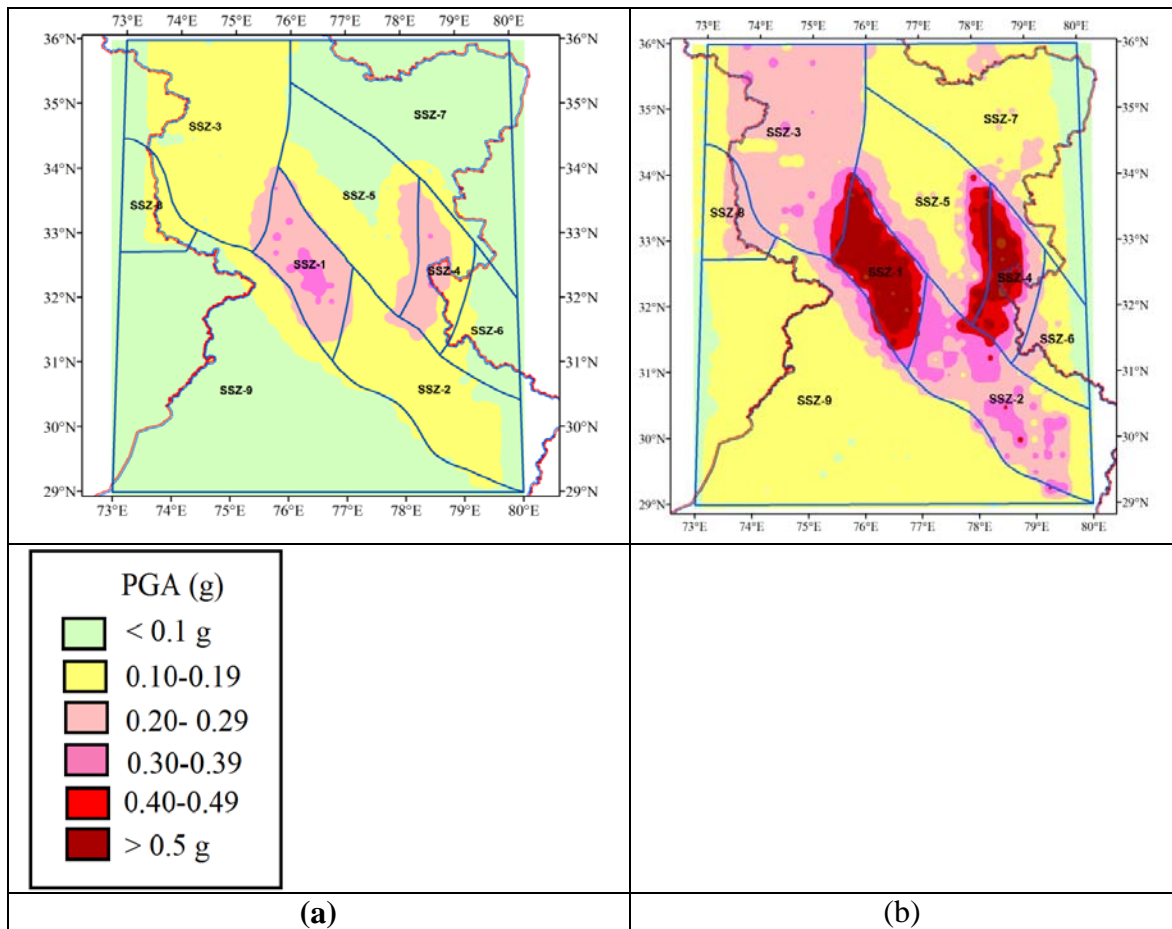


**Figure 7.6:** Hazard maps as per PSHA-2 for; (a) 10% probability of exceedance in 50 years for a return period of 475 years, (b) 2% probability of exceedance in 50 years for a return period of 2,475 years.

### 7.2.8 Interpretation of PSHA hazard map

Interpretation of hazard map shown in figure 7.6(a) is given here. PGA in the entire study area varied between 0.013 to 0.315g for 10% probability of exceedance in 50 years for a return period of 475 years. PGA greater than 0.30g was observed as one large area and several small islands around it in Kangra SSZ, encompassing the districts of Kangra, Chamba, Mandi in HP, and Doda and Kathua districts of J&K, in addition to Lahual & Spiti district of HP and Laddakh in Kaurik SSZ, along the Kaurik Fault System.

The next PGA contour is in the range 0.20 to 0.29g, which occupied almost the entire area of Kangra SSZ. Prominent tectonic elements which traverse these contours are Kangra segment of MBT, Chenab segment of MCT, Kishtwar fault, Jwalamukhi and Vaikrita thrusts. In addition to this large area, this PGA range extended beyond the Kangra SSZ in all other neighbouring zones, viz. Uttarakhand SSZ (encompassing small and contiguous parts of Kullu

and Mandi districts), Kashmir Syntaxis SSZ (Doda and Anantnag, north west of Kishtwar fault), Kargil Laddakh SSZ, and Indo Gangetic SSZ (small and contiguous parts of Una and Bilaspur districts). Another prominent region was located along the Kaurik fault system, partially in Kaurik SSZ and partially in Kargil Laddakh SSZ, encompassing Kinnaur, Kullu and Lahual & Spiti districts, on MCT.

The next PGA contour is in the range 0.10 to 0.19 g, and is depicted by a large region encompassing the above PGA contour. Almost 20% of the study area is occupied by this PGA contour and is spread in several SSZs. In SSZ1, it occupies small parts of Bilaspur, Hamirpur, Kangra, Mandi and Solan districts in HP. Prominent tectonic features in this SSZ are Kangra segment of MBT, Chenab segment of MCT, Drang thrust, Kishtwar fault, Jwalamukhi thrust, Sundernagar fault and Vaikrita thrust. The entire SSZ2 shows PGA of this range. In Himachal Pradesh it encompasses parts of Kullu, Kinnaur, Mandi, Sirmaur, Shimla and Solan districts, in Uttarakhand it encompasses Almora, small parts of Bageshwar, Chamoli, Dehradun, Nainital, Pauri Garhwal, Rudraprayag, Tehri Garhwal and Uttarkashi districts. It includes the region between Kangra, Dehradun and Nainital segments of MBT and Kinnaur and Uttarkashi and Bageshwar segments of MCT. Alaknanda Fault, North Almora thrust, Ramgarh thrust, South Almora Thrust, complex tectonic units in the form of closed loops and several lineaments are prominent in this SSZ. In SSZ3, Anantnag, Doda, Jammu, Srinagar and Udhampur districts of J&K and more than 30% of SSZ4 which includes Kinnaur in HP and south eastern Leh (Laddakh) show this PGA range. Kaurik fault System and ISZ are prominent tectonic units in this SSZ. It includes Chamba and Lahaul & Spiti districts of HP and Laddakh in SSZ5. Parts of SSZ8 and SSZ9 also show this PGA range.

The lowest PGA contour is for PGA less than 0.10g. It exists in SSZ5, SSZ6, SSZ7 SSZ8 and SSZ9. Several slivers of ISZ are prominent tectonic units within SSZ5 and SSZ6. Karakoram fault and Jhelum fault are associated with SSZ7 and SSZ8, respectively.

### **7.3 Discussion**

PGA computed in the present study was compared with the PGA recorded at near field stations for three recent earthquakes, viz. Dharamshala earthquake of 26<sup>th</sup> April, 1986, Uttarkashi earthquake of 20<sup>th</sup> October, 1991 and Chamoli earthquake of 28<sup>th</sup> March, 1999, similar to as was done in section 6.4 for DSHA. This comparison was carried out at relevant site and also at station location.

Maximum PGA for the Dharamshala earthquake of 26<sup>th</sup> April 1986, 0.244g, was recorded at Dharamshala station, at an epicentral distance of 10 km (Chandrasekaran, 1988). In

the present study PGA was checked at the site nearest to the recording station. This was 0.30 g at site #105. The recording station is at a distance of 15km from site #105 and the PGA at recording station is 0.28g, as per figure 7.7(a). Therefore, for Dharamshala earthquake, calculated PGA is comparable to the recorded PGA.

A similar exercise was carried out for Uttarkashi earthquake of 20<sup>th</sup> October, 1991 and Chamoli earthquake of 28<sup>th</sup> March, 1999. Maximum PGA, 0.313g, for Uttarkashi earthquake of 20<sup>th</sup> October, 1991, was recorded at Uttarkashi station, at epicentral distance of 34 km (Chandrasekaran and Das, 1991, 1992). In the present study PGA was checked at the site nearest to the recording station. This was 0.14g at site #151. The recording station is at a distance of 20 km from site #151 and the PGA computed at recording station is 0.13g, as per figure 7.7(b). Therefore, for Uttarkashi earthquake, calculated PGA is lower than the recorded PGA. Maximum PGA, 0.359 g, for Chamoli earthquake of 28<sup>th</sup> March, 1999, was recorded at Chamoli station, at epicentral distance of 14 km (DEQ report, 2000). In the present study PGA was checked at the site nearest to the recording station. This was 0.16g at site #167. The recording station is at a distance of 14 km from site #167 and the PGA at recording station is 0.11g, as per figure 7.7(c). Therefore, for Chamoli earthquake, calculated PGA is lower than the recorded PGA. Table 7.8 shows the highest PGA obtained at the site nearest to the recording station and PGA obtained at station.

Hazard estimated in the present study was compared with PSHA studies carried out by those authors who estimated hazard in the Indian sub continent, and in parts of the Himalayan arc. These results are discussed in section 1.2.4 and are listed in table 7.9. It was observed that PGA obtained in the present study in PSHA-2 is comparable to that estimated by Bhatia *et al.* (1999) and Mahajan *et al.* (2010), NDMA (2011), and Rout *et al.* (2015) for 10% probability of exceedance in 50 years for a return period of 475 years. However, when compared with Khattri *et al.* (1984) and Nath and Thingbaijam (2012), the results obtained in PSHA-2 study are on the lower side, whereas, results of Patil *et al.* (2014) yield the lowest hazard of all studies. It implies that hazard estimation is dependent on many factors varying from author to author and GMPE used.

**Table 7.8:** PGA values computed in this study compared with observed PGA, for Dharamshala earthquake of 1986, Uttarkashi earthquake of 1991 and Chamoli earthquake of 1999. (<sup>1</sup>Chandrasekaran, 1988; <sup>2</sup>Chandrasekaran and Das, 1991; 1992; <sup>3</sup>DEQ report, 2000).

Earthquake Parameters as per MHD Catalogue	PGA at Station, Computed	Maximum PGA at nearest site, Computed	Station Coordinates	Recorded PGA/ Epicentral Distance, $\Delta$
Dharamshala earthquake, 26 <sup>th</sup> April, 1986, $M_w = 5.8$ , 32.15 °N, 76.40 °E	0.28g	0.3g at site #105	Dharamshala station <sup>1</sup> 32.21 °N, 76.32 °E	0.244g <sup>1</sup> $\Delta = 10$ km
Uttarkashi earthquake, 20 <sup>th</sup> October, 1991, $M_w = 6.8$ , 30.77 °N, 78.79 °E	0.14 g	0.14 g at site #151	Uttarkashi Station <sup>2</sup> 30.73 °N, 78.44 °E	0.313g <sup>2</sup> $\Delta = 34$ km
Chamoli earthquake, 28 <sup>th</sup> March, 1999, $M_w = 6.7$ , 30.51 °N, 79.42 °E	0.11 g	0.16g at site #167	Chamoli station <sup>3</sup> 30.41 °N, 79.32 °E	0.359g <sup>3</sup> $\Delta = 14$ km

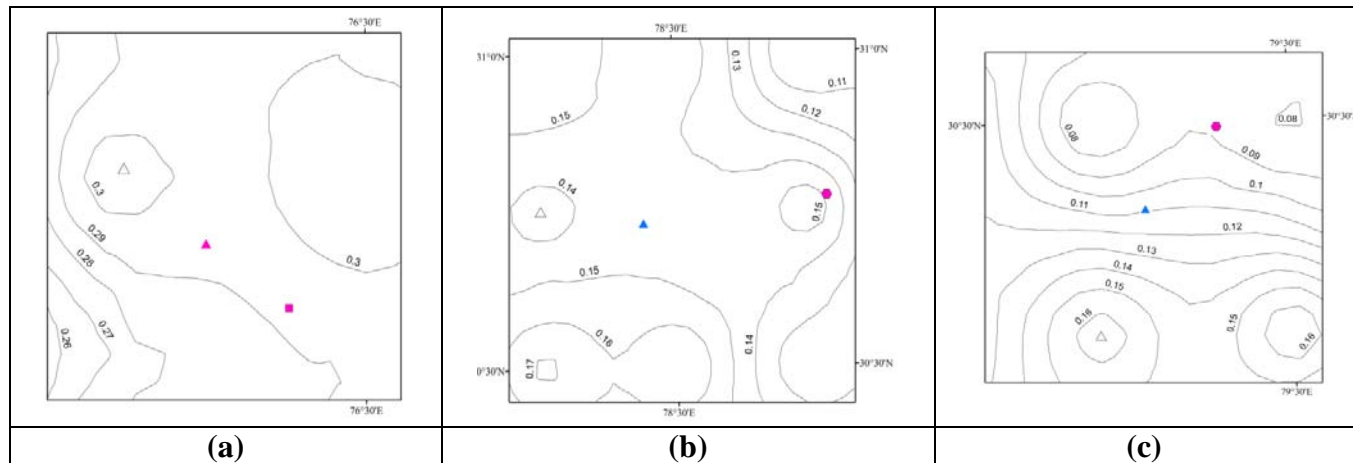


**Figure 7.7** Comparison of PGA computed in the present study, with the PGA recorded at near field stations for several recent earthquakes. Recording station is shown by colored triangle, color of station is as per site classification given in figure 6.4(b), magnitude of epicenter is as per legend of seismicity map (figure 2.4), and site at which maximum PGA obtained in this study is shown by hollow triangle. (a) Dharamshala earthquake of 26<sup>th</sup> April, 1986,  $M_w = 5.8$ , (b) Uttarkashi earthquake of 20<sup>th</sup> October, 1991,  $M_w = 6.8$ , (c) Chamoli earthquake of 28<sup>th</sup> March, 1999,  $M_w = 6.7$ .

**Table 7.9:** PGA values for 10% probability of exceedance computed by different authors compared with this study.

PSHA carried out by Author/Agency	Range of PGA (g)/ hazard parameter	Region / Study area
	10% probability of exceedance	
Khattri <i>et al.</i> (1984)	0.40 – 0.70	India and adjoining regions
Bhatia <i>et al.</i> (1999) GSHAP	0.10 – 0.40	India and adjoining regions
Mahajan <i>et al.</i> (2010)	Kashmir region (0.70 g), Kangra region (0.50 g), Kaurik-Spiti region (0.45 g), Garhwal region (0.50 g) Dharchula region (0.50 g)	NW Himalaya and its adjoining area
NDMA (2010)	0.35 – 0.55	India
Nath and Thingbaijam (2012)	0.05- 0.65	India
Patil <i>et al.</i> (2014)	0.08 – 0.15, b-varying	Himachal Pradesh and adjoining regions
	0.12- 0.23, b-constant	
Rout <i>et al.</i> (2015)	0.09 – 0.39	NW and central Himalayas and the adjoining region
This study: PSHA-1	0.022 - 0.289	North west Himalaya, 7° by 7° area longitude: 73°E - 80°E latitude: 29°N - 36°N
PSHA-2	0.013-0.315	

## 7.4 Conclusions

Computation of seismic hazard using probabilistic approach was attempted and was discussed in this chapter. Nine seismogenic source zones were delineated using a combination of seismicity and tectonic data with segmented MBT and MCT. Fault plane solutions were also taken into consideration. Seismic hazard parameters were computed for each SSZ. The highest observed magnitude in SSZ1 was 8.0, and the calculated maximum magnitude was  $8.71 \pm 0.87$ , which means that it can vary between  $M_w = 7.8$  and 9.5. The return period of the highest observed magnitude,  $M_w = 8.0$ , in the study area was the lowest compared to all other SSZs, 141 years, in SSZ1. In addition, a very low value of 'b', 0.51, for SSZ1, indicates that this zone has a relative likelihood of frequent occurrence of high magnitude earthquakes. Recent epicenters from MHD catalogue-2 superimposed on the SSZ map showed maximum, i.e. 24/80, epicenters

are located within SSZ1. PGA was computed for 10 % and 2 % probability of exceedance in 50 years for a return period of 475 and 2,475 years, respectively. In both the studies the highest PGA was obtained for Kangra and Chamba districts in SSZ1.

This leads to the conclusion that the most vulnerable zone in the entire 7° by 7° area is the Kangra seismogenic source zone, SSZ1. This is indicated in terms of estimated hazard parameters viz.  $M_{\max,obs}$ , 'a', 'b' value, return periods,  $M_{\max,cal}$ , computed PGA and hazard map. This underlines the urgency for estimating populations that are at risk within Kangra SSZ, future implications of which are tremendous and are discussed briefly in the next chapter. An attempt is also made in the next chapter, Chapter 8, to consolidate and integrate the results of various studies carried out for identifying susceptible areas identified in Chapter 4, segments of MBT and MCT from Chapter 5, DSHA study in Chapter 6 and SSZ and return periods from this chapter, and to hypothesize a predictive model for the Kangra SSZ.



## CHAPTER 8

### DISCUSSION AND CONCLUSIONS

---

#### 8.1 Summary

In this research work four studies, viz. identification of seismically susceptible areas, segmentation of MBT and MCT, assessment of deterministic seismic hazard (DSHA), and probabilistic seismic hazard assessment were carried out for a  $7^\circ$  by  $7^\circ$  study area centered on the epicenter of the great Kangra earthquake of 1905. The  $7^\circ$  by  $7^\circ$  area is bounded by longitude:  $73^\circ\text{E}$  to  $80^\circ\text{E}$  and latitude:  $29^\circ\text{N}$  to  $36^\circ\text{N}$ . A summary of this work is presented here. An attempt is made in this chapter to consolidate and integrate these results, in section 8.2, and to hypothesize a predictive model for the Kangra SSZ, in section 8.3. On the basis of the training exercise and decisions made thereafter, the study area was divided into three susceptible areas: Area A: Most susceptible area; Area B: Moderately susceptible area; Area C: Least susceptible area, using Pattern Recognition technique as discussed in Chapter 4. These areas are shown in figure 4.9. Area A represents the area having  $M_w \geq 5.5$  as per training exercise; therefore, it may be considered as the most susceptible area. Seven islands of area A exist in the study area. The largest island of A occupies approximately  $1/5^{\text{th}}$  of the study area and consists of 38 sites out of 196 sites. It encompasses epicenters of several major destructive earthquakes such as the great Kangra earthquake of 1905 ( $M_w = 8.0$ ), Dharamshala earthquake of 1986 ( $M_w = 5.8$ ), Kinnaur earthquake of 1975 ( $M_w = 6.5$ ), Uttarkashi earthquake of 1991 ( $M_w = 6.8$ ) and Chamoli earthquake of 1999 ( $M_w = 6.7$ ). Major tectonic units in this area are MBT, MCT, Sundarnagar fault, Kishtwar fault, Jwalamukhi thrust, Drang thrust, Kaurik fault system, NAT, SAT and closed thrusts in the form of loops between MBT and MCT. Recent higher magnitude earthquakes which were not part of the training exercise originated within area A, and this area can be considered where future earthquakes can be expected.

Seismic hazard assessment of the study area was carried out to assign PGA to the entire study area. Since length of tectonic units plays an important role in assigning maximum magnitude to an earthquake, segmentation of MBT and MCT was first carried out before assessing hazard.

Segmentation of MBT and MCT was carried out in Chapter 5. The longest segment in the study area, the MBT, was segmented on the combined basis of cross over epicenters obtained from PR exercise, observed change in strike of the highly contorted MBT, sharp bends in the MBT, change in seismicity pattern along this thrust and presence of transverse tectonic units associated with the MBT. MBT was finally divided into 6 segments, named as MBT-1,..., MBT-6. These are from west to east: the Poonch segment, Udhampur segment, Kangra segment, Solan segment, Dehradun segment and Nainital segment. Details of these segments are given in table 5.4. A similar exercise was performed for the 800 km long MCT, which was divided into 5 segments named as MCT-1,...,MCT-5. These are the Mashko segment, Chenab segment, Kinnaur segment, Uttarkashi segment and Bageshwar segment. Details of these segments are given in table 5.6.

The DSHA was carried out by considering epicentral data from MHD catalogue and 127 tectonic units, including segmented MBT and MCT, assigning maximum magnitude to each tectonic unit and calculating PGA using a New Generation Attenuation (NGA) relationship. The hazard map prepared for this revealed that PGA in the study area varied between 0.056 - 0.581 g and this hazard map can be used to assign PGA to the entire study area. This map was validated using recent epicenters from MHD catalogue-2.

The study area was divided into nine seismogenic source zones on the combined basis of seismicity from MHD catalogue and 127 tectonic units. Seismic hazard parameters were computed for each SSZ. The most hazardous zone in the entire  $7^{\circ}$  by  $7^{\circ}$  area is the Kangra seismogenic source zone, SSZ1. This is indicated in terms of estimated hazard parameters viz.  $M_{\max,obs}$ , 'a', 'b' value, return periods,  $M_{\max,cal}$ , computed PGA and hazard map. This underlines the urgency of estimating future implications for the Kangra source zone.

## **8.2 Integrated Results for Kangra SSZ**

The Kangra SSZ covers an area of 24,013 sq km, and it covers large parts of Himachal Pradesh and small parts of contiguous Jammu & Kashmir. The boundaries of Kangra SSZ are defined by Jwalamukhi thrust in the south, Chenab segment of MCT in the north, Kishtwar fault in west and Sundarnagar fault in east. It consists of Hamirpur district and parts of Chamba, Kangra, Mandi, Bilaspur, Solan, Lahaul Spiti, Kullu and Una districts of Himachal Pradesh and parts of Kathua, Doda and Udhampur districts of Jammu & Kashmir. The Kangra SSZ is going through a rapid phase of techno-economic development and hydro electric potential is tremendous in this

Himalayan region due to the presence of many rivers and their tributaries. These are shown in figure 8.1. Magnitude wise distribution of seismicity and prominent tectonic units within this source zone are shown in table 7.1.

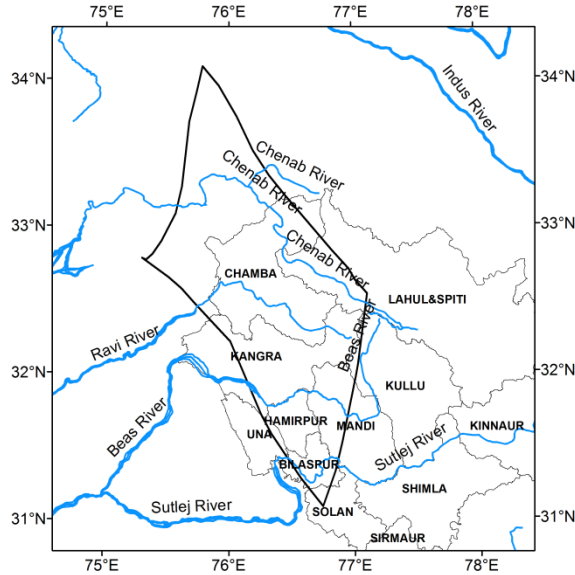


**Figure 8.1:** Districts of Himachal Pradesh, drawn after Survey of India (2011), and rivers (redrawn after SEISAT) superimposed on Kangra SSZ.

Susceptible area map, figure 4.9, when overlain on figure 8.1, and truncated to Kangra SSZ is shown in figure 8.2. Almost, 73% area of Kangra SSZ comprises of susceptible area 'A' i.e., 17496 km<sup>2</sup>, i.e. approximately 17500 km<sup>2</sup>, and the rest is 'B'. Further implications are presented here for this truncated area. Recent epicenters from MHD catalogue-2 for validation, which were not part of the training exercise, when superimposed on figure 8.2, showed that out of 24 epicenters which were located in SSZ1, 23 were located within the truncated area. This is shown in figure 8.3. This leads to the perception that the truncated area can be considered to be an area where current events are located. It is pertinent to note that all these 23 epicenters are located in the region between the Kangra segment of MBT and Chenab segment of MCT. PGA contours in the truncated area varied between 0.37g and 0.58g as per DSHA. This is shown in figure 8.4. District wise and tehsil wise breakup of this area according to PGA is given in table 8.1. Within the island of zone V, as per Seismic zoning map of India, BIS: 1893–2002, corresponding to PGA range 0.24-0.36g, the PGA range obtained in DSHA study is much higher. PGA values > 0.5g were estimated at 6 sites (site #104, 105, 106, 119, 120 and 121), shown in figure 8.4. It implies that

PGA calculated in the present study is much higher than that assigned to zone V in BIS: 1893 – 2002.

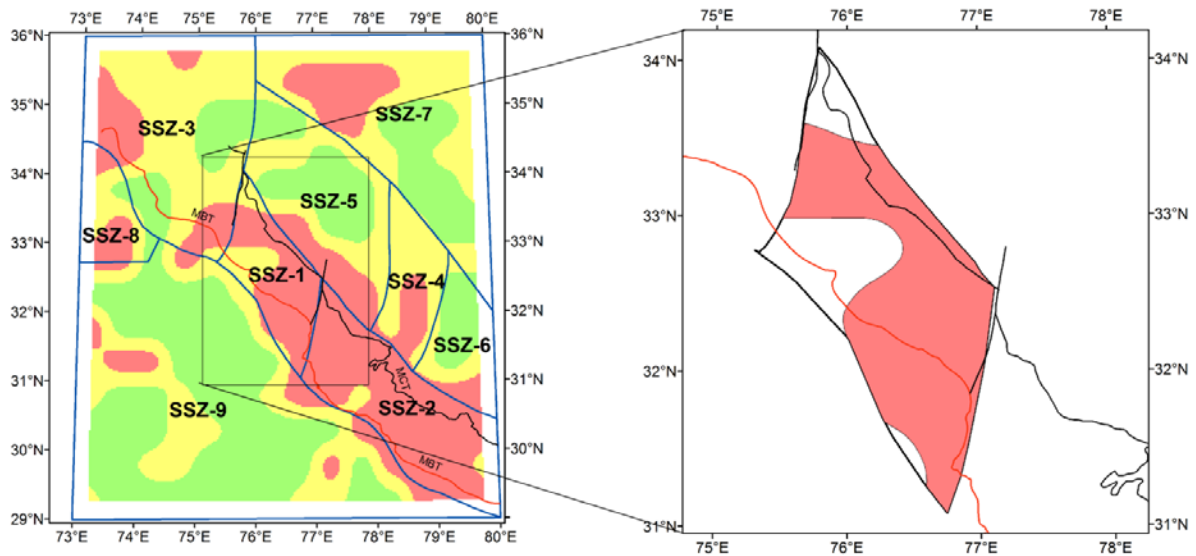


**Figure 8.2** Seismically susceptible areas, as per figure 4.9, superimposed on seismogenic source zones, as per figure 7.2(a) for the entire study area. Common area of Kangra SSZ and largest area of susceptible areas 'A' is shown by box. This area is called truncated area, henceforth.

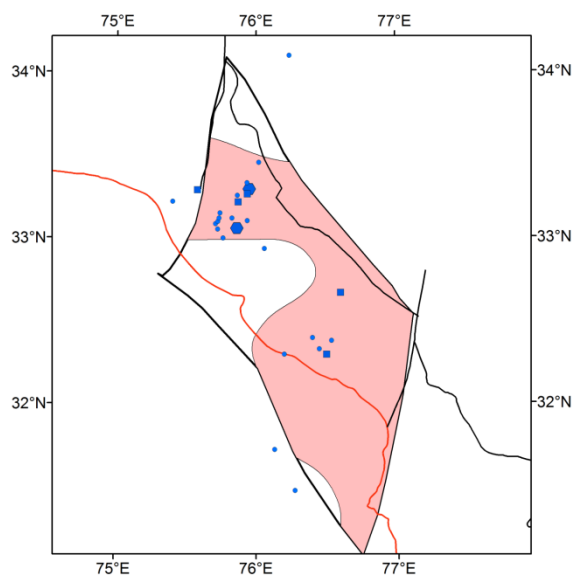


**Figure 8.3:** Seismicity as per MHD catalogue-2 plotted on the truncated area.

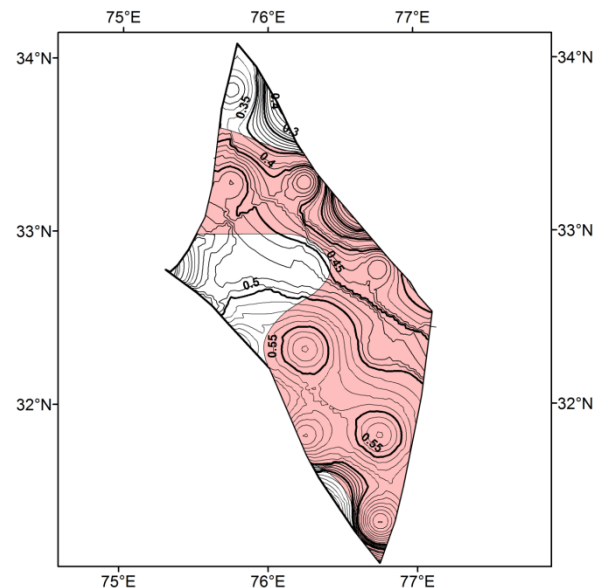


**Figure 8.4:** PGA contours, as per figure 6.7(a), superimposed on the truncated area.

Risk to loss of human life was calculated in those districts which are common to the truncated area and zone V, viz. Kangra, Chamba, Bilaspur, Hamirpur and Mandi. Parameters used in assessing seismic risk were: building types and grade of damage, housing data, seismic zoning map of India (BIS: 1893- 2002), population of each district, and time of occurrence of the earthquake. The study indicates that Kangra district would suffer maximum human casualty, with 9,524 persons at risk. Similar computations were made for other districts, and the risk in decreasing order is for Mandi, Hamirpur, Bilaspur and Chamba districts.

According to the seismic zoning map of India, BIS: 1893-2002, PGA assigned to zone V is in the range 0.24-0.36g and risk was computed for zone V based on this range. However, in the present study PGA in the same area is always more than 0.36 g and can be as high as 0.58g. Therefore, actual risk is expected to be much higher than that computed (Rajput *et al.*, 2016). Therefore, the populations at risk due to these high accelerations will be more than that computed as per BIS zoning map.

When the isoseismal map of the great Kangra earthquake of 1905 was superimposed on figure 8.2, it showed that large parts of the higher isoseismals: X, IX and VIII (on the RF scale) were well within the truncated area, as shown in figure 8.5 (a). The same applies for the Chamba earthquakes of 1945 and 1995 and Dharamshala earthquake of 1986, as shown in figures 8.5 (b, c, d). Intensity for these earthquakes is given tehsil wise in table 8.1. This leads to the observation that maximum damage due to these four destructive events is concentrated within the truncated area and this area is under an enhanced threat perception.

### **8.3 Predictive Model for Kangra SSZ**

After all these studies the following can be deduced for the truncated area. It is an area where the following are concentrated: current events are located, meizo-seismal areas of four destructive earthquakes are located, computed PGA values are in the range 0.39 g to 0.58 g and risk to population is high.

Return periods computed for earthquakes of magnitude 4.5 to 8.0, indicate that an earthquake of  $M_w$  8.0 will occur between the years 2003 to 2109, earthquakes of magnitude 7.0 and 6.0 are overdue since 1964 and 1966, respectively and it was observed that earthquakes of

magnitude 5.0 - 5.7 are occurring more frequently than computed. This implies that an impending disaster is overdue in the Kangra source zone.

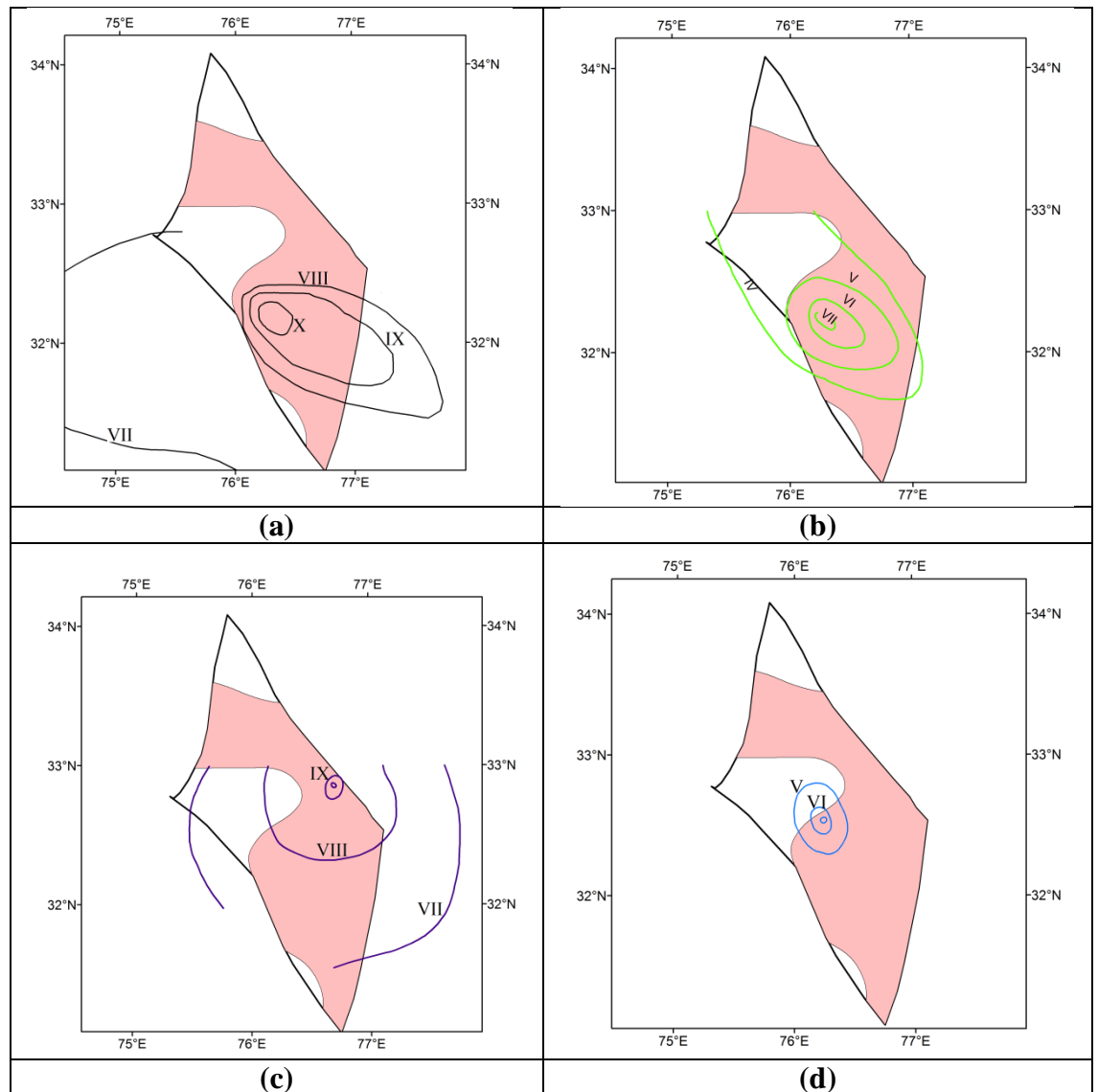


**Figure 8.5:** Isoseismals of four destructive earthquakes plotted on the truncated area:

- (a) The great Kangra earthquake of 4<sup>th</sup> April, 1905. Isoseismals are on RF scale (Redrawn after Middlemiss, 1910).
- (b) Dharamshala earthquake of 26<sup>th</sup> April, 1986. Isoseismals are on MMI scale (Redrawn after SEISAT, 2010).
- (c) Chamba earthquake of 22<sup>nd</sup> June, 1945. Isoseismals are on MM scale (Redrawn after SEISAT, 2010).
- (d) Chamba earthquake of 24<sup>th</sup> March, 1995. Isoseismals are on MSK scale (Redrawn after SEISAT, 2010).

**Table 8.1:** District wise and tehsil wise breakup of truncated area according to PGA are shown in this table. **A:** Intensities of the great Kangra earthquake of 4<sup>th</sup> April, 1905 on RF scale, **B:** Intensities of Dharamshala earthquake of 26<sup>th</sup> April, 1986 on MMI scale, **C:** Intensities of Chamba earthquake of 22<sup>nd</sup> June, 1945 on MM scale, **D:** Intensities of Chamba earthquake of 24<sup>th</sup> March, 1995 on MSK scale.

PGA	District	Tehsil	A	B	C	D
> 0.5 g	Bilaspur	Namhol	VII	VII	–	–
		Bilaspur Sadar	VII	VII	–	–
		Ghumarwin	VII	VII	–	–
		Jhanduta	VII	VII	–	–
		Shri Naina Devi Ji	VII	VII	V	–
		Bharari	VII	VII	V	–
	Chamba	Bhattiyat	IX	VII	V	–
		Saluni	VII	VII	IV	–
		Chaurah	VII	VII	V	–
		Brahmaur	IX	VIII	VI	–
		Chamba	IX	VIII	V	IX
		Dalhosi	VII	VII	IV	–
	Hamirpur	Barsar	VII	VII	V	–
		Bhoranj	VIII	VII	IV	–
		Hamirpur	IX	VII	V	–
		Nadaun	VIII	VII	V	–
		Tira Sujampur	IX	VII	V	–
		Galore	VII	VII	V	–
	Kangra	Badoh	VIII	VII	V	–
		Jaswan	VII	VII	V	–
		Jawali	IX	VII	V	–
		Baijnath	IX	VII	V	–
		Dehra Gopipur	VIII	VII	V	–
		Dharmshala	X	VII	VII	–
		Dhira	X	VII	V	–
		Fateh Pur	VII	VII	V	–
		Har Chakkian	IX	VII	V	–
		Indora	VII	VII	V	–
		Jaisinghpur	IX	VII	V	–
		Kangra	X	VII	VI	VIII
Khundiya		IX	VII	V	–	
Nurpur		VII	VII	V	–	
Palampur	X	VII	VI	–		
Rakar	VII	VII	V	–		
Shahpur	X	VII	VII	–		

PGA	District	Tehsil	A	B	C	D
	Kullu	Thural	IX	VII	V	–
		Kullu	IX	VII	V	–
	Mandi	Chachyot	IX	VII	V	–
		Jogidarnagar	VIII	VII	V	–
		Bali Chauki	IX	VII	V	–
		Karsog	IX	VII	V	–
		Mandi	IX	VII	IV	–
		Padhar	IX	VII	V	–
		Sarkaghat	VIII	VII	–	–
		Thunag	IX	VII	V	–
	Solan	Arki	VII	VII	V	–
		Nalagarh	VII	VII	V	–
		Ramshahr	VII	VII	V	–
	Una	Amb	VII	VII	–	–
		Bangana	VII	VII	–	–
Bharwain		VII	VII	–	–	
0.40-0.49 g	Bilaspur	Jhanduta	VII	VII	V	–
		Shri Naina Devi Ji	VII	VII	V	–
	Chamba	Saluni	VII	VIII	V	–
		Chaurah	VII	VII	V	–
		Brahmaur	IX	VII	V	–
		Pangi	VII	IX	V	–
		Chamba	IX	VII	V	–
	Hamirpur	Barsar	VII	VII	V	–
	Kangra	Baijnath	IX	VII	V	–
	Kullu	Kullu	IX	VII	V	–
		Manali	IX	VII	V	–
	Lahul&Spiti	Kyelang	VII	IX	V	–
Una	Bangana	VII	VII	V	–	
0.37-0.39 g	Lahul&Spiti	Kyelang	VII	VII	V	–
	Chamba	Chaurah	VII	VII	V	–
		Chamba	IX	VII	V	–



## 8.4 Conclusions

After fulfilling the objectives of this research work the following conclusions are drawn.

1. Three types of seismically susceptible areas were identified: A, B and C.
2. Maximum number of recent epicenters was located in area" A which implies that recent seismic activity is concentrated within this area.
3. Six segments of MBT were identified: the Poonch segment, Udhampur segment, Kangra segment, Solan segment, Dehradun segment and Nainital segment.
4. Five segments of MCT were identified: the Mashko segment, Chenab segment, Kinnaur segment, Uttarkashi segment and Bageshwar segment.
5. These mega thrusts are not active over their entire length. The Poonch and Udhampur segment of MBT are active in the north western part of the study area whereas Uttarkashi and Bageshwar segments of MCT are active in the eastern part of the study, are as borne out by recent seismic activity. In central portion of the study area both MBT and MCT seem to be active.
6. Seismic hazard assessed by deterministic and probabilistic methods showed that DSHA gave higher PGA values than PSHA.
7. The results obtained by DSHA provided PGA values to seismically susceptible areas. The PGA values obtained by DSHA are much higher than that assigned to zone V as per seismic zoning map of India, BIS: 1893-2002.
8. Nine seismogenic source zones were identified in the study area: Kangra SSZ, Uttarakhand SSZ, Kashmir Syntaxis SSZ, Kaurik SSZ, Kargil Laddakh SSZ, Western Nepal SSZ, Karakoram SSZ, Jhelum SSZ, and Indo Gangetic SSZ.
9. The Kangra seismogenic source zone, SSZ1, was the most hazardous zone in terms of hazard parameters.
10. Return periods of all magnitude earthquakes were the lowest in this zone. The occurrence of any destructive event in the Kangra seismogenic source zone (SSZ) is expected to be catastrophic.
11. Starting with a  $7^{\circ}$  by  $7^{\circ}$  study area the results were narrowed down to hypothesize a predictive model for a smaller area,  $17500 \text{ km}^2$ , where destructive earthquakes are expected in the near future. Therefore, immediate and urgent preparedness, emergency responses and disaster mitigation measures are required in this area.

12. The integrated study discussed in section 8.2, for Kangra SSZ is valid for all other eight SSZ also, especially for Uttarakhand SSZ, Kashmir Syntaxis SSZ and Kaurik SSZ, and has tremendous implications for future.

### 8.5 Future Scope

The present study has the potential to be extended in future. Some of the suggested areas are:

1. A predictive model similar to that made for Kangra SSZ can be made for each SSZ.
2. Appropriate disaster mitigation measures can be formulated for each SSZ.
3. In the MHD catalogue-2 used for validation of results the maximum magnitude earthquake was  $M_w = 5.7$ , which occurred between the years 2013-2015. Therefore, large magnitude earthquakes within this time span, which occurred outside and near the boundaries of the study area, could not be validated for this study. These earthquakes are Nepal earthquake of 25<sup>th</sup> April, 2015 ( $M_w=7.8$ , epicentre: 84.70°E, 28.14°N, USGS) and Hindu Kush earthquake of 26<sup>th</sup> October, 2015 ( $M_w=7.5$ , epicentre: 36.44°N 70.71°E, USGS). This implies that the study area needs to be extended in the east and west to cover a larger part of the seismotectonically active Himalayan arc.
4. Segmentation of other long tectonic units, such as Karakoram F, Drang thrust, ISZ, Jwalamukhi thrust, MMT and closed loops between MBT and MCT will be more relevant for future DSHA and PSHA studies.
5. DEM data was not available for the entire study area like for Tibet, China and parts of Jammu and Kashmir. Therefore, while identifying seismically susceptible areas, it is recommended either to modify the study area to those areas for which DEM's are available or to drop this feature during the PR training exercise.
6. Extensive studies in these areas are required for large civil structures.
7. Ground effects such as landslide, liquefaction, and rockfall were not incorporated in this study area of rugged mountain terrain for hazard estimation. These terrain effects need to be inclusive in future studies.
8. It is recommended that area A'', a continuous and large area between and along the MBT and MCT, extending from J&K, HP and upto Uttarakhand be considered as zone V in the seismic zoning map of India, BIS: 1893-2002, the PGA ranges be revised upwards in these areas. Similar exercise needs to be carried out for zone IV.

## BIBLIOGRAPHY

1. Abrahamson, N. A., and Litehiser, J. J. (1989), Attenuation of vertical peak acceleration. *Bulletin of the Seismological Society of America*, 79(3), 549-580.
2. Aguilar, J. (2004), Statistical pattern recognition problems and the multiple classes random neural network model. In *Progress in Pattern Recognition, Image Analysis and Applications*, Springer Berlin Heidelberg, 336-341.
3. Alfahaid, W. M., Khan, A. I., and Amin, A. H. M. (2012), A combined pattern recognition scheme with genetic algorithms for robot guidance using Wireless Sensor Networks. *Control Automation Robotics and Vision (ICARCV), 12<sup>th</sup> IEEE International Conference*, 759-764.
4. Ali, A., and Aggarwal, J. K. (2001), Segmentation and recognition of continuous human activity. *Proceedings of IEEE Workshop on Detection and recognition of events in video*, 28-35.
5. Allen, C. R. (1968), The tectonic environments of seismically active and inactive areas along the San Andreas fault system. *Stanford University Publications. Geological Sciences*, 11, 70-80.
6. Ambraseys, N., and Bilham, R. (2000), A note on the Kangra  $M_s = 7.8$  earthquake of 4 April 1905. *Current Science-Bangalore*, 79(1), 45-50.
7. Ameer, A. S., Sharma, M. L., Wason, H. R., and Alsinawi, A. (2005), Markov model for earthquake occurrence as implication in PSHA from revised Iraq seismicity catalogue. *Proceeding of Symposium on Seismic Hazard Analysis and Microzonation*, Sept. 23-24, IIT Roorkee, 167-179.
8. Aminzadeh, F. (1987), Pattern Recognition and Image Processing: *Handbook of Geophysical Exploration*. Geophysical Press, 20.
9. Aminzadeh, F. (2005), Applications of AI and soft computing for challenging problems in the oil industry. *Journal of Petroleum Science and Engineering*, 47(1), 5-14.
10. Aminzadeh, F., and Chatterjee, S. (1984), Applications of clustering in exploration seismology. *Geoexploration*, 23(1), 147-159.

11. Anbazhagan, P., Vinod, J. S., and Sitharam, T. G. (2009), Probabilistic seismic hazard analysis for Bangalore. *Natural Hazards*, 48(2), 145-166.
12. Andras, P. (2005), Neural activity pattern systems. *Neurocomputing*, 65, 531-536.
13. Antani, S., Kasturi, R., and Jain, R. (2002), A survey on the use of pattern recognition methods for abstraction, indexing and retrieval of images and video. *Pattern Recognition*, 35(4), 945-965.
14. Ardeleanu, L., Leydecker, G., Bonjer, K. P., Busche, H., Kaiser, D., and Schmitt, T. (2005), Probabilistic seismic hazard map for Romania as a basis for a new building code. *Natural Hazards and Earth System Science*, 5(5), 679-684.
15. Arya, A. S., Gupta, S. P., Lavania, B. V. K., and Kumar A. (1986), Report on Dharamshala, Himachal Pradesh earthquakes, April 26, 1986: seismicity, building and recommendations for strengthening and reconstruction. *Department of Earthquake Engineering, University of Roorkee, Roorkee*, 80 p.
16. Atkinson, G. M., and Boore, D. M. (2006), Earthquake ground-motion prediction equations for eastern North America. *Bulletin of the Seismological Society of America*, 96(6), 2181-2205.
17. Basu, S., and Nigam, N. C. (1977), Seismic risk analysis of Indian peninsula. *Proceeding 6<sup>th</sup> World Conference Earthquake Engineering*, New Delhi, 1,782-788.
18. Basu, S., and Nigam, N. C. (1978), On seismic zoning map of India. *Proceedings of the 6<sup>th</sup> Symposium of Earthquake Engineering*, 83-90.
19. Benito, M. B., Navarro, M., Vidal, F., Gaspar-Escribano, J., García-Rodríguez, M. J., and Martínez-Solares, J. M. (2010), A new seismic hazard assessment in the region of Andalusia (Southern Spain). *Bulletin of Earthquake Engineering*, 8(4), 739-766.
20. Berrueta, L. A., Alonso-Salces, R. M., and Héberger, K. (2007), Supervised pattern recognition in food analysis. *Journal of Chromatography A*, 1158(1), 196-214.
21. Bezdek, J. C., Hall, L. O., and Clarke, L. (1992), Review of MR image segmentation techniques using pattern recognition. *Medical Physics*, 20(4), 1033-1048.

22. Bhatia, S. C., Chetty, T. R. K., Filimonov, M. B., Gorshkov, A. I., Rantsman, E. Y., and Rao, M. N. (1992), Identification of potential areas for the occurrence of strong earthquakes in Himalayan arc region. *Proceedings of the Indian Academy of Sciences-Earth and Planetary Sciences*, 101(4), 369-385.
23. Bhatia, S. C., Kumar, M. R., and Gupta, H. K. (1999), A probabilistic seismic hazard map of India and adjoining regions. *Annals of Geophysics*, 42(6), 1154-1164.
24. Bhatia, S., and Amati, J. P. (2010), "If These Women Can Do It, I Can Do It, Too": Building Women Engineering Leaders through Graduate Peer Mentoring. *Leadership and Management in Engineering*, 10(4), 174-184.
25. Bommer, J. J., and Abrahamson, N. A. (2006), Why do modern probabilistic seismic-hazard analyses often lead to increased hazard estimates?. *Bulletin of the Seismological Society of America*, 96(6), 1967-1977.
26. Boominathan, A., Dodagoudar, G. R., Suganthi, A., and Maheswari, R. U. (2008), Seismic hazard assessment of Chennai city considering local site effects. *Journal of Earth System Science*, 117(2), 853-863.
27. Boore, D. M., and Atkinson, G. M. (2008), Ground-motion prediction equations for the average horizontal component of PGA, PGV, and 5%-damped PSA at spectral periods between 0.01 s and 10.0 s. *Earthquake Spectra*, 24(1), 99-138.
28. Boore, D. M., and Joyner, W. B. (1982), The empirical prediction of ground motion. *Bulletin of the Seismological Society of America*, 72(6B), S43-S60.
29. Boore, D. M., Joyner, W. B., and Fumal, T. E. (1997), Equations for estimating horizontal response spectra and peak acceleration from western North American earthquakes: a summary of recent work. *Seismological Research Letters*, 68(1), 128-153.
30. Borok Keilis, V. I., and Kossobokov, V. G. (1990), Premonitory activation of earthquake flow: algorithm M8. *Physics of the Earth and Planetary Interiors*, 61(1), 73-83.
31. Borok Keilis, V. I., Knopoff, L., and Rotvain, I. M. (1980). Bursts of aftershocks, long-term precursors of strong earthquakes. *Nature*, 283, 259-263.

32. Bureau of Indian Standards (2002), *BIS-1893 (Part 1): 2002*, Indian Standard Criteria for Earthquake Resistant Design of Structures. 5<sup>th</sup> rev., Bureau of Indian Standards, New Delhi, 40p.
33. Campbell, K. W. (1981), Near-source attenuation of peak horizontal acceleration. *Bulletin of the Seismological Society of America*, 71(6), 2039-2070.
34. Campbell, K. W. (1985), Strong motion attenuation relations: a ten-year perspective. *Earthquake Spectra*, 1(4), 759-804.
35. Caputo, M., Keilis-Borok, V., Oficerova, E., Ranzman, E., Rotwain, I., and Solovjeff, A. (1980), Pattern recognition of earthquake-prone areas in Italy. *Physics of the Earth and Planetary Interiors*, 21(4), 305-320.
36. Central water commission NCS DP Guidelines (2011), Guidelines for preparation and submission of site specific seismic study report of river valley project to national committee on seismic design parameters, Government of India.
37. Chandra, U. (1977), Earthquakes of peninsular India—a seismotectonic study. *Bulletin of the seismological Society of America*, 67(5), 1387-1413.
38. Chandrasekaran, A. R. (1988), Analysis of strong motion accelerogram of Dharamshala earthquake of 26<sup>th</sup> April. *Earthquake Engineering Studies*, EQ 88-10, 90.
39. Chandrasekaran, A. R., and Das, J. D. (1991), Analysis of strong ground motion accelerograms of Uttarkashi earthquake of October 20, 1991, *Department of Earthquake Engineering, Indian Institute of Technology, Roorkee*, EQ 91-10.
40. Chandrasekaran, A. R., and Das, J. D. (1992), Analysis of strong motion accelerograms of Uttarkahi earthquake of October 20, 1991. *Bulletin of the Indian Society of Earthquake Technology*, 29(1), 35-55.
41. Chang, J. K., Ryoo, S., and Lim, H. (2013), Real-time vehicle tracking mechanism with license plate recognition from road images. *The Journal of Supercomputing*, 65(1), 353-364.
42. Chawla, M. P. S., Verma, H. K., and Kumar, V. (2008), RETRACTED: A new statistical PCA–ICA algorithm for location of R-peaks in ECG. *International Journal of Cardiology*, 129(1), 146-148.

43. Chen, C. H., and Fu, H. (1987), A comparison of decision rules for seismic classification. *In: Pattern Recognition and Image Processing: Handbook of Geophysical Exploration, Section I*, (Seismic Exploration, K. Helbig and S. Treitel, Eds.) Geophysical Press, London, 568.
44. Chen, C. H., and Ho, P. G. P. (2008), Statistical pattern recognition in remote sensing. *Pattern Recognition*, 41(9), 2731-2741.
45. Chiou, B. S. J., and Youngs, R. R. (2008), Empirical ground motion model for the average horizontal component of Peak ground Acceleration and pseudo-spectral acceleration for spectral periods 0.01 to 10 s. *Earthquake Spectra*, 24 (S1), 173-216.
46. Chu, M. L., Gradisar, I. A., Railey, M. R., and Bowling, G. F. (1976), Detection of knee joint diseases using acoustical pattern recognition technique. *Journal of Biomechanics*, 9(3), 111-114.
47. Chunga, K., Michetti, A., Gorshkov, A., Panza, G., Soloviev, A., Martillo, C. (2010), Identificación de nudos sismogénicos capaces de generar potenciales terremotos de  $M > 6$  y  $M > 6.5$  en la Región costera y cadenas montañosas de los Andes Septentrionales del Ecuador. *Revista ESPOL - RTE*, 23(3), 61-89.
48. Cisternas, A., Godefroy, P., Guishiani, A., Gorshkov, A. I., Kosobokov, V., Lambert, M., Rantsman, E., Sallantin, J., Saldano, H., Soloviev, A., and Weber, C. (1985), A dual approach to recognition of earthquake prone areas in the Western Alps. *Annales Geophysicae*, Gauthier-Villars, 3(2), 249-269.
49. Coppersmith, K. J. (1991), Seismic source characterization for engineering seismic hazard analysis. *Proceeding of 4<sup>th</sup> International Conference on Seismic Zonation*, Vol. I, Earthquake Engineering Research Institute, Oakland, California, 3-60.
50. Cornell, C. A. (1968), Engineering seismic risk analysis. *Bulletin of the Seismological Society of America*, 58(5), 1583-1606.
51. Courtney, J. W., Magee, M. J., and Aggarwal, J. K. (1984), Robot guidance using computer vision. *Pattern Recognition*, 17(6), 585-592.
52. Cramer, C. H. (2001), A seismic hazard uncertainty analysis for the New Madrid seismic zone. *Engineering Geology*, 62(1), 251-266.

53. Das, S., Gupta, I. D., and Gupta, V. K. (2006), A probabilistic seismic hazard analysis of Northeast India. *Earthquake Spectra*, 22(1), 1-27.
54. Davies, D. (1971), Seismic methods for monitoring underground explosions. *Progress Report (No. NP--19237)*, Stockholm International Peace Research Institute (Sweden).
55. Davis, J. C. (2002), Statistics and data analysis in geology, *Third edition*, John Wiley and Sons, 638 p.
56. Delac, K., and Grgic, M. (2004), A survey of biometric recognition methods. *Electronics in Marine, 2004. Proceedings of ELMAR-2004, 46<sup>th</sup> International Symposium*, IEEE, 184-193.
57. DePolo, C. M., Clark, D. G., Slemmons, D. B., and Ramelli, A. R. (1991), Historical surface faulting in the Basin and Range province, western North America: implications for fault segmentation. *Journal of Structural Geology*, 13(2), 123-136.
58. DEQ Report (2000), A damage survey report of Chamoli earthquake Garhwal Himalayas India, *Department of Earthquake Engineering*, Indian Institute of Technology, Roorkee.
59. Desai, S., and Choudhury, D. (2014), Deterministic seismic hazard analysis for greater Mumbai, India. In *Geo-Congress 2014 Technical Papers@ sGeo-characterization and Modeling for Sustainability* , ASCE, 389-398.
60. Dong, W., Kim J. E., Felix, S. W., and Shah, H. C. (1990), A Knowledge-Based Seismic Risk Evaluation System for the Insurance and Investment Industries (IRAS), *ISET Journal of Earthquake Engineering*, Paper No. 292, 27, 3.
61. Dong, W., Shah, H. C., Bao, A., and Mortgat, C. P. (1984), Utilization of geophysical information in Bayesian seismic hazard model. *International Journal of Soil Dynamics and Earthquake Engineering*, 3(2), 103-111.
62. Douglas, J. (2001), A comprehensive worldwide summary of strong-motion attenuation relationships for peak ground acceleration and spectral ordinates (1969 to 2000). *Imperial College of Science, Technology and Medicine*, Civil Engineering Department.
63. Douglas, J. (2011), Investigating possible regional dependence in strong motions. *Earthquake Data in Engineering Seismology*. S. Skkar, P. Gulkan, T. Van Eck (eds.), Springer Ltd, 29-38.



64. Duda, R. O., Hart, P. E., and David, G. S. (2001), *Pattern Classification. (2nd edition)*, Wiley, New York, ISBN 0-471-05669-3.
65. Duin, R. P., and Pekalska, E. (2005), Open issues in pattern recognition. *Computer Recognition Systems*, Springer Berlin Heidelberg, 27-42.
66. Earthquake Engineering Research Institute EERI (2005), First report on the Kashmir earthquake of October 8, 2005, EERI Special Earthquake Report, December 2005.
67. Eremenko, N. A., and Negi, B. S. (1968), Tectonic map of India, 1: 2,000,000 scale Oil and Natural Gas Commission, Dehradun, India.
68. Esteban, M. A., Martínez-Álvarez, F., Troncoso, A., Justo, J. L., and Rubio-Escudero, C. (2010), Pattern recognition to forecast seismic time series. *Expert Systems with Applications*, 37(12), 8333-8342.
69. Faulkner, B. (2001), Towards a framework for tourism disaster management. *Tourism Management*, 22(2), 135-147.
70. Fukuda, T., and Shibata, T. (1992), Theory and applications of neural networks for industrial control systems. *IEEE Transactions on industrial electronics*, 39(6), 472-489.
71. Fukui, I. (1981), TV image processing to determine the position of a robot vehicle. *Pattern Recognition*, 14(1), 101-109.
72. Fukushima, Y., and Tanaka, T. (1990), A new attenuation relation for peak horizontal acceleration of strong earthquake ground motion in Japan. *Bulletin of the Seismological Society of America*, 80(4), 757-783.
73. Ganapathy, G. P. (2010), A deterministic seismic hazard analysis for the major cultural heritage sites of Tamil Nadu, India. *International Journal of Geomatics and Geosciences*, 1(3), 529.
74. Gardner, J. K., and Knopoff, L. (1974), Is the sequence of earthquakes in southern California, with aftershocks removed, Poissonian. *Bulletin of Seismological Society of America*, 64(5), 1363-1367.

75. Gelfand, I. M., Guberman, S. A., Keilis-Borok, V. I., Knopoff, L., Press, F., Ranzman, E. Y., ... and Sadovsky, A. M. (1976), Pattern recognition applied to earthquake epicenters in California. *Physics of the Earth and Planetary Interiors*, 11(3), 227-283.
76. Gelfand, I. M., Guberman, S. I., Izvekova, M. L., Keilis-Borok, V. I., and Ranzman, E. J. (1972), Criteria of high seismicity, determined by pattern recognition. *Tectonophysics*, 13(1), 415-422.
77. Gelfand, I. M., Guberman, Sh. A., Keilis-Borok, V. I., Ranzman, E., Rotwain, I. M., and Zhidkov M. P. (1974b), Recognition of places where strong earthquakes may occur III, the case when the boundaries of disjunctive knots are unknown (In Russian).
78. Gelfand, I. M., Guberman, Sh. A., Izvekova, M. L., Keilis-Borok, V. I. and Ranzman, E. (1973a), Recognition of places where strong earthquake may occur, I. Pamir and Tien Shan. *Computational Seismology*, 6, (In Russian).
79. Gelfand, I. M., Guberman, Sh. A., Kaletskaja, M. S., Keilis-Borok, V. I., Ranzman, E., Rotwain, I. M., and Zhidkov, M. P. (1974a), Recognition of places where strong earthquakes may occur II, four regions of Asia Minor and S-E Europe (In Russian).
80. Gelfand, I. M., Guberman, Sh. A., Kaletskaja, M. S., Keilis-Borok, V. I., Ranzman, E., and Zhidkov, M. P. (1973b), On transfer of criterion of high seismicity from Central Asia to Anatolia and adjacent regions (In Russian).
81. Geological Survey of India (1992), Uttarkashi Earthquake of October 20, 1991. *Special Publication* no. 30.
82. Geological Survey of India (2001), Chamoli Earthquake of March 29, 1999. *Bulletin Series-B*, No. 53.
83. Giardini, D., Grünthal, G., Shedlock, K. M., and Zhang, P. (1999), The GSHAP global seismic hazard map. *Annals of Geophysics*, 42(6).
84. Gir, R., and Gir, S. M. (1981), A comment on the use of spectral characteristics of teleseismic body waves to evaluate fine crustal structure. *Pure and Applied Geophysics*, 119(6), 1180-1189.

85. Gir, R., Subhash, S. M. G., and Choudhury, M. A. (1978), Investigation of crustal structure by the analysis of reverberation periodicities. *Bulletin of the Seismological Society of America*, 68(5), 1387-1397.
86. Gir, S. S. M., and Choudhury, M. A. (1979), Coda power and modulation characteristics of a complex P signal from underground nuclear explosions. *Tectonophysics*, 53(1), T33-T39.
87. Gir, S. S. M., and Gir, R. (1979), Test of surface-body wave hypothesis for the Q-frequency dependence of coda. *Tectonophysics*, 57(2), T27-T33.
88. Gir, R., Subhash, S. M. G., and Choudhury, M. A. (1977), The resolution power of spectral ratio method in crustal structure studies. *European Seism. Comm.*, Krakaw, Poland, *Pub. Inst. Geophys. Pol. Acad. Sci.*, A-4 (115), 297- 311.
89. Göbel, R., Almer, A., Blaschke, T., Lemoine, G., and Wimmer, A. (2005), Towards an integrated concept for geographical information systems in disaster management. *Geo-information for Disaster Management*, Springer Berlin Heidelberg, 715-732.
90. Gonzalez, R. C. (2008), Digital Image Processing using MATLAB, *Prentice Hall International publications*.
91. Gorshkov, A. I., Mokhtari, M., and Piotrovskaya, E. P. (2009), The alborz region: identification of seismogenic nodes with morphostructural zoning and pattern recognition. *Journal of Seismology and Earthquake Engineering*, 11, 1-16.
92. Gorshkov, A. I., Kuznetsov, I. V., Panza, G. F., and Soloviev, A. A. (2000), Identification of future earthquake sources in the Carpatho-Balkan orogenic belt using morphostructural criteria. *Pure and Applied Geophysics*, 157(1-2), 79-95.
93. Gorshkov, A. I., Panza, G. F., Soloviev, A. A., and Aoudia, A. (2002), Morphostructural zonation and preliminary recognition of seismogenic nodes around the Adria margin in peninsular Italy and Sicily. *Journal of Seismology and Earthquake Engineering*, 4(1), 1.
94. Gorshkov, A. I., Panza, G. F., Soloviev, A. A., and Aoudia, A. (2004), Identification of seismogenic nodes in the Alps and Dinarides. *Bollettino Della Società Geologica Italiana*, 123(1), 3-18.

95. Gorshkov, A. I., Soloviev, A. A., Jiménez, M. J., García-Fernández, M., and Panza, G. F. (2010), Recognition of earthquake-prone areas  $\geq (M5.0)$  in the Iberian Peninsula. *Rendiconti Lincei*, 21(2), 131-162.
96. Gorshkov, A., Parvez, I. A., and Novikova, O. (2012), Recognition of earthquake-prone areas in the Himalaya: validity of the results. *International Journal of Geophysics*, 2012.
97. Gorshkov, A., Zhidkov, M., Rantsman, E., Tumarkin, A. (1991), Morphostructures of the Lesser Caucasus and places of earthquakes,  $M \geq 5.5$ , *Izv. Acad. Sci. SSSR, Phys Earth*. 6, 30-38
98. Green, M. W. (1999), The Appropriate and Effective Use of Security Technologies in US Schools. *A Guide for Schools and Law Enforcement Agencies*.
99. Grzelak, M. D., Maurer, B. W., Pullen, T. S., Bhatia, S. K., and Ramarao, B. V. (2011), A comparison of test methods adopted for assessing geotextile tube dewatering performance. *J. Han and D.E. Alzamora (Eds.), Geo-Frontiers 2011, Advances in Geotechnical Engineering Reston, VA: ASCE*, 3050-3058.
100. Gupta, A., Kripakaran, P., Mahinthakumar, G., and Baugh Jr, J. W. (2005), Genetic algorithm-based decision support for optimizing seismic response of piping systems. *Journal of Structural Engineering*, 131(3), 389-398.
101. Gupta, I. D. (2002), The state of the art in seismic hazard analysis. *ISET Journal of Earthquake Technology*, 39(4), 311-346.
102. Gupta, I. D., and Pattanur, L. (2012), PSHA using different attenuation relationships for different seismic sources. *ISET Golden Jubilee Symposium*, IIT Roorkee.
103. Gupta, I. D., Joshi, R. G., and Rambabu, V. (2001), An example of seismic zoning using PSHA. *MAEER's MIT Pune Journal*, 107-116.
104. Gupta, I., and Sinvhal, A. (2010), Assessment of seismic risk in a microzone. *Proceedings of 14<sup>th</sup> Symposium on Earthquake Engineering*, IIT Roorkee, 224-232.
105. Gupta, I., Sinvhal, A., and Shankar, R. (2006), Himalayan population at earthquake risk: strategies for preparedness. *Disaster Prevention and Management: An International Journal*, 15(4), 608-620.

106. Gutenberg, B., and Richter, C. F. (1944), Frequency of earthquake is California. *Bulletin of Seismological Society of America*, 134, 4, 1985-1988.
107. Gvishiani A., Gorshkov A., Kossobokov V., Cisternas A., Philip H., and Weber C. (1987), Identification of Seismically Dangerous Zones in the Pyrenees. *Annales Geophysicae*, 5 B(6), 681-690.
108. Gvishiani, A. D., and Soloviev, A. A. (1984), Recognition of places on the Pacific coast of the South America where strong earthquakes may occur. *Earthquake Prediction Research*, 2(4), 237-243.
109. Gvishiani, A. D., Zhidkov, M. P., and Soloviev, A. A. (1984), On application of the criteria of high seismicity of Andean mountain belt to Kamchatka. *Izv. Akad Nauk SSSR, Fiz. Zemli*, 1, 20-33.
110. Gvishiani, A.D., Gorshkov, A.I., Ranzman, E.Ya., Cisternas, A, and Soloviev, A.A. (1988). Prognozirovanie mest zemletryaseni v regionakh umerennoi seismichnosti (Forecasting the Earthquake Locations in the Regions of Moderate Seismic Activity), Moscow: Nauka, 1988. 187 p.
111. Hamzehloo, H. (2005), Determination of causative fault parameters for some recent Iranian earthquakes using near field SH-wave data. *Journal of Asian Earth Sciences*, 25(4), 621-628.
112. Hamzehloo, H., Rahimi, H., Sarkar, I., Mahood, M., Alavijeh, H. M., and Farzanegan, E. (2010), Modeling the strong ground motion and rupture characteristics of the March 31, 2006, Darb-e-Astane earthquake, Iran, using a hybrid of near-field SH-wave and empirical Green's function method. *Journal of Seismology*, 14(2), 169-195.
113. Hamzehloo, H., Vaccari, F., and Panza, G. F. (2007), Towards a reliable seismic microzonation in Tehran, Iran. *Engineering Geology*, 93(1), 1-16.
114. Hanks, T. C., and Kanamori, H. (1979), A moment magnitude scale. *Journal of Geophysics Research*, 84, 2348-2350.
115. Harvard: HRV, <http://www.seismology.harvard.edu/projects/CMT>.

116. Hasegawa, H. S., Basham, P. W., and Berry, M. J. (1981), Attenuation relations for strong seismic ground motion in Canada. *Bulletin of the Seismological Society of America*, 71(6), 1943-1962.
117. Hofmann, M., Steinke, F., Scheel, V., Charpiat, G., Farquhar, J., Aschoff, P., ... and Pichler, B. J. (2008), MRI-based attenuation correction for PET/MRI: a novel approach combining pattern recognition and atlas registration. *Journal of Nuclear Medicine*, 49(11), 1875-1883.
118. Huang, K. Y., and Fu, K. S. (1987), Detection of seismic bright spots using pattern recognition techniques. *Handbook of Geophysical Exploration: Section I. Seismic Exploration*, 20, 263-301.
119. Hull, A. G., Augello, A., and Yeats, R. S. (2003), Deterministic seismic hazard analysis in Northwest Oregon, USA. *Pacific conference of earthquake engineering. Paper* (No. 157).
120. Ikeda, M., Toda, S., Kobayashi, S., Ohno, Y., Nishizaka, N., and Ohno, I. (2009). Tectonic model and fault segmentation of the Median Tectonic Line active fault system on Shikoku, Japan. *Tectonics*, 28(5), 1-22.
121. IS: 1893-1962, Indian standard Criteria for earthquake resistant design of structures. *Indian Standard Institution*, New Delhi.
122. IS: 1893-1966, Indian standard Criteria for earthquake resistant design of structures. First revision, *Indian Standard Institution*, New Delhi.
123. IS: 1893-1984, Indian standard Criteria for earthquake resistant design of structures. Fourth revision, *Bureau of Indian Standards*, New Delhi.
124. ISC Catalogue: <http://www.isc.ac.uk/iscbulletin/search/bulletin> (International Seismological Center).
125. ISRO digital elevation model (DEM): Cartosat-1 data user's handbook, given by [http://bhuvan.nrsc.gov.in/bhuvan\\_links.php](http://bhuvan.nrsc.gov.in/bhuvan_links.php).
126. Itakura, F., and Saito, S. (1970), A statistical method for estimation of speech spectral density and formant frequencies. *Electronics and Communications in Japan*, 53A, 36-43.
127. Jain, A. K. (2007), Technology: biometric recognition. *Nature*, 449(7158), 38-40.

128. Jain, A. K., Ross, A., and Prabhakar, S. (2004), An introduction to biometric recognition. *IEEE Transactions on Circuits and Systems for Video Technology*, 14(1), 4-20.
129. Jain, P., Deo, M. C., Latha, G., and Rajendran, V. (2011), Real time wave forecasting using wind time history and numerical model. *Ocean Modelling*, 36(1), 26-39.
130. Jaiswal, K. S., and Sinha, R. (2008), Estimating Seismic Hazard for Central and Southern India. *The 14<sup>th</sup> World Conference on Earthquake Engineering*, October 12-17, 2008, Beijing, China.
131. Joshi, A., Kumar, A., Castanos, H., and Lomnitz, C. (2013b), Seismic Hazard of the Uttarakhand Himalaya, India, from deterministic modeling of possible rupture planes in the area. *International Journal of Geophysics*, 1-12.
132. Joshi, A., Kumar, A., Mohan, K., and Rastogi, B. K. (2013a), Hybrid attenuation model for estimation of peak ground accelerations in the Kutch region, India. *Natural Hazards*, 68(2), 249-269.
133. Joshi, A., Mohanty, M., Bansal, A. R., Dimri, V. P., and Chadha, R. K. (2010b), Use of strong motion data for frequency dependent shear wave attenuation studies in the Pithoragarh region of Kumaon Himalaya. *Indian Society of earthquake Technology*, 47, 1, 25-46.
134. Joshi, A., Mohanty, M., Bansal, A. R., Dimri, V. P., and Chadha, R. K. (2010a), Use of spectral acceleration data for determination of three-dimensional attenuation structure in the Pithoragarh region of Kumaon Himalaya. *Journal of Seismology*, 14(2), 247-272.
135. Joshi, A., Mohanty, M., Teotia, S. S., Bansal, A. R., Dimri, V. P., and Chadha, R. K. (2009), Crustal attenuation of shear waves in Pithoragarh region, *Journal of Ind. Geophys. Union*, 13,137-146.
136. Joshi, A., Sinvhal, A., and Sinvhal, H. (1999), A strong motion model for the Uttarkashi earthquake of October 20, 1991. *Gondwana Research Group Memoir-6*, 329-334.
137. Joshi, D. D., and Khan, A. A. (2009), Seismic vulnerability vis-à-vis active faults in the Himalaya-Hindukush belt. *Journal of South Asia Disaster Studies*, 2(1), 197-243.
138. Joyner, W. B. and Boore, D. M. (1988). Measurement, characterization and prediction of strong ground motion. *Proceedings of Earthquake Engineering and Soil Dynamics-II*, 43-

100.

139. Joyner, W. B., and Boore, D. M. (1981), Peak horizontal acceleration and velocity from strong-motion records including records from the 1979 Imperial Valley, California, earthquake. *Bulletin of the Seismological Society of America*, 71(6), 2011-2038.
140. Kagan, Y., and Knopoff, L. (1978), Statistical study of the occurrence of shallow earthquakes. *Geophysical Journal International*, 55(1), 67-86.
141. Kaman, E. J., Van Riel, P., Young, I. T., and Protais, J. C. (1987), The application of pattern recognition in detailed target model inversion. *Pattern Recognition and Image Processing, Seismic Exploration*, 312-335.
142. Kataria, N. P., Shrikhande, M., and Das, J. D. (2013), Deterministic seismic hazard analysis of Andaman and Nicobar Islands. *Journal of Earthquake and Tsunami*, 7(04), 1350035-1-1350035-19.
143. Kebeasy, R. M., Hussein, A. I., and Dahy, S. A. (1998), Discrimination between natural earthquakes and nuclear explosions using the Aswan Seismic Network. *Annals of Geophysics*, 41(2), 127-140.
144. Kebede, F., and Van Eck, T. (1996), Probabilistic seismic hazard assessment for the Horn of Africa based on seismotectonic regionalization. *Tectonophysics*, 270, 221-237.
145. Khan, A. A. (2012), Seismogenic sources in the Bay of Bengal vis-a-vis potential for tsunami generation and its impact in the northern Bay of Bengal coast. *Natural Hazards*, 61(3), 1127-1141.
146. Khan, A. A. (2014), Earthquake hazard vulnerability constraints from geophysical characterization – a case study from Dhaka megacity, Bangladesh. *Natural Hazards*.
147. Khan, A. A., and Hossain, M. S. (2005), Recurrence of 1885 Bengal earthquake and hazard vulnerability status of Dhaka Metropolitan City, Bangladesh. *Oriental geographer*, 49(2), 205-216.
148. Khattri, K. N. (1987), Great earthquakes, seismicity gaps and potential for earthquake disaster along the Himalaya plate boundary. *Tectonophysics*, 138(1), 79-92.



149. Khattri, K. N., Rogers, A. M., Perkins, D. M., and Algermissen, S. T. (1984), A seismic hazard map of India and adjacent areas. *Tectonophysics*, 108(1-2), 93111-108134.
150. Khattri, K., Rai, K., Jain, A. K., Sinvhal, H., Gaur, V. K., and Mithal, R. S. (1978), The Kinnaur earthquake, Himachal Pradesh, India, of 19 January, 1975. *Tectonophysics*, 49(1), 1-21.
151. Kijko, A. (2004), Estimation of the maximum earthquake magnitude,  $m_{max}$ . *Pure and Applied Geophysics*, 161(8), 1655-1681.
152. Kijko, A. and Öncel, A. O. (2000), Probabilistic seismic hazard maps for Japanese islands. *Journal of Soil Dynamics and Earthquake Engineering*, Wessex Institute of Technology, 20, 485-491.
153. Kijko, A., and Graham, G. (1998), Parametric-historic procedure for probabilistic seismic hazard analysis Part I: estimation of maximum regional magnitude  $M_{max}$ . *Pure and Applied Geophysics*, 152(3), 413-442.
154. Kijko, A., and Graham, G. (1999), "Parametric-historic" Procedure for Probabilistic Seismic Hazard Analysis Part II: Assessment of Seismic Hazard at Specified Site. *Pure and Applied Geophysics*, 154(1), 1-22.
155. King, G. C. P. (1986), Speculations on the geometry of the initiation and termination processes of earthquake rupture and its relation to morphology and geological structure. *Pure and Applied Geophysics*, 124(3), 567-585.
156. King, G., and Nábělek, J. (1985), Role of fault bends in the initiation and termination of earthquake rupture. *Science*, 228(4702), 984-987.
157. King, G., and Yielding, G. (1984), The evolution of a thrust fault system: processes of rupture initiation, propagation and termination in the 1980 El Asnam (Algeria) earthquake. *Geophysical Journal International*, 77(3), 915-933.
158. Klügel, J. U. (2008), Seismic hazard analysis—Quo vadis?. *Earth-Science Reviews*, 88(1), 1-32.
159. Knopoff, L., Levshina, T., Keilis-Borok, V. I., and Mattoni, C. (1996), Increased long-range intermediate-magnitude earthquake activity prior to strong earthquakes in California. *Journal of Geophysical Research: Solid Earth*, 101(B3), 5779-5796.

160. Kramer, S.L. (2009). Geotechnical Earthquake Engineering. Prentice –Hall Publications, 626 p.
161. Krinitzsky, E. L. (2003), How to combine deterministic and probabilistic methods for assessing earthquake hazards. *Engineering Geology*, 70, 157-163.
162. Kripakaran, P., Gupta, A., and Baugh, J. W. (2007), A novel optimization approach for minimum cost design of trusses. *Computers and Structures*, 85(23), 1782-1794.
163. Kripakaran, P., Gupta, A., and Matzen, V. C. (2008), Computational framework for remotely operable laboratories. *Engineering with Computers*, 24(4), 405-415.
164. Kulkarni, R. B., Youngs, R. R., and Coppersmith, K. J. (1984), Assessment of confidence intervals for results of seismic hazard analysis. *Proceedings of the Eighth World Conference on Earthquake Engineering*, 1, 263-270.
165. Kumar, D., Khattri, K. N., Teotia, S. S., and Rai, S. S. (1999), Modelling of accelerograms of two Himalayan earthquakes using a novel semi-empirical method and estimation of accelerogram for a hypothetical great earthquake in the Himalaya. *Current Science*, 76(6), 819-830.
166. Kumar, D., Sarkar, I., Sriram, V., and Khattri, K. N. (2005), Estimation of the source parameters of the Himalaya earthquake of October 19, 1991, average effective shear wave attenuation parameter and local site effects from accelerograms. *Tectonophysics*, 407(1), 1-24.
167. Kumar, D., Sarkar, I., Sriram, V., and Teotia, S. S. (2012), Evaluating the seismic hazard to the National Capital (Delhi) Region, India, from moderate earthquakes using simulated accelerograms. *Natural Hazards*, 61(2), 481-500.
168. Kumar, D., Sriram, V., Sarkar, I., and Teotia, S. S. (2008), An estimate of a scaling law of seismic spectrum for earthquakes in Himalaya. *Indian Minerals*, 61(3-4), 1-4.
169. Kumar, D., Teotia, S. S., and Khattri, K. N. (1997), The representability of attenuation characteristics of strong ground motions observed in the 1986 Dharmasala and 1991 Uttarkashi earthquakes by available empirical relations. *Current science*, 73(6), 543-548.

170. Kumar, D., Teotia, S. S., and Sriram, V. (2011), Modelling of strong ground motions from 1991 Uttarkashi, India, Earthquake using a hybrid technique. *Pure and Applied Geophysics*, 168(10), 1621-1643.
171. Kumar, M., Wason, H. R., and Das, R. (2013), Deterministic seismic hazard assessment of Dehradun city. *Proceedings of Indian Geotechnical Conference-2013*, IIT Roorkee, December 22-24.
172. Kumar, P., Kumar, A., and Sinvhal, A. (2011), Assessment of seismic hazard in Uttarakhand Himalaya. *Disaster Prevention and Management: An International Journal*, 20(5), 531-542.
173. Kumar, P., Kumar, A., Pandey, A. D., Sharma, R., and Emami P. K. (2014), Seismic hazard map of Uttarakhand using NGA relationship. *Proceedings of 15<sup>th</sup> Symposium on Earthquake Engineering*, IIT Roorkee, 141-150.
174. Liew, A. W. C., Yan, H., and Yang, M. (2005), Pattern recognition techniques for the emerging field of bioinformatics: A review. *Pattern Recognition*, 38(11), 2055-2073.
175. Lindholm, C. D., and Bungum, H. (2000), Probabilistic seismic hazard: a review of the seismological frame of reference with examples from Norway. *Soil Dynamics and Earthquake Engineering*, 20(1), 27-38.
176. Lombardi, A. M., Akinci, A., Malagnini, L., and Mueller, C. S. (2005), Uncertainty analysis for seismic hazard in Northern and Central Italy. *Annals of Geophysics*, 8, 853-866.
177. Ma'hood, M., Hamzehloo, H., and Doloei, G. J. (2009), Attenuation of high frequency P and S waves in the crust of the East-Central Iran. *Geophysical Journal International*, 179(3), 1669-1678.
178. Mahajan, A. K., Thakur, V. C., Sharma, M. L., and Chauhan, M. (2010), Probabilistic seismic hazard map of NW Himalaya and its adjoining area, India. *Natural Hazards*, 53(3), 443-457.
179. Maiti, S. K., Nath, S. K., Sengupta, P., and Dasadhikari, M. (2010), Seismic hazard assessment in central India in both the deterministic and probabilistic framework, **PAGEOPH**.

180. Mäntyniemi, P., Marza, V., Kijko, A., and Retief, P. (2003), A new probabilistic seismic hazard analysis for the Vrancea (Romania) seismogenic zone. *Natural Hazards*, 29(3), 371-385.
181. Mark, R. K. (1977), Application of linear statistical models of earthquake magnitude versus fault length in estimating maximum expectable earthquakes. *Geology*, 5(8), 464-466.
182. Markušić, S., Gülerce, Z., Kuka, N., Duni, L., Ivančić, I., Radovanović, S., Glavatović B, Milutinović Z, Akkar S, Kovačević S and Mihaljević, J. (2016), An updated and unified earthquake catalogue for the Western Balkan Region. *Bulletin of Earthquake Engineering*, 14(2), 321-343.
183. Matsuo, Y., Shirahama, K., and Uehara, K. (2003), Video data mining: Extracting cinematic rules from movie. *Proceedings of International Workshop Multimedia Data Management (MDM-KDD), 2003*.
184. [Mayordomo G., J., Gaspar-Escribano, J. M., and Benito, B. \(2007\), Seismic hazard assessment of the Province of Murcia \(SE Spain\): analysis of source contribution to hazard. \*Journal of Seismology\*, 11\(4\), 453-471.](#)
185. McGuire, R. K. (1976), Deterministic vs. probabilistic earthquake hazards and risks, *Soil Dynamics and Earthquake Engineering*, 21(5), 377-384.
186. McGuire, R. K. (1977), Seismic design spectra and mapping procedures using hazard analysis based directly on oscillator response. *Earthquake Engineering and Structural Dynamics*, 5(3), 211-234.
187. McGuire, R. K. (2004), Seismic hazard and risk analysis. *Earthquake Engineering Research Institute (EERI)*.
188. Menon, A., Ornthammarath, T., Corigliano, M., and Lai, C. G. (2010), Probabilistic seismic hazard macrozonation of Tamil Nadu in Southern India. *Bulletin of the Seismological Society of America*, 100(3), 1320-1341.
189. Middlemiss, C. S. (1910), The Kangra earthquake of 4<sup>th</sup> April, 1905. *Memoirs of Geological Survey of India*, 38, 409 p.
190. Miller, J. C., Smith, M. L., and McCauley, M. E. (1998), Crew fatigue and performance on us coast guard cutters (TRID Report No. CG-D-10-99).

191. Mittal, H., Kumar, A., and Ramhmachhuani, R. (2012), Indian national strong motion instrumentation network and site characterization of its stations. *International Journal of Geosciences*, 3(06), 1151.
192. Mohan, K., Joshi, A., and Patel, R. C. (2008), The assessment of seismic hazard in two seismically active regions in Himalayas using deterministic approach. *Journal of Indian Geophys Union*, 12(33), 97-107.
193. Mohan, K., Joshi, A., and Patel, R. C. (2008), The assessment of seismic hazard in two seismically active regions in Himalayas using deterministic approach. *Journal of Indian Geophys Union*, 12(33), 97-107.
194. Molnar, P., and Lyon-Caent, H. (1989), Fault plane solutions of earthquakes and active tectonics of the Tibetan Plateau and its margins. *Geophysical Journal International*, 99(1), 123-153.
195. Moratto, L., Orlecka-Sikora, B., Costa, G., Suhadolc, P., Papaioannou, C., and Papazachos, C. B. (2007), A deterministic seismic hazard analysis for shallow earthquakes in Greece. *Tectonophysics*, 442(1), 66-82.
196. [Mridula, Sinvhal, A. and Wason, H. R. \(2014\), Probabilistic seismic hazard assessment in the vicinity of MBT and MCT in western Himalaya, \*Research Inventy: International Journal of Engineering and Science\*, 4\(11\), 21-34.](#)
197. Mualchin, L. (2005), Seismic hazard analysis for critical infrastructures in California. *Engineering Geology*, 79(3), 177-184.
198. Mukhopadhyay, B. (2011), Clusters of Moderate Size Earthquakes along Main Central Thrust (MCT) in Himalaya. *International Journal of Geosciences*, 2(03), 318.
199. Mukhopadhyay, B., Acharyya, A., and Dasgupta, S. (2011), Potential source zones for Himalayan earthquakes: constraints from spatial-temporal clusters. *Natural Hazards*, 57(2), 369-383.
200. Mukhopadhyay, B., and Dasgupta, S. (2015), Seismic hazard assessment of Kashmir and Kangra valley region, Western Himalaya, India. *Geomatics, Natural Hazards and Risk*, 6(2), 149-183.

201. Muñoz, D., and Udías, A. (1992), Earthquake occurrence and seismic zonation in South Spain. *Proceedings of the World Conference on Earthquake Engineering, Madrid, Spain*, 483-487.
202. Musson, R. M. W., Toro, G. R., Coppersmith, K. J., Bommer, J. J., Deichmann, N., Bungum, H., ... and Abrahamson, N. A. (2005), Evaluating hazard results for Switzerland and how not to do it: A discussion of “Problems in the application of the SSHAC probability method for assessing earthquake hazards at Swiss nuclear power plants” by JU Klügel. *Engineering Geology*, 82(1), 43-55.
203. Nagy, G. (2005), Interactive, mobile, distributed pattern recognition. *Image Analysis and Processing–ICIAP 2005*, Springer Berlin Heidelberg, 37-49.
204. Naik, N., and Choudhury, D. (2015), Deterministic seismic hazard analysis considering different seismicity levels for the state of Goa, India. *Natural Hazards*, 75(1), 557-580.
205. Narula, P. L., Acharyya, S. K., and Banerjee, J. (2000), Seismotectonic atlas of India and its environs. *Geological Survey of India*.
206. Nath, S. K., and Thingbaijam, K. K. S. (2012), Probabilistic Seismic hazard assessment of India. *Seismological Research Letters*, 83,135-149.
207. Nath, S. K., Maity, S. K., Bora, S. S., Singh, Y., Yadav, A. K., and Dasadhikari, M. (2010a), Deterministic seismic hazard assessment for Indian subcontinent. *Earth Science Reviews*.
208. Nath, S. K., Maity, S. K., Bora, S. S., Yadav, A. K., and Sengupta, P. (2010b), Seismic hazard assessment for Gujarat, Western India in both deterministic and probabilistic framework. *Journal of Earth System Science*.
209. Nath, S. K., Thingbaijam, K. K. S., and Raj, A. (2008), Earthquake hazard in Northeast India—a seismic microzonation approach with typical case studies from Sikkim Himalaya and Guwahati city. *Journal of Earth System Science*, 117(2), 809-831.
210. NDMA (2011), Development of probabilistic seismic hazard map of India (2011). *Technical Report, National Disaster Management Authority (NDMA), Government of India, New Delhi, 2011*.

211. Ni, J., and Barazangi, M. (1984), Seismotectonics of the Himalayan collision zone: geometry of the underthrusting Indian plate beneath the Himalaya. *Journal of Geophysical Research: Solid Earth*, 89(B2), 1147-1163.
212. Nitzan, D. (1988), Three-dimensional vision structure for robot applications. *IEEE Transactions on Pattern Analysis and Machine Intelligence*, 10(3), 291-309.
213. Novikova, O., and Gorshkov, A. (2013), Recognition of Earthquake Prone Areas (M<sup>3</sup> 6.0) in the Kopet Dagh Region Using the GIS Technology. *Journal of Seismology and Earthquake Engineering*, 15(2), 101.
214. Oldham, T. (1883), Catalogue of Indian Earthquakes from the Earliest Time to the End of AD 1869. *Geological Survey of India*.
215. Ordaz, M., Martinelli, F., Aguitar, A., Arboleda, J., Meletti C., and Amico V. D., (2012). CRISIS Ver. 4.4 Program for Computing Seismic Hazard, *Instituto de Ingenieria, UNAM, Mexico, 2007*.
216. Orhan, A., Seyrek, E., and Tosun, H. (2007), A probabilistic approach for earthquake hazard assessment of the Province of Eskisehir, Turkey. *Natural Hazards Earth Syst. Sci.*, 7, 607–614.
217. Orozova, I. M., and Suhadolc, P. (1999), A deterministic–probabilistic approach for seismic hazard assessment. *Tectonophysics*, 312(2), 191-202.
218. Pailoplee, S., Sugiyama, Y., and Charusiri, P. (2010), Probabilistic seismic hazard analysis in Thailand and adjacent areas by using regional seismic source zones. *Terrestrial, Atmospheric and Oceanic Sciences*, 21(5), 757-766.
219. Papaioannou, C. A., and Papazachos, B. C. (2000), Time-independent and time-dependent seismic hazard in Greece based on seismogenic sources. *Bulletin of the Seismological Society of America*, 90(1), 22-33.
220. Parvez, I. A., and Ram, A. (1997), Probabilistic assessment of earthquake hazards in the north-east Indian peninsula and Hindukush regions. *Pure and Applied Geophysics*, 149(4), 731-746.
221. Parvez, I. A., and Ram, A. (1999), Probabilistic assessment of earthquake hazards in the Indian subcontinent. *Pure and Applied Geophysics*, 154(1), 23-40.

222. Parvez, I. A., Vaccari, F., and Panza, G. F. (2003), A deterministic seismic hazard map of India and adjacent areas. *Geophysical Journal International*, 155(2), 489-508.
223. Patil, N. S., Das, J., Kumar, A., Rout, M. M., and Das, R. (2014), Probabilistic seismic hazard assessment of Himachal Pradesh and adjoining regions. *Journal of Earth System Science*, 123(1), 49-62.
224. Peng, K. Z., Wu, F. T., and Song, L. (1985), Attenuation characteristics of peak horizontal acceleration in Northeast and Southwest China. *Earthquake Engineering and Structural Dynamics*, 13(3), 337-350.
225. Peresan, A., Gorshkov, A., Soloviev, A., and Panza, G. F. (2015), The contribution of pattern recognition of seismic and morphostructural data to seismic hazard assessment. *Bollettino di Geofisica Teorica e Applicata*, 56, 295-328.
226. Peresan, A., Panza, G. F., Gorshkov, A. I., and Aoudia, A. (2002), Pattern recognition methodologies and deterministic evaluation of seismic hazard: a strategy to increase earthquake preparedness. *Bollettino Della Società Geologica Italiana*, 121(1), 37-46.
227. Peresan, A., Zuccolo, E., Vaccari, F., Gorshkov, A., and Panza, G. F. (2011), Neo-deterministic seismic hazard and pattern recognition techniques: time-dependent scenarios for North-Eastern Italy. *Pure and Applied Geophysics*, 168(3-4), 583-607.
228. Petricoin, E. F., and Liotta, L. A. (2004), SELDI-TOF-based serum proteomic pattern diagnostics for early detection of cancer. *Current Opinion in Biotechnology*, 15(1), 24-30.
229. Rabiner, L. R., and Juang, B. H. (2004), Statistical methods for the recognition and understanding of speech. *Encyclopedia of language and linguistics*.
230. Rabiner, L. R., Levinson, S. E., Rosenberg, A. E., and Wilpon, J. G. (1979), Speaker-independent recognition of isolated words using clustering techniques. *IEEE Transactions on Acoustics, Speech and Signal Processing*, 27(4), 336-349.
231. Rajput, S.S., Mridula, Sinvhal, A., Wason, H. R., and Dixit P. (2016). Seismic Hazard and Risk Assessment in Kangra Seismogenic Source Zone, *Sixth International Conference on Recent Advances in Geotechnical Earthquake Engineering and Soil Dynamics*, Accepted.
232. Rao, B. R., and Rao, P. S. (1984), Historical seismicity of peninsular India. *Bulletin of the Seismological Society of America*, 74(6), 2519-2533.



233. Reasenber, P. (1985), Second-order moment of central California seismicity, 1969–1982. *Journal of Geophysical Research: Solid Earth*, 90(B7), 5479-5495.
234. Reiter, L. (1990), Earthquake hazard analysis: issues and insights, Columbia University Press, New York, 254.
235. Ristau, J., Rogers, G. C., and Cassidy, J. F. (2005), Moment magnitude–local magnitude calibration for earthquakes in western Canada. *Bulletin of the Seismological Society of America*, 95(5), 1994-2000.
236. Robbert, J. S. (1992), Pattern recognition: statistical, structural and neural approaches. Wiley, New York, ISBN 0-471-052974-5, 1992.
237. Rosenfeld, A. (1976), Pattern recognition and image processing. *IEEE transactions on computers*, (12), 1336-1346.
238. Rout, M. M., Das, J., and Das, R. (2015), Probabilistic seismic hazard assessment of NW and central Himalayas and the adjoining region. *Journal of Earth System Science*, 124(3), 577-586.
239. Rydelek, P. A., and Sacks, I. S. (1989), Testing the completeness of earthquake catalogues and the hypothesis of self-similarity. *Nature*, 337(6204), 251-253.
240. Sabetta, F., Lucantoni, A., Bungum, H., and Bommer, J. J. (2005), Sensitivity of PSHA results to ground motion prediction relations and logic-tree weights. *Soil Dynamics and Earthquake Engineering*, 25(4), 317-329.
241. Sayed A. D., and Hassib, H. G. (2009), Discriminating nuclear explosions from earthquakes at teleseismic distances. *European Journal of Applied Sciences*, 4(1), 47-52.
242. Scarpetta, S., Giudicepietro, F., Ezin, E. C., Petrosino, S., Del Pezzo, E., Martini, M., and Marinaro, M. (2005), Automatic classification of seismic signals at Mt. Vesuvius volcano, Italy, using neural networks. *Bulletin of the Seismological Society of America*, 95(1), 185-196.
243. Scherbaum, F., Bommer, J. J., Bungum, H., Cotton, F., and Abrahamson, N. A. (2005), Composite ground-motion models and logic trees: methodology, sensitivities, and uncertainties. *Bulletin of the Seismological Society of America*, 95(5), 1575-1593.

244. Schwartz, D. P., and Coppersmith, K. J. (1986), Seismic hazards: new trends in analysis using geologic data. *Active Tectonics*, National Academy Press, Washington, D.C., 215-230
245. Schwartz, D. P., Coppersmith, K. J., and Swan III, F. H. (1984), Methods for estimating maximum earthquake magnitudes. *Proceedings of the Eighth World Conference on Earthquake Engineering*, 1, 279-285.
246. Scott, W. E., Pierce, K. L., and Hait, M. H. (1985), Quaternary tectonic setting of the 1983 Borah Peak earthquake, central Idaho. *Bulletin of the Seismological Society of America*, 75(4), 1053-1066.
247. Shah, H., Ghazali, R., and Nawi, N. M. (2011), Using artificial bee colony algorithm for MLP training on earthquake time series data prediction. *arXiv preprint arXiv:1112.4628*.
248. Shah, M. A., Qaisar, M., Iqbal, J. and Ahmed, S. (2012), Deterministic seismic hazard assessment of Quetta, Pakistan. *Proceedings of 15<sup>th</sup> World Conference on Earthquake Engineering*, 214-219.
249. Shakal, A. F., and Bernreuter, D. L. (1980), Empirical analyses of near-source ground motion. (No. NUREG/CR-2095; UCRL-53028), Lawrence Livermore National Lab., CA (USA).
250. Sharma, M. L. (1998), Attenuation relationship for estimation of peak ground horizontal acceleration using data from strong-motion arrays in India. *Bulletin of the Seismological Society of America*, 88(4), 1063-1069.
251. Sharma, M. L. (2000), Attenuation Relationship for Estimation of Peak Ground Vertical acceleration Using Data from Strong Motion Arrays in India, *Proceedings of 12<sup>th</sup> World Conference on Earthquake Engineering*, Paper No. 1964, 1-8.
252. Sharma, M. L., and Lindholm, C. (2012), Earthquake hazard assessment for Dehradun, Uttarakhand, India, including a characteristic earthquake recurrence model for the Himalaya Frontal Fault (HFF), *Pure and Applied Geophysics*, 169(9), 1601-1617.
253. Sharma, M. L., and Malik, S. (2006), Probabilistic seismic hazard analysis and estimation of spectral strong ground motion on bed rock in north east India. *4<sup>th</sup> International Conference on Earthquake Engineering, Taipei, Taiwan, Paper (No. 15)*.

254. Sharma, M. L., and Wason, H. R. (2004), Estimation of Seismic Hazard and Seismic Zonation at Bed Rock Level for Delhi Region, India, 13<sup>th</sup> World Conference on Earthquake Engineering. Paper No. 2046
255. Sharma, M. L., Douglas, J., Bungum, H., and Kotadia, J. (2009), Ground-motion prediction equations based on data from the Himalayan and Zagros regions. *Journal of Earthquake Engineering*, 13(8), 1191-1210.
256. Sharma, M. L., Wason, H. R., and Dimri, R. (2003), Seismic zonation of the Delhi region for bedrock ground motion. *Pure and Applied Geophysics*, 160(12), 2381-2398.
257. Shin, H., and Markey, M. K. (2006), A machine learning perspective on the development of clinical decision support systems utilizing mass spectra of blood samples. *Journal of Biomedical Informatics*, 39(2), 227-248.
258. Shitong, W., and Min, W. (2006), A new detection algorithm (NDA) based on fuzzy cellular neural networks for white blood cell detection. *IEEE Transactions on Information Technology in Biomedicine*, 10(1), 5-10.
259. Shrimali, V., Anand, R. S., Kumar, V., and Srivastav, R. K. (2009), Medical feature based evaluation of structuring elements for morphological enhancement of ultrasonic images. *Journal of Medical Engineering and Technology*, 33(2), 158-169.
260. Shukla, J., and Choudhury, D. (2012), Estimation of seismic ground motions using deterministic approach for major cities of Gujarat. *Natural Hazards and Earth System Science*, 12, 2019-2037.
261. Sil, A., Sitharam, T. G., and Kolathayar, S. (2013), Probabilistic seismic hazard analysis of Tripura and Mizoram states. *Natural Hazards*, 68(2), 1089-1108.
262. Singh, B., Mittal, A., and Ghosh, D. (2011a), An evaluation of different feature extractors and classifiers for offline handwritten Devnagari character recognition. *Journal of Pattern Recognition Research*, 2, 269-277.
263. Singh, B., Mittal, A., Ansari, M. A., and Ghosh, D. (2011b), Handwritten Devanagari Word Recognition: A Curvelet Transform Based Approach. *International Journal on Computer Science and Engineering*, 3(4), 1658-1665.

264. Singh, R. P., Aman, A., and Prasad, Y. J. J. (1996), Attenuation relations for strong seismic ground motion in the Himalayan region. *Pure and Applied Geophysics*, 147(1), 161-180.
265. Singh, S., Jain, A. K., Singh, V. N., and Srivastava, L. S. (1977), Damage during Kinnaur earthquake of January 19, 1975 in Himachal Pradesh, India. *Proceedings of Sixth World Conference on Earthquake Engineering, New Delhi*, 10-14.
266. Sinha, A. K. (2006), Simplified method for seismic vulnerability assessment. *Journal of the Bridge and Structural Engineer*, 36, 25-28.
267. Sinha, A. K. et al. (1998), Problem and growth management in the city of Delhi: planning for sustainable development. *Journal of Indian Building Congress*, 5, 73-80.
268. Sinha, A. K. et al. (2001a), Creating community awareness for seismic disaster mitigation. *Journal of Indian Building Congress*, 8, 346-352.
269. Sinha, A. K. et al. (2001b), Rescue after earthquake. *Journal of Indian Building Congress*, 8, 391-397.
270. Sinvhal A., 1979, Application of seismic reflection data to discriminate between subsurface litho-Stratigraphy, Ph.D. thesis. Department of Earth Sciences, University of Roorkee, India, 218 p.
271. Sinvhal, A. (2012), Understanding Earthquake Disasters, *Tata McGraw-Hill Education private limited*, New Delhi, 283 p.
272. Sinvhal, A. (2012), Seismic modelling and pattern recognition in oil exploration. *Springer Science and Business Media*. Kluwer Academic Publisher, The Netherlands, 178
273. Sinvhal, A. and Sinvhal, H. (1992), Seismic modeling and pattern recognition in oil exploration. *Kluwer Academic Publisher, The Netherlands*, 178 p.
274. Sinvhal, A., and Khattri, K. (1983), Application of seismic reflection data to discriminate subsurface lithostratigraphy. *Geophysics*, 48(11), 1498-1513.
275. Sinvhal, A., Joshi, G., Sinvhal, H., and Singh, V. N. (1990), A pattern recognition technique for microzonation. *Proceedings Ninth Symposium on Earthquake Engineering, Roorkee, India*, 1, 24-30.

276. Sinvhal, A., Khattri, K. N., Sinvhal, H., and Awasthi, A. K. (1984), Seismic indicators of stratigraphy. *Geophysics*, 49(8),1196-1212.
277. Sinvhal, A., Pandey, A. D., and Pore, S. M. (2005), Preliminary report on 8<sup>th</sup> October 2005 Kashmir Earthquake. *Department of Earthquake Engineering*, IIT Roorkee, 60 p.
278. Sinvhal, A., Sinvhal, H., and Joshi, G. (1991), A valid pattern of microzonation. *Proceedings of the Fourth International Conference on Seismic Zonation*, Stanford University, USA, 641-648.
279. Sitharam, T. G., Anbazhagan, P., and Ganesha Raj, K. (2006), Deterministic Seismic Hazard Analysis and Estimation of PHA for Bangalore City. *International Conference on Earthquake Engineering*,1-8.
280. Sitharam, T. G., and Sil, A. (2014), Comprehensive seismic hazard assessment of Tripura and Mizoram states. *Journal of Earth System Science*, 123(4), 837-857.
281. Smith, J., and Bhatia, S. (2009), Bioimprovement of Soils for Highway Applications Using Rolled Erosion Control Products. *Transportation Research Record: Journal of the Transportation Research Board*, (2108), 117-126.
282. Smith, P., Lobo, N. D. V., and Shah, M. (2005), Temporal boost for event recognition. *Tenth IEEE International Conference on Computer Vision ICCV*, 1, 733-740.
283. Sokolov, V. Y., Wenzel, F., and Mohindra, R. (2009), Probabilistic seismic hazard assessment for Romania and sensitivity analysis: a case of joint consideration of intermediate-depth (Vrancea) and shallow (crustal) seismicity. *Soil Dynamics and Earthquake Engineering*, 29(2), 364-381.
284. Sokolov, V., Wenzel, F., Mohindra, R., Grecu, B., and Radulian, M. (2007), Probabilistic seismic hazard assessment for Romania considering intermediate-depth (Vrancea) and shallow (crustal) seismicity. *In International symposium on strong Vrancea earthquakes and risk mitigation*.
285. Soloviev, A. A., Novikova, O. V., Gorshkov, A. I., and Piotrovskaya, E. P. (2013), Recognition of potential sources of strong earthquakes in the Caucasus region using GIS technologies. In *Doklady Earth Sciences*, Springer Science and Business Media, 450(2), 658.

286. Srinivasan, K., Porkumaran, K., Sainarayanan, G. (2009), Improved background subtraction techniques for security in video applications. *Proceedings of 3rd International Conference on Anti-counterfeiting, Security, and Identification in Communication*, 114 – 117.
287. Srivastava, H. B. (2009), Image pre-processing algorithms for detection of small/point airborne targets. *Defence Science Journal*, 59(2), 166.
288. Srivastava, H. N., and Ramachandran, K. (1983), New catalogue of earthquakes for peninsular India during 1839-1900. *Mausam*, 36(3), 351-358.
289. Stepp, J. C. (1972), Analysis of completeness of the earthquake sample in the Puget Sound area and its effect on statistical estimates of earthquake hazard. *Proceeding of the 1<sup>st</sup> Int. Conf. on Microzonation, Seattle*, 2, 897-910.
290. Stirling, M. W., Mc Verry, G. H., and Berryman, K. R. (2002), A new seismic hazard model for New Zealand. *Bulletin of the Seismological Society of America*, 92(5), 1878-1903.
291. Survey of India, (2011), Administrative Body Database For entire country Up to Taluk level with HQ, Code: OVLSF/1M/37, Single licensed digitized map.
292. Tandon, A. N., and Srivastava, H. N. (1974), Earthquake occurrence in India. *Earthquake Engineering: Jai Krishna Sixtieth Birth Anniversary Commemoration*, 1-48.
293. Tewatia, S. K., and Bose, P. R. (2006), Discussion on" A Study on the Beginning of Secondary Compression of Soils" by RG Robinson. *Journal of Testing and Evaluation*, 34(5), 453.
294. Tewatia, S. K., Bose, P. R., and Sridharan, A. (2013), Fastest rapid loading methods of vertical and radial consolidations. *International Journal of Geomechanics*, 13(4), 332-339.
295. Tewatia, S. K., Bose, P. R., Sridharan, A., and Rath, S. (2007), Stress induced time dependent behavior of clayey soils. *Geotechnical and Geological Engineering*, 25(2), 239-255.
296. Theodulidis, N., Lekidis, V., Margaris, B., Papazachos, C., Papaioannou, C., & Dimitriou, P. (1998), Seismic hazard assessment and design spectra for the Kozani-Grevena region (Greece) after the earthquake of May 13, 1995. *Journal of Geodynamics*, 26(2), 375-391.

297. Tselentis, G. A., and Danciu, L. (2010), Probabilistic seismic hazard assessment in Greece–Part 1: Engineering ground motion parameters. *Natural Hazards Earth Syst. Sci*, 10, 25-39
298. Tselentis, G. A., Danciu, L., and Sokos, E. (2010), Probabilistic seismic hazard assessment in Greece–Part 2: Acceleration response spectra and elastic input energy spectra. *Natural Hazards and Earth System Science*,10(1), 41-49.
299. Tuyen, N. H., Thi, L., and Gorshkov, I. (2012), Recognition of earthquake-prone area ( $M \geq 5.0$ ) applied for North Vietnam and Adjacency. *Journal of Sciences of the Earth*, 34 (3), 251-265.
300. USGS Catalogue: <http://earthquake.usgs.gov/earthquakes/eqarchives> (United States Geological Survey).
301. Ustundag, B. (2008), Pattern based cognitive communication system. *Patent Application, Turkish Patent Institute*.
302. Valafar, F. (2002), Pattern recognition techniques in microarray data analysis. *Annals of the New York Academy of Sciences*, 980(1), 41-64.
303. Varunoday, G. V., and Wason, H. R. (1979), Spatial prediction of earthquakes in Kumaon Himalaya by pattern recognition. *Mausam*, 30, 253-264.
304. Veneziano, D., Cornell, C. A., and O’Hara, T. (1984), Historic method for seismic hazard analysis. Interim report, May 1984 (No. EPRI-NP-3438). Yankee Atomic Electric Co., Framingham, MA (USA).
305. Walt, C. M., and Barnard, E. (2007), Data characteristics that determine classifier performance, *SAIEE Africa Research Journal*, 98(3), 87-93.
306. Walter, W. R., Matzel, E., Pasyanos, M. E., Harris, D. B., Gok, R., and Ford, S. R. (2007), Empirical observations of earthquake-explosion discrimination using P/S ratios and implications for the sources of explosion S-waves. *Lawrence Livermore National Lab CA*.
307. Wang, J. P., Huang, D., and Yang, Z. (2012), Deterministic seismic hazard map for Taiwan developed using an in-house Excel-based program. *Computers and Geosciences*, 48, 111-116.

308. Wason, H. R., Das, R., and Sharma, M. L. (2012), Magnitude conversion problem using general orthogonal regression. *Geophysical Journal International*, 190(2), 1091-1096.
309. Wells, D. L., and Coppersmith, K. J. (1994), New empirical relationships among magnitude, rupture length, rupture width, rupture area, and surface displacement. *Bulletin of the seismological Society of America*, 84(4), 974-1002.
310. Wiemer, S. (2001), Software Package to Analyze Seismicity: ZMAP. *Seismological Research Letters*, 72, 373-382. Z- Map: <http://mercalli.ethz.ch/~eberhard/zmap.zip>.
311. Wiemer, S., and Wyss, M. (2000), Minimum magnitude of completeness in earthquake catalogs: examples from Alaska, the western United States, and Japan. *Bulletin of the Seismological Society of America*, 90(4), 859-869.
312. Woessner, J., and Wiemer, S. (2005), Assessing the quality of earthquake catalogues: Estimating the magnitude of completeness and its uncertainty. *Bulletin of the Seismological Society of America*, 95(2), 684-698.
313. Wu, X., Kumar, V., Quinlan, J. R., Ghosh, J., Yang, Q., Motoda, H., ... and Zhou, Z. H. (2008), Top 10 algorithms in data mining. *Knowledge and information systems*, 14(1), 1-37.
314. Wyss, M., Hasegawa, A., Wiemer, S., and Umino, N. (1999), Quantitative mapping of precursory seismic quiescence before the 1989, M 7.1 off-Sanriku earthquake, Japan.
315. Yadav, R. B. S., Bayrak, Y., Tripathi, J. N., Chopra, S., Singh, A. P., and Bayrak, E. (2012), A probabilistic assessment of earthquake hazard parameters in NW Himalaya and the adjoining regions. *Pure and Applied Geophysics*, 169(9), 1619-1639.
316. Yielding, G., Jackson, J. A., King, G. C. P., Sinval, H., Vita-Finzi, C., and Wood, R. M. (1981), Relations between surface deformation, fault geometry, seismicity, and rupture characteristics during the El Asnam (Algeria) earthquake of 10 October 1980. *Earth and Planetary Science Letters*, 56, 287-304.
317. Youngs, R. R., Chiou, S. J., Silva, W. J., and Humphrey, J. R. (1997), Strong ground motion attenuation relationships for subduction zone earthquakes. *Seismological Research Letters*, 68(1), 58-73.



318. Zhang, D. Q., and Chen, S. C. (2004), A novel kernelized fuzzy c-means algorithm with application in medical image segmentation. *Artificial Intelligence in Medicine*, 32(1), 37-50.
319. Zhao, J. X., Zhang, J., Asano, A., Ohno, Y., Oouchi, T., Takahashi, T., Ogawa, H., Irikura, K., Thio, H.K., Somerville, P.G. and Fukushima, Y. (2006), Attenuation relations of strong ground motion in Japan using site classification based on predominant period. *Bulletin of the Seismological Society of America*, 96(3), 898-913.
320. Zhong, H., Shi, J., and Visontai, M. (2004), Detecting unusual activity in video. *CVPR 2004. Proceedings of the 2004 IEEE Computer Society Conference on Computer Vision and Pattern Recognition*, 2, II-819.
321. Zhu, H., Sun, W., Wu, M., Guan, G., and Guan, Y. (2008), Pre-processing of X-ray medical image based on improved temporal recursive self-adaptive filter. *The 9<sup>th</sup> International Conference Young Computer Scientists, 2008. ICYCS 2008*, 758-763.
322. Zhu, X., Wu, X., Elmagarmid, A. K., Feng, Z., and Wu, L. (2005), Video data mining: semantic indexing and event detection from the association perspective. *IEEE Transactions on Knowledge and Data Engineering*, 17(5), 665-677.



## LIST OF PUBLICATIONS

### Journals

1. **Mridula**, Sinvhal A and Wason H R (2015), Identification of seismically susceptible areas in the western Himalaya using pattern recognition, Accepted on 1<sup>st</sup> February, 2016, *Journal of Earth System Science*.
2. **Mridula**, Sinvhal A and Wason H R (2014), Probabilistic seismic hazard assessment in the vicinity of MBT and MCT in western Himalaya, Research Inveny: International Journal of Engineering and Science, 4(11), 21-34.

### Conferences/ Symposium

1. **Mridula**, Sinvhal A and Wason H R (2013), A review on pattern recognition techniques for seismic hazard analysis. *In Proceedings of International Conference on Emerging Trends in Engineering and Technology*, 854-858.
2. Rashmi, **Mridula**, Sinvhal A and Wason H R (2014), *Probabilistic seismic hazard Assessment of Himachal Pradesh and contiguous regions*, Proceedings volume, 15<sup>th</sup> Symposium on Earthquake Engineering, , 110 - 121.
3. Rajput S S, **Mridula**, and Sinvhal A (2014), Vulnerability assessment of area and structures, Proceedings volume, 15<sup>th</sup> Symposium on Earthquake Engineering, 2014, 1099 - 1108.
4. **Mridula**, Sinvhal A. and Wason H R (2014), Seismic hazard zonation of Himachal Pradesh, Northwest Himalaya, in *National workshop on Status of natural hazards in Himachal Pradesh (NHHP-14)*, 6-8 November, 2014 conducted by Central University of Himachal Pradesh, Shahpur, Dharamsala, Abstract.
5. **Mridula**, Rajput S S, Sinvhal A and Wason H R (2015), Seismic Hazard and Vulnerability Assessment of Himachal Pradesh and Contiguous Regions, *EMI 2015*, Stanford, Abstract.
6. Rajput S S, **Mridula**, A Sinvhal, Wason H R and Dixit Prashansa, Seismic hazard and risk assessment in Kangra seismogenic source zone, *Sixth International conference on recent advances in geotechnical earthquake engineering and soil dynamics*, Accepted on 20<sup>th</sup> April, 2016.

### Communicated

1. **Mridula**, A. Sinvhal and H. R. Wason, 2015, Segmentation of Main Boundary Thrust and Main Central Thrust in Western Himalaya for assessment of seismic hazard, Natural hazards, Communicated.